NOVEL GROUP 9 CATALYSTS FOR THE CARBONYLATION OF METHANOL

Andrew Craig Marr

A Thesis Submitted for the Degree of PhD
at the
University of St Andrews

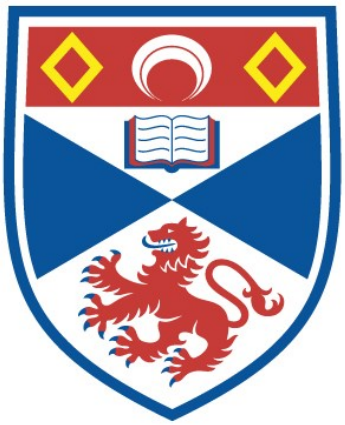

1998

Novel Group 9 Catalysts for the Carbonylation of Methanol

A thesis presented by Andrew Craig Marr BSc.,

to

the University of St. Andrews

in application for the degree of Doctor of Philosophy

September 1998

TL D150

DECLARATION

I, Andrew Craig Marr, hereby certify that this thesis, has been written by me, that it is a record of work carried out by me and that it has not been submitted in any previous application for a higher degree.

Signed ___ ____ Date 23rd Sept 1998

I was admitted as a research student in September 1995 as a candidate for the degree of Doctor of Philosophy; the higher study for which this is a record was carried out in the University of St. Andrews between September 1995 and September 1998.

Signed _ _____ Date 23rd Sept. 1998

I hereby certify that the candidate has fulfilled the conditions of the Resolution and Regulations appropriate for the degree of Doctor of Philosophy in the University of St. Andrews and that the candidate is qualified to submit this thesis in application for that degree.

Signed Date 23rd September, 1998

DECLARATION

In submitting this thesis to the University of St. Andrews I wish access to be subject to the following conditions: for a period of 5 years from the date of submission, the thesis shall be withheld from use. I understand, however, the title and abstract of the thesis will be published during this period of restricted access; and that after the expiry of this period the thesis will be made available for use in accordance with the regulations of the University Library for the time being in force, subject to any copyright in the work not being affected thereby, and a copy of the work may be made and supplied to any *bone fide* library or research worker.

Signed

Date 3/11/98

Table of Contents

CHAPTER 1

INTRODUCTION.

CHAPTER 2:

CATALYST SOLUTIONS CONTAINING ONLY CO, PHOSPHINE AND IODIDE LIGANDS.

CHAPTER 3:

CYCLOPENTADIENYL COBALT CARBONYL, A CARBONYLATION CATALYST?

CHAPTER 4:

IMPROVING CYCLOPENTADIENYL COBALT CARBONYL CATALYSTS

CHAPTER 5:

DISCUSSION AND FURTHER WORK.

CHAPTER 6:

EXPERIMENTAL.

ACKNOWLEDGEMENTS.

I would like to express my gratitude to the following people:

My supervisor Prof. David Cole-Hamilton for teaching me how to be a research chemist and for preventing me from getting too carried away with all the Cp ligands.

My industrial supervisors Dr. Andrew Poole and Dr. Evert Ditzel for being friendly as well as helpful.

All those who have tolerated my crazed madness in lab.334 and especially to Al. Brown and Gary Schwarz for joining in.

All the people who have given freely of their time in order to talk sense in to / discuss chemistry with me, you are too numerous to mention, but you know who you are.

All the practical people without whom crazy ideas on paper would have stayed that way. The technical staff in St. Andrews were great friends as well as great assistance.

All my family and in particular my mother for finally getting me to take an interest in studying.

To my wife, a very special woman who keeps me organised, makes me smile and lets me be insane.

Finally, this project would not have been possible without the financial backing of the EPSRC and B.P. Chemicals.

ABSTRACT.

The carbonylation of methanol catalysed by Group 9 metals is the principle industrial route to acetic acid. It has been one of the most important applications of homogeneous catalysts for thirty years. In that time the preferred catalytic species has descended the group from cobalt, through rhodium, and recently to iridium with the introduction of B.P. Chemical's Cativa process.

Rhodium and iridium are precious metals, it would be advantageous to develop a catalytic system which does not depend on a rare metal. One way this could be achieved is by improving cobalt catalysed carbonylation.

Work has concentrated on the ability of the cyclopentadienyl, pentamethylcyclopentadienyl and triethyl phosphine ligands to promote cobalt catalysts. Several novel cobalt catalysts and one novel rhodium catalyst have been discovered for the carbonylation of methanol to methyl acetate.

$$CH_3OH + ROH \xrightarrow[\text{Catalyst}]{CO} CH_3COOR + H_2O$$

At 120 °C using $[Cp^*Co(CO)_2]$ and PEt_3 as catalyst precursors rates of methanol carbonylation have been achieved which are, to our knowledge, far greater than any previously reported for cobalt catalysts. The initial rate of carbonylation compares favourably with that of rhodium based systems.

High Pressure Infrared Spectroscopy has been utilised extensively as a tool for investigating the solution behaviour of the novel catalyst precursors $[CpCo(CO)PMe_2Ph]$, $[CpCo(CO)_2]$, $[Cp^*Co(CO)_2]$ and $[Cp^*Rh(CO)_2]$.

Table of Contents

CHAPTER 1

INTRODUCTION.

CHAPTER 2:

CATALYST SOLUTIONS CONTAINING ONLY CO, PHOSPHINE AND IODIDE LIGANDS.

CHAPTER 3:

CYCLOPENTADIENYL COBALT CARBONYL, A CARBONYLATION CATALYST?

CHAPTER 4:

IMPROVING CYCLOPENTADIENYL COBALT CARBONYL CATALYSTS

CHAPTER 5:

DISCUSSION AND FURTHER WORK.

CHAPTER 6:

EXPERIMENTAL.

ACKNOWLEDGEMENTS.

I would like to express my gratitude to the following people:

My supervisor Prof. David Cole-Hamilton for teaching me how to be a research chemist and for preventing me from getting too carried away with all the Cp ligands.

My industrial supervisors Dr. Andrew Poole and Dr. Evert Ditzel for being friendly as well as helpful.

All those who have tolerated my crazed madness in lab.334 and especially to Al. Brown and Gary Schwarz for joining in.

All the people who have given freely of their time in order to talk sense in to / discuss chemistry with me, you are too numerous to mention, but you know who you are.

All the practical people without whom crazy ideas on paper would have stayed that way. The technical staff in St. Andrews were great friends as well as great assistance.

All my family and in particular my mother for finally getting me to take an interest in studying.

To my wife, a very special woman who keeps me organised, makes me smile and lets me be insane.

Finally, this project would not have been possible without the financial backing of the EPSRC and B.P. Chemicals.

ABSTRACT.

The carbonylation of methanol catalysed by Group 9 metals is the principle industrial route to acetic acid. It has been one of the most important applications of homogeneous catalysts for thirty years. In that time the preferred catalytic species has descended the group from cobalt, through rhodium, and recently to iridium with the introduction of B.P. Chemical's Cativa process.

Rhodium and iridium are precious metals, it would be advantageous to develop a catalytic system which does not depend on a rare metal. One way this could be achieved is by improving cobalt catalysed carbonylation.

Work has concentrated on the ability of the cyclopentadienyl, pentamethylcyclopentadienyl and triethyl phosphine ligands to promote cobalt catalysts. Several novel cobalt catalysts and one novel rhodium catalyst have been discovered for the carbonylation of methanol to methyl acetate.

$$CH_3OH + ROH \xrightarrow[\text{Catalyst}]{CO} CH_3COOR + H_2O$$

At 120 °C using $[Cp^*Co(CO)_2]$ and PEt_3 as catalyst precursors rates of methanol carbonylation have been achieved which are, to our knowledge, far greater than any previously reported for cobalt catalysts. The initial rate of carbonylation compares favourably with that of rhodium based systems.

High Pressure Infrared Spectroscopy has been utilised extensively as a tool for investigating the solution behaviour of the novel catalyst precursors $[CpCo(CO)PMe_2Ph]$, $[CpCo(CO)_2]$, $[Cp^*Co(CO)_2]$ and $[Cp^*Rh(CO)_2]$.

CHAPTER 1: INTRODUCTION.

SECTION 1.1: ACETATES DERIVED FROM C1 PRECURSORS

1.1a. Introduction. [1]

In organic chemistry the carbonyl group is of prime importance. The reactivity of this functional group makes it a useful starting point for the synthesis of many classes of compound. The formation of compounds containing the carbon to carbonyl linkage is a carbon - carbon bond forming reaction of vital importance.

The simplest and cheapest source of the carbonyl group is carbon monoxide generated from fossil fuels, with the help of metal catalysts organic compounds can be built containing carbon derived solely from carbon monoxide gas. An example of such a process is the synthesis of acetic acid. Carbon monoxide and hydrogen are converted to methanol, and then this organic compound is carbonylated with CO gas using a homogeneous transition metal carbonyl catalyst.

1.1b. Obtaining Pure CO. [2]

In recent times the principle source of carbon monoxide containing gases has been from steam reforming or partial oxidation of liquid or gaseous hydrocarbons but it can also be derived from coal.

Exothermic Partial Oxidation Process: ΔH

$$CH_4 + 1/2O_2 \longrightarrow CO + 2H_2 \quad -40\ kJ/mol$$

Endothermic Steam Reforming Process:

$$CH_4 + H_2O \longrightarrow CO + 3H_2 \quad +205\ kJ/mol$$

1.1c. Methanol Production. [1,2]

Methanol is obtained from carbon monoxide and hydrogen in an exothermic reaction which liberates 90.8 kJ/mol:

$$CO + 2H_2 \rightleftharpoons CH_3OH$$

Although thermodynamically feasible methanol formation is less favourable than the formation of other alcohols and alkanes and a heterogeneous catalyst is required to promote methanol production. The process is promoted by high pressure and low

temperature and a copper / zinc catalytic system operates under fairly mild conditions of 250°C and 50 bar. Various promotors are added to enhance the activity and stability, these include chromium, aluminium and vanadium / manganese additives. The product is removed and the resultant gas is recycled as the yield is low.

1.1d. Acetic Acid Synthesis

1.1d i. Uses of Acetic Acid.[1,3]

Acetic acid is a very important feedstock chemical. It has found application as a solvent and as a starting material in the pharmaceutical and polymer industries, furthermore conversion to inorganic acetates renders acetic acid useful in the textile, leather and paint industries. Acetic acid and acetates are also useful lab reagents as solvents, and as cheap starting materials and ligands for synthetic work. Amongst the largest uses of acetic acid are the production of the vinyl acetate monomer, cellulose acetate and terephthalic acid.

1.1d ii. Acetic Acid Synthesis from Methanol and CO.

About 5.5 million tonnes of acetic acid is synthesised from methanol and CO every year. [3] Acetic acid is simply the product of methanol carbonylation on a homogeneous metal catalyst.

Its synthesis represents the synthesis of a C_2 oxygenated compound from two C_1 units, both of which started as carbon monoxide. It is an example of a homogeneous catalytic system used for large scale industrial synthesis and has been commercialised employing three different metals: cobalt, rhodium and iridium.

In recent times the coupling of carbon monoxide and methanol has become the preferred route to acetic acid.

$$CH_3OH + CO \longrightarrow CH_3COOH$$

The transition metal catalyst facilitates coupling of the CH_3 and CO units and an iodide promotor activates the methyl unit.

Since the first commercialised process in the 60's the passage of time has seen the technology descend group 9 from cobalt in 1966, through rhodium in 1970, to iridium in 1996.

SECTION 1.2: THE COBALT CATALYSED ACETIC ACID PROCESS: THE B.A.S.F. PROCESS

1.2a. Introduction: The B.A.S.F. Process.

The B.A.S.F. process was the first process for the catalytic carbonylation of methanol to acetic acid. It has been used to prepare acetic acid on an industrial scale since 1966. Cobalt is introduced as CoI_2. The operating conditions are harsh for a homogeneous process 200 - 250°C and 500 - 700 bar, and the concentration of cobalt is high, approximately 0.1 mol dm^{-3}. [4] The high temperatures and metal concentrations are required to enhance the rate as cobalt is a poor catalyst. High pressures are required to stabilise the metal carbonyl species. [5] Under optimised conditions the selectivity to acetic acid production is 90% based on methanol. [4] The solvent system consisted mainly of methanol, water, acetic acid, methyl acetate and methyl iodide, hydrogen can be added as a promotor. [6]

1.2b. The Mechanism.

The mechanism of the cobalt catalysed carbonylation of methanol has never been elucidated. There are several reasons for this. Firstly the conditions at which the process operates are too harsh for spectroscopic methods. Secondly, the reaction chemistry of cobalt is very complex and the reaction solution contains a mixture of many species in equilibria. Thirdly, most cobalt carbonyl complexes are unstable and highly reactive as the cobalt to carbon bond in carbonyl and alkyl compounds is weak. In the absence of stabilising ligands such as PPh_3 most alkyl and acyl cobalt carbonyls are very air sensitive oils. These rapidly decompose, even under inert atmospheres at low temperatures preventing isolation, purification and characterisation. [7,8] Fourthly, it is difficult to obtain good quality NMR data, partly because cobalt is a quadripolar nucleus of spin I = 7/2, with the effect of broadening the signals of nuclei coupled to it and, more detrimental to the quality of spectrum, is the propensity of cobalt to form Co (II) species. These compounds have unpaired electrons and are therefore paramagnetic. The presence of paramagnetic species serves to shift and broaden the resonances. Most of the information is lost, even at low levels. Co (II) is especially accessible from Co (O) and Co (I) via disproportionation and oxidation processes. Solutions must be kept rigorously free from air as cobalt has a high affinity for oxygen.

The mechanistic discussion that follows is based on a general knowledge of cobalt carbonyl chemistry and studies done on the homologation of methanol to ethanol using synthesis gas.

1.2b i. Cobalt Chemistry: Species in Solution.[5]

Solutions containing low valent cobalt species are very complex. The ligands of cobalt carbonyl compounds are very labile and have an extensive and varied reaction chemistry. Cobalt is capable of heterolytic and homolytic bond cleavage lending to ionic and radical chemistry simultaneously. Cobalt complexes can undergo disproportionation and conproportionation reactions leading to many species in equilibria. Small changes in conditions can greatly affect the nature of a solution containing low valent cobalt.
Due to the nature of cobalt chemistry the discussion of mechanistics is not as useful as it is for catalysts with simpler chemistry. It is very unlikely that we will be able to predict the effect of an added species or a change in conditions! However it is very helpful to gain knowledge of the processes occuring in solution and to find out which species are active carbonylation catalysts. This may help us to choose conditions favouring carbonylation and design better catalysts. To this end we will consider the reactions which could be occurring in a solution containing cobalt, iodide, methanol, water, acetic acid, methyl acetate, methyl iodide and hydrogen at high pressures of carbon monoxide and high temperatures.

1.2b ii. The Conditions in Solution.

In a typical carbonylation solvent system the main organic equilibria in solution are:

Organic Equilibria:

$$MeCOOH + MeOH \rightleftharpoons MeCOOMe + H_2O$$

$$2MeOH \rightleftharpoons MeOMe + H_2O$$

$$MeOH + HI \rightleftharpoons MeI + H_2O$$

$$MeCOOMe + HI \rightleftharpoons MeI + MeCOOH$$

$$MeOMe + HI \rightleftharpoons MeI + MeOH$$

and to a lesser extent: [9]

$$HI \rightleftharpoons I_2 + H_2$$

$$MeOH + HI \rightleftharpoons MeOH_2^+ + I^-$$

The medium is very acidic due to the presence of the mineral acid HI and quite polar due to the high concentrations of acetic acid, methanol and water.

1.2b iii. The Catalyst Precursor CoI_2.

CoI_2 can undergo a number of transformations in the reaction media. It is widely accepted that the catalytic cycle involves cobalt intermediates in low oxidation states. In a CO atmosphere two likely routes to Co (0) are: [6,9]

$$2CoI_2 + 2H_2O + 10CO \longrightarrow Co_2(CO)_8 + 4HI + 2CO_2$$

$$2CoI_2 + 2H_2 + 8CO \longrightarrow Co_2(CO)_8 + 4HI$$

Co (II) and Co (0) are in equilibrum as oxidising agents are also available: [20]

$$Co_2(CO)_8 + 4HI \longrightarrow 2CoI_2 + 2H_2 + 8CO$$

Co (II) can also form anionic tetrahedral iodides $[CoI_4]^{2-}$. [10]

The cobalt-cobalt bond of $[Co_2(CO)_8]$ is very labile in donor solvents, in the resulting reaction cobalt again changes oxidation state, it can be reduced. [11] oxidised, [12,6,9] or it can disproportionate. [C12, C26]

Reduction

$$Co_2(CO)_8 + 2A^+I^- + H_2 \longrightarrow 2A^+[Co(CO)_4]^- + 2HI$$

$$Co_2(CO)_8 \longrightarrow 2[Co(CO)_4]^-$$

Oxidation

$$Co_2(CO)_8 + H_2 \longrightarrow 2HCo(CO)_4$$

$$Co_2(CO)_8 + H_2O + CO \longrightarrow 2HCo(CO)_4 + CO_2$$

Disproportionation

$$3Co_2(CO)_8 + 4A^+I^- \rightleftharpoons 2CoI_2 + 4A^+[Co(CO)_4]^- + 8CO$$

$$3Co_2(CO)_8 + nMeOH \rightleftharpoons 2\{[Co(MeOH)_n][Co(CO)_4]_2\} + 8CO$$

$[Co(CO)_4]^-$ and $[CoH(CO)_4]$ can be interconverted by the action of acid and base. [8]

The result of all these reaction pathways is a complex mixture of cobalt species in different oxidation states and with different co-ordination spheres, in equilibria with each other:

DIAGRAM 1: Cobalt Species in Solution.

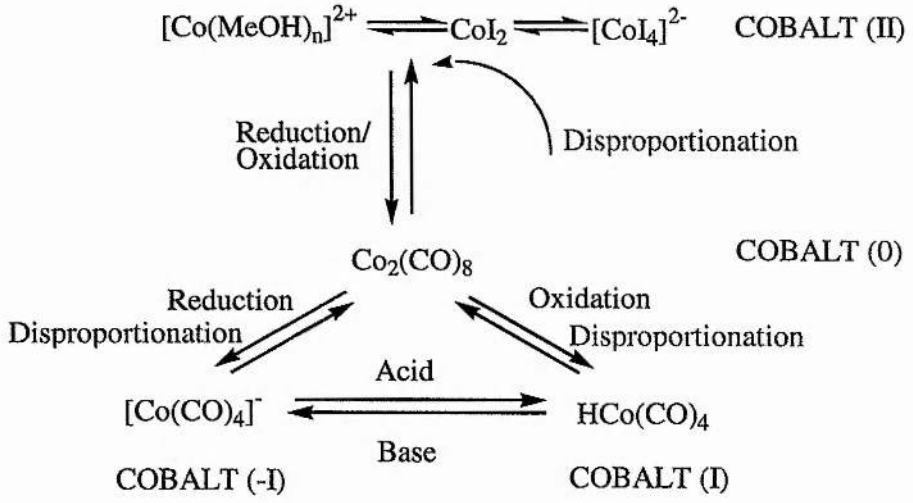

1.2b iv. Cobalt-Carbon Bond Formation.

Mononuclear Co carbonyls can act as nucleophiles and attack electrophilic carbon atoms. [12] Methyl must be activated by attachment to a leaving group, this can occur by protonation of methanol, [13] but it is more likely that the active form of CH_3 is methyl iodide, formed in the organic equilibria listed in section 1.2b ii.

$$ACo(CO)_4 + MeI \longrightarrow MeCo(CO)_4 + AI$$

A = H or counter ion

1.2b v. Migratory Insertion of CO.

Heck and Breslow [12] demonstrated that the action of CO on $[CoR(CO)_4]$ generated $[Co(RCO)(CO)_4]$, it is widely accepted that the mechanism is CO migratory insertion followed by ligand co-ordination. [12,7]

$$[Co(Me)(CO)_4] \rightleftharpoons [Co(COMe)(CO)_3]$$

$$[Co(COMe)(CO)_3] \xrightarrow{L} [Co(COMe)(CO)_3L]$$

L = CO, PR_3, I^-

1.2b vi. Product Formation.

$[Co(RCO)(CO)_n]$ readily decomposes with the loss of the acetyl unit. It is particularly susceptible to attack of nucleophiles at the electron deficient carbon, as demonstrated by Heck and Breslow. [c3]

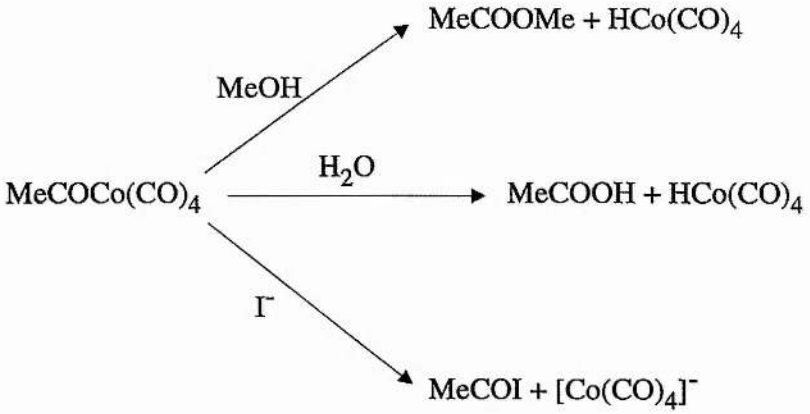

The product of decomposition is one of the simple cobalt carbonyls. During the catalytic cycle RCO could be intercepted by MeOH, H_2O or I^-. Acetic acid and methyl acetate are in equilibrium. Acetyl iodide is readily hydrolysed to acetic acid or alcoholysed to methyl acetate.

1.2b vii. The Catalytic Cycle.

From these simple steps we can construct a first approximation of the catalytic cycle for the cobalt catalysed carbonylation of methanol.

DIAGRAM 2: The Mechanism of the B.A.S.F. Process.

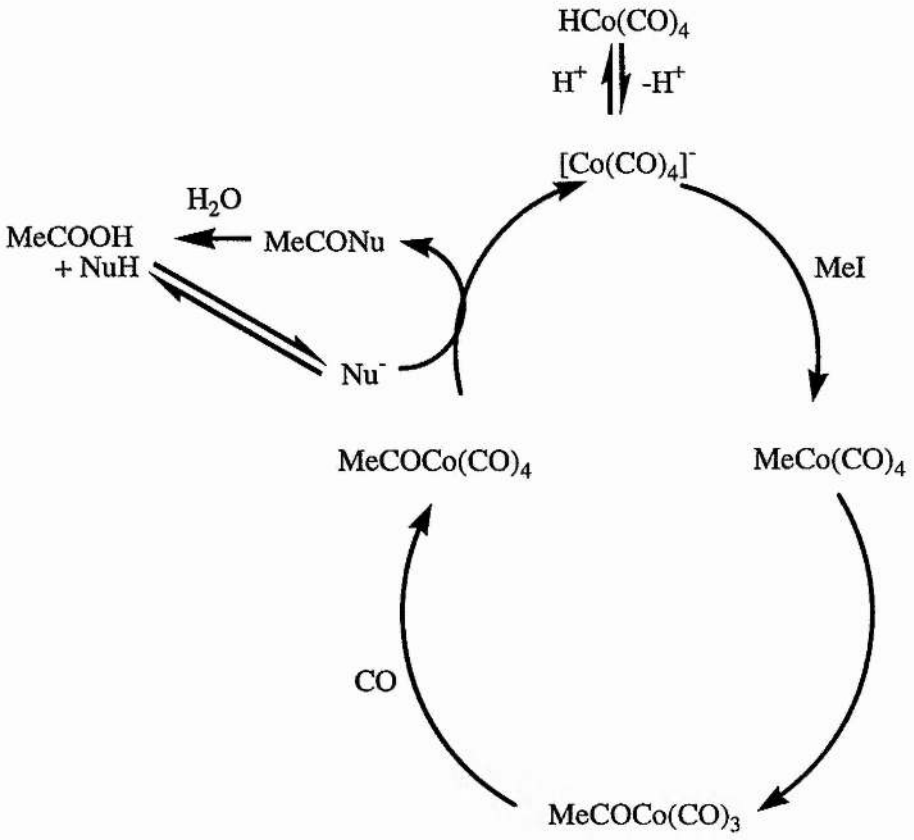

1.2c. Kinetics.

No in-depth kinetic analysis has been published in the literature. The rate of the process varies with most of the species present depending on conditions.

Hohenschutz *et al* reported that the concentration of methanol governed the rate of product formation in the B.A.S.F. process. [6] In order to keep rates high but minimise methyl acetate production water is added. Fast rates are also dependent on high carbon monoxide concentrations. This is thought to be related to the concentration of active carbonyl species. [14]

Mizoroki *et al* measured the conversion of methanol to acetates for different MeI : Co ratios in methanol, acetic acid and water. [15] They found that the conversion increased to a maximum at a MeI : Co ratio of 0.75 and then decreased as the methyl iodide concentration was increased further.

The rate of carbonylation can also be enhanced by adding hydrogen, [14] but this is detrimental to selectivity.

The reaction has been reported to be first order in methanol, carbon monoxide, iodide and

cobalt under process conditions.[C22]

1.2d. Side Products.

1.2d i. Methanol Conversion.

The selectivity with respect to methanol is 90 %. 2 % is lost during processing and 4.5 % is consumed in the production of liquid by-products. [6]

Side products involving methanol consumption can be divided in to two categories. The first category is the side products which are in equilibria with the reactants and products. The major side products generated in this way are dimethyl ether and methyl acetate produced in the organic equilibria on page 4. [6] Dimethyl ether can also be prepared by the action of methyl iodide on methanol.

$$MeI + MeOH \rightleftharpoons MeOMe + HI$$

The concentration of these species increases as the concentration of methanol increases. The addition of water shifts the equilibria away from the side products.

The second category of side products are formed at the catalytic centre. The major side products, acetaldehyde and methane, are formed in this way from activated methyl units. The reaction mixture contains $[Co(Me)(CO)_4]$ and $[Co(MeCO)(CO)_3]$ in equilibrium, these species are thought to be responsible for side product formation.

Methane may be generated from homolytic cleavage of the carbon-cobalt bond in $[Co(Me)(CO)_4]$. [9] Alkyl cobalt carbonyl are known to be in equilibrium with the products of homolytic and heterolytic cleavage. [7]

DIAGRAM 3: The Homolytic Cleavage of the Co-Me Bond.

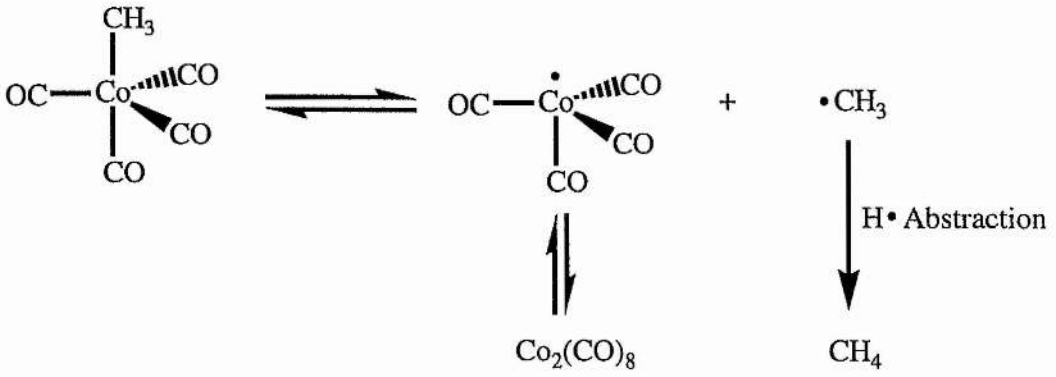

Methane could also be generated via the reaction of $[Co(R)(CO)_4]$ and HI. [7]

$$Co(Me)(CO)_4 + HI \longrightarrow MeH + Co(CO)_4I$$

The production of hydrocarbon side products is increased by increasing the reaction temperature. [14] Methane production would also be expected to increase as the concentration of hydrogen is increased.

The cobalt catalysed production of acetaldehyde is well known and provides the basis for the homologation reaction which converts methanol to ethanol under similar conditions and increased hydrogen partial pressure.[13, 16, 17, 18] The pathway to $[Co(COMe)(CO)_4]$ is thought to be similar. This acyl Co (I) species can now react with a source of hydrogen, either $[Co(H)(CO)_4]$, HI or H_2, to generate acetaldehyde. Under homologation conditions the reaction with hydrogen is thought to be the most significant. One possible mechanism is contained in diagram 4.

DIAGRAM 4: The Production of Acetaldehyde: One Possible Route.

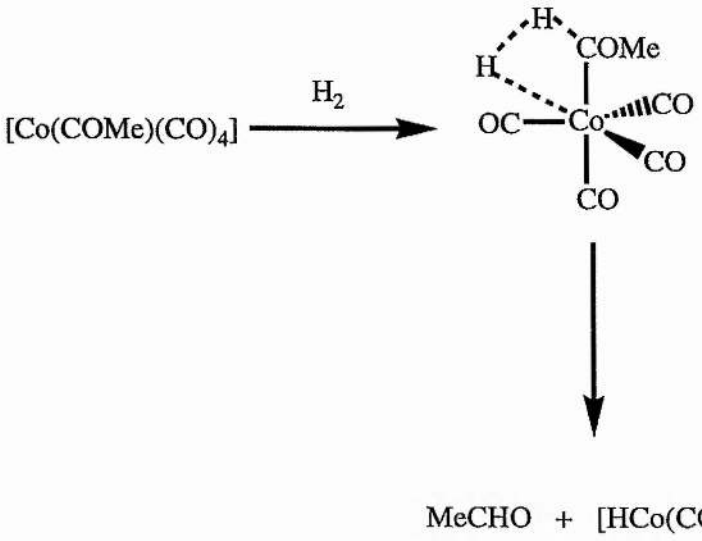

$$MeCHO + [HCo(CO)_4]$$

The production of acetaldehyde and acetates occur under the same conditions.

Acetaldehyde can also be generated from the reaction of $[Co(COMe)(CO)_4]$ and HI: [8]

$$Co(COMe)(CO)_4 + HI \longrightarrow MeCHO + Co(CO)_4I$$

Acetaldehyde is only detected in trace amounts as it reacts rapidly with other compounds present by subsequent hydrogenation, carbonylation, hydrocarbonylation, aldolisation and esterification reactions.

Two subsequent reactions of acetaldehyde dominate:

i. If the concentration of hydrogen is high hydridocobalt carbonyl will act as a hydrogenation catalyst and convert acetaldehyde to ethanol (the homologation reaction).
ii. At high methanol concentration the acetaldehyde reacts with two equivalents of methanol to generate the acetal 1,1-dimethoxyethane. The reaction is acid catalysed:

$$CH_3CHO + 2CH_3OH\ (H^+) \longrightarrow CH_3CH(OCH_3)_2 + H_2O$$

Three equivalents of methanol are consumed in this reaction.

1.2d ii. CO Conversion:

Selectivity is 70 % with respect to CO. [19] The major CO derived side products are CO_2 and formic acid and its esters.

10 % of the carbon monoxide is converted in to carbon dioxide in the water gas shift reaction: [6]

$$CO + H_2O \rightleftharpoons CO_2 + H_2$$

This reaction is metal catalysed. It probably involves Co (II) reduction and Co (0) oxidation half reactions in which H_2 is evolved during the oxidation step and CO_2 during the reduction step, [20] similar reactions occur in the rhodium catalysed system but involve Rh (I) and Rh (III) (see section 1.3e).

Reduction

$$2CoI_2 + 2H_2O + 10CO \longrightarrow Co_2(CO)_8 + 4HI + 2CO_2$$

Oxidation

$$Co_2(CO)_8 + 4HI \longrightarrow 2CoI_2 + 2H_2 + 8CO$$

The production of methyl formate from methanol and CO is thermodynamically possible under the reaction conditions, however derivatives of formic acid are only minor side products. [14]

$$MeOH + CO \longrightarrow HCOOMe$$

1.2e. The Effects of Promoters.

1.2e i. Bifunctional Organics.

Prior to the B.A.S.F. process Reppe *et al* patented a similar process involving cobalt acetate a source of iodine and a polyfunctional organic compound containing at least two hydroxy, carboxy, nitrile, keto or amino groups. [21] This non olefinic additive was believed to co-ordinate to the metal centre and activate it in some way. The catalytic

system produced acetic acid in methanol and water (5 - 30 %) at 200 °C and 200 - 700 Atm. It was reusable under these conditions. The addition of such promoters has been discontinued.

1.2e ii. Hydrogen.

The addition of hydrogen increases the rate of cobalt catalysed carbonylations. [9, 14] Hydrogen increases the concentration of active cobalt by facilitating the formation of $[CoH(CO)_4]$. [9] However selectivity to acetic acid is reduced as more ethanol, the homologation product, is formed.

1.2e iii. Water.

The inclusion of added water reduces the concentration of side products methyl acetate and dimethyl ether according to organic equilibria on page 4.

1.2e iv. Iodide and Acetate.

Acetates and inorganic iodides (e.g. LiI) are promoters for the cobalt catalysed carbonylation of methanol. Mizoroki *et al* carried out preliminary investigations in to the role of sodium iodide and acetate as promotors for methanol carbonylation. [10, 22] They found that iodide and acetate increased the rate of carbonylation, particularly when used together. These additives have also been found to enhance rhodium catalysed carbonylation (see section 1.3f). The group suggested that the added acetate increased the concentration of the active species. Furthermore they noted that HI had an inhibitory effect. This may be due to side reactions involving HI oxidative addition that decrease the concentration of cobalt in the lower oxidation states. The two effects can be brought together by suggesting that acetate reduces the concentration of HI in solution.
Where M is a metal such as Li.

$$AcOM + HI \rightleftharpoons AcOH + MI$$

Added acetate may also remove H^+ from $[CoH(CO)_4]$ increasing the electron density on cobalt. [23]

The promoting affect of a range of iodides has been contrasted by Gauthier-Lafaye *et al.* [17] Employing $[Co_2(CO)_8]$ as a homologation catalyst in pure methanol they established an order of promoter efficiency by measuring the rate of consumption of CO / H_2.

$$MeI >> MePBu_3I > CsI \sim KI > LiI$$

There was no great change in selectivity for the different sources of iodide. Covalent iodide was found to be a much more active promoter that ionic iodide. They observed that the rate could be enhanced much further by using both forms of iodide together revealing a synergic effect.

The main role of molecular iodide is well established. MeI provides an electrophilic methyl unit which is readily attacked by the cobalt nucleophile, this substantially increases the rate of the first step in the cycle. Roper *et al* contrasted the reactivity of this species with that of methanol and showed that $[Co_2(CO)_8]$ reacted preferentially with methyl iodide. [18] Roper *et al* showed that inorganic iodides can serve as precursors to MeI. The additional role of inorganic iodides is not so well understood. The first role of iodide in solution may be to help form the active catalyst. Braterman *et al* found that halide ions catalysed $[Co_2(CO)_8]$ disproportionation to form $[Co(CO)_4]^-$ and solvated Co^{2+}. [11] the reaction could be carried out in the aprotic solvents such as ethers.

Mizoroki *et al* made a number of suggestions to explain the observed effect of NaI on the $Co_2(CO)_8$ + MeI catalytic system involving every step of the catalytic cycle [24] If oxidative addition is rate limiting iodide ions may replace CO ligands in the catalytic species and increase the nucleophilicity of the catalyst and hence enhance its reactivity towards MeI. If migratory insertion is rate limiting iodide may promote insertion reactions according to:

$$RCo(CO)_4 + L \longrightarrow RCOCo(CO)_3L$$

Finally if the rate determining step of carbonylation were the removal of the acyl grouping, a trans iodide ligand would increase the reaction rate by having a labilising effect on the metal to carbon bond. The removal of the acyl grouping may also occur via reductive elimination of acetyl iodide.

A likely role of iodide is as a nucleophile, attacking the acyl carbon atom and therefore facilitating its removal. Zoeller [23] suggested one final role for iodide. Iodides may speed up the conversion of methyl acetate to methyl iodide and inorganic acetate important when MeOAc is used as a co-solvent. In this capacity iodide not only produces methyl iodide, consistent with Roper's work, but generates the promoter MOAc. He summarised his ideas in his proposed mechanism, diagram 5.

$$MeOAc + MI \rightleftharpoons MeI + MOAc$$

M = Metal e.g. Li^+

DIAGRAM 5: Zoeller's Mechanism for the Co Catalysed Carbonylation of Methanol.

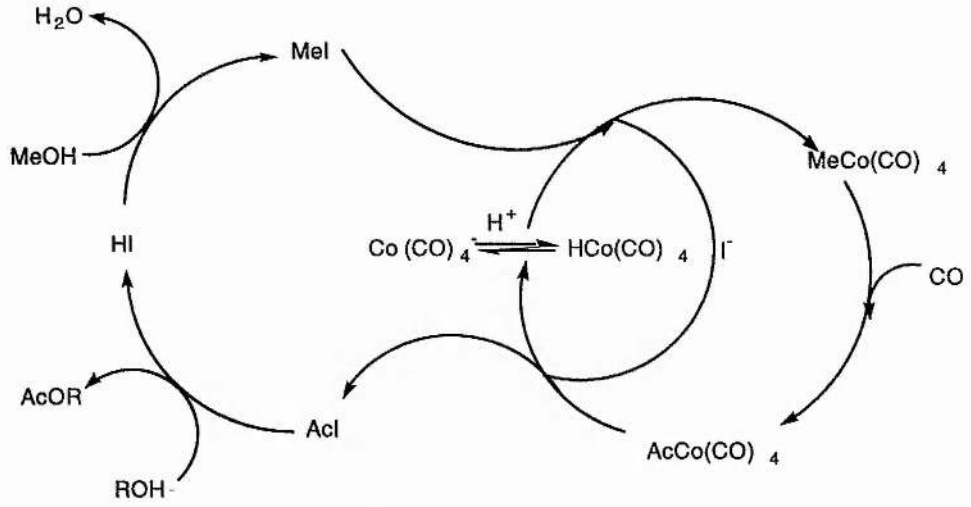

The effects of these promoters are dependent on the reaction conditions. Mizoroki *et al* found that too much acetate led to inhibition.[10] During *in situ* absorption spectroscopy the group discovered the presence of high concentrations of tetrahedral Co (II) mixed iodo acetate complexes $[Co(OAc)_nI_{(4-n)}]^{2-}$. It may be that high concentrations of acetate favour the formation of these inactive species. A similar effect has been noted at high concentrations of iodide. Acetic acid production catalysed by $[Co_2(CO)_8]$ is inhibited by high concentrations of MeI; under the same conditions no inhibition was observed using NaI [15]

Pretzer *et al* followed the homologation reaction by *in situ* infrared spectroscopy and found the major species to be $[Co(CO)_4]^-$. This, they reasoned, was the catalytic species. [8] They investigated the effect of adding different concentrations of iodine. At high concentrations of iodine the CO stretch due to $[Co(CO)_4]^-$ diminished in size. They believed that the iodine was acting as an oxidising agent removing active cobalt, and forming insoluble iodo complexes. Forster *et al* suggested high concentrations of iodide lead to the formation of inactive $[CoI_4]^-$. [9]

SECTION 1.3 THE RHODIUM CATALYSED ACETIC ACID PROCESS: THE MONSANTO PROCESS.

1.3a. Rhodium Catalysed Acetic Acid Synthesis: The Monsanto Process. [25]

In 1966 The Monsanto Company began developing the process that dominated acetic acid production for over two decades: The rhodium catalysed iodide promoted carbonylation

of methanol. The first plant was opened in 1970, the yields of acetic acid based on methanol were over 99 % [26] The catalyst operates effectively under a variety of conditions 30-60 atm pressure, 150 - 200 °C, [27] and in a variety of solvents, the preferred solvent systems are based on acetic acid and methyl acetate. The concentration of rhodium is approximately 0.001mol dm^{-3}. [4, 46]

1.3b. The Mechanism.

The importance of this process is such that academic papers began appearing almost as soon as the process was on line and have continued steadily until the present day.
In the seventies and early eighties Denis Forster published some pioneering work on the mechanism of the process. [4, 28, 29, 30, 31,] In these papers he identified the active catalyst as $[Rh(CO)_2I_2]^-$ [31] and followed the steps of the catalytic cycle by infrared spectroscopy. [30, 31]
He found that the behaviour was similar in a variety of solvents, CH_3OH, $CHCl_3$, CH_3NO_2, $C_6H_5NO_2$, C_6H_5Cl, CH_2Cl_2. [30]
Forster found that, at room temperature and in the presence of excess MeI, $[Rh(CO)_2I_2]^-$ reacts generating $[Rh(COCH_3)(CO)I_3]^-$. When CO is bubbled through the solution $[Rh(COCH_3)(CO)_2I_3]^-$ is formed. This species decomposes slowly to yield the starting material. The infrared stretches that Forster observed are in table 1, he did not observe the methyl species.

TABLE 1.1: Infrared ν_{CO} of Intermediates in the Monsanto Process

Species Present	ν_{CO} / cm^{-1}	Temp. / °C	P^{CO} / Atm.
$[Rh(CO)_2I_2]^-$	2064, 1989	room temp.	0
$[Rh(COMe)(CO)I_3]^-$	2062, 1711	room temp.	0
$[Rh(COMe)(CO)_2I_3]^-$	2141, 2084, 1708	room temp.	1
$[Rh(CO)_2I_2]^-$	2067, 1996	100	6

The catalytic cycle Forster proposed was: [4]

DIAGRAM 6: Mechanism for the Monsanto Process With Forster's Infrared Assignments.

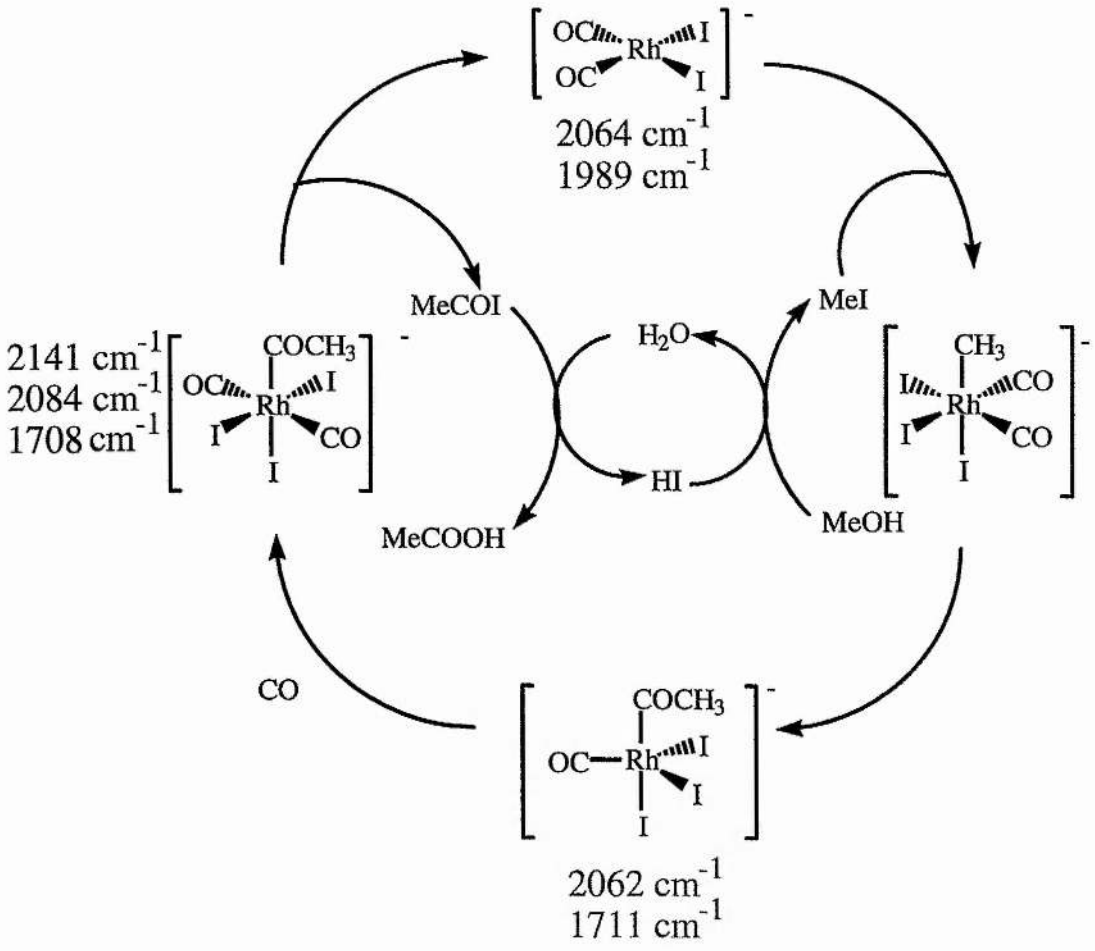

Using the high temperature, high pressure infrared cell [32] developed in the Monsanto laboratories Forster observed the carbonylation of methanol in heptanoic acid at 100 °C. He monitored the changes in the CO stretching region of the infrared spectrum when he exposed $RhCl_3.3H_2O$ to methyl iodide, water and methanol. The bands he saw were due to $[Rh(CO)_2I_2]^-$.

1.3b i. Oxidative Addition and Migratory Insertion [27, 33, 34]

The oxidative addition of methyl iodide to $[Rh(CO)_2I_2]^-$ cannot be considered alone as the first new species encountered in solution is $[Rh(COMe)(CO)I_3]^-$. The low steady state concentration of the oxidative addition product $[Rh(Me)(CO)_2I_3]^-$ has prevented its observation in normal solvent systems. Haynes *et al* [34] reasoned that there were two

possible explanations for this low concentration:

i. A rapid migratory insertion step removing the alkyl species as soon as it is formed. In this case oxidative addition of MeI would be rate limiting.

ii. Facile reductive elimination of MeI from $[Rh(Me)(CO)_2I_3]^-$ leading to an equilibrium lying towards $[Rh(CO)_2I_2]^-$. In this case migratory insertion is rate limiting.

DIAGRAM 7: Oxidative Addition and Reductive Elimination in The Monsanto Process.

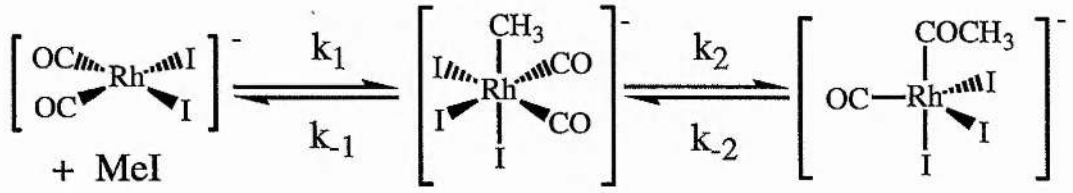

In order to observe the methyl rhodium species the group carried out their investigations in pure methyl iodide. This served to push the first equilibrium towards $[Rh(Me)(CO)_2I_3]^-$ and to slow down migratory insertion as MeI is non polar and alkyl migrations are slower in non polar media.[33,34]

At 25 °C they observed a very weak CO stretch at 2104 cm^{-1}, this was larger at 5 °C and at this temperature they could see the peak decay at the same rate as those assigned to $[Rh(CO)_2I_2]^-$. The rate of formation of the acetyl species increased as the concentration of the 2104 cm^{-1} stretch increased. The stretch was assigned to the symmetric stretch of $[Rh(Me)(CO)_2I_3]^-$. It is thought that the antisymmetric stretch is under the acyl 2061 cm^{-1} peak which is broad and shouldered as it represents a collection of isomers.[34] They concluded that $[Rh(CO)_2I_2]^-$ and $[Rh(Me)(CO)_2I_3]^-$ are in equilibrium in pure MeI and that insertion migration is rapid leading to a low standing concentration of $[Rh(Me)(CO)_2I_3]^-$. Although migratory insertion is very fast Haynes *et al* have shown that it is reversible in the presence of methyl iodide in CH_2Cl_2 at ambient temperatures.[27,34]

The isotopic labelling studies carried out by Bunel *et al* illustrate the reversibility of alkyl migration. They followed the isomerisation of $[AsPh_4][Rh(COMe)(^{13}CO)(CD_3CN)I_3]$, which is formed in CD_3CN from $[AsPh_4]_2[Rh(COMe)(^{13}CO)I_3]_2$ by ^{13}C n.m.r and assigned their spectra as detailed in diagram 8.[35]

DIAGRAM 8: The Isomerisation of $[AsPh_4][Rh(COMe)(^{13}CO)(CD_3CN)I_3]$.

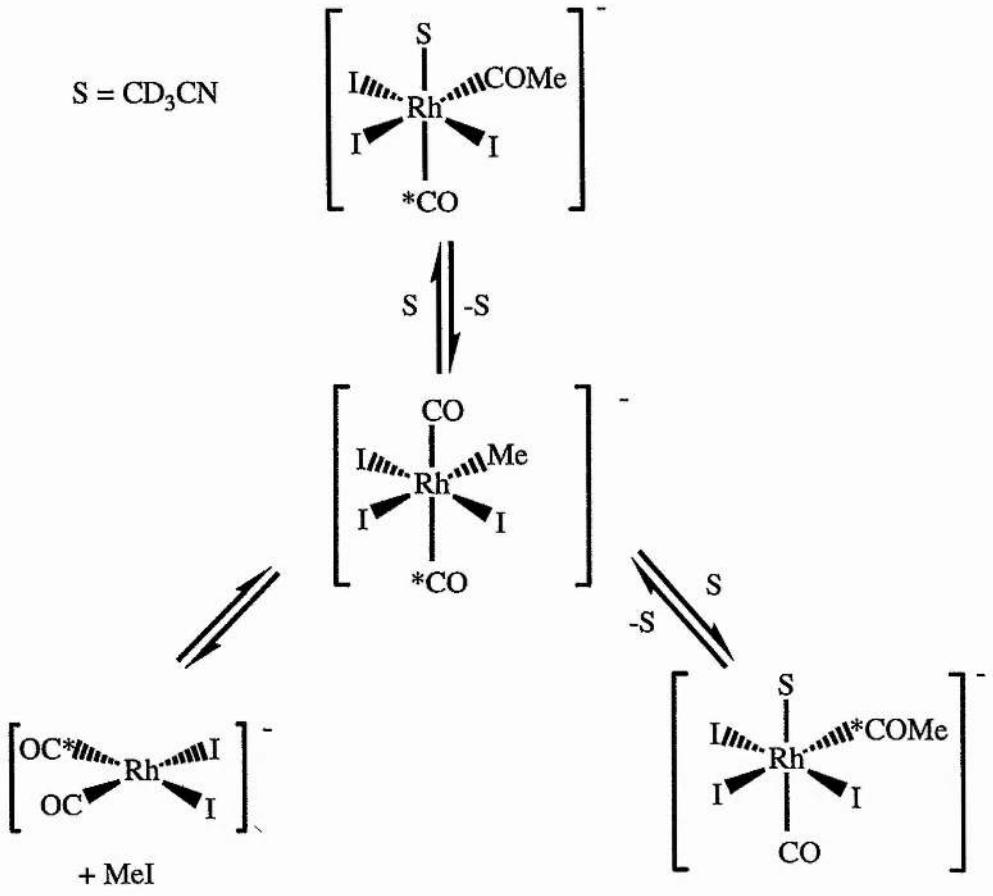

1.3b ii. CO Co-ordination.

Forster and co-workers showed that $[Rh(COMe)(CO)I_3]^-$ exists as a dimer in the solid state bridged through weak iodide bridges. [28] It is likely that this complex is monomeric in donor solvents [35, 36] Kent *et al* followed the uptake of ^{13}CO by $[Rh_2(^{13}COMe)_2(^{13}CO)_2I_6]^{2-}$ in CD_2Cl_2 by ^{13}C n.m.r. (see diagram 9). [37] The product had a trans arrangement of carbonyl ligands. The fac-cis and mer-trans isomers are in equilibrium [30] It is the fac-cis isomer that undergoes reductive elimination to give cis $[Rh(CO)_2I_2]^-$.

DIAGRAM 9: CO Co-ordination Followed by Isomerisation.

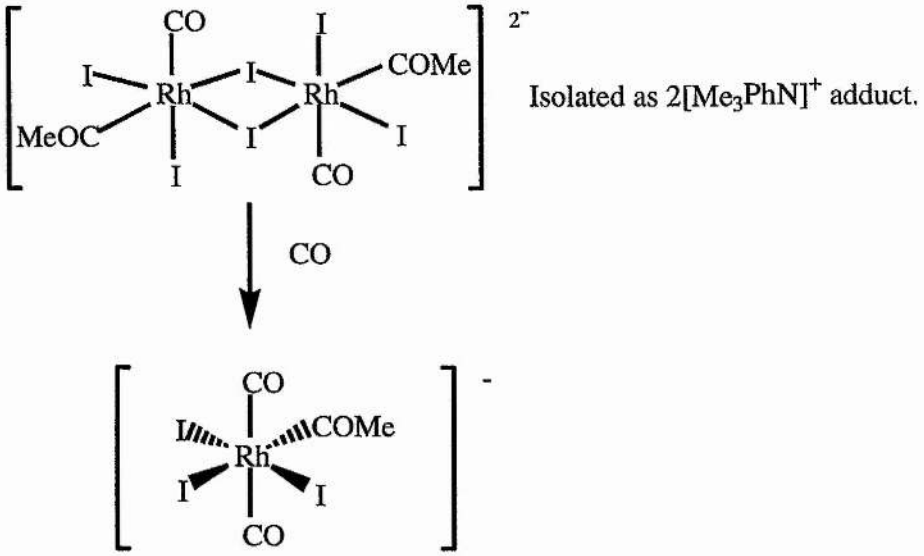

CO co-ordination is reversible, [35, 37] Bunel *et al* generated mer-trans $[Rh(COMe)(CO)_2I_3]^-$ by reacting $[Rh(CO)_2I_2]^-$ with acetyl iodide at room temperature. [35] Making use of isotope enriched n.m.r studies they followed the behaviour of the acetyl species under a variety of conditions. When the reaction between $[Rh(^{13}CO)_2I_2]^-$ and acetyl iodide was carried out in CD_2Cl_2 at 25 °C and in the presence of CO the initial product was fac-cis $[Rh(COMe)(^{13}CO)_2I_3]^-$. This readily underwent cis-trans isomerisation to the mer-trans isomer. The mer-trans isomer could be converted to $[Rh_2(COCH_3)_2(CO)_2I_6]^{2-}$ under vacuum. Dimers of this sort were disrupted by dissolving them in polar solvents yielding solvated monomeric monocarbonyls.

DIAGRAM 10: Monocarbonyl - Dicarbonyl Isomerisation in Donor Solvents.

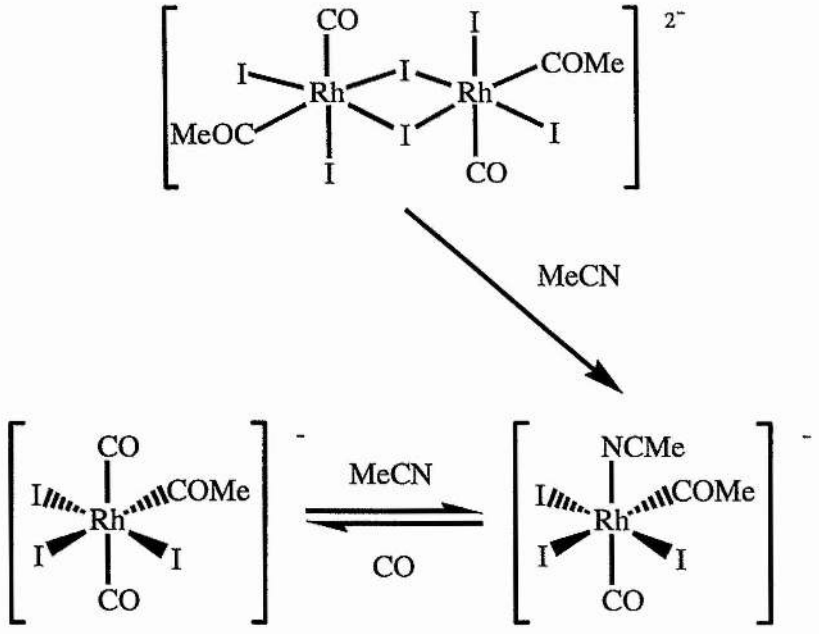

Bunel *et al* followed the behaviour of $[AsPh_4]_2[Rh(MeCO)(CO)I_3]$ in $CDCl_3$ at 50 °C in the presence of ^{13}CO. They observed complete CO scrambling, revealing that CO co-ordination and methyl migration are reversible under these conditions.

1.3b iii. Rh-COMe Bond Cleavage.

$[Rh(MeCO)(CO)_2I_3]^-$ may expel COMe in two ways:

i. Nucleophilic attack as in the proposed B.A.S.F. cycle, (see section 1.2b),

ii. Reductive elimination of acetyl iodide. Acetyl iodide is then hydrolysed by water to generate acetic acid irreversibly driving the process.

The production of acetyl iodide is the generally accepted route based on the observation of acetyl iodide during the carbonylation of methyl iodide,[30] acetyl iodide cannot be observed in solutions containing water (or methanol) as its hydrolysis is too rapid. Nucleophilic attack cannot be ruled out, and is found to compete in some model studies. [27]

1.3c. Kinetics.

The rate of reaction is first order with respect to the concentration of rhodium and methyl iodide and zero order with respect to the concentration of methanol and carbon monoxide. [4,39] This, coupled with the observation of only $[Rh(CO)_2I_2]^-$ ν_{CO} bands in solution under catalytic conditions, [30,31] led to the suggestion that oxidative addition of methyl iodide was

the rate determining step. [4] Employing the strategy of Fulford *et al* [38] let us consider all the processes possible during oxidative addition and migratory insertion, the first two bond forming steps in Forster's mechanism:

DIAGRAM 11: Oxidative Addition and Migratory Insertion in The Monsanto Process.

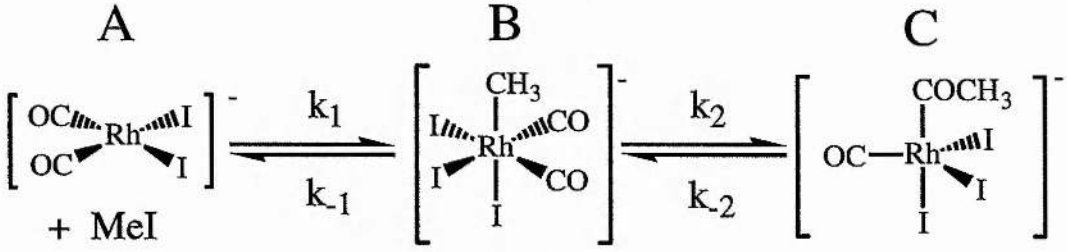

The rate of the overall process worked out by following the rate of consumption of $[Rh(CO)_2I_2]^-$ in the infrared, by invoking the Lambert-Beer law:

Absorbance (Abs) = (concentration)(extinction coefficient)(pathlength).

Fulford *et al* [38] determined pseudo first order rate constants for the overall reaction in an excess of methyl iodide. For a pseudo first order process:

Rate = $k_{obs}[A]$

The rate constant can be obtained from the infrared absorbance. If Abs_0 is the absorbance at time zero and Abs_t is the absorbance at time t:

$Ln (Abs_t/Abs_0) = -k_{obs}t$

That is a graph of $Ln (Abs_t/Abs_0)$ against t has slope $-k_{obs}$ and intercepts the origin.

In order to obtain the value for k_2 we need an equation that related k_2 to the rate constant we can observe k_{obs}. Under conditions of very high MeI concentration the rate will be pseudo first order and they worked out the equation for k_2 as:

$k_2 = k_{obs}Abs_A\varepsilon_B(Abs_B\varepsilon_A)^{-1}$

We can see that the equation involves a measurement of the absorbance of B. Therefore it can only be observed in very high concentrations of MeI and low to ambient temperatures in order to increase the concentration of $[Rh(Me)(CO)_2I_2]^-$ (B). Under these conditions k_2 can be calculated directly from the infrared data. Analyses like these enabled them to obtain the constants for the forward and reverse oxidative addition and migratory insertion steps.

DIAGRAM 12: Oxidative Addition and Reductive Elimination in The Monsanto Process.

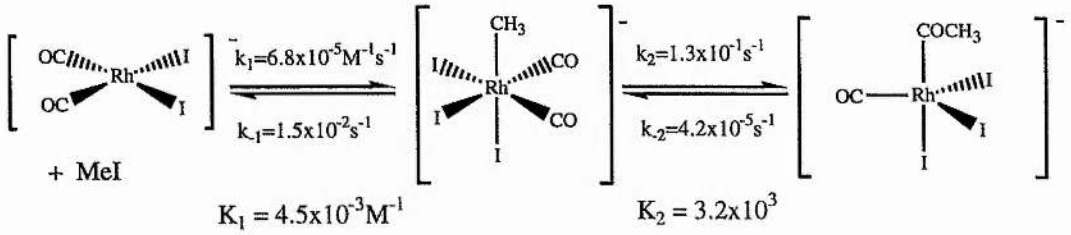

Also quoted are the equilibrium constants calculated from

$\mathbf{K_c = k_1/k_{-1}}$

Under the conditions of these measurements the rate of migratory insertion is an order of magnitude faster than the rate of reductive elimination of MeI. Oxidative addition is comparatively slow. This shows that slow oxidative addition and fast migratory insertion causes the high steady state concentration of $[Rh(CO)_2I_2]^-$.

1.3d. Thermodynamic Parameters.

DIAGRAM 13: A Reaction Profile.

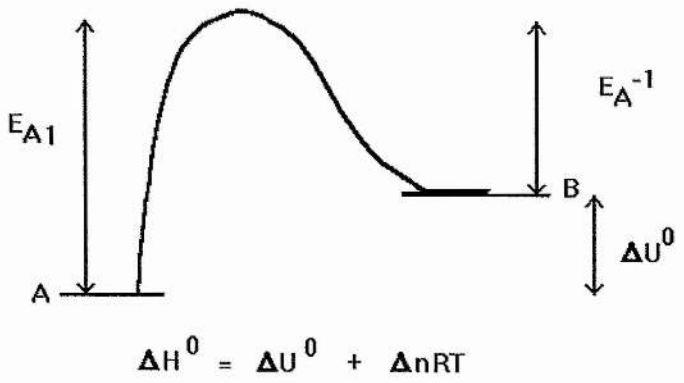

Measuring the rate constants for oxidative addition and migratory insertion at different temperatures and constructing an Arrhenius plot allows calculation of the activation energies E_A and pre-exponentional factors A (plot of lnk versus 1/T gives gradient $-E_a/R$ and intercept lnA) for the reactions.

$\mathbf{\ln k = \ln A - E_A/RT}$

The activation energies of the forward and reverse processes allow calculation of $\Delta U°$ and

$\Delta H°$ according to:

$$\Delta U° = E_{A1} - E_{A-1}$$

$$\Delta H° = \Delta U° + \Delta nRT$$

$\Delta H°$ = standard enthalpy

$\Delta U°$ = change in internal energy

Δn = change in no. moles

R = gas constant, 8.314 J mol^{-1} K^{-1}

The pre-exponential factors of the forward and reverse processes are related to the entropy change for the reaction $\Delta S°$ according to:

$$\ln(A_1/A_{-1}) = \Delta S°/R - (1 + \ln[R'T])$$

R' = 0.0821 atm $mol^{-1}K^{-1}$

The free energy for a process ΔG:

$$G = H - TS$$

$$\Delta G = -RT\ln K_p$$

$$K_p = K_c(R'T)^{\Delta n}$$

The enthalpy of activation can be calculated from transition state theory:

$$\Delta H^{\#} = E_A + (\Delta n^{\#} - 1)RT$$

depicts value refers to activation.

The entropy of activation $\Delta S^{\#}$ can be calculated from transition state theory:

$$A = [k_B/h]Te^{-(\Delta n^{\#} - 1)} e^{\Delta S^{\#}/R}$$

k_B = Boltzmann's constant, 1.381×10^{-23} J K^{-1}

h = Planck constant, 6.626×10^{-34} J s

$\Delta H^{\#}$ and $\Delta S^{\#}$ can be fed in to the equation for ΔG.

$$\Delta G^{\#} = \Delta H^{\#} - T\Delta S^{\#}$$

$-\Delta G^{\#}/RT$ is proportional to lnk.

Haynes *et al* constructed a free energy diagram [27] for the interconversions at 35 °C in CH_2Cl_2 - MeI:

DIAGRAM 14: Reaction Profile of the Monsanto Process.

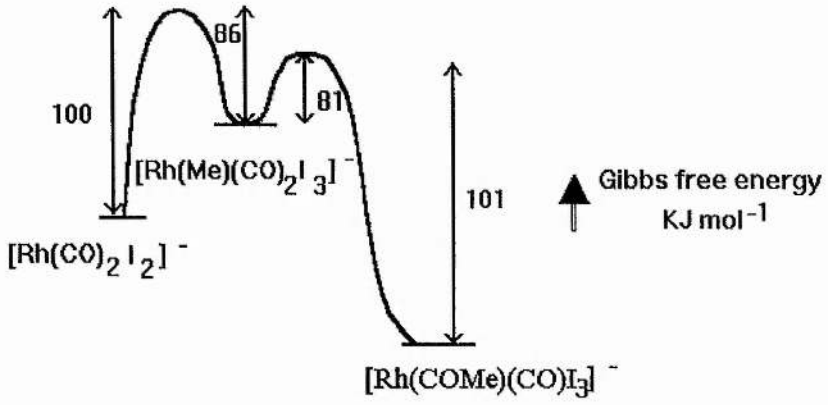

$[Rh(Me)(CO)_2I_3]^-$ is unstable to reductive elimination of MeI and migratory insertion. Migratory insertion is the faster process. Oxidative addition of methyl iodide is confirmed as the rate limiting step.

1.3e. Side Reactions.

As mentioned earlier the rhodium and iodide catalysed carbonylation of methanol is a very selective reaction, however, certain side products are formed.

1.3e i. Loss of Methanol:

Selectivities based on methanol are over 99 %. [4] Propanoic acid is the major side product involving methanol although some methane is produced. [19]

1.3e ii. Loss of CO:

Loss of CO is far more significant. Selectivity based on CO is > 85 %. [46] CO loss is due to the major competing reaction the Water Gas Shift reaction.

The Water-Gas Shift Reaction [19, 40]

$$H_2O + CO \rightleftharpoons H_2 + CO_2$$

The conversion of carbon monoxide and water to hydrogen and carbon dioxide is catalysed by rhodium and iodide promoters. The reaction is facile under mild temperatures and pressures, $\Delta G^\circ_{298} = -4.76$ kcal mol^{-1}. Due to a considerable activation energy barrier rates are only significant at higher temperatures, i.e. the rate is increased by

increasing the temperature.

Baker *et al* [40] studied the kinetics of the process in a water and acetic acid solvent system containing HCl, NaI and $[Rh(CO)_2Cl]_2$. They found that the reaction was first order in [Rh], second order in [I⁻] at low temperature and low [I⁻] but had order -1 in [I⁻] at high temperature and that order with respect to p_{co} was complex and pH dependent. At low pH the rate was almost independent of p_{co} (showing a slight increase), but at high pH increased pH inhibited the reaction.

Infrared spectra of the reaction mixtures revealed the presence of $[Rh(CO)_2I_2]^-$, trans $[Rh(CO)_2I_4]^-$ (ν_{CO} 2092 cm^{-1} in acetic acid, 2084 cm^{-1} in KBr as the $AsPh_4$ salt), $[Rh(CO)I_4]^-$and $[Rh(CO)I_5]^-$(ν_{CO} 2035 cm^{-1} in KBr as the $AsPh_4$ salt)

The ratio of Rh(I) : Rh(III) was found to be very dependent on the reaction conditions. [19, 40] $[Rh(CO)_2I_4]^-$ was the dominant species under low water, high acid, high iodide, low p_{co} or high temperature conditions, whereas $[Rh(CO)_2I_2]^-$ dominated otherwise.

From this wealth of information a cycle has been elucidated. The water-gas shift catalytic cycle can be split in to two domains oxidation and reduction. If Rh(I) builds up oxidation is rate limiting, if Rh(III) builds up reduction is rate limiting. The oxidation process involves HI uptake and CO and H_2 evolution, the reduction process involves CO and H_2O uptake and HI and CO_2 evolution.

DIAGRAM 15: The Monsanto Water Gas Shift Cycle.

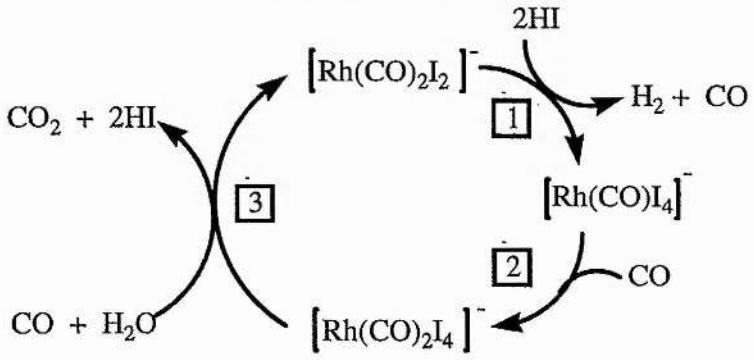

In terms of organics the process is:

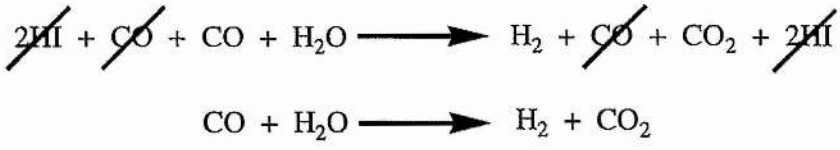

The uptake of water is rate limiting for reduction, the uptake of HI is rate limiting for oxidation. At low temperatures oxidation is rate limiting, at high temperatures reduction is rate limiting. Reduction is also slowed by excessive acidity suggesting a mechanism involving evolution of H^+ in the rate determining step. This may involve nucleophilic attack of water at a carbonyl carbon to produce a hydroxycarbonyl ligand and H^+. [19]

1.3e. iii. The Water Gas-Shift Reaction in the Monsanto Process.

Under methanol carbonylation conditions the water-gas shift reaction is relatively slow. Despite this water-gas shift behaviour still constitutes a major problem. The conditions in the reaction vessel can be equated with the high temperature regime discussed in section 1.3e ii. This coupled with the high standing concentration of Rh means that the water-gas shift oxidation process dominates. The conversion of $[Rh(CO)_2I_2]^-$ to $[Rh(CO)_2I_4]^-$ leads to a reduction in the active concentration of Rh and a reduction in rate of carbonylation. Even more problematic is formation of insoluble Rh(III) iodides in the reaction media. $[Rh(CO)_2I_4]^-$ is susceptible to loss of CO and can be converted in to RhI_3 via $[Rh(CO)I_4]^-$, RhI_3 precipitates from the reaction medium and rhodium is lost. [41]

We can see from the mechanism that a high water concentration and a low HI concentration will lead to a higher concentration of Rh(I) relative to Rh(III), these conditions are necessary in order to prevent rhodium precipitating. Although reducing the concentration of HI retards the water-gas shift reaction and speeds up conversion of inactive Rh(III) to active Rh(I) a standing concentration of HI in solution is necessary to convert methanol and methyl acetate to methyl iodide.

If the CO pressure is too low this will retard the water-gas shift reduction step and lead to a reduction in active rhodium.

1.3f. The Effects of Promoters.

There have been many papers published on the effect of promoters on the rhodium catalysed carbonylation of methanol. [19, 29, 38, 39, 41, 42, 43, 44, 45] In order to consider these effects we must have an understanding of the processes occurring in solution. The basic solvent system is acetic acid, water, methyl iodide and methyl acetate, originally iodide was introduced as HI. As discussed previously the major equilibria within such a feed are:

$$MeCOOH + MeOH \rightleftharpoons MeCOOMe + H_2O \quad (1)$$

$$2MeOH \rightleftharpoons MeOMe + H_2O \quad (2)$$

$$MeOH + HI \rightleftharpoons MeI + H_2O \quad (3)$$

$$MeCOOMe + HI \rightleftharpoons MeI + MeCOOH \quad (4)$$

$$MeOMe + HI \rightleftharpoons MeI + MeOH \quad (5)$$

Equilibria 3,4 and 5 lie towards MeI under process conditions, this leads to high carbonylation and low water-gas shift rates. [19] High methanol concentrations are not employed as these lead to a high equilibrium concentration of MeOMe. [42, 46]

It is likely that the majority of promoters operate in a similar way, changing the equilibrium concentrations of important species within the reaction media. Water, acetate and iodide deserve special treatment as they are particularly effective for promoting rhodium catalysed carbonylation.

1.3f i. Hydrogen.

The presence of hydrogen has no effect on the catalytic system.

1.3f ii. Water. [41, 45]

Water is a very important component of the catalytic system. It has three main roles in solution.

Firstly it acts to trap the acetyl group from acetyl iodide irreversibly producing acetic acid. This process is very rapid and drives the carbonylation process. [4] Secondly the presence of high concentrations of water converts $[Rh(CO)_2I_4]^-$ to $[Rh(CO)_2I_2]^-$, preventing loss of rhodium and increasing the active concentration of the catalyst. Thirdly water increases the rate of oxidative addition. Fulford *et al* found considerable rate enhancements when they added water to $[Rh(CO)_2I_2]^-$ and MeI in methanol and a variety of aprotic solvents. [38] They also found that the rate was faster in protic solvents than aprotic solvents. The group proposed that a hydrogen bonding interaction helps hold the reactants in a well ordered transition state.

If water concentrations are too high methyl iodide becomes insoluble and the rate is retarded. [41, 43]

1.3f iii. Inorganic Iodide and Acetate.

Two comprehensive treatments have been carried out on the effect of such promoters, The Celanese Chemical Company studied their effect on the overall process. [41, 45] More recently Maitlis *et al* investigated the effect of iodide on the oxidative addition of MeI. [38, 47]

The Celanese group wanted to decrease the concentration of water in the reaction solution and therefore reduce the cost of water removal. They added a variety of compounds to the reaction mixture and found the addition of inorganic iodide or inorganic acetate allowed them to maintain catalyst stability at lower water levels. The rate was increased compared with low water runs in the absence of promoters. The selectivity was increased relative to the high water process. Lithium salts were used as these are highly soluble in the reaction media.

The group explained the effects of both salts in terms of the equilibrium:

Where M = metal e.g. Li

$$MI + MeOAc \rightleftharpoons MeI + MOAc$$

They found that the best carbonylation effects were obtained under conditions that favoured LiOAc formation and they concluded that this was a better promoter than LiI. The position of this equilibrium is very dependent on the concentration of water.

The Celanese group believed that promotion was mainly due to two effects.

Firstly the presence of LiOAc leads to a reduction in the equilibrium concentration of HI due to the equilibrium.

$$LiOAc + HI \rightleftharpoons HOAc + LiI$$

This increases the concentration of $[Rh(CO)_2I_2]^-$ relative to Rh(III). By this route high initial methyl acetate concentration therefore favours the production of $[Rh(CO)_2I_2]^-$.

Secondly the presence of I^- was thought to prevent loss of iodide by $[Rh(CO)_2I_4]^-$ preventing its degradation to insoluble RhI_3. [48]

LiOAc may also serve to increase the rate of the oxidative addition step, (see below) and the rate of reductive elimination.

DIAGRAM 16: Proposed Mechanism of Reductive Elimination facilitated by Lithium Acetate. Where A is the counter ion for the complex.

$$[Rh(COMe)(CO)_2I_3]^-A^+ \quad + \quad LiOAc$$

$$\downarrow$$

$$[Rh(CO)_2I_3]^{2-}A^+Li^+ \quad + \quad AcOAc$$

$$\downarrow H_2O$$

$$[Rh(CO)_2I_2]^-A^+ \quad + \quad 2AcOH \quad + \quad I^- \quad + \quad Li^+$$

Operating with high concetrations of inorganic iodide enabled the rhodium catalysed acetic acid process to be run with a reduced water concentration. [48] Hoechst Celanese operate the rhodium catalysed acetic acid process in this way. Iodide is added as LiI and the methyl acetate concentration is kept high. The iodide assumes the same role as water, that is it increases the reaction rate and helps prevent rhodium precipitating as RhI_3. In addition to these benefits the selectivity is improved, in particular there is a reduction of water-gas shift reaction products giving more efficient use of CO. The increased selectivity can be explained because under low water, high iodide and high methyl acetate conditions, the concentration of HI is very low.

Maitlis *et al* looked at the effect of iodide on the oxidative addition step of the cycle. Iodide was found to promote the oxidative addition of MeI to $[Rh(CO)_2I_2]^-$. [38, 47] They found very little dependence on the cation in most cases. One possible mechanism for the promotive effect is the formation of very nucleophilic di-anionic five co-ordinate $[Rh(CO)_2I_3]^{2-}$ which would be expected to act as a better nucleophile towards MeI and react faster than $[Rh(CO)_2I_2]^-$. [41, 45] Maitlis *et al* searched for spectroscopic evidence for this dianion but no conclusive evidence for its existence has been found. Alternatively iodide may stabilise the transition state of the oxidative addition process. [38]

SECTION 1.4: THE IRIDIUM CATALYSED ACETIC ACID PROCESS: THE CATIVA PROCESS

1.4a. Introduction: The Cativa Process. [49]

The Cativa process is operated under mild conditions of temperature and pressure similar to those of the Monsanto Process. The catalyst consists of a soluble iridium precursor, MeI and an additional promoter, usually a soluble ruthenium complex.

The solvent system is essentially the same as that employed in the Monsanto process. The intermediates in the cycle are more stable than their rhodium equivalents, this affords the process greater flexibility and the relative concentrations of the different solvent constituents can be altered more freely. The plant is operated under lower water concentrations than the Monsanto process. This reduces the cost of running the process as water is expensive to remove from the product mixture. [50]

The Cativa process shows even greater selectivity than the Monsanto process.

1.4b. Kinetics and Mechanism: The Iridium Catalysed Carbonylation of Methanol.

In the absence of promoters iridium and rhodium catalyse methanol carbonylation to a similar extent.

The composition of the iridium solution is very dependent on the exact conditions. Forster *et al* looked at the effect of changing the reactant concentrations and found that the effects were complex, he used infrared spectroscopy to probe the species in solution. Forster assumed the same unit processes as the Monsanto process and separated the behaviour into three extremes. [4, 9, 20, 51]

1.4b i. Low Iodide and Water Concentration.

The concentration of methyl iodide is rate limiting. Increasing the CO pressure inhibits the reaction.

The major iridium species was identified as $[Ir(CO)_3I]$. In this complex the iridium centre is relatively electron poor due to back donation in to the antibonding orbitals of three carbonyl ligands. Forster demonstrated that this species is a poor nucleophile and reasoned that it would require loss of a carbonyl ligand to render it nucleophilic enough to interact with MeI at a significant rate. The suggested rate determinig step is oxidative addition of MeI involving prior CO dissociation.

$$[Ir(CO)_3I] \xrightarrow[-CO]{S} [Ir(CO)_2(S)I] \xrightarrow[-S]{MeI} [Ir(Me)(CO)_2I_2]$$

S = donor solvent

1.4b ii. Higher Iodide Concentration.

Increasing the iodide concentration decreases the rate of carbonylation. Increasing carbon monoxide pressure promotes the reaction.

The major species in solution is $[Ir(Me)(CO)_2I_3]^-$ this suggests an ionic pathway initiated by the replacement of CO by I^- in $[Ir(CO)_3I]$ to generate a nucleophile analogous to the Monsanto catalyst $[Ir(CO)_2I_2]^-$, this is a function of the raised iodide level. Oxidative addition of MeI to this nucleophile is very rapid (quicker than for the Monsanto catalyst) and $[Ir(Me)(CO)_2I_3]^-$ is generated. Methyl migration in this complex is slower than in the rhodium analogue, this is thought to be because the iridium to methyl carbon bond is stronger. In order to form the acyl iridium intermediate iodide must be replaced by CO this weakens the iridium to carbon bond. This less electron rich neutral species $[Ir(Me)(CO)_3I_2]$ undergoes methyl migration readily in a CO atmosphere. Iodide substitution occurs via a dissociative pathway and is facilitated by the trans labilising effect of the methyl unit. [27]

The rate determining step is the replacement of iodide by CO, this is promoted by CO and inhibited by I^-.

$$[Ir(Me)(CO)_2I_3]^- \xrightarrow{-I^-} [Ir(Me)(CO)_2I_2] \xrightarrow{CO} [Ir(Me)(CO)_3I_2] \downarrow [Ir(COMe)(CO)_2I_2]$$

The intermediate $[Ir(Me)(CO)_2I_2]$ is common to both the neutral and anionic pathways.

1.4b iii. High Methanol or Water Concentrations.

The reaction rate depends on the concentration of methanol but the rate is zero order in CO pressure at high concentration of water or methanol. The mechanism under these conditions is believed to be a variation of the anionic pathway. The major form of iridium is $[IrH(CO)_2I_3]^-$. The water-gas shift and carbonylation processes are now in direct

competition. $[Ir(CO)_2I_2]^-$ generated can react with HI or MeI. HI oxidative addition is more rapid and this is why there is a large standing concentration of $[IrH(CO)_2I_3]^-$. The reaction with HI is reversible and a rapid equilibrium is established between $[IrH(CO)_2I_3]^-$ and $[Ir(CO)_2I_2]^-$. The irreversibility of MeI oxidative addition, presumably due to the high Ir-C bond strength, enables carbonylation to be the dominant process.

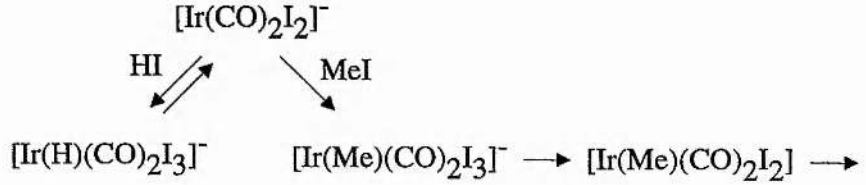

Methanol is known to facilitate removal of iodide from iridium complexes [52] and may promote the reaction by ensuring the standing concentration of $[Ir(Me)(CO)_2I_3]^-$ is low and the reaction is pulled towards the carbonylation pathway.

Forster's Infrared assingments are detailed in table 2.

TABLE 1.2: Infrared assignments: [51] in methyl acetate or nonanoic acid solvents.

Complex	ν_{CO} / cm^{-1}
$[Ir(CO)_3I]$	2073, 2046
$[Ir(Me)(CO)_2I_2]$	2118, 2077
$[Ir(Me)(CO)_2I_3]^-$	2096, 2046

1.4b iv. The Catalytic Cycle:

Dekleva and Forster [9] proposed two cycles with some common intermediates for the unpromoted catalytic carbonylation of methanol.

DIAGRAM 17: Catalytic Cycle for the Iridium Catalysed Carbonylation of Methanol.

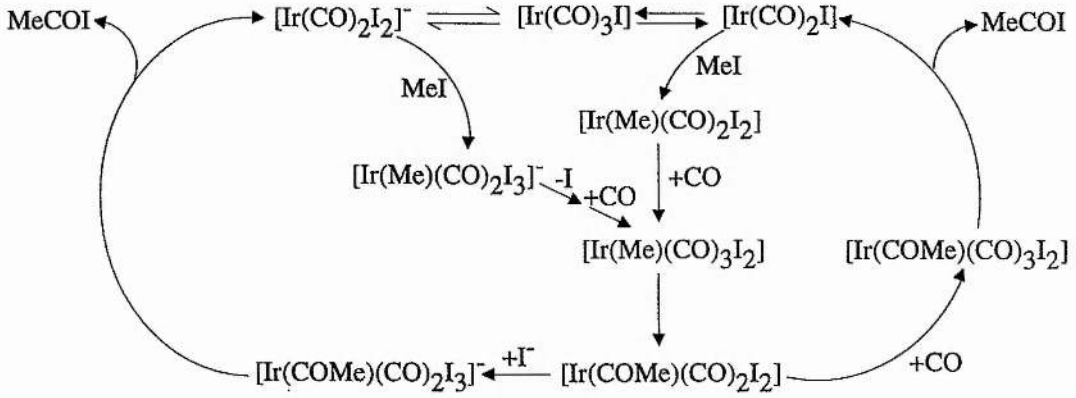

1.4c. Side Reactions.

As with rhodium catalysts the selectivity is very high under most conditions. There are two major side reactions, methane production and the water gas shift reaction.

1.4c i. Methane Production.

When there is a high standing concentration of methyl iridium species in solution the production of methane can become significant. [20, 51] The problem is greatest when $[Ir(Me)(CO)_2I_3]^-$ is the major species and the carbonylation pathway is inhibited by excess iodide or too little CO or MeI.

Haynes *et al* have studied the production of methane from $[Ir(Me)(CO)_2I_3]^-$. [52] It is likely that methane production is the result of Ir-Me bond cleavage by hydrogen from H_2 gas or RCOOH. The reaction with HI was ruled out as a pathway to MeH. In propanoic acid and the absence of H_2 the process is inhibited by I^- and CO suggesting a mechanism involving ligand dissociation.

As expected from these studies adding hydrogen to the catalytic system increases methanol hydrogenolysis to methane.

1.4c ii. The Water-Gas Shift Reaction.

$$H_2O + CO \rightleftharpoons H_2 + CO_2$$

As mentioned in section 1.4b this reaction becomes significant when the water or methanol concentration is high and $[IrH(CO)_2I_3]^-$ is the major species in solution. The mechanism under these conditions is similar to that of rhodium catalysed water-gas shift. [51]

DIAGRAM 18: The Water-Gas Shift Reaction Catalysed by $[Ir(CO)_2I_2]^-$

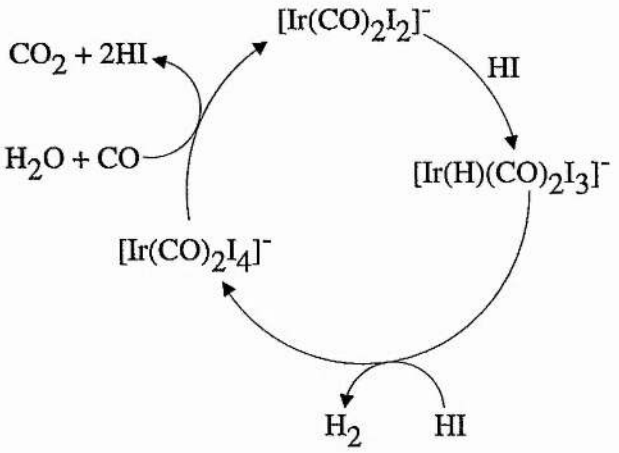

The iridium catalysed water gas shift reaction is more robust than the rhodium catalysed process and operates under a wider range of conditions

The neutral iridium catalyst $[Ir(CO)_3I]$ is also believed to catalyse the the water-gas shift reaction: [9]

DIAGRAM 19: The Water-Gas Shift Reaction Catalysed by $[Ir(CO)_3I]$

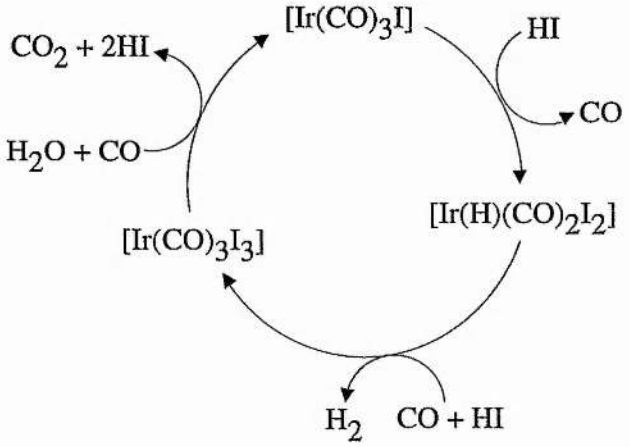

1.4d. The Effects of Additives.

The effects of additives are dependent on the precise conditions and cannot be generalised. In order to consider the effect of the Cativa promoter we must consider the mechanistics of the process under process conditions.

1.4d i. Under Process Conditions.

Under the process conditions two forms of iridium are present $[Ir(Me)(CO)_2I_3]^-$ and $[Ir(CO)_2I_4]^-$. [50] Both are present in Forster's anionic pathway, (see section 1.4b) in which some of the iridium is tied up in the water-gas shift process as Ir (III). $[Ir(Me)(CO)_2I_3]^-$ builds up because loss of iodide and co-ordination of CO is required in order to form an iridium species capable of sufficient rates of methyl migration and this is rate limiting. $[Ir(CO)_2I_2]^-$ reacts with two equivalents of HI as part of the water-gas shift cycle, this leads to a build up of $[Ir(CO)_2I_4]^-$ as the slowest step in the cycle is reduction.

1.4d ii. The Promoter.

The Cativa process differs from the B.A.S.F. and Monsanto processes as it involves a promoter besides MeI. The promoter increases the activity, selectivity and stability of the process and reduces the volatility of the iridium mixture. [49, 50]

The promoter employed is usually a soluble ruthenium species, [49] although a range of molecular metal iodides and transition metal carbonyl iodides can be employed. [50]

To have such a beneficial effect on iridium catalysed carbonylation of methanol under the process conditions the promoter must be carrying out one or a combination of the following tasks:

a. Facilitating methyl migration by accepting iodide from $[Ir(Me)(CO)_2I_3]^-$. This would be analogous to promotive effects that have been attributed to methanol and SnI_2. [52]

b. Facilitating methyl migration by donating CO to $[Ir(Me)(CO)_2I_2]$ to form $[Ir(Me)(CO)_3I_2]$.

c. Preventing the water-gas shift reaction by removing active HI from solution.

The observation that all the promoters can form Lewis acids suggests that the removal of iodide is important to their functioning. Ghaffar *et al* have performed the stoichiometric reaction:

$$2[Ir(Me)(CO)_2I_3]^- \xrightarrow{-I^-} [Ir(Me)(CO)_2I_2]_2$$

Using InI_3 to abstract iodide and have measured the relative rates of migration for the two pathways. $[IrMe(CO)_3(I)_2]$ undergoes migratory insertion approximately 800 times faster than $[Ir(Me)(CO)_2(I)_3]^{1-}$. They have suggested a promotion pathway involving iodide abstraction. [53]

DIAGRAM 19: Mechanism for the Promotion of th Cativa Process:

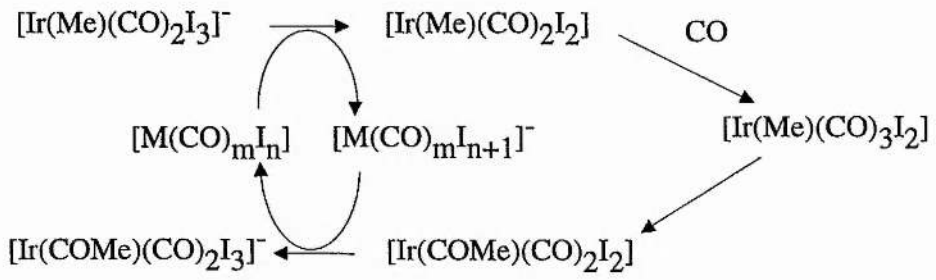

SECTION 1.5: COMPARING COBALT, RHODIUM AND IRIDIUM CATALYSTS.

1.5a Comparing Co, Rh and Ir Methanol Carbonylation Catalysts.

1.5a i Iodide Promoted Group 9 Catalysts for the Carbonylation of Methanol.

In general the transition metal centre is required to carry out five consecutive tasks, where M = Co, Rh or Ir:

1. Form a carbonyl complex with a nucleophilic metal centre:

$$M + CO \longrightarrow M(CO)$$

2. React with an electrophilic methyl carbon to form an alkyl metal carbonyl:

$$M(CO) + MeI \longrightarrow [MeM(CO)]^+ + I^-$$

$$\text{or } M(CO) + MeI \longrightarrow MeM(CO)I$$

3. Carry out migratory insertion to bind Me and CO together and form an acyl metal carbonyl:

MeCOM

4. Take up another CO ligand.

$$MeCOM + CO \longrightarrow MeCOM(CO)$$

5. Evolve the acyl unit to regenerate the nucleophilic metal carbonyl:

$$MeCOM(CO) + H_2O \longrightarrow M(CO) + MeCOOH + H^+$$

Although the finer points of the Co, Rh and Ir methanol carbonylation mechanisms are very different all three share considerable common ground.

- There is good evidence that the nucleophilic metal carbonyl is anionic,
- The preferred form of the methyl unit is methyl iodide,
- The acyl grouping is formed by an alkyl migration reaction.

The three processes differ considerably in the nature of the specific intermediates, and in particular the number of iodide ligands attached to the metal centre. This reflects the change in chemistry as you descend group 9, not surprisingly the behaviour of the rhodium and iridium systems are similar but quite different from that of cobalt.

Prior to the discovery of the Cativa technology many catalytic chemists believed that rhodium was the perfect metal for carbonylation catalysts, we shall compare the three metals of group 9 in order to discover why.

1.5b. The Catalyst: Desirable Properties.

As mentioned earlier the simplest possible carbonylation catalyst must perform:

a. Attachment to Me and CO.

b. Creation of the Me-CO bond.

c. Removal of the acyl unit and incorporation into CH_3COOH.

The properties required from the metal centre are:

a. High nucleophilicity to attack Me,

b. Availability of oxidation states two units apart,

c. An alkyl species which is unstable towards migratory insertion of CO,

d. A sufficiently labile acyl-metal bond.

Each of these processes will now be considered in turn with reference to the three metals in the group and the B.A.S.F., Monsanto and Cativa processes.

1.5b ii Forming the M-CH_3 Bond.[57]

In order to discuss the metal's behaviour we must divide the group in two:

The active cobalt catalyst is formally Co (-I) d^{10}, whilst rhodium and iridium catalysts

have M (I) d^8 metal centres. All the catalysts are four co-ordinate.

The creation of the M-CH_3 can generate a five or a six coordinate product. Direct nucleophilic attack on the methyl unit generates a five co-ordinate methyl complex, this may go on to undergo CO insertion immediately or it may add iodide to form a six co-ordinate complex. In both cases the formal oxidation state of the metal is increased by two.

Cobalt favours a five co-ordinate intermediate, $[Co(CO)_4]^-$ is an 18 electron complex and the product will be Co (I) with a relatively small metal centre. An oxidative addition would lead to a 20 electron Co (I) species, this is not favourable. In addition a six coordinate Co (I) would be sterically crowded. For rhodium and iridium there is a drive towards a six co-ordinate metal (III) complex, as the metal (I) complex is a 16 electron species this metal (III) complex will be 18 electron. Rh (III) and Ir (III) are frequently six co-ordinate and this is a relatively stable arrangement.

The reaction of $[Co(CO)_4]^-$ with MeI generates a cobalt (I) complex, methyl and acyl cobalt (I) carbonyls are susceptible to a wide range of side reactions. It is probable that $[Co(CO)_4]^-$ is generated instead of $[Co(CO)_2I_2]^-$ due to poor Co-I orbital overlap. The cobalt centre is smaller and has a lower affinity to the iodide ligand than Rh and Ir, in many cases iodide ligands can be substituted for carbonyls in a CO atmosphere.

In the rhodium catalysed process the oxidative addition of methyl iodide is rate limiting and this leaves the resting state $[Rh(CO)_2I_2]^-$ susceptible to competing oxidative addition of HI, because of this a high concentration of water is required to maintain a high concentration of the active catalytic species, (section 1.2d). When the electron density on the metal is further increased by descending group 9 to iridium the rate of oxidative addition is enhanced. Unfortunately this is the case for HI as well as for MeI.

1.5b iii The Migratory Insertion Step.

$[CoMe(CO)_4]$ and $[RhMe(CO)_2I_3]^-$ are both unstable towards migratory insertion. The conversion is complete as the five co-ordinate acyl complex is thermodynamically stable relative to the methyl complex and the square planar starting complex.[54] It has been suggested that the presence of iodide increases the rate of migratory insertion on to rhodium.[55] $[CoMe(CO)_4]$ and $[Co(MeCO)(CO)_3]$ are in equilibrium as the reverse reaction has a similar rate. The methyl iridium complex $[IrMe(CO)_2I_3]^-$ is fairly stable towards CO insertion. Ir (III) is an inherently stable oxidation state which forms isolable alkyl

complexes. The reluctance of $[IrMe(CO)_2I_3]^-$ to form an acyl species may be attributed in part to the strength of the carbon-iridium (III) bond.[56] This is backed up by the comparitive ease of migration of $[IrMe(CO)_3I_2]$, the replacement of an iodide ligand for a carbonyl will serve to draw electron density from the Ir-Me linkage.

1.5b iv Forming Acetate.

There are two major mechanisms by which the removal of the acyl group is facilitated:

a. For anionic M (III) complexes with three iodides reductive elimination of acetyl iodide is possible to regenerate an anionic M (I) complex. This process is very fast for the acyl rhodium (III) species in the presence of a trap for acetyl iodide such as water.

b. Alternatively the electron deficient carbonyl ligand of the acyl grouping may be attacked by a nucleophile, i.e. MeOH, H_2O or I^- to generate MeCOOMe, MeCOOH or MeCOI respectively.

The latter route is the most likely for the B.A.S.F. process. The need for nucleophilic attack in the B.A.S.F. process is obvious as iodide is not coordinated to the metal centre. It is generally accepted that the major process is reductive elimination in the Monsanto process. In the Cativa process anionic and neutral processes can operate and it is likely that both mechanisms of acetyl iodide formation will operate.

1.5c Conclusions From the Comparison.

In conclusion the carbonylation of methanol is simply and easily effected by a rhodium catalyst. For simple rhodium precursors such as RhI_3 the electronic properties of the species formed in solution are perfect for the oxidative addition and reductive elimination steps. The Rh (I) and Rh (III) states are both accessible and furthermore the methyl rhodium (III) complex is unstable and readily undergoes alkyl migration. Subsequent reductive elimination regenerates the catalyst. Furthermore the rate of water-gas shift is very low under the process conditions. In the B.A.S.F. process the cobalt centre is Co (-I), on exposure to carbonylation conditions there is no highly nucleophilic iodo Co (I) complex formed and $[Co(CO)_4]^-$ is formed instead, this leads to many side reactions which reduce the efficiency of the process. The Iridium centre $[Ir(CO)_2I_2]^-$ is more electron rich than rhodium, this speeds up the oxidative addition of MeI but water-gas shift behaviour is also promoted, the resulting methyl species $[Ir(Me)(CO)_2I_3]^-$ is too stable and does not readily undergo CO insertion followed by reductive elimination. The problem is

overcome by reducing the electron density, replacing an anionic electron donating iodide ligand with a neutral carbonyl ligand capable of accepting electron density from the metal centre. The result is a complex that readily undergoes CO insertion and expulsion of the acyl unit.

1.5d Why Iridium?

Considering the chemistry of the three processes it seems strange that the Cativa process was developed until we consider the process as a whole, that is incorporating the process engineering and economic forces at work. The stability and durability of the iridium species has allowed an increase in catalyst concentration, this has increased the rate of acetic acid production. It has also given the engineers greater flexibility, facilitating a reduction in water concentration and a decrease in the number of costly purification steps.

1.5e A Future for Cobalt?

Most of the problems of the iridium catalysed carbonylation of methanol were solved by the addition of a promoter. The cobalt process presents a greater challenge as the chemistry and conditions of the B.A.S.F. process must be completely changed in order to make the process commercially viable.

In this project we suggest that the problems associated with cobalt carbonylation can be solved by providing ligands which stabilise an electron rich Co (I) catalyst.

The development of an active catalyst based on a cheap metal which could operate under mild conditions, would be of great benefit. As cobalt is cheap and of comparatively low molecular weight the concentration of the catalyst in solution could be quite high, this opens the opportunity to access the kind of rates enjoyed by the Monsanto and Cativa processes.

CHAPTER 2: CATALYST SOLUTIONS CONTAINING ONLY CO, PHOSPHINE AND IODIDE LIGANDS.

SECTION 2.1: INTRODUCTION.

2.1a Dicobalt Octacarbonyl.[1,2]

The simplest cobalt carbonyl used as a catalyst precursor is dicobalt octacarbonyl. Dicobalt octacarbonyl is a thermally and air sensitive volatile crystalline solid. In low polarity solvents it exists in bridged and non-bridged forms (diagram 20). At room temperature carbonyl site exchange occurs very rapidly.

DIAGRAM 20: The three forms of dicobalt octacarbonyl:

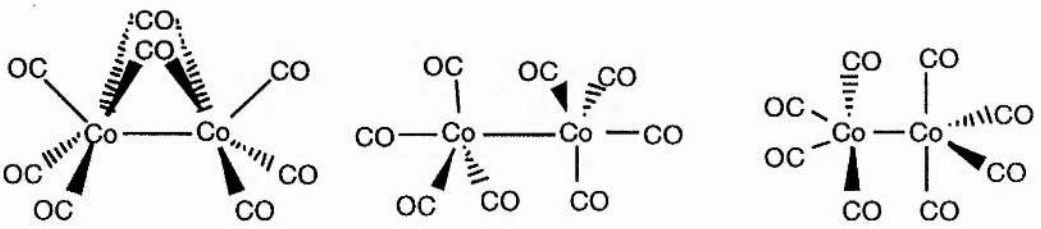

As the temperature is raised the proportion of the unbridged isomers increases.

In polar solvents dicobalt octacarbonyl can disproportionate. [3] Where L= solvent,

$$3Co_2(CO)_8 + 2nL \longrightarrow 2\{[CoLn]\,[Co(CO)_4]_2\}$$

6xCo(0) 2xCo(II) 4xCo(-1)

The carbonylate anion is a nucleophile and attacks methyl iodide to yield alkyl cobalt (I) tetracarbonyl. Subsequent CO insertion and reaction with ROH should produce acetic acid esters. It is sensible therefore to postulate the carbonylate anion as a possible catalytic species for methanol carbonylation. If the proposed B.A.S.F. mechanism is obeyed dicobalt octacarbonyl should catalyse the production of methyl acetate from methanol, methyl iodide and carbon monoxide.

2.1b The Catalytic Activity of Dicobalt Octacarbonyl.

Dicobalt octacarbonyl has been employed as a carbonylation catalyst in a wide variety of

reactions. The products obtained are very dependent on the concentration of hydrogen in the system.

2.1b i. Carbonylation Reactions That Do Not Required Hydrogen.

Examples of the application of dicobalt octacarbonyl to catalytic processes involving carbon monoxide and no added hydrogen include acetic acid synthesis, (see section 1.2), and ester formation. [1]

Ester Formation:

a. In systems similar to the B.A.S.F. process acetic acid esters are formed when alcohols attack the acyl cobalt (I) intermediate:

$$2CH_3OH + CO \longrightarrow CH_3COOCH_3 + H_2O$$

b Alkyl halides can also be converted into esters. Catalysis is performed by the tetracarbonyl cobaltate (-1) ion. [1]

$$RX + R'OH + CO \longrightarrow RCOOR' + HX$$

The addition of a tertiary amine regenerates the anion. Once more catalysis proceeds via an acyl intermediate susceptible to attack by ROH and other nucleophiles. This is evidence for the proposed pathway to alcohol carbonylation.

2.1b ii. Carbonylation Reactions Requiring Hydrogen.

Dicobalt octacarbonyl also catalyses some noteworthy reactions involving both CO and H_2 i.e. synthesis gas:

a. Hydroformylation of unsaturated compounds. [2] (Diagram 21). Dicobalt octacarbonyl is a source of hydridocobalt tricarbonyl for catalysing the conversion of alkenes to aldehydes at high temperatures (150°C-180°C) and pressures (>200 atm).

DIAGRAM 21: Hydroformylation of alkenes:

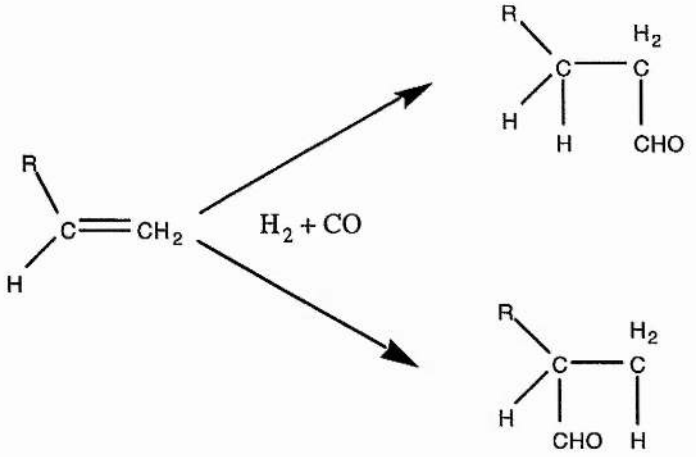

The product mixture is about 3:1 linear to branched aldehydes or alcohols.

One possible mechanism for the production of the linear aldehyde is as follows:

DIAGRAM 22: The Mechanism of alkene hydroformylation by $Co_2(CO)_8$:

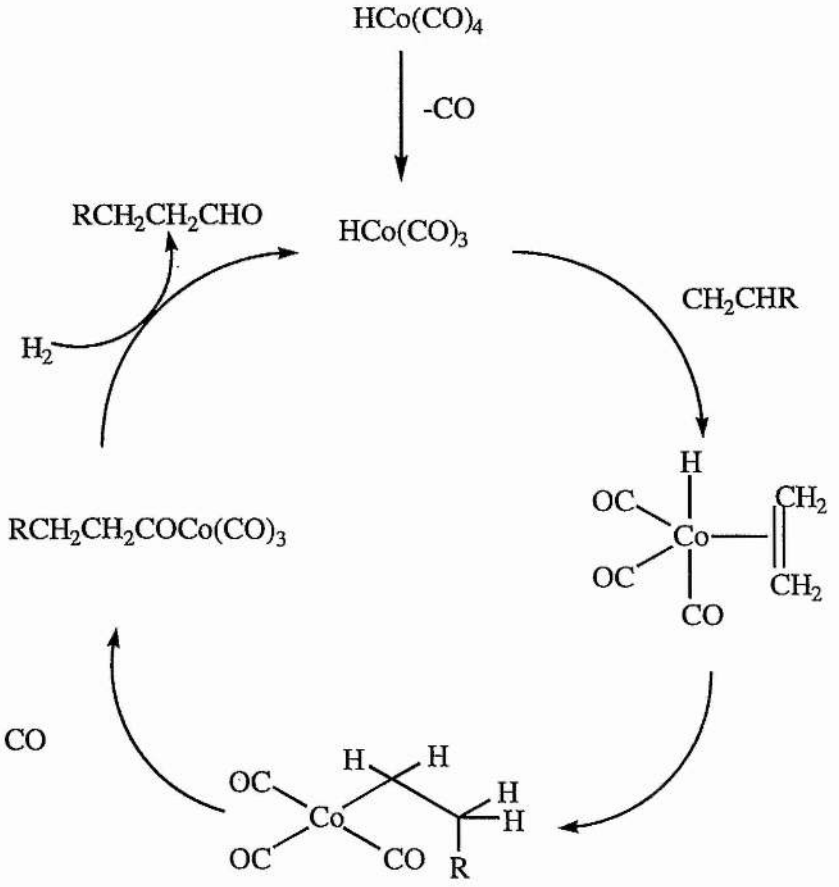

This is not the only pathway available, and the mechanism by which the acyl grouping is

removed from the metal centre as an aldehyde may involve an H_2 σ bond metathesis or an intermolecular reaction, exploiting the strong acidity of hydridocobalt tetracarbonyl in polar solvents:

$$RCOCo(CO)_3 + HCo(CO)_4 + CO \longrightarrow RCHO + Co_2(CO)_8$$

It is believed that under hydroformylation conditions the reaction with H_2 is the dominant pathway.[4]

The rate determining step is the loss of carbon monoxide from pentaco-ordinate hydridocobalt carbonyl, this involves a change from an 18 electron to a 16 electron complex. The instability of $[CoH(CO)_3]$ is thought to be the reason why it has not been directly observed. The reaction rate is inversely proportional to the pressure of carbon monoxide. Despite this, high pressures of CO are utilised in the industrial process to stabilise the catalytic species.

b. Reductive carbonylation.[1,2] Hydridocobalt carbonyls can also act as hydrogenation catalysts. The homologation reaction involves reductive carbonylation of an alcohol to an aldehyde followed by hydrogenation to the higher alcohol. Iodides are essential to attain appreciable rates.

$$ROH + 2H_2 + CO \longrightarrow RCH_2OH + H_2O$$

The two steps are as follows:

i: $CH_3OH + H_2 + CO \longrightarrow CH_3CHO + H_2O$

ii: $CH_3CHO + H_2 \longrightarrow CH_3CH_2OH$

2.1c Improving on the B.A.S.F. Dicobalt Octacarbonyl / Methyl Iodide Carbonylating System.

The ideal catalytic system for methanol carbonylation would be cheap, available, selective, active and stable. It may be possible to improve the activity and selectivity of acetate production by either:

i: Changing the catalytic species and therefore by-passing the B.A.S.F. cobalt (I) dominated mechanism. It may be possible to carry out cobalt catalysed carbonylation via a catalytic cycle that is driven by the oxidative addition of methyl iodide this would hopefully lead to much greater selectivity.

ii: Changing the reaction medium and increasing the rate of carbonylation relative to the other processes occurring; one possible medium is a supercritical carbon dioxide / methanol mixture.

This project was mainly concerned with the former strategy.

Before any amendments could be made it was important to understand the workings and limitations of the traditional system. The B.A.S.F. process operates under much harsher conditions than the Monsanto and Cativa processes. Our aim was to operate a cobalt catalyst under the sort of mild conditions possible with rhodium and iridium systems. Consequently all catalyst testing was done at low temperatures 100 °C - 185 °C and lower pressures p_{CO} 40 - 80 bar.

2.2 BATCH AUTOCLAVE EXPERIMENTS INVOLVING $[Co_2(CO)_8]$

2.2a Results.

Batch autoclave studies are a useful starting point at which to determine whether a proposed catalyst precursor is active under the sorts of conditions of interest. The catalyst and substrate are heated and stirred under pressure in an autoclave for a set time period and the resulting solution analysed by capillary gas chromatography.

The methyl iodide promoted $[Co_2(CO)_8]$ catalytic system was employed as our baseline in order to evaluate the effectiveness of novel systems. Consequently through the course of our studies the system was tested under a variety of conditions to coincide with the conditions at which we tested the novel catalysts.

2.2a i. Methanol to Methyl Acetate Catalysed by Dicobalt Octacarbonyl and Methyl Iodide.

Dicobalt Octacarbonyl will catalyse the carbonylation of methanol to methyl acetate under mild conditions of temperature and pressure, methyl acetate is easy to quantify by capillary g.c. analysis. Acceptable rates are obtained at higher catalyst concentrations (~ 0.1 mol dm^{-3}), lower temperatures (100 - 140 °C) and higher CO pressures (p_{CO} 60-80 bar) than the Monsanto and Cativa processes. These conditions help maintain a high concentration of the active catalyst.

The rate data for reactions carried out under a variety of different conditions are shown in table 2.1.

TABLE 2.1: Batch Autoclaves $Co_2(CO)_8$ + MeI in MeOH.

Expt. No	[Co] / mol dm^{-3}	Autoclave S = Steel H = Hastelloy	Temp. / °C E=External I = Internal	P / bar RO = Room temp. RE = Reaction Temp.	MeOH / g	MeI / g	Volume / cm^3	Run Time / hr	[MeOAc] / mol dm^{-3}	Rate / mol $dm^{-3}hr^{-1}$	Rate / turnover hr^{-1}
ACM 43	0.122	S. 250 cm^3	100 E	60 RO	3.16	1.60	4.7	4	0.50	0.125	1.04
ACM 72	0.058	S. 250 cm^3	100 E	80 RO	3.16	0.68	4.3	4	0.31	0.078	1.35
ACM 113	0.134	H. 28 cm^3	100 I	80 RO	1.58	0.80	2.3	4	0.26	0.065	0.44
ACM 151	0.045	H. 28 cm^3	140 I	60 RO	3.16	2.28	5.0	24	2.46	0.103	2.28
ACM 181	0.148	H. 300 cm^3	120 I	100 RE	28.877	17.354	44.1			0.64	4.3

TABLE 2.2: Batch Autoclaves $Co_2(CO)_8$ + MeI, Effect of [MeI]:

Expt. No	[Co] / mol dm^{-3}	Autoclave S = Steel H = Hastelloy	Temp. / °C E=External I = Internal	P / bar RO = Room temp. RE = Reaction Temp.	MeOH / g	MeI / g	Volume / cm^3	Run Time / hr	[MeOAc] / mol dm^{-3}	Rate / mol $dm^{-3}hr^{-1}$	Rate / turnover hr^{-1}
ACM 15.2	0.133	S. 250 cm^3	100 E	60 RO	3.16	0.68	4.3	4	0.29	0.073	0.55
ACM 15.1	0.129	S. 250 cm^3	100 E	60 RO	3.16	0.91	4.4	4	0.33	0.083	0.64
ACM 15.7	0.126	S. 250 cm^3	100 E	60 RO	3.16	1.37	4.6	4	0.53	0.133	1.05
ACM 15.6	0.125	S. 250 cm^3	100 E	60 RO	3.16	1.60	4.7	4	0.56	0.140	1.12
ACM 15.5	0.119	S. 250 cm^3	100 E	60 RO	3.16	2.05	4.9	4	0.30	0.075	0.63
ACM 15.4	0.107	S. 250 cm^3	100 E	60 RO	3.16	3.42	5.5	4	0.25	0.063	0.58

DIAGRAM 23: The g.c. Trace From ACM151: A 24 Hour $Co_2(CO)_8$ Catalysed Catalytic Run.

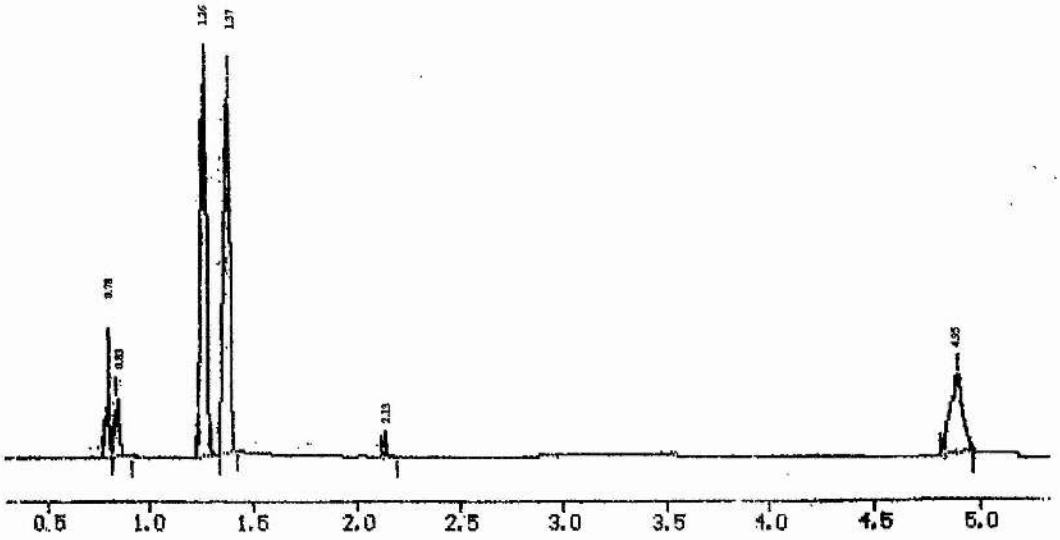

MeOMe, MeOH, MeI, MeOAc, **1,1-dimethoxyethane,** **THP, internal standard**

Experiments ACM 43, 72 and 113 were simple batch autoclaves to give an indication of the magnitude of the reaction rates under various conditions. Average rates are obtained by dividing the methyl acetate production by the reaction time. ACM 151 was run over a 24 hour period in order to analyse the side products formed. The g.c trace of the product solution reveals that the process is very selective towards methyl acetate production under these conditions.

The peaks in diagram 23 in order of increasing retention times are dimethyl ether, methanol, methyl iodide, methyl acetate, 1,1-dimethoxy-ethane and the internal standard tetrahydropyran. The reaction is virtually complete after 24 hours. 0.0986 moles of methanol were in the original 5 cm^3 solution, a molarity of 19.7 mol dm^{-3}. If all the methanol were converted this would correspond with the production of approximately 10 mol dm^{-3} methyl acetate, a rate of 0.41 mol $dm^{-3} hr^{-1}$, approximately 9 turnovers per hour, a reduction in the final reaction volume suggests that some methanol had been lost so the rate was less than this. A g.c / m.s trace suggested that traces of acetaldehyde and water may also be present.

2.2a ii. The Effect of [MeI], see table 2.2.

We investigated the effect of varying the methyl iodide concentration on the conversion of methanol to methyl acetate. This has been investigated in methanol, acetic acid, THF and water at 215 °C and 350 kg cm^{-2} (= 350 bar).by Mizoroki and Nakayama. [3] They reported that methyl iodide had a promoting effect to a limiting value but strongly inhibited the reaction of methanol and carbon monoxide at higher concentrations. The optimum ratio of MeI / Co from their studies was 0.75.

For our investigation the operating conditions of the catalytic system were set at 100°C, CO (60 bar), 4 cm^3 methanol reacting for 4 hours. We were able to optimise the methyl iodide concentration by varying the amount of methyl iodide added, (0.3, 0.4, 0.6, 0.7, 0.8, 0.9 and 1.5 cm^3). The results are in table 2.2 and diagram 24.

DIAGRAM: 24: Graph of Methyl Acetate Turnover as a Function of Methyl Iodide Concentration:

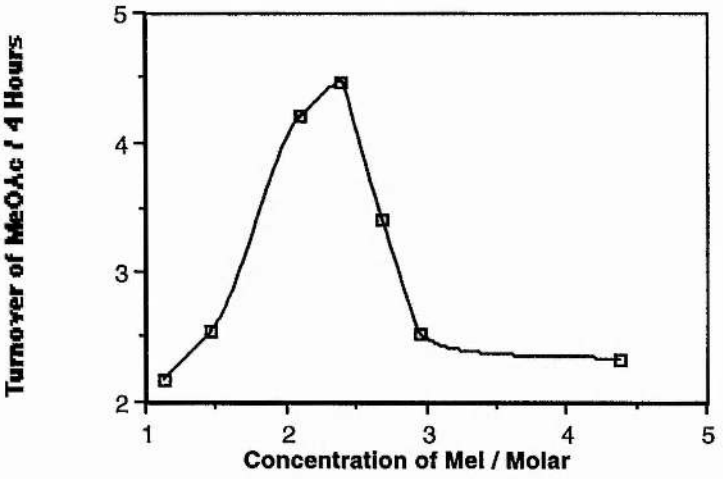

The reaction solution which gave optimised results in the Co : MeI experiments contained: 0.1002g of dicobalt octacarbonyl ($2.930 * 10^{-4}$ moles), 4 cm^3 of methanol and 0.7 cm^3 of methyl iodide (0.01124 moles). This corresponds with an optimum Co : MeI ratio of 1: 19.2. The morphology of the curve is very similar to that observed by Mizoroki *et al.* The experiments were conducted by varying the amount of MeI added and keeping the quantity of all other constituents constant. As the concentration of methyl iodide was increased, the concentration of the catalyst was reduced in the overall solution, this is because the overall volume of the solution was increased. To account for this the rate is expressed in terms of turnover number. By comparing the results of ACM 15.6 table 2.2 and ACM 43 table 2.1 we can see that the repeatability of our experiments is reasonable. The experiments were carried out using very similar component mixtures and the average result was 1.08 + / - 0.04, turnovers per hour a 4 % error.

In these experiments 1,1-dimethoxyethane is observed at a low concentration ~ 2-6 x 10^3. The concentration of this species increases as the concentration of methyl iodide is increased to the optimum for carbonylation and then stays more or less constant when the concentration of MeI is increased further.

The promotion of carbonylation at lower concentration and inhibition at higher concentration can be clearly seen. The effect of methyl iodide on methanol carbonylation is discussed extensively in chapter 1 and is summarised here.

The promoting effect is most likely to be due to:

i. the increased nucleophilicity of methyl iodide compared with methanol:

$$[Co(CO)_4]^- + CH_3I \longrightarrow [CH_3Co(CO)_4] + I^-$$

ii. or the acceleration of the acetyl removal step by iodide:

$$[MeCOCo(CO)_4] + I^- \longrightarrow MeCOI + [Co(CO)_4]^-$$

At high concentrations the inhibition observed may be due to the formation of an inactive iodo cobalt species such as $[CoI_4]^{2-}$.[1] CoI_2 is not a catalytic precursor for the carbonylation of methanol under these conditions.

Zoeller [5] included these mechanisms of iodide promotion in his proposed catalytic cycle (diagram 25).

DIAGRAM 25: Zoeller's mechanism for the methyl iodide promoted carbonylation of methanol:

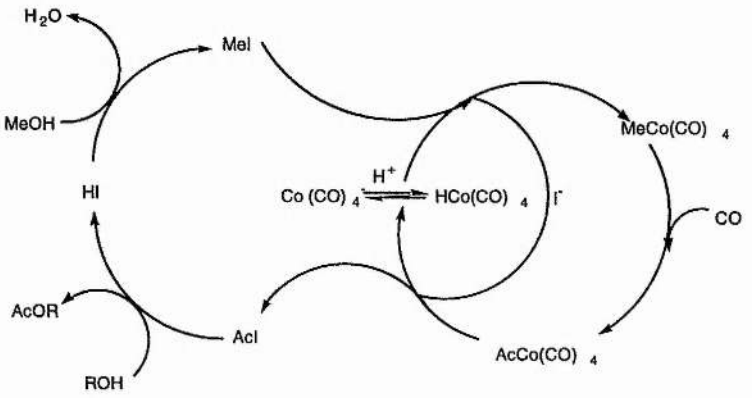

2.3. RATE OF CO UPTAKE FOR $[Co_2(CO)_8]$.

The rate of selective carbonylation reactions can be measured by following the rate of uptake of CO from a high pressure reservoir or ballast vessel see diagram 26. The pressure and temperature in the reaction vessel is held constant. Rate of uptake of CO = the rate of formation of carbonylated products.

DIAGRAM 26: Apparatus for Measuring the Rate of CO Uptake in to a Catalyst Solution.

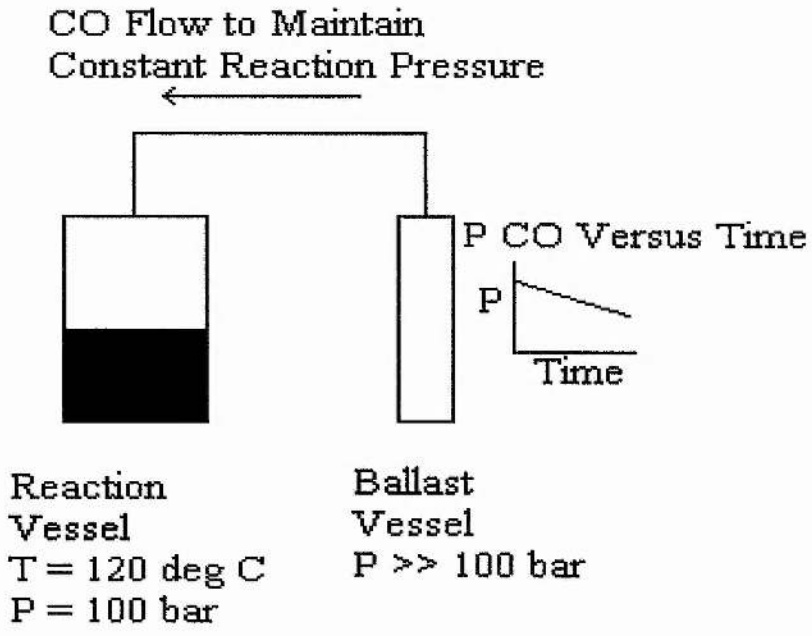

DIAGRAM 27: Dicobalt Octacarbonyl Catalytic System CO Uptake ACM 181.

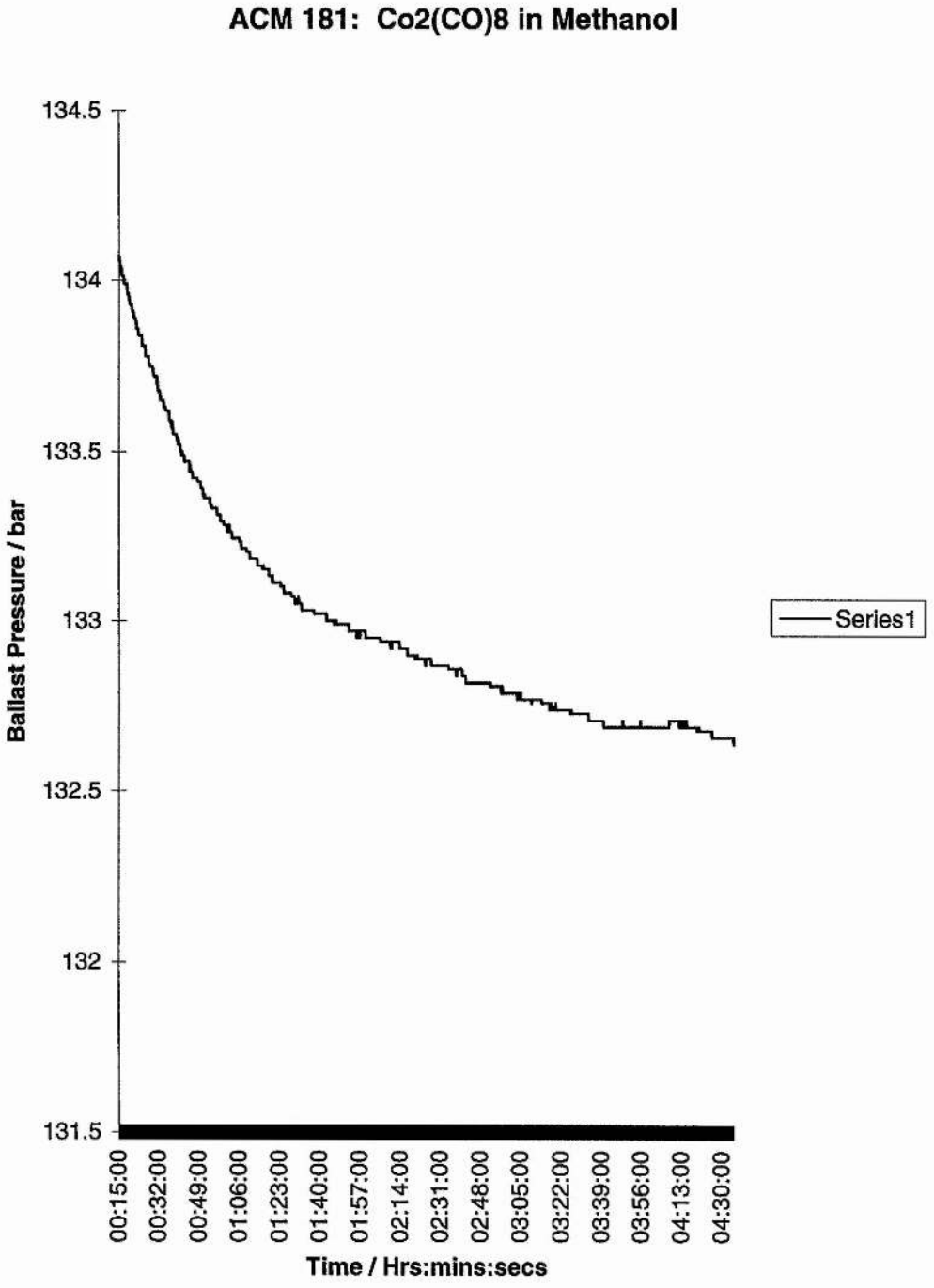

DIAGRAM 28: Dicobalt Octacarbonyl Catalytic System CO Uptake ACM 182.

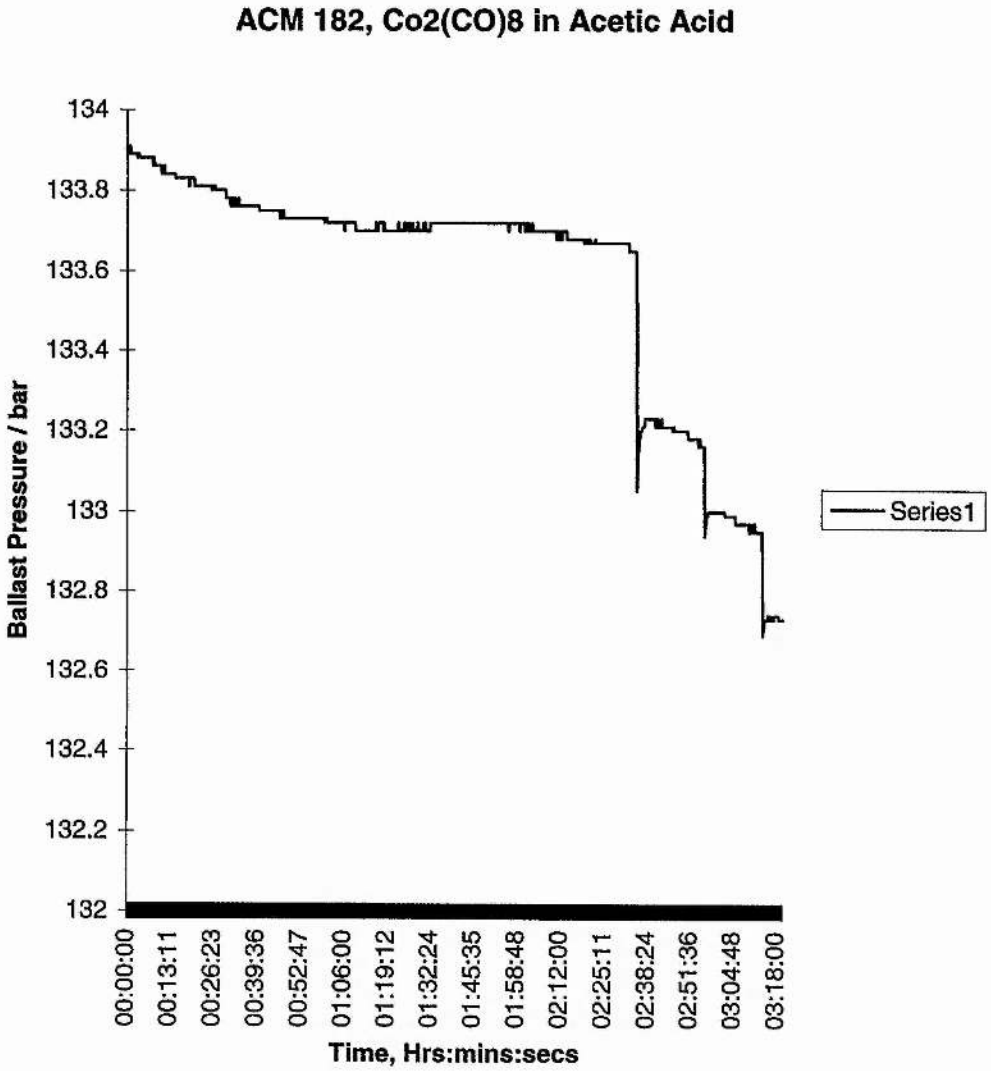

2.3a. Results.

The rate of CO uptake was measured in pure methanol for the $[Co_2(CO)_8]$ + MeI catalytic system, see diagram 27 The reaction was carried out at B.P. Chemicals Hull with the assistance of Evert Ditzel and technical assistance of David Serero. The initial rate was 0.64 mol $dm^{-3}hr^{-1}$. The rate decayed rapidly over the course of the reaction. Comparing the conditions of ACM 181 with those of the 24 hour run ACM 151 (table 2.1), the relative concentration of cobalt is much higher in ACM 181 leading to a faster rate of carbonylation and a lower ratio of MeI / Co. As the ACM 151 catalytic system carbonylated the majority of the methanol reactant in 24 hours at a high relative concentration of iodide it is unlikely that the observed loss of activity is due to catalyst deactivation by reaction with iodide. In experiment ACM 181 approximately 25 % of the methanol has been carbonylated and we propose that the loss of activity is due to the conversion of methanol to methyl acetate, this suggests a rate dependency on methanol concentration. The graph is roughly zero order for the first 40 minutes and undergoes a first order decay after 2 hours, the shape of the curve is typical of saturation kinetics. Table 2.3 contains the results of the product composition analysis carried out by the B.P. Chemicals Hull analytical department, the methyl acetate concentration was calculated from the total uptake of CO.

2.3a i. Methanol to Acetic Acid Catalysed by Dicobalt Octacarbonyl and Methyl Iodide.

see table 2.4, 2.5.

The Cativa and Monsanto processes for the carbonylation of methanol are operated in acetic acid and water. The substrate is tied up in the form of methyl acetate. Methyl acetate reacts with HI to generate methyl iodide and acetic acid and start the catalytic cycle. An important driving force in the development of new catalysts for the carbonylation of methanol is the reduction of water concentrations in solution, this will reduce purification costs. A novel catalytic system with similar rates of carbonylation to the Monsanto and Cativa processes may be commercialised if it can operate in a low water acetic acid solvent. To this end we measured the CO uptake from such a solution containing $[Co_2(CO)_8]$ in acetic acid containing 7 % water at B.P. Hull, see table 2.4, diagram 28. At 140 °C and 100 bar the rate was very low and the opening and closing of the control valve between the ballast and reaction vessel can be clearly seen on diagram 28. The rate was measured at approximately 0.5 $moldm^{-3}hr$, this is just less than the rate

obtained in pure methanol at 120 °C operated at 2.77 mol dm^{-3} MeI, ACM 181 (see table 2.1).

As the graph of ballast pressure against time is so poor few conclusions can be drawn from it but it seems that the system is still active after 3 hours. The reduction in activity relative to the pure methanol run and the constant rate in acetic acid (which is essentially unchanged over the course of the measurements) are consistent with a stable system that is dependent on the concentration of methanol. Another possible explanation for the low activity is the low concentration of MeI. The concentration of MeI in the commercial solution recipe was 1.17 mol dm^{-3}. The rate may be enhanced by increasing this.

In order to warrant commercial application the rate of carbonylation would have to be increased by more than an order of magnitude.

TABLE 2.3: Products from ACM 181

Expt. No.	Catalyst	CH_3COOCH_3 / mol dm^{-3}	CH_3CH_2COOH / mol dm^{-3}	CH_3CHO / mol dm^{-3}	Acetone / mol dm^{-3}	EtOAc / mol dm^{-3}	PropI / mol dm^{-3}	Ethylidene diacetate / mol dm^{-3}
ACM181	$Co_2(CO)_8$	0.808	0.01055		0.045			0.00106

TABLE 2.4: Batch Autoclaves $Co_2(CO)_8$ + MeI in AcOH / MeOAc / H_2O.

Expt. No	[Co] / mol dm^{-3}	Autoclave S = Steel H = Hastelloy	Temp. / °C E=External I = Internal	P / bar RO = Room temp. RE = Reaction Temp.	AcOH / g	MeOAc / g	H_2O / g	MeI / g	Volume / cm^3	Rate / mol dm^{-3} hr^{-1}	Rate / turnover hr^{-1}
ACM 182	0.134	H. 250 cm^3	140 I	100 RE	32.006	7.150	3.553	7.532	45.28	0.5	3.7

Table 2.5: Product Composition in Low Water Acetic Acid Solvent.

Expt. No.	Catalyst	CH_3COOH /mol dm^{-3}	CH_3CH_2COOH /mol dm^{-3}	ACETONE /mol dm^{-3}	EtI /mol dm^{-3}	EtOAc /mol dm^{-3}	Ethylidene Diacetate
ACM182	$Co_2(CO)_8$	0.636	0.05936	0.00057	0.01275		

2.4. MECHANISTIC STUDIES: DICOBALT OCTACARBONYL AS A CARBONYLATION CATALYST.

2.4a. Studying the Mechanism of a Catalytic Carbonylation Processes:

The study of mechanism is very important to the catalytic chemist. Understanding what the metal is doing in solution has two major benefits: Firstly we can identify the unit processes necessary to transform the organic, this should allow us to make necessary changes to speed up the slowest step. Secondly we can identify the side reactions associated with the cycle and minimise them in order to increase the concentration of active catalytic sites in solution.

In the following studies the primary technique used for probing the mechanisms of the catalytic carbonylation processes was infrared spectroscopy. High pressure infrared spectroscopy can be carried out under the sort of temperatures and pressures at which methanol carbonylation catalysts operate allowing the metal species to be observed *in situ*. In addition the short timescale and high sensitivity of infrared spectroscopy makes it the ideal technique for *in situ* study.

We followed the carbonyl stretching frequencies in the reaction media. The CO stretching frequencies in the infrared spectra may let us identify a compound by comparing the spectrum with the available literature, failing that they give two levels of information on an unknown:

Firstly on the nature of the carbonyl compound from the frequency,

Terminal: 2120 - 1850 cm^{-1},

Bridging: 1850 -1750 cm^{-1},

Acyl: 1750 - 1650 cm^{-1}.

and from the number of stretches.

Secondly, and particularly for terminal carbonyl ligands, infrared spectroscopy gives a feel for the electron density on the metal centre. The stretching frequency will decrease as electron density on the metal centre increases due to increased backbonding to the carbon to oxygen antibonding orbitals which weakens the C-O bond.

Once the infrared spectrum has been analysed compounds isolated from the product liquor can be compared with this data and further characterised by NMR and X - ray crystallography.

2.4b. ACM 73: Infrared Study of Dicobalt Octacarbonyl Under Mild Catalytic Conditions.

No detailed *in situ* HPIR study of cobalt catalysed carbonylation of methanol has been reported in the literature.

$[Co_2(CO)_8]$ and methyl iodide, molar ratio 1:18, in methanol, were injected in to the HPIR autoclave and pressurised to 60 bar with CO. The autoclave was warmed and infrared spectra were recorded, these are presented as infrared spectra 1-4.

As the autoclave was heated to 60 °C the spectra collected were similar (infrared spectra 1 and 2), spectrum 2 shows the terminal stretches of an active system as the CO stretching frequency of methyl acetate is growing at 1727 cm^{-1}. The infrared absorptions observed can be assigned by considering some literature values:

Some examples of cobalt carbonyls expected in solution are[6] (In hydrocarbon solvents unless otherwise stated):

C_{3v}:	$[CoH(CO)_4]$:	2116 (A_1), 2053 (A_1) and 2030 (E) cm^{-1}
C_{3v}:	$[CoMe(CO)_4]$:	2105 (A_1), 2036 (A_1) and 2019 (E) cm^{-1}
C_{3v}:	$[Co(RCO)(CO)_4]$:	2120 (A_1), 2060 (A_1) and 2020 (E) cm^{-1}, (acyl 1680 cm^{-1})
	$[Co_2(CO)_8]_{bridged}$:	2112w, 2071s, 2042s, 2001w
		1863w, 1853s.
	$[Co_2(CO)_8]_{unbridged}$:	2106w, 2069s, 2031s, 2022s, 1991m (^{13}CO) cm^{-3}.
	$[Co(CO)_4]^-$ in MeOH:	1900 cm^{-1} [7]

The terminal carbonyl absorptions in spectra 1 and 2 are at 2006, 2024, 2047 and 2107 cm^{-3}, this resembles the spectra of $[CoMe(CO)_4]$ and $[Co(RCO)(CO)_4]$. The presence of four peaks instead of three can be explained by a breakdown in the degeneracy of the stretch with E symmetry. This occurs due to restricted rotation of the acyl group around the Co-C axis. The acyl grouping's $p\pi$ and $p\pi^*$ orbitals and the metal centre's $d\pi$ orbitals interact fixing the conformation and reducing the overall symmetry. This splitting is well known for species of general formula $[Co(RCO)(CO)_3L]$, where L is a stabilising ligand such as PPh_3 which have been isolated and characterised.[8]. We assign the spectra to trigonal bipyramidal $[Co(CH_3CO)(CO)_4]$ with the acyl grouping in an axial position, this structure has C_s symmetry and therefore 4 stretching modes. The acyl CO stretch is not detected due to noise resulting from the water and methanol, these are difficult to subtract from the region below 1700 cm^{-1}.

In infrared spectrum 3 we can only detect stretches due to the product methyl acetate at

1728 cm^{-1}. The relative intensity of the terminal carbonyls is vastly reduced, this is interesting as the autoclave experiments suggest that the system is still active at this point. It may be that the activity of the cobalt catalyst is quite high but the concentration of the catalytic species is very low. The region below 2000 cm^{-1} is very noisy and it is very difficult to determine whether there is a signal due to $[Co(CO)_4]^-$, comparison with spectrum 2 suggests not as there is no great change in this region.

Infrared spectrum 4 is an enlargement of the region above 2000 cm^{-1} for a spectrum that has been at 100 °C for 30 minutes. The spectrum is consistent with a $[Co(MeCO)(CO)_4]$ distorted by the 'noise' from the other species. The additional stretches may be due to another species, this is most likely to be $[CoMe(CO)_4]$.

TABLE 2.6: Assignment of ACM 73, room temperature to 60 °C:

ν_{co} / cm^{-1}	Species	Assignment
1727 - 1728	MeCOOMe	Acyl CO
2006 - 2008	$Co(MeCO)(CO)_4$	Terminal CO (E)
2024 - 2026	$Co(MeCO)(CO)_4$	Terminal CO (E)
2047 - 2050	$Co(MeCO)(CO)_4$	Terminal CO (A_1)
2107 - 2108	$Co(MeCO)(CO)_4$	Terminal CO (A_1)

$[Co(MeCO)(CO)_4]$ is observed as the major species during catalysis in pure methanol at 100 °C and CO (60 bar) (at room temperature). This suggests that the slowest step in the catalytic cycle is the breaking of the Co-COMe bond. A long lifetime for this intermediate is consistent with the production of the side product 1,1-dimethoxyethane (see section 2.2c).

INFRARED 1: ACM 73: $Co_2(CO)_8$ + MeOH + MeI, 60 bar CO at room temp. 34 °C.

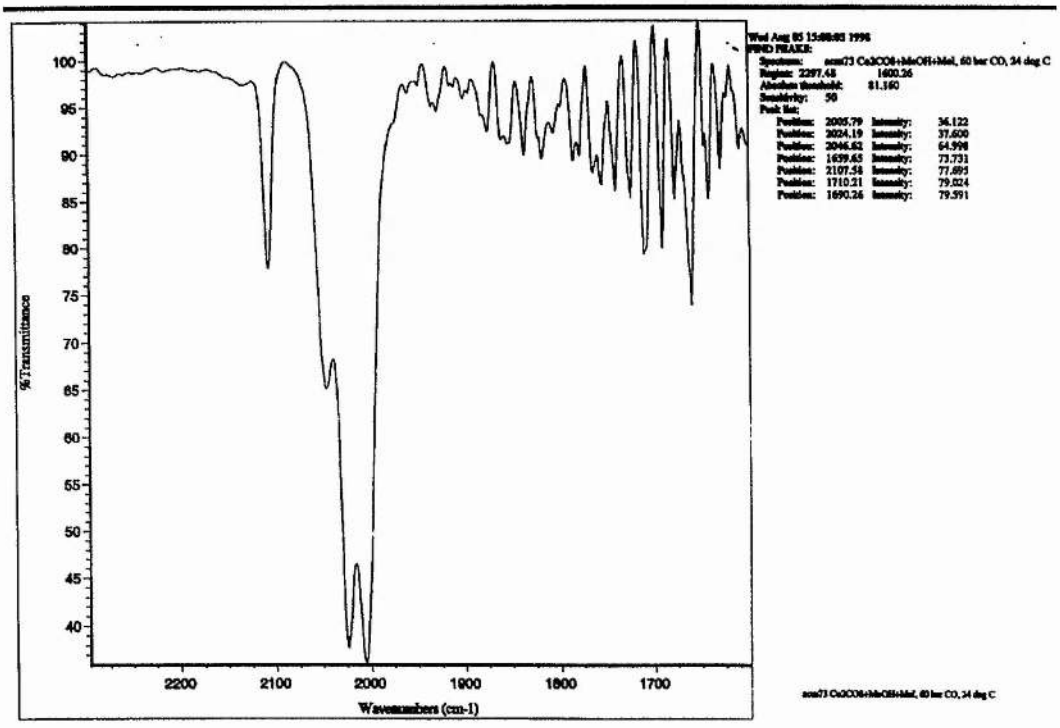

INFRARED 2: ACM 73 at 60 °C.

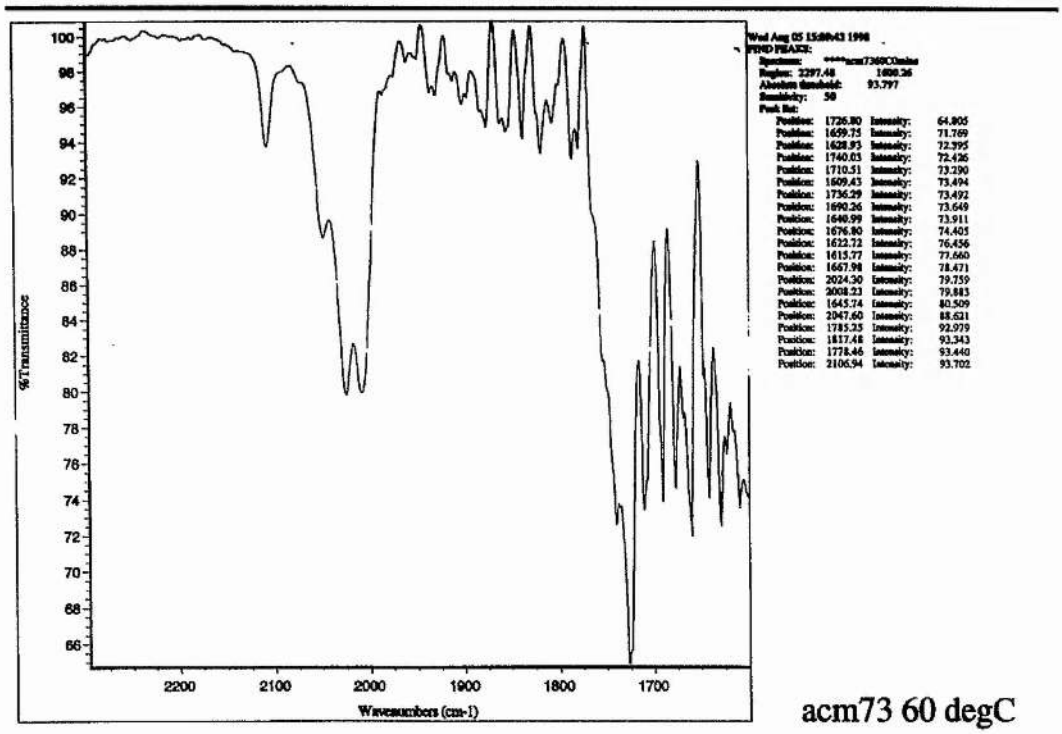

INFRARED 3: ACM 73, 80 °C.

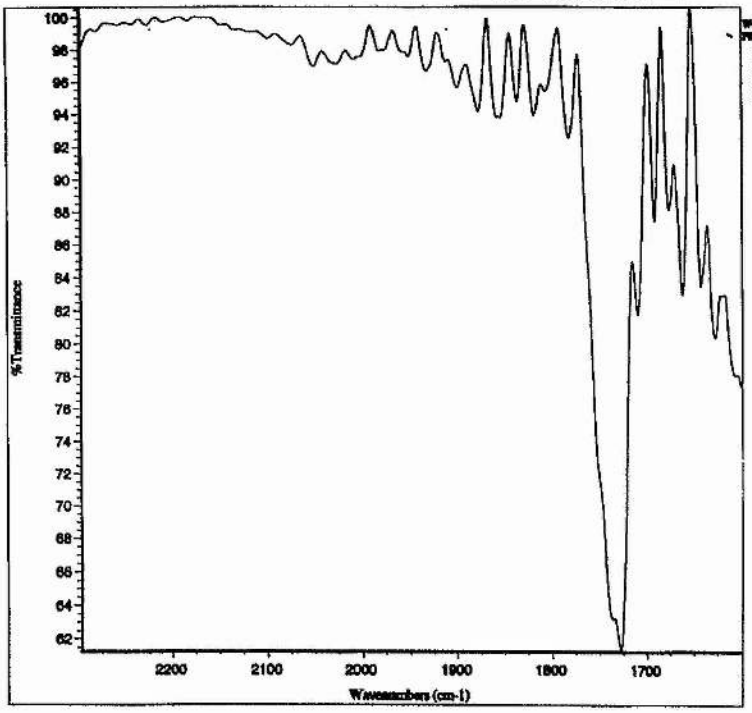

acm73 80 degC

INFRARED 4: ACM 73, 100 degC for 30 minutes, enlargement.

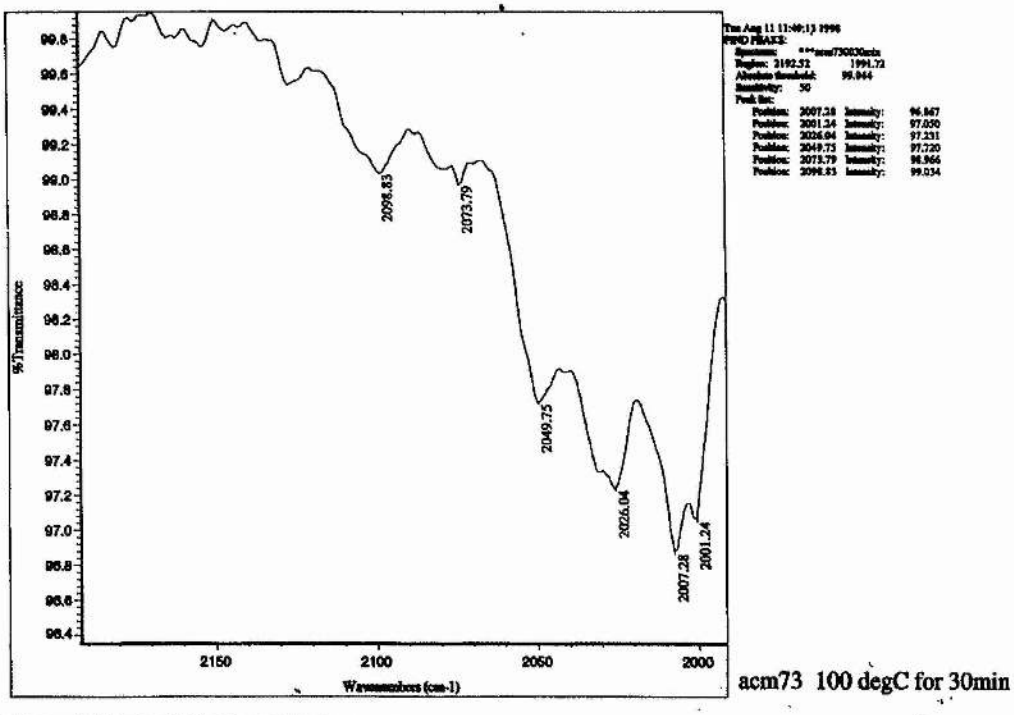

2.5. DISCUSSION: $[Co_2(CO)_8]$ AS A CATALYST FOR METHANOL CARBONYLATION

2.5a. Rationalising the Observed Products.

The three main products of the reaction of methanol and CO in the presence of dicobalt octacarbonyl and methyl iodide are dimethyl ether, methyl acetate, and 1,1-dimethoxy-ethane, the concentration of acetaldehyde is very low.

Dimethyl Ether: Dimethyl ether can be generated by the nucleophilic attack of methanol on methyl iodide or $[CoMe(CO)_4]$, or it can also be generated from the acid catalysed reaction of two molecules of methanol. The reaction of methanol with methyl iodide is thought to be the most important as iodide is a good leaving group. It is generated in the absence of catalytic activity.

Methyl Acetate: It is likely that methyl acetate is generated by cobalt catalysed carbonylation occuring via a Zoeller-like mechanism (see diagram 25).

Acetaldehyde and 1,1-Dimethoxyethane: These and most of the other documented side products in cobalt catalysed alcohol carbonylation reactions are the result of acetaldehyde production by the hydridocobalt carbonyl catalysed reductive carbonylation of methanol. Acetaldehyde is formed as detailed in section 1.2d.

When there is a low hydrogen concentration and high methanol concentration the acetaldehyde reacts with two equivalents of methanol to generate 1,1-dimethoxyethane. The reaction is acid catalysed:

$$CH_3CHO + 2CH_3OH \xrightarrow[H^+]{} CH_3CH(OCH_3)_2 + H_2O$$

Three equivalents of methanol are consumed in this reaction, two of which are recoverable.

2.6. THE EFFECT OF ADDITIVES ON DICOBALT OCTACARBONYL AND METHYL IODIDE IN METHANOL.

2.6a. Batch Autoclave Experiments.

see table 2.7

The effect of various additives on the catalytic activity of dicobalt octacarbonyl in neat methanol are summarised in table 2.7. ACM 28: Ruthenium trichloride inhibited the reaction under the conditions tested. The conversion compares unfavourably with that of ACM 15.6, (table 2.2) carried out under very similar conditions with no ruthenium. Lithium iodide was added in ACM 75, this batch autoclave can be compared with experiment ACM 72 (table 2.1). In the four hour period the production of methyl acetate is reduced, this may be due to a slower rate of carbonylation or quicker degradation to an inactive Co (II) iodo species, the latter is likely as initial rates should be enhanced due to an increase in the rate of Co-COMe bond breaking.

PEt_3 was added in an attempt to increase the electron density on the metal centre and therefore enhance its reactivity with MeI and tendency to form Co (III) intermediates. Triethyl phosphine has been employed in this way to promote the rhodium catalysed carbonylation of methanol.[9] There are four major forms that phosphine can take in the reaction:

- $[MePEt_3]I$: formed from the reaction of MeI and PEt_3. We assume that this is the major form in the initial reaction solution as quaternisation is fast and complete in dichloromethane at room temperature. This formation of this is equivalent to replacing methyl iodide with inorganic iodide.
- PEt_3: We have observed free phosphine in the product solutions when $[Cp^*Co(CO)_2]$ and PEt_3 are employed as catalyst precursors (see chapter 4). The concentration of free phosphine is expected to be low but may be significant when the initial solution contains a high concentration of PEt_3.
- Co-PEt_3: The formation of active cobalt phosphine compounds would be expected to significantly change the CO uptake profile.
- PEt_3O: This may be generated from the decomposition of cobalt phosphine compounds. J. Rankin *et al* observed the generation of PEt_3O when $[Rh(CO)(PEt_3)I_3]$ was heated with MeI under CO in the presence of water and suggested a mechanism which involved

TABLE 2.7: Batch Autoclaves $Co_2(CO)_8$ + MeI + Additive in Methanol.

Expt. No	[Co] / mol dm^{-3}	Additive [Additive] / mol dm^{-3}	Autoclave S = Steel H = Hastelloy	Temp. / °C E=External I = Internal	P / bar RO = Room temp. RE = Reaction Temp.	MeOH / g	MeI / g	Volume / cm^3	Run Time / hr	[MeOAc] / mol dm^{-3}	Rate / mol dm^{-3} hr^{-1}	Rate / turnover hr^{-1}
ACM 28	0.124	$RuCl_3.H_2O$ 0.1	S. 250 cm^3	100 E	60 RO	3.16	1.60	4.7	4	0.17	0.043	0.34
ACM 75	0.062	LiI 0.628	S. 250 cm^3	100 E	80 RO	3.16	0.73	4.32	4	0.14	0.035	0.56
ACM 160	0.036	PEt_3 0.35	H. 28 cm^3	140 I	60 RO	3.16	2.28	4.90	1	0.064	0.064	1.76
ACM 170	0.147	PEt_3 0.8	H. 28 cm^3	150 I	80 RO	3.80	1.37	5.15	2	2.163	1.082	7.35
ACM 179	0.148	PEt_3 0.88	H. 300 cm^3	120 I	100 RE	66.09	23.50	88.96			1.38	9.2

TABLE 2.8: Product Compositions for Experiments ACM 179 and 181.

Expt. No.	Catalyst	CH_3COOCH_3 / mol dm^{-3}	CH_3CH_2COOH / mol dm^{-3}	CH_3CHO / mol dm^{-3}	Acetone / mol dm^{-3}	EtOAc / mol dm^{-3}	PropI / mol dm^{-3}	Ethylidene diacetate / mol dm^{-3}
ACM179	$Co_2(CO)_8 + PEt_3$	4.803	0.04982			0.00026		
ACM181	$Co_2(CO)_8$	0.808	0.01055		0.045			0.00106

reductive elimination of Et_3PI_2 followed by hydrolysis.[10]

The results ACM 160, 170, 179, table 2.7, were promising. ACM 179 was measured as the rate of CO uptake.

2.6b. The Rate of CO Uptake.

The rate of CO uptake to a methanol solution containing $[Co_2(CO)_8]$, MeI and PEt_3 was measured at B.P. Chemicals Hull. The ballast pressure versus time graph is diagram 29. Comparing $[Co_2(CO)_2]$ in methanol with and without PEt_3 (ACM 179 and 181) reveals that the addition of phosphine has facilitated an increase in turnover number from 4.3 to 9.2.hr^{-1} The rate of carbonylation falls through time as it did in the absence of phosphine but the shape of the ballast pressure time graph is more complex as there is an initiation period whilst the catalyst forms. After the period of induction there follows a period of zero order kinetics and finally tailing to virtually no activity.

The increase in carbonylation rate on adding phosphine could have two possible routes. The first possibility is the generation of more active cobalt phosphine compounds, the second is an increase in the rate of Co-COMe cleavage by iodide attack. The strange shape of the pressure time curve opens the possibility that there is a novel species in solution thus explaining the induction period. This novel species may decompose to give a $[Co_2(CO)_8]$ + iodide catalytic system. A mechanistic study is required to establish whether this is the case. The reduction in rate at approximately 50 % conversion may be due to a dependence on a high concentration of methanol.

The product compositions for the reactions with and without phosphine are given in table 2.7. The addition of phosphine has rendered this catalytic system more active and more selective. The improved selectivity may be due to a reduction in the standing concentration of acetyl cobalt tetracarbonyl. This may be affected by cleavage of the the cobalt carbon bond by nucleophilic attack of iodide forming CH_3COI.

DIAGRAM 29: Dicobalt Octacarbonyl + PEt_3 CO Uptake vs. Time ACM 179.

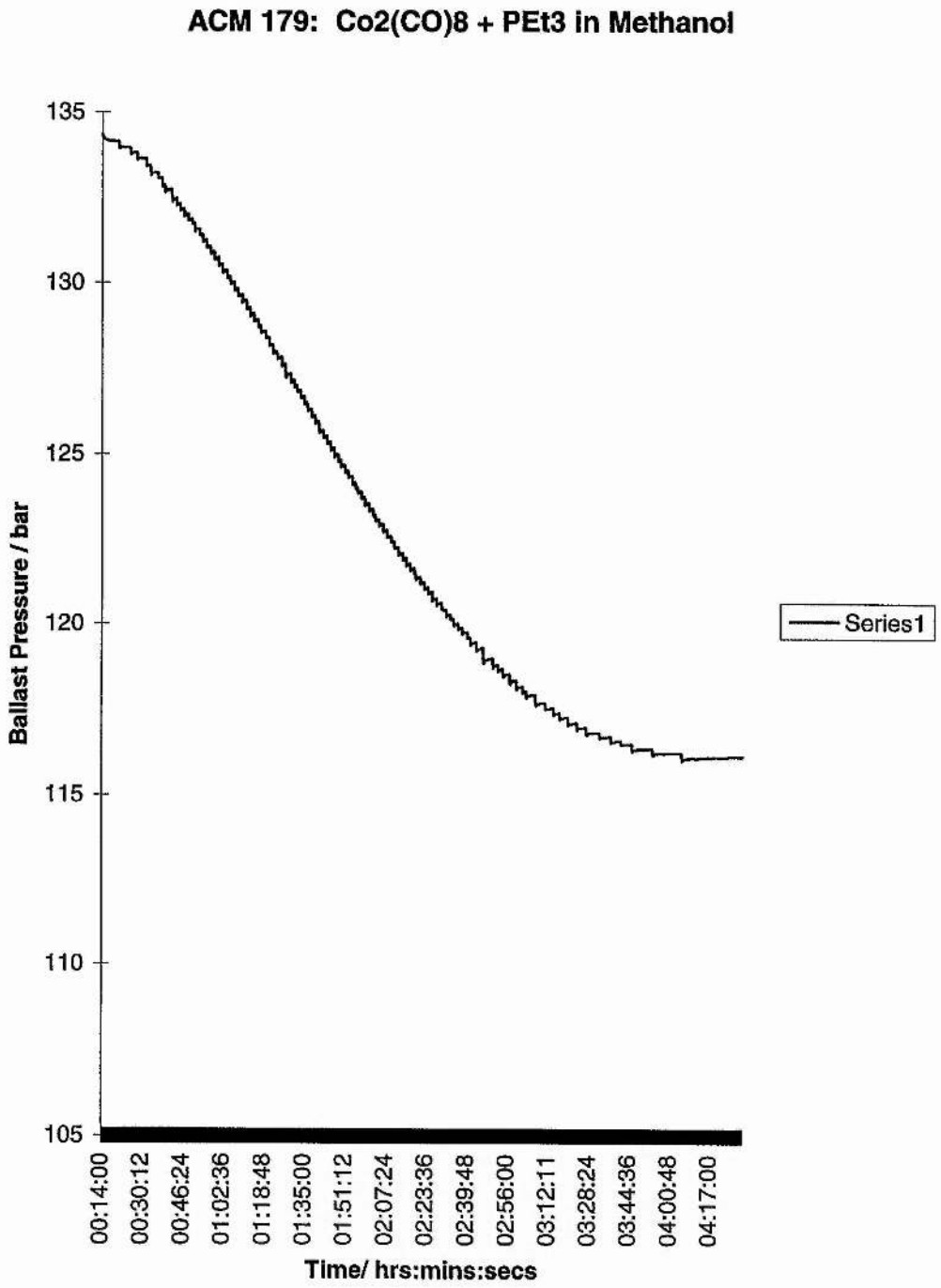

2.7. CLEANER SOLVENTS FOR $[Co_2(CO)_8]$ CATALYSED CARBONYLATION OF METHANOL.

2.7a. Introduction.

It may be advantageous to replace the conventional organic solvent systems with cleaner media such as supercritical CO_2 / methanol.

Supercritical fluids can be used to overcome some of the problems associated with homogeneous catalysis.

Homogeneous catalysis in liquid solvents can:

. be limited by the rate of dissolution and overall concentration of a gaseous reactant,

. be retarded by slow diffusion of reactants, solvation shells and cage effects,

. be wasteful and time consuming as catalysts and solvent are often difficult to remove from the products,

. be dangerous and environmentally damaging as the solvents can be flammable and toxic.

The application of solvent systems like supercritical CO_2 can help to overcome all the above problems:

. Gases are generally completely miscible with supercritical fluids,

. As the physical properties of supercritical fluids are those of gases, short distance diffusion is very rapid; and as the solvation shells are very weak, therefore the reactants are in a more reactive state,

. CO_2 and catalyst are easily separated from the products by selective precipitation involving careful pressure changes,

. Carbon dioxide has no toxicity or flammability.

Some further advantages of the carbon dioxide system are:

- its cheapness;
- its high quadripolar moment which enables it to dissolve polar molecules better than most supercritical fluids;
- its low critical points ($T_C = 31°C$ $p_C = 73.8$ Atm.) allowing supercritical conditions to be attained at temperatures at which most catalytic complexes are stable.

(N.B. At 31°C and 73.8 atm the critical density of CO_2 is 0.47g cm^{-3}).

Supercritical carbon dioxide mixed with methanol solvates volatile, nonpolar, saturated,

aprotic organic solutes most efficiently.

In order to achieve a homogeneous solution it is advisable to work well above the critical point of the supercritical solvent as the solutes reduce its solvating power. Problems may arise if the catalytic cycle involves ionic intermediates as these are insoluble, e.g. the tetracarbonyl cobaltate (-1) ion.

Carbonylation of methanol catalysed by dicobalt octacarbonyl may be operated in supercritical CO_2 as it may involve exclusively neutral intermediates $[CoH(CO)_4]$, $[CoMe(CO)_4]$ and $[CoMeCO)(CO)_4]$ and radical pathways. These species are known to be soluble in supercritical CO_2.[32]

DIAGRAM 30: Possible Scheme For Carbonylation in Supercritical CO_2.

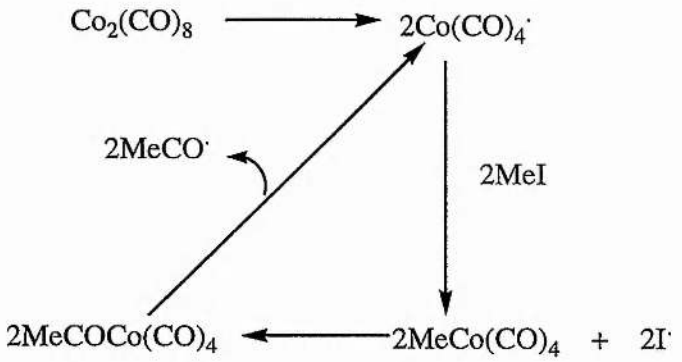

2.7b. Results.

Quoted in table 2.9 are the results of preliminary experiments in CO_2 / MeOH. The autoclave was charged with the catalyst, methanol and methyl iodide, it was pressurised with CO and then CO_2 was pumped in using an HPLC pump. The autoclave was now heated and stirred like a normal batch autoclave run. Methyl acetate was detected in both experiments but the concentration was low in ACM 112. In ACM 114 1,1-dimethoxyethane was also produced concentration ~ 2×10^{-3} moldm^{-3}. If the mixture is in the supercritical phase then the catalyst concentration is 0.0107 moldm^{-3} as the solution will expand to fill the 28 cm^3 autoclave, low catalyst concentrations would be expected to lead to low reaction rates.

The turnover for ACM 114 is greater than the turnover for ACM 113 (table 2.1) which involved a similar feed and a greater catalyst concentration. In ACM 113 the autoclave was loaded with CO (80 bar) at room temperature in ACM 114 only 42 bar, despite this the results suggest that the concentration of CO is rate limiting. The concentrations of all

other species are reduced due to the expansion of the fluid to fill the vessel and the effective concentration of CO is increased as gas diffusion is more rapid in a supercritical fluid. Comparing the two resultant solutions, ACM 113 has produced roughly twice the methyl acetate and twice the 1,1-dimethoxyethane so the selectivity is similar in the two media.

Although the calculated rates are higher in this new medium in order to achieve industrially significant rates of acetate production we must increase the concentration of catalyst, this will require an in depth study of phase behaviour in order to maintain a homogeneous supercritical phase. One way that the integrity of a supercritical fluid can be monitored is by incorporating a sapphire window in the side of the autoclave.

TABLE 2.9: Batch Autoclaves $Co_2(CO)_8$ + MeI in CO_2 / MeOH.

Expt. No	[Co] / moles x 10^{-4}	CO_2 added / bar	CO added / bar	Autoclave S = Steel H = Hastelloy	Temp. / °C E=External I = Internal	P / bar RO = Room temp. RE = Reaction Temp.	MeOH / g	MeI / g	Run Time / hr	[MeOAc] / mol dm^{-3}	Rate / mol $dm^{-3}hr^{-1}$
ACM 112	2.761	62 RO	31.5 RO	H. 28 cm^3	100 I	197 RE	1.58	0.80	1	trace	
ACM 114	3.000	49 RO	42 RO	H. 28 cm^3	100 I	167 RE	1.58	0.80	4	0.14	0.038

TABLE 2.10: $[Co(CO)_2(PMe_2Ph)_2I]$

Expt. No	[Co] / mol dm^{-3}	Autoclave S = Steel H = Hastelloy	Temp. / °C E=External I = Internal	P / bar RO = Room temp. RE = Reaction Temp.	MeOH / g	MeI / g	Volume / cm^3	Run Time / hr	[MeOAc] / mol dm^{-3}	Rate / mol $dm^{-3}hr^{-1}$	Rate / turnover hr^{-1}
ACM 158	0.0027	H. 28 cm^3	100 I	60 RO	3.16	2.28	5.0	24	0.094	0.004	1.45

2.8. POSSIBLE IMPROVEMENTS TO THE COBALT CATALYSED CARBONYLATION OF METHANOL.

2.8a. Introduction.

The selectivity and activity of a process can be improved to a point by optimising the reaction conditions. For example the g.c trace of ACM 151 (diagram 23) contains virtually no side products whereas significant amounts of 1,1-dimethoxyethane were produced in ACM 15 (see section 2.2a ii.).

A more radical approach is to try and change the mechanism of the process. The production of 1,1-dimethoxyethane as a side product is the result of having a high standing concentration of $[Co(CH_3CO)(CO)_4]$ in a solvent rich in methanol.

In order to improve the selectivity it would be advantageous to avoid such an acyl cobalt (I) intermediate, this may be done by attaching basic ligands to the metal thus stabilising the Co (III) oxidation state relative to Co (I).

Adding PEt_3 to the $Co_2(CO)_8$ system in methanol does not greatly change the behaviour of the system as the CO uptake is similar in each case (compare diagrams 27 and 29), therefore we decided to prepare a range of cobalt compounds with basic ligands attached and test them for cobalt catalysed carbonylation.

2.8b. Cobalt Carbonyl Phosphine Compounds as Catalysts for Methanol Carbonylation.

Two cobalt carbonyl phosphine compounds were tested as carbonylation catalysts.

2.8b. i. Monophosphine Cobalt Carbonyls.

$[Co_2(CO)_6(PEt_3)_2]$ can be prepared from $[Co_2(CO)_8]$ and PEt_3 in toluene, no catalytic activity was observed in a solution of the complex (0.0057 $moldm^{-3}$) in methanol (4 cm^3) and methyl iodide (1 cm^3) loaded with CO (60 bar) (at room temperature) at 140 °C over a 4 hour period, nor was there any activity at 0.0013 $moldm^{-3}$ concentration in methanol (4 cm^3) and methyl iodide (0.7 cm^3) loaded with CO (60 bar) (at room temperature) at 100 °C for four hours. It is interesting that this shows no activity as cleavage of the Co-PEt_3 was expected to form $[Co_2(CO)_8]$.

2.8b. ii. Bisphosphine Cobalt Carbonyls.

We have evidence that trans $[Co(CO)_2(PR_3)_2I]$ compounds act as carbonylation catalysts where PR_3 is PEt_3 or PMe_2Ph, a discussion of this work is contained in the subsequent chapters as it involves $Cp^{(*)}$ catalyst precursors. Unfortunately these trigonal bipyramidal compounds are difficult to prepare as there is not a reliable synthetic route to them. One catalytic run was carried out with pure trans $[Co(CO)_2I(PMe_2Ph)_2]$, the details are in table 2.10.

The average rate at 100 °C measured over 24 hours was 1.45 turnovers per hour. The selectivity of the system appears to be good as no appreciable 1,1-dimethoxyethane was detected, there was evidence for traces of acetaldehyde from the g.c. / m.s. Water and dimethyl ether were also detected.

The catalytic activity of the rhodium species $[Rh(CO)(PEt_3)_2I]$ was measured by Rankin *et al.* This compound was found to be a very efficient methanol carbonylation catalyst under mild conditions. [9] This compound is closely related to $[Co(CO)_2(PMe_2Ph)_2I]$.

2.8c. Further Work:

The application of trans $[Co(CO)_2I(PR_3)_2]$ compounds to carbonylation of methanol was promising. The poor stability of these compounds could be enhanced by replacing the two phosphine ligands by a diphosphine ligand.

CHAPTER 3: CYCLOPENTADIENYL COBALT CARBONYL, A CARBONYLATION CATALYST?

3.1 CYCLOPENTADIENYL COBALT (I) CARBONYL COMPOUNDS AS CATALYST PRECURSORS.

3.1a The Cyclopentadienyl Ligand.

The synthetic routes to cobalt (I) phosphines are poorly defined so we had to find another method of imparting a high electron density on to a Co (I) centre. The literature contains another electron donating ligand capable of activating group 9 metals to the oxidative addition of alkyl halides namely the cyclopentadienyl ligand.

Cyclopentadienyl cobalt (I) carbonyl complexes contain a very basic cobalt atom. $[CpCo(CO)_2]$ is commercially available as it catalyses the trimerisation of alkynes to benzene[1] and its derivatives and $[Cp^*Co(CO)_2]$ are easily synthesised from $[Co_2(CO)_8]$ [2]. Lichtenberger *et al* analysed the bonding in $[CpCo(CO)_2]$, [3] and discovered considerable electron donation to the cobalt centre from the Cp ring. The outer orbitals of the complex involve the cyclopentadienyl π orbitals and the d_{XZ} and d_{YZ} of the metal, see diagram 31. The carbonyls lie in the yz plane and the interaction of the carbonyls with the d_{YZ} metal orbital results in an antibonding orbital that is the LUMO. The HOMO is the antibonding orbital derived from the overlap between d_{XZ} and the cyclopentadienyl ligand.

The electron donation from the cyclopentadienyl e_1^- to the d_{YZ} is greater than that from the other cyclopentadienyl π orbital the e_1^+ therefore the e_1^+ makes more of a contribution in to the carbon-carbon bonding of the cyclopentadienyl ring. The result is a distorted ring which resembles an isolated double bond connected to an allyl group. Although π back donation to the cyclopentadienyl group is possible there is no evidence for this [4]. The molecular orbital structure of $[Cp^*M(CO)_2]$ (M = Co, Rh) systems has also been discussed. [4,5,6] As in $[CpCo(CO)_2]$ the HOMO is due to the interaction between an orbital derived from the metal d_{xz} and the $Cp^* e_1^+$ orbital.

DIAGRAM 31: The Bonding in Cyclopentadienyl Cobalt Dicarbonyl:

Sigma Bonding in $CpCo(CO)_2$

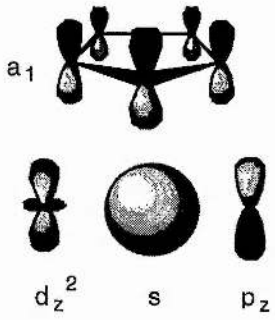

Pi bonding in cyclopentadienyl cobalt dicarbonyl:

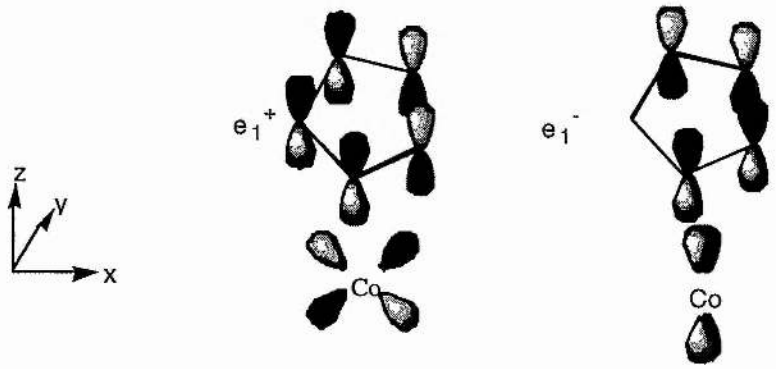

LUMO and HOMO of cyclopentadienyl cobalt dicarbonyl:

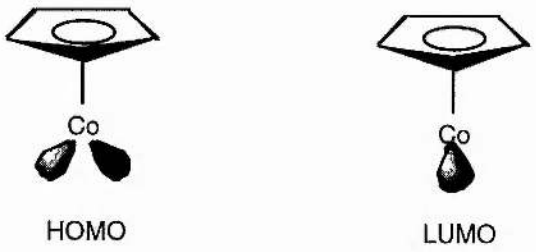

3.1b The Reactivity of $[CpCo(CO)_2]$.

3.1b i. CO Substitution Reactions.

The substitution of CO by other ligands is retarded by the electron donation from the Cp ring relative to simple cobalt carbonyls. A computational molecular orbital study on

cyclopentadienyl cobalt dicarbonyl was carried out in the 1970's. [7]. The author used the results to explain how $[CpCo(CO)_2]$ reacts in CO substitution reactions. $C_5H_5^-$ is an electron donor and this, coupled with the geometry of the $[Co(CO)_2]^+$ moiety, promotes back donation from the d_{xy} and d_{yz} orbitals of the electron rich metal centre in to the antibonding π^* orbitals of CO. This strengthens the M-C bond and weakens the C-O bond. It is the high metal to carbon bond order that slows the rate of CO substitution with nucleophiles such as PPh_3. CO dissociation is less likely and reactions involving second order kinetics are more probable. The mechanism adopted for substitution reactions is therefore usually associative not dissociative. Metals which contain η^5-cyclopentadienyl ligands are capable of ring slippage to facilitate associative substitution reactions. [8]

3.1b ii. The Reaction of $[CpCo(CO)_2]$ With Methyl Iodide.

In order to catalyse methanol carbonylation $[CpCo(CO)_2]$ must react with methyl iodide. No literature was found on the interaction of $[CpCo(CO)_2]$ with simple alkyl halides. Cyclopentadienyl cobalt dicarbonyl does oxidatively add perfluorinated iodides yielding black volatile solids of general formula $[CpCo(CO)(R_F)I]$; ($R_F = CF_3$, C_2F_5, C_3F_7). [9] The electronegative fluorine atoms increase the electron deficiency of the carbon atom in CF_3 and speed up the nucleophilic attack by cobalt.

Oxidative addition of MeI to $[CpCo(CO)_2]$, and therefore the methanol carbonylation catalysed by $[CpCo(CO)_2]$ is likely to be promoted by increasing the electron density on the metal centre. This could be achieved in three ways:

- By replacing CO with an electron donating group, e.g. a trialkyl phosphine,
- By introducing electron donating groups to the Cp ring, e.g employing the pentamethyl cyclopentadienyl ligand,
- By changing the metal and descending group 9 in order to increase the rate of oxidative addition.

In this chapter we will be dealing with the first strategy, the second strategy is dealt with in chapter 4, we embark upon the third strategy in chapter 5.

3.1c Cyclopentadienyl Metal Carbonyl Phosphines.

When [$CpCo(CO)_2$] is modified by replacing a carbonyl ligand with an electron donating ligand such as trialkyl phosphine the reaction with alkyl halides is initiated. [$CpCo(CO)PMe_3$] will react at room temperature[10] These trialkyl, triaryl and mixed alkyl-aryl phosphine substituted cyclopentadienyl cobalt carbonyls can be prepared from the reaction of cyclopentadienyl cobalt dicarbonyl with the appropriate phosphine [11,10] These compounds undergo a reaction with methyl iodide to yield acyl cobalt (III) species, see diagram 32.

DIAGRAM 32: The Synthesis of Cyclopentadienyl Cobalt (I) Phosphines and their reaction with Methyl Iodide.

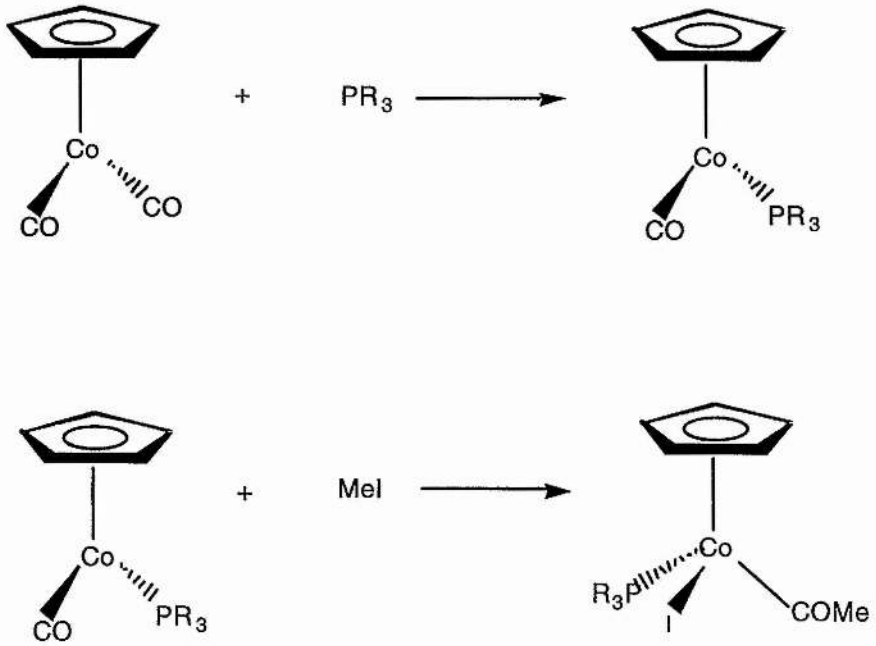

The reaction occurs via an ionic pathway. [11] This involves nucleophilic attack on methyl iodide and the formation of an electron deficient methyl intermediate. Methyl migration and attack of iodide occur rapidly generating the 18 electron iodo cyclopentadienyl acyl cobalt (III) phosphine. (see diagram 33). The reaction is first order in the metal complex and MeI consistent with a bimolecular mechanism in which the rate determining step is the nucleophilic attack on the methyl unit.

DIAGRAM 33 The mechanism of formation of the acyl cobalt complex.

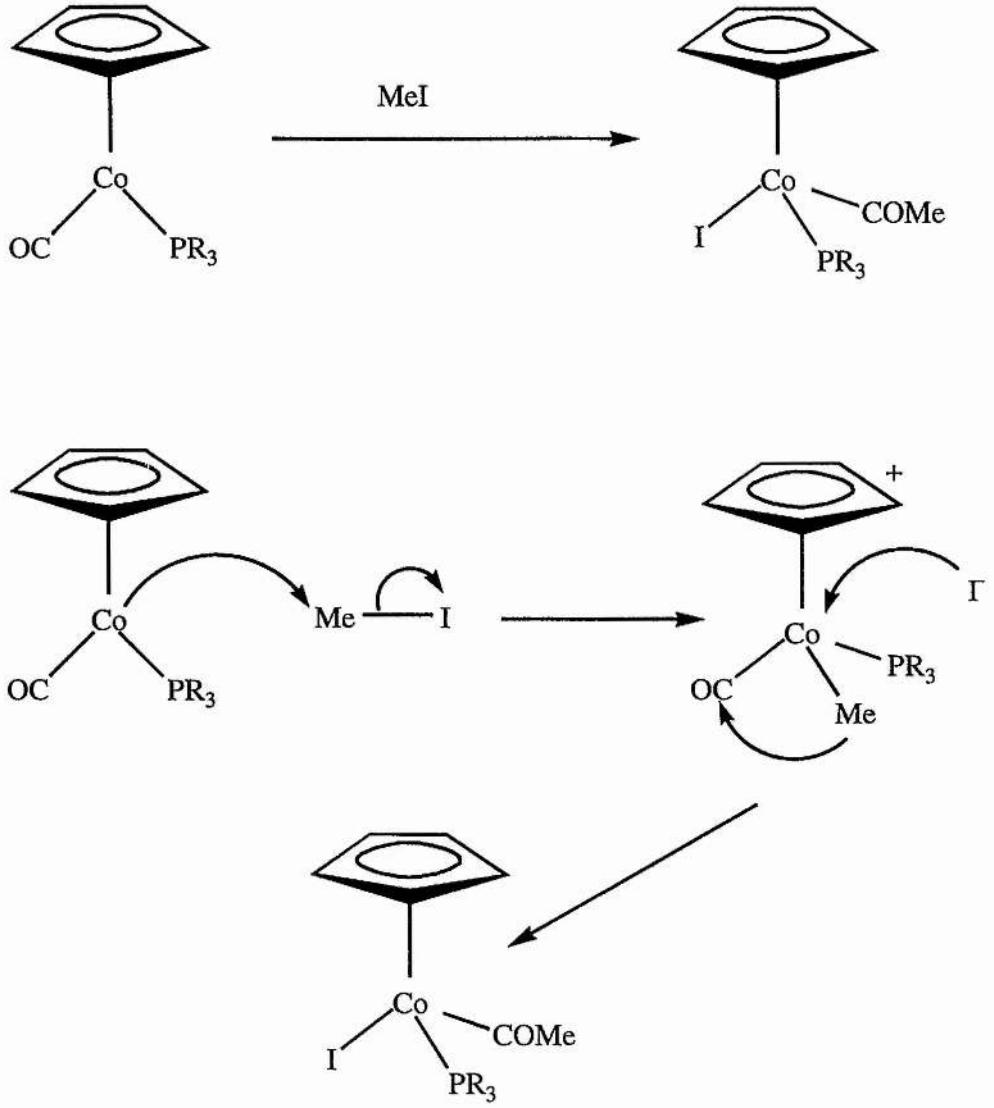

Hart-Davis and Graham carried out a comparative study of the reaction of MeI with the cyclopentadienyl complexes with ligands PPh_3, PPh_2Me, $PPhMe_2$ and $P(C_6H_{11})_3$. [11] They discovered that the rate of the reaction increased in the order: $P(C_6H_{11})_3 < PPh_3 < PPh_2Me < PPhMe_2$. This order of reactivity cannot be attributed to the electronic effect of the ligand and is in fact predicted from a purely steric model.

Once the acyl cobalt (III) species has formed reductive elimination and carbonyl co-ordination steps would be required for the synthesis of acetic acid and to recover the starting complex (diagram 34).

DIAGRAM 34: A proposed mechanism for catalytic methanol carbonylation:

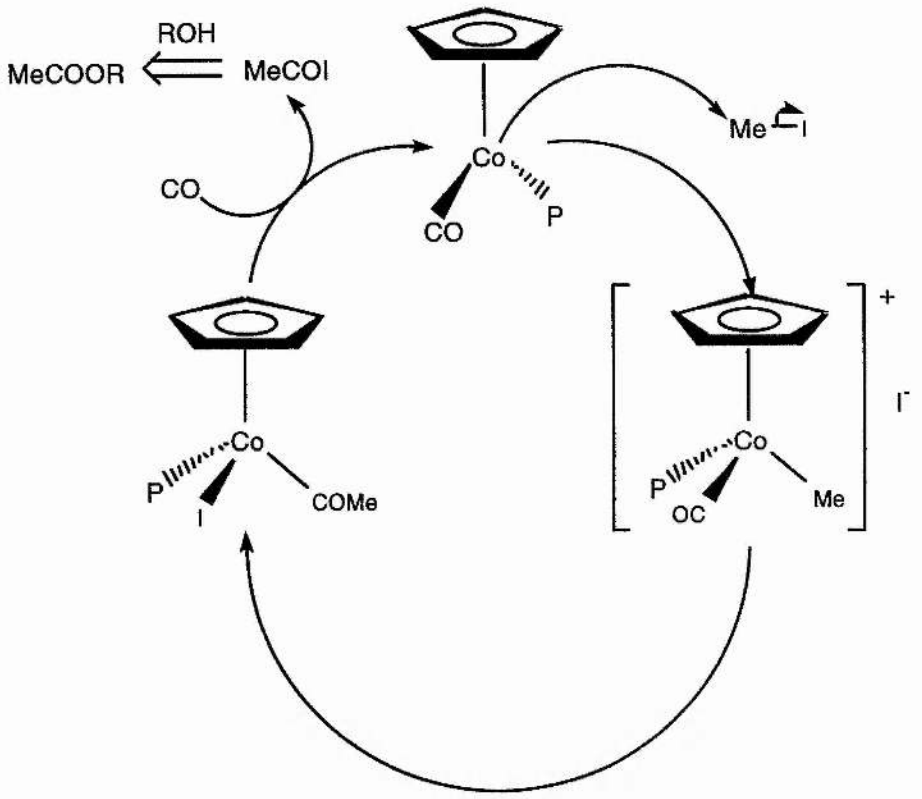

3.1d. Summary.

Cyclopentadienyl ligands could be perfect ligands for cobalt carbonylation catalysts,as:

- they donate considerable electron density to the metal centre with little or no back donation,
- they are very efficient at stabilising higher oxidation states,
- they occupy three co-ordination sites with minimal steric hindrance, (they are virtually planar),
- they are highly chelating and therefore less likely to decomplex, (a very important consideration in the extreme conditions of methanol carbonylation),
- Cp metal complexes are known to undergo the reactions necessary for Monsanto-like carbonylation: oxidative addition and CO insertion.

3.2. RESULTS FROM [CpCo(CO)P] EXPERIMENTS.

3.2a Novel Catalysts: Testing Cyclopentadienyl Cobalt Monocarbonyl Trialkylphosphine Compounds.

A range of cyclopentadienyl cobalt carbonyl phosphine compounds has been investigated for the carbonylation of methanol.

3.2a i. Synthesis.

The compounds were prepared by a simple substitution reaction between the dicarbonyl and phosphine. The more basic phosphines reacted more vigorously. [$CpCo(CO)PPh_3$], [$CpCo(CO)PPh_2Me$], [$CpCo(CO)PPhMe_2$], [$CpCo(CO)PMe_3$] and [$CpCo(CO)PEt_3$] were all prepared in this way. [$CpCo(CO)PMe_3$] and [$CpCo(CO)PEt_3$] were obtained as distillable oils, the rest are crystalline solids. As the electron density on the metal is increased the carbonyl stretching frequency in the infrared decreases. These are quoted in table 3.1, (all spectra were run in hexane).

TABLE 3.1: The Infrared Stretching Frequencies of [CpCo(CO)P] in Hexane:

Complex Added.	ν_{co} / cm^{-1}
[$CpCo(CO)_2$]	2030, 1970
[$CpCo(CO)PPh_3$]	1938
[$CpCo(CO)PPh_2Me$]	1933
[$CpCo(CO)PPhMe_2$]	1932
[$CpCo(CO)PMe_3$]	1929
[$CpCo(CO)PEt_3$]	1928

TABLE 3.2: Batch Autoclaves of CpCo(CO)P Complexes As Catalyst Precursors.

Catalyst	[Co] / mol dm^{-3}	Expt. No.	Autoclave S = Steel H = Hastelloy	Temp. / °C E=External I = Internal	P / bar RO = Room temp. RE = Reaction Temp.	MeOH / g	MeI / g	Volume / cm^3	Run Time / hr	[MeOAc] / mol dm^{-3}	Rate / mol dm^{-3} hr^{-1}	Rate / turnover hr^{-1}
$CpCo(CO)_2$	0.126	ACM 40	S. 250 cm^3	100 E	60 RO	3.16	1.60	4.70	4	trace		
$CpCo(CO)PMe_3$	0.122	ACM 36	S. 250 cm^3	100 E	60 RO	3.16	1.37	4.60	4	0.08	0.020	0.16
$CpCo(CO)PEt_3$	0.125	ACM 37	S. 250 cm^3	100 E	60 RO	3.16	1.37	4.60	4	0.09	0.023	0.18
$CpCo(CO)PEt_3$	0.106	ACM 41	S. 250 cm^3	100 E	60 RO	3.16	1.37	4.60	24	0.44	0.018	0.17
$CpCo(CO)PEt_3$	0.135	ACM 47	S. 250 cm^3	140 E	60 RO	3.16	1.82	4.80	24	0.74	0.031	0.23
$CpCo(CO)PPh_3$	0.092	ACM 49	S. 250 cm^3	100 E	60 RO	3.16	1.14	4.50	4	0.04	0.010	0.11
$CpCo(CO)PMe_2Ph$	0.135	ACM 52	S. 250 cm^3	100 E	60 RO	3.16	1.60	4.70	4	0.09	0.021	0.16
$CpCo(CO)PMePh_2$	0.107	ACM 53	S. 250 cm^3	100 E	60 RO	3.16	1.37	4.60	4	0.15	0.038	0.35
$CpCo(CO)PMe_2Ph$	0.131	ACM 54	S. 250 cm^3	100 E	60 RO	3.16	2.10	4.75	4	0.25	0.063	0.48
$CpCo(CO)PMe_2Ph$	0.090	ACM 62	S. 250 cm^3	100 E	60 RO	3.16	1.14	4.50	4	0.07	0.019	0.20

3.2a ii. Batch Autoclaves Involving [CpCo(CO)P]. See table 3.2

The first reaction carried out in each case was under conditions analogous to those of the optimised dicobalt octacarbonyl system, (see section 2.2c). The results of tesing $[CpCo(CO)_2]$, $[CpCo(CO)PPh_3]$, $[CpCo(CO)PPh_2Me]$, $[CpCo(CO)PPhMe_2]$, $[CpCo(CO)PMe_3]$ and $[CpCo(CO)PEt_3]$ are in table 3.2.

Comparing these results with the results from experiment ACM 15 table 2.2. reveals that the rate of methyl acetate production for the novel catalytic precursors is lower than for the dicobalt octacarbonyl system. It must be noted however that the dicobalt octacarbonyl system is operating under an optimised Co : MeI ratio and the novel systems are not optimised. $[CpCo(CO)PEt_3]$, $[CpCo(CO)PMe_3]$, $[CpCo(CO)PMe_2Ph]$ and $[CpCo(CO)PMePh_2]$ catalysed the carbonylation of methanol to methyl acetate. Over the four hour period the best results were obtained for $[CpCo(CO)PMe_2Ph]$ and $[CpCo(CO)PMePh_2]$. The production of methyl acetate from $[CpCo(CO)_2]$ and $[CpCo(CO)PPh_3]$ was not significant.

In all cases the g.c traces revealed a fairly pure liquid product. The selectivity towards methyl acetate would appear to be very high for all four catalysts. The products obtained were dimethyl ether and methyl acetate almost exclusively with only traces of other compounds. Dimethyl ether production is a consequence of the methanol solvent system and is avoided in industry by running in an acetic acid, methyl acetate and water mix. The trace peaks are thought to be 1,1-dimethoxyethane, acetic acid and a cyclopentadiene derivative.

Comparison of the yield after 24 hours (ACM 41), with that obtained after 4 hours for the $[CpCo(CO)PEt_3]$ catalyst shows that the system retains its activity for a prolonged period. Increasing the external temperature to 140°C over a 24 hour period (ACM 47) gave an increase in turnover frequency. The liquid product mixture remained very clean. At 140°C more 1,1-dimethoxyethane was detected than before, but levels were still very low. $[CpCo(CO)PEt_3]$ and $[CpCo(CO)PMe_3]$ were tested as crude oils. These species are very air sensitive. The catalyst was synthesised as close in time to the catalyst testing as possible in a order to keep the catalyst fresh and was not stored for more than a few days. The composition of the catalytic oil would appear to be fairly uniform as the results were reasonably repeatable.

3.2a iii. Further Work.

The batch autoclave runs had given us a feel for which cobalt (I) precursors may be employed as carbonylation catalysts and the conditions at which they could be applied. The improved selectivity obtained for these new precursors suggested a novel catalytic system had been discovered. At this point we endeavoured to prove this using high pressure infrared spectroscopy.

[CpCo(CO)PMe_2Ph] was chosen for the investigation as it provides a compromise:

The two methyl groups give this complex:

- a high electron density on the metal like the trialkyl phosphine compounds,
- a lower steric hindrance and higher solubility in methanol / methyl iodide than [CpCo(CO)$PMePh_2$],

The phenyl grouping confers to the complex:

- a greater crystallinity, making it and its derivatives easier to work with and easier to clean.

It is known that this complex reacts with MeI to give [CpCo(COMe)(PMe_2Ph)I] with ν_{co} at 1658 cm^{-1}.

3.2b Mechanistic Studies on [CpCo(CO)$PPhMe_2$] as a catalyst for Methanol Carbonylation.

Experiments were geared towards detecting the active species under catalytic conditions.

3.2b i. Experiments in the High Pressure Infra Red Autoclave, Results.

H.P.I.R. studies were carried out in a hastelloy high pressure vessel incorporating a single crystal silicon rod for cylindrical internal reflectance (a CIR cell).

[CpCo(CO)$PPhMe_2$] + MeI in Dichloromethane Under a CO Atmosphere, ACM 83, 84:

The solvent dichloromethane allows us to observe the metal-acyl ν_{co} stretching region. [CpCo(CO)$PPhMe_2$] was dissolved in dichloromethane and methyl iodide was added. The solution was injected in to the H.P.I.R. autoclave.

The first infra red spectrum ACM 83 infrared spectrum 5 revealed that all the [CpCo(CO)$PPhMe_2$] had been completely converted to [CpCo(I)(COMe)$PPhMe_2$] at room

temperature in about six minutes. We have isolated a quantitative yield of [CpCo(I)(COMe)PPhMe$_2$] in this way. In cyclohexane the product has a large acyl CO stretch at 1658 cm^{-1}. The autoclave was pressurised to 60 bar with CO and infrared spectra 6,7 and 8 were collected. There was little change at room temperature. As the autoclave was heated to 40°C the spectrum changed as [CpCo(I)(COMe)PPhMe$_2$] gave off the acyl grouping. The major peak is at 1980 cm^{-1}, once the acyl cobalt species was almost completely depleted (after 19 hours at 40 degC) the other important stretches were 1981, 2024, 2033 and 1915 cm^{-1}. These carbonyl stretching frequencies recur throughout our work involving Cp, Cp* and phosphine ligands, see chapters 4 and 5. At this point we did not have enough evidence to assign this spectrum but it is important to note that [CpCo(I)(COMe)PPhMe$_2$] did not regenerate [CpCo(CO)PPhMe$_2$].

[CpCo(CO)PPhMe$_2$] + MeI in Methanol Under a CO Atmosphere, ACM 122, 191: Infrared spectra 9, 10, 11 and 12.

CO (60 bar)

In order to establish the effect of the solvent on the decomposition of [CpCo(COMe)(I)(PPhMe$_2$)] it was necessary to carry out the infrared analysis in methanol, using the same procedure as before. This had two effects on the spectrum. Firstly the change to a protic donor solvent led to the production of a broader acyl band. Secondly the solvent subtraction is much poorer in methanol partly due to the very broad band due to traces of water at approximately 1600 cm^{-1}. These changes combine to make the spectrum almost impossible to assign in the region below 1700 cm^{-1}.

In methanol at room temperature and CO (60 bar) loading pressure, the first species observed is [CpCo(I)(COMe)PPhMe$_2$] (infrared spectrum 9). This decomposes to give compounds with infrared absorptions at 1984, 2053 and 2135 cm^{-3}, the 1984 and 2053 cm^{-3} absorptions increase at 40 °C and change in relative intensity until the peak at the lower frequency dominates.

INFRARED 5: ACM 83 $CpCo(CO)PMe_2Ph$ + MeI in CH_2Cl_2 at room temperature.

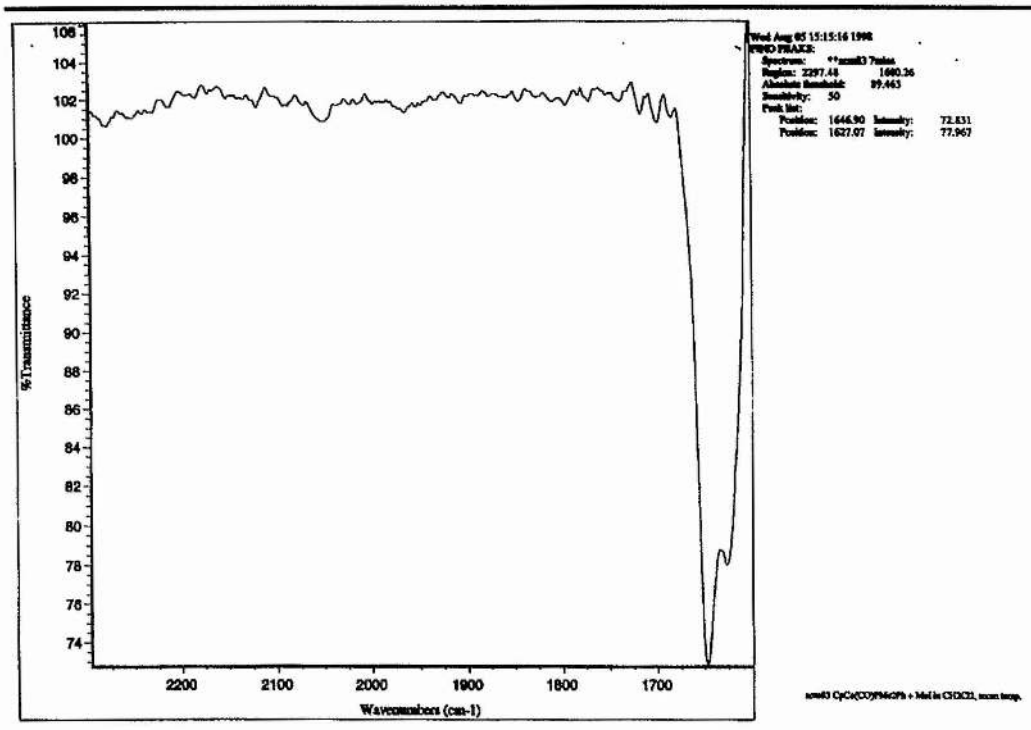

INFRARED 6: ACM 83 + 60 bar CO, at 40 degC

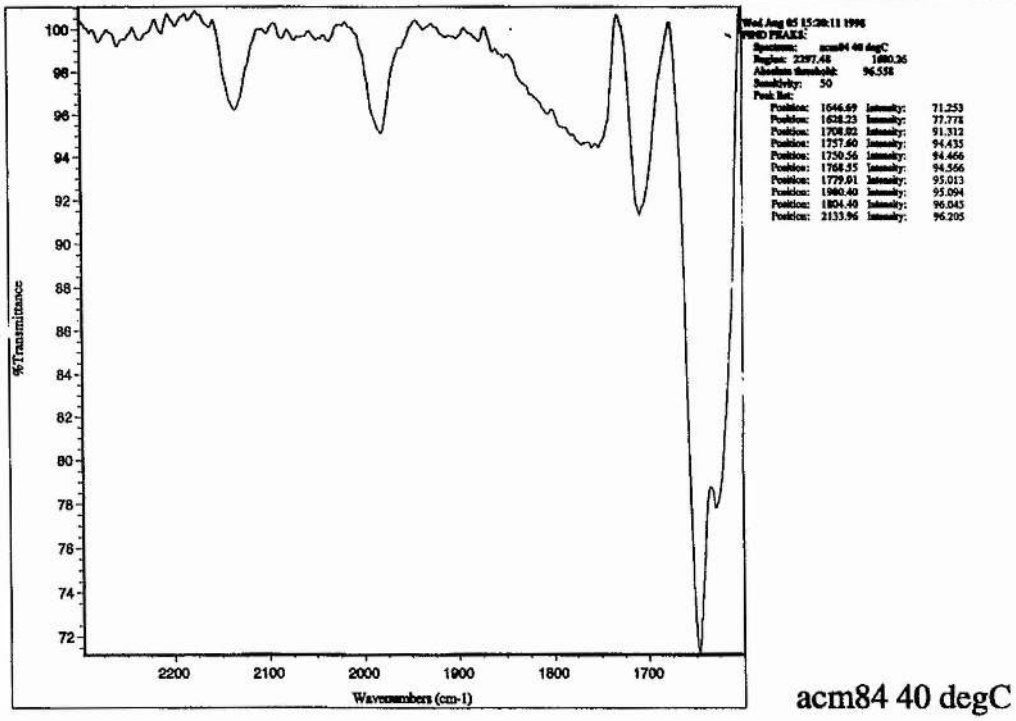

INFRARED 7: ACM 84, 40 degC for 6 hours.

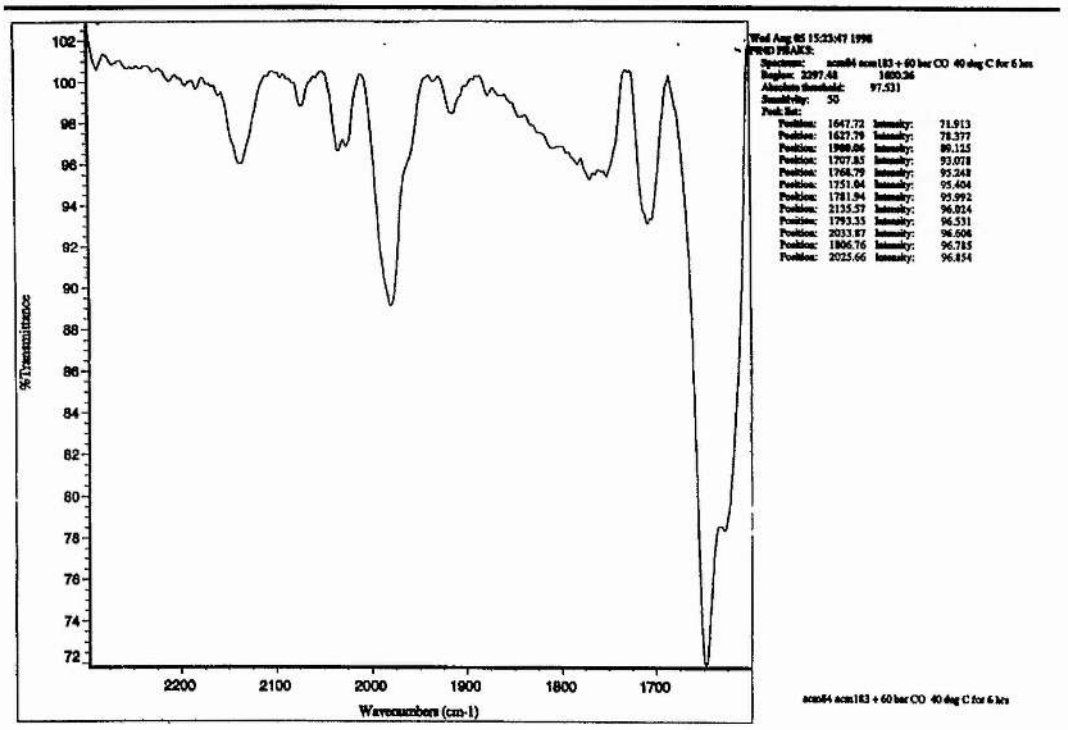

INFRARED 8: ACM 84, at 40 degC for 19 hours.

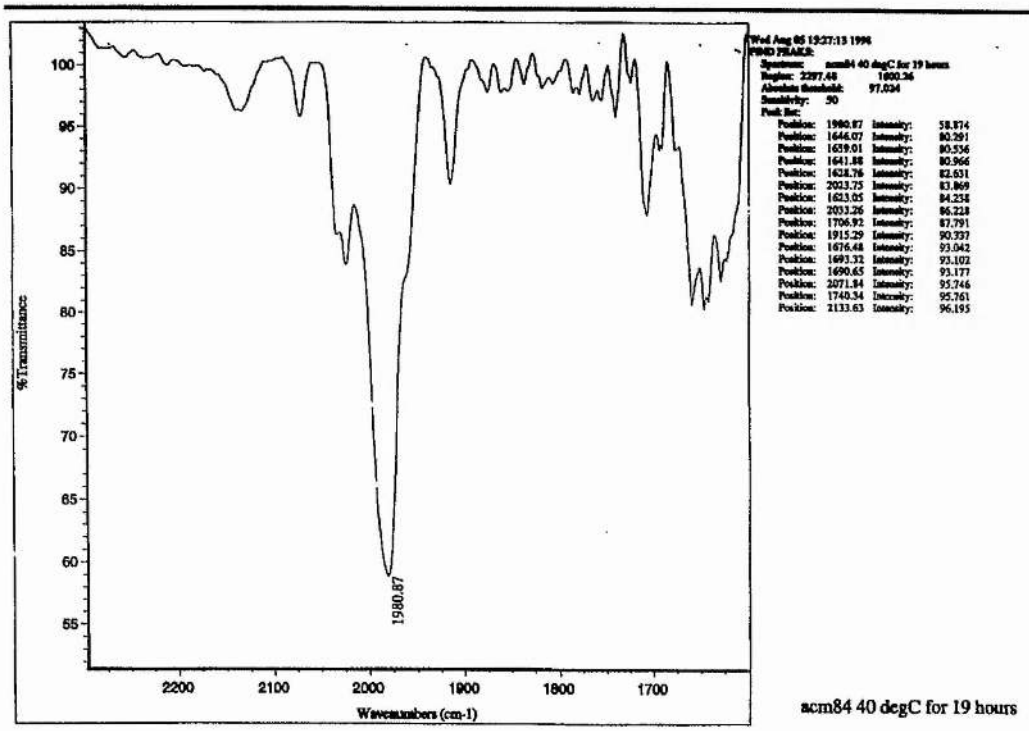

INFRARED 9: ACM 122 $CpCo(CO)PMe_2Ph$ in MeOH / MeI, 60 bar CO, room temperature.

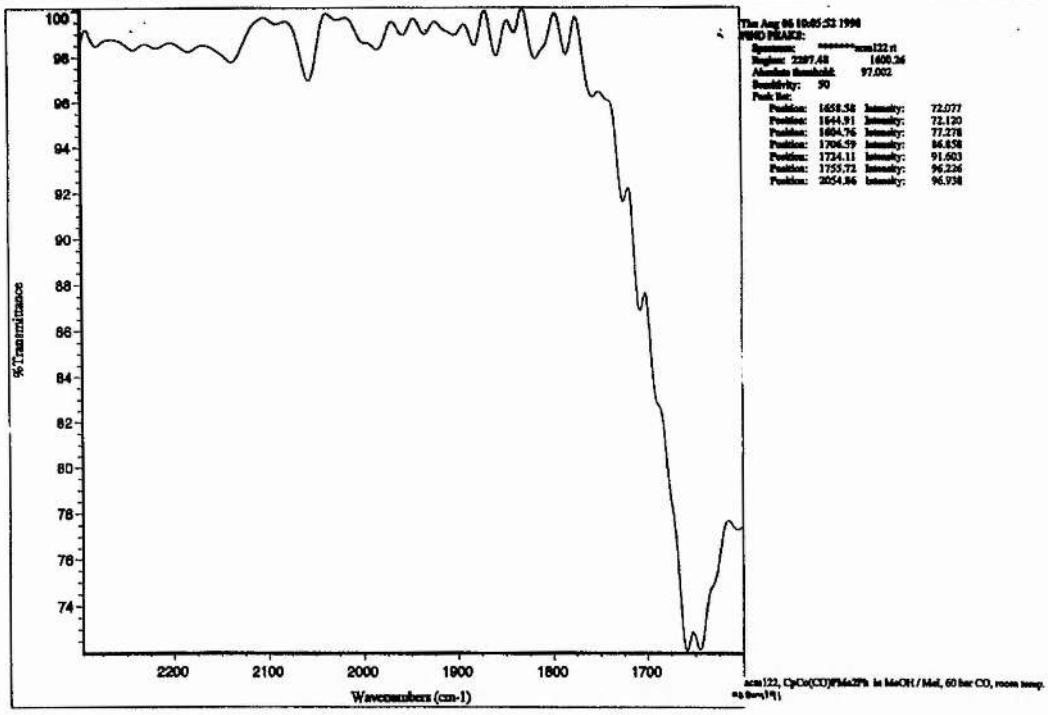

INFRARED 10: ACM 191, $CpCo(CO)PMe_2Ph$ in MeOH / MeI, 57 bar CO, 21 degC.

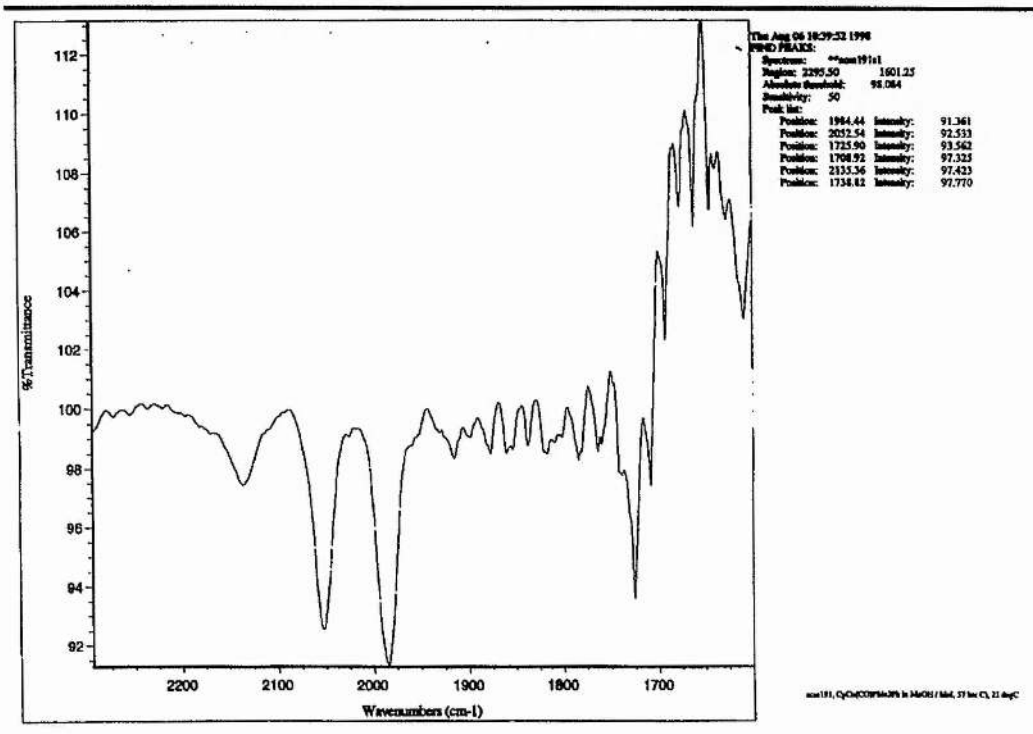

INFRARED 11: ACM 191, 40 degC.

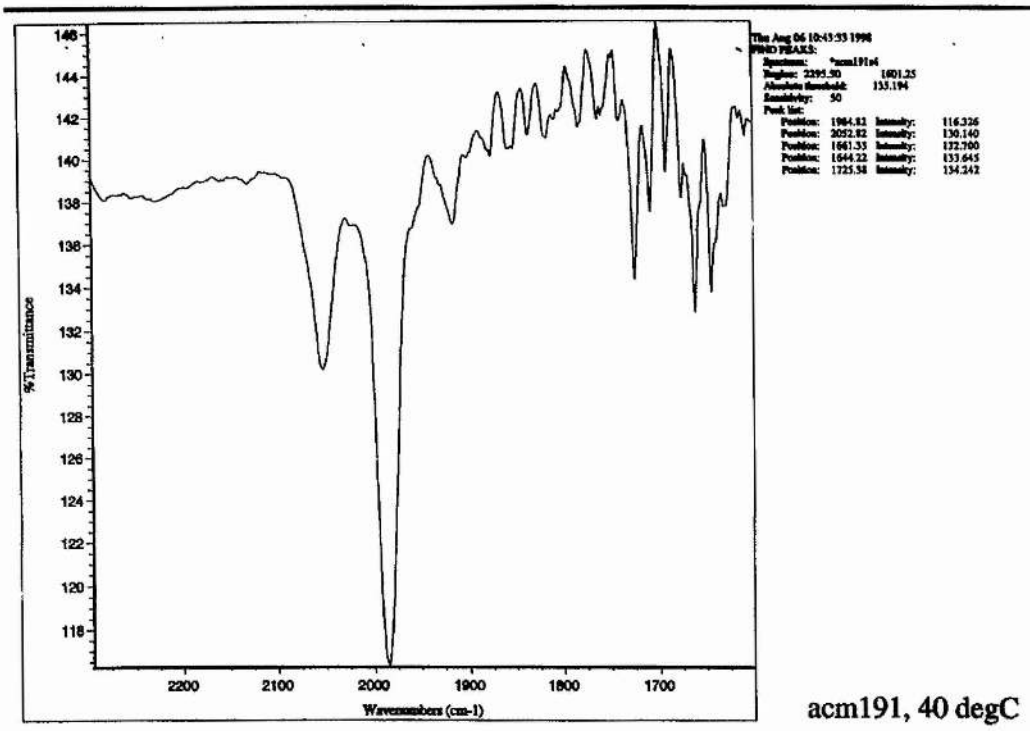

INFRARED 12: ACM 191, 40 degC for 45 mins then cooled to room temperature.

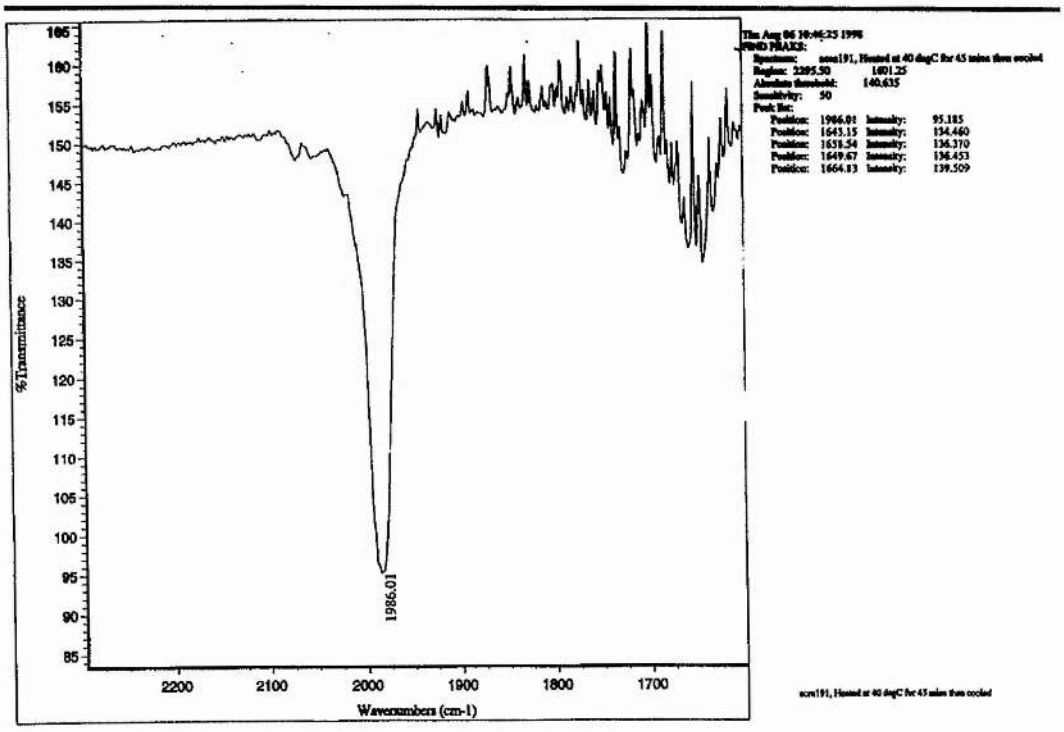

INFRARED 13: $CpCo(CO)PMe_2Ph$ in MeOH / MeI, 10 bar CO, 22 degC.

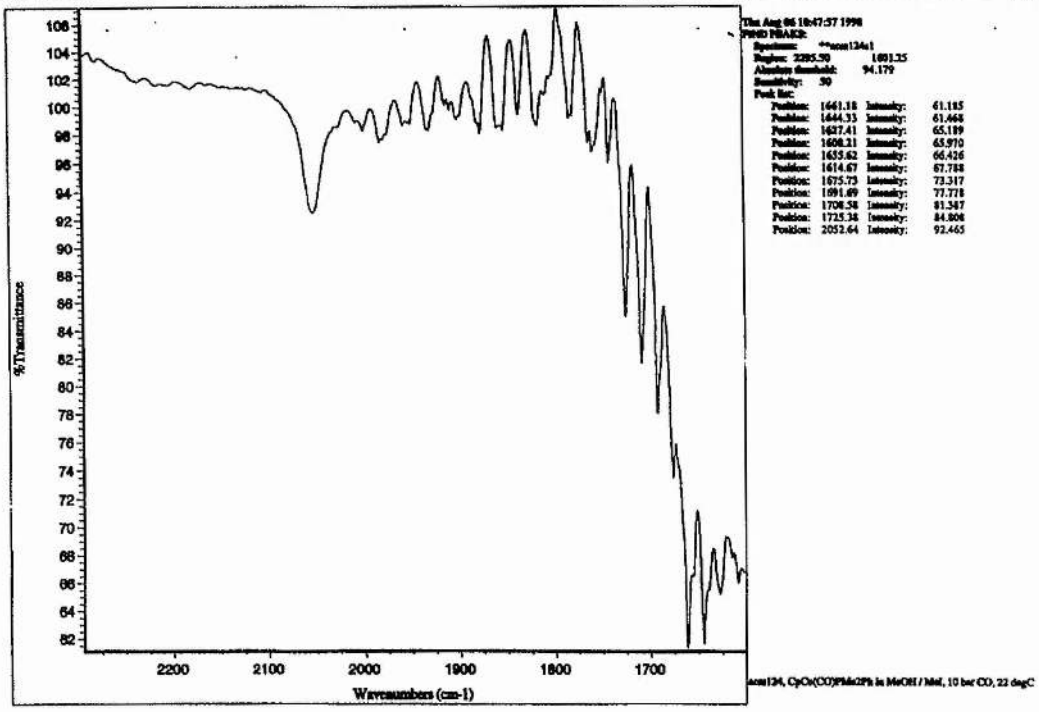

INFRARED 14: ACM 124, 40 degC.

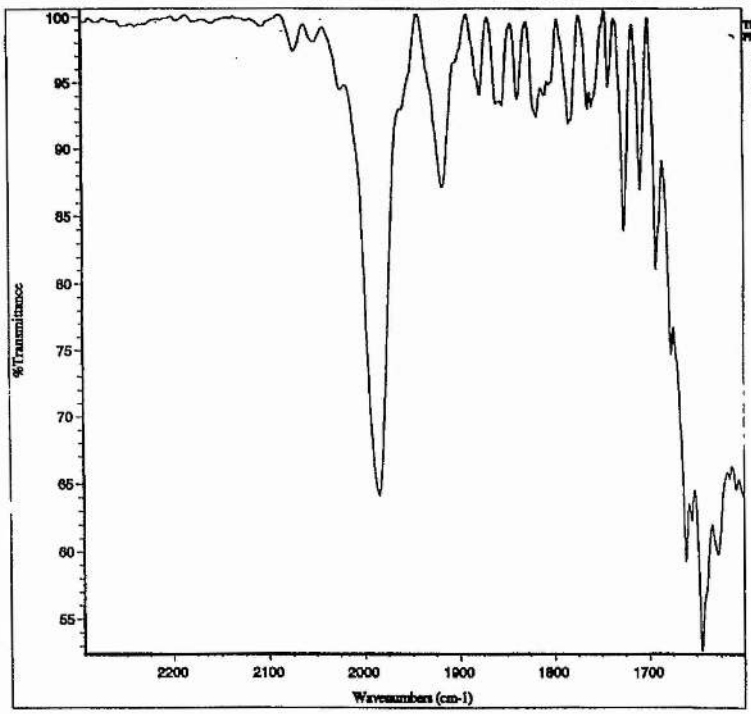

acm124, 40 degC

10 Bar CO, ACM 124, Infrared Spectra 13 and 14:

The experiment was repeated under 10 bar of CO, spectra 13, 14. An additional peak was detected at 1917 cm^{-1} at a lower relative intensity; this is believed the same peak that was detected from the overnight run in dichloromethane at CO (60 bar).

3.2b ii. Attempts to Assign the Infrared Spectra: Isolating the Complexes in Solution.

Procedure and IR Spectra:

Many attempts have been made to isolate the compounds observed *in situ*. We report the successful experiments only.

The ACM 124 Solution, 10 bar CO in Methanol, ACM 132:

Infrared spectra 15, 16.

The methanol solution from the 10 bar CO high pressure infrared study was degassed and handled under argon. Solvent was slowly removed under reduced pressure without heating until a brown red solid precipitated. The solid was insoluble in diethyl ether and liable to go off when left in methylene chloride so it was recrystallised from methanol. The resulting infrared in dichloromethane revealed stretches at 1915, 1920 and a smaller stretch at 1982 cm^{-1} spectrum 15.

When recrystallised again very slowly from methanol X-ray quality hexagonal brown plates were obtained, the infrared spectrum of these in dichloromethane is shown in infrared spectrum 16.

The plate crystals in dichloromethane had only two CO stretches: A very strong stretch at 1916 cm^{-1} and a medium stretch at 1982 cm^{-1}, this suggests the antisymmetric and symmetric stretches of a dicarbonyl complex. The NMR and X-ray analysis of this solid revealed it to be $[Co(PMe_2Ph)_2(CO)_2(I)]$. The crystal structure is contained in appendix 1 and contains trans phosphine ligands. In the ^1H n.m.r. spectrum of the trans phosphine ligands gave rise to a $H_6PP'H'_6$ second order multiplet which can be assigned to the CH_3 groups of PMe_2Ph, see diagram 35A, the ^{13}C n.m.r. spectrum as reproduced in diagram 35B and both spectra assigned in chapter 6.

DIAGRAM 35A: ^{1}H N.m.r. Spectrum of $[Co(PMe_2Ph)_2(CO)_2I]$ in C_6D_6:

$Co(CO)_2(P(CH_3)_2Ph)_2I$, $H_6PP'H'_6$

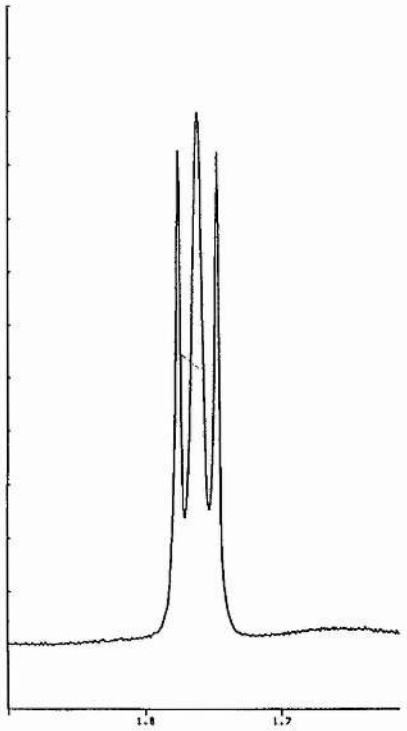

DIAGRAM 35B ^{13}C N.m.r. of $[Co(CO)_2(PMe_2Ph)_2I]$ in CD_3OD.

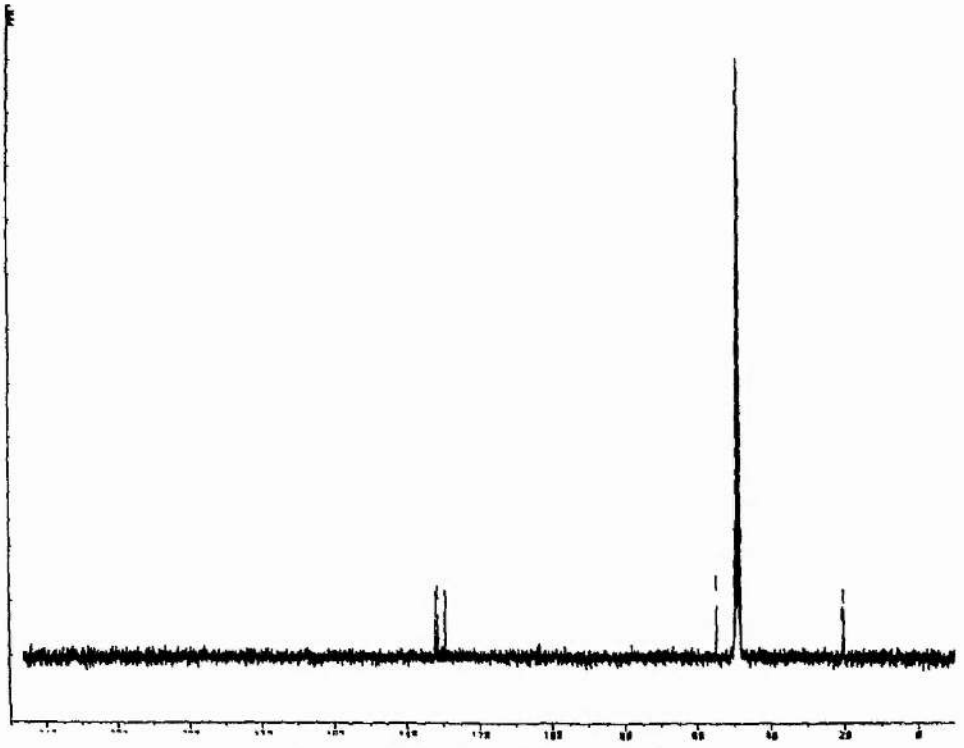

^{13}C, δ, 20.18, 20.42, 20.66 ppm, $[Co(CO)_2(P(CH_3)_2Ph)_2I$, m, AXX', $^{1}J_{C\text{-}P} + {}^{1}J_{C\text{-}P'} = 144.9$ Hz], 129.43, 129.49, 129.55, 131.48, 132.11, 132.17 ppm, $[Co(CO)_2(P(CH_3)_2Ph)_2I]$ + solvent C's.

SPECTRUM 15: Solid from ACM 124.

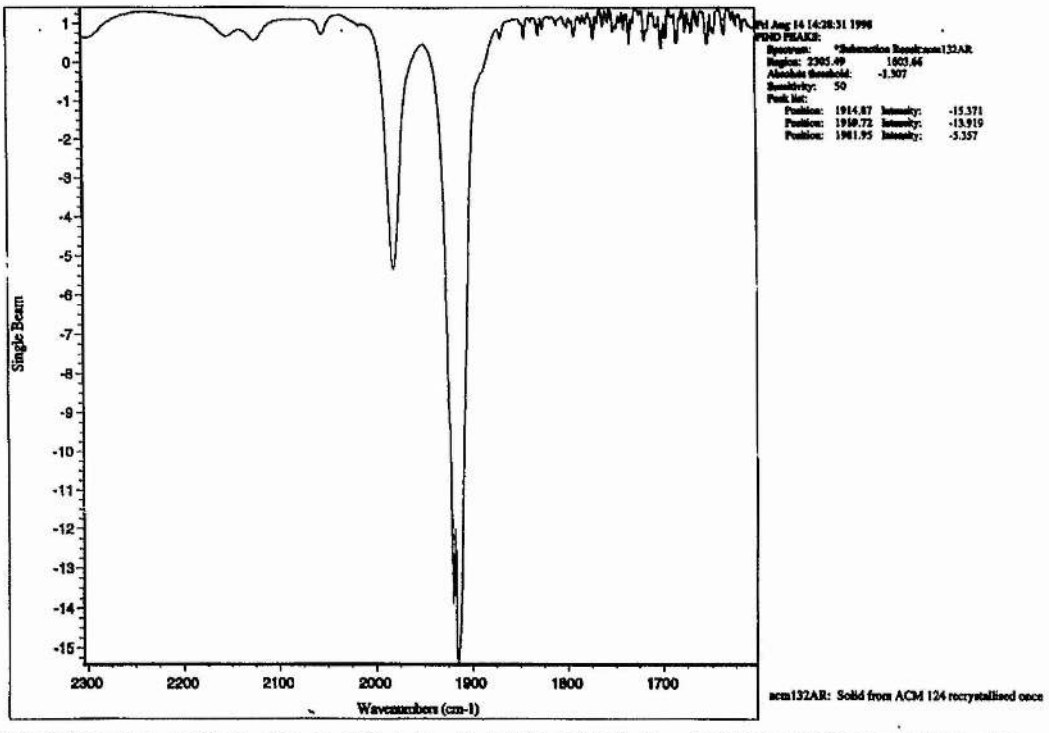

SPECTRUM 16: Recrystallised solid from ACM 124.

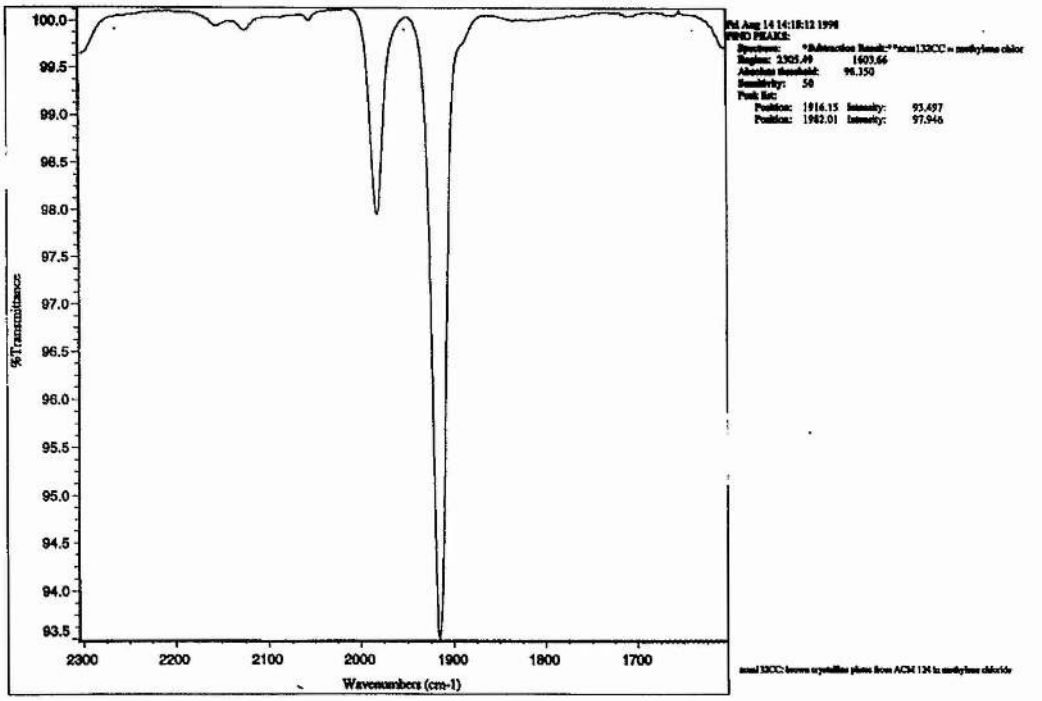

$[Co(PMe_2Ph)_2(CO)_2(I)]$ accounts for one of the peaks detected *in situ* and part of the broad 1985 cm^{-1} peak but cannot account for the whole of the 1985 cm^{-1} peak as the relative intensities of the peaks are reversed in ACM 124.

In addition to the crystals a solid sludge was collected from the methanol solution which was fairly insoluble and its spectrum was recorded as a nujol mull, infrared spectrum 16. The peaks not detected in spectrum 15 were at 1981 and 2002 cm^{-1}. The 1733 cm^{-1} peak was an impurity in the nujol. This sludge is believed to consist of a mixture of the compounds detected *in situ* and decomposition products derived from them. The unknown strong absorption from 1980-90 cm^{-1} is detected but further attempts to purify and characterise this compound failed.

[CpCo(CO)PMe_2Ph] + CO (57 bar) in MeOH / MeI, ACM 191.

The deep red / brown solution from experiment ACM 191 was cathetered from the autoclave under nitrogen and CD_3OD was added to a sample. The ^{13}C and ^{1}H n.m.r. spectra were recorded.

The n.m.r. Spectra:

The proton spectrum was paramagnetically line broadened and only methanol and methyl iodide could be observed. The carbon spectrum was more interesting, see diagram 36. The peak at -24.99 ppm is from methyl iodide and the peaks 48 - 50 ppm are due to methanol and deuterated methanol. The multiplet at 20.28 ppm looks like the second order spectrum expected for PCH_3 in $[Co(CO)_2(PMe_2Ph)_2I]$, this is consistent with the multiple peaks in the PC_6H_5 region, this would give a value of $^{1}J_{C\text{-}P} + {}^{1}J_{C'\text{-}P'}$ of about 142 Hz, this is very similar to the value for $[Co(CO)_2(PMe_2Ph)_2I]$, see section 6.2a ix. That leaves one unassigned peak in the sp^3 carbon region at 19.81 ppm this may be part of a doublet that is overlapping with the peak at 20.28 ppm, this would give a doublet of chemical shift ~ 20.0 ppm. This resonance is downfield with reference to the free phosphine PMe_2Ph (δ_C 14.37, 14.54 ppm in $CDCl_3$ [12]) and this suggests that represents a complexed phosphine ligand, this is backed up by the complexity of the peaks around 130 ppm which cannot be assigned solely to $[Co(CO)_2(PMe_2Ph)_2I]$. The absence of a Cp carbon peak at 83 ppm rules out the starting material [CpCo(CO)PMe_2Ph]. The peak at 92.19 ppm can be assigned to the carbon atoms of a Cp group. The position of the Cp group can tell us something of the nature of the metal centre.

TABLE 3.3: The δ_c of some Cp groups.

Compound	Solvent	δ_c of Cp / ppm
$CpCo(CO)_2$	CD_3OD	85.91
$CpCo(CO)PMe_2Ph$	CD_3OD	82.96
$CpCo(CO)PEt_3$	CD_2Cl_2	81.27
$CpCo(COMe)(PMe_2Ph)I$	CD_2Cl_2	88.81

As the electron density on the metal decreases there is an increase in the value of δ_c for Cp. This would suggest that the 92.19 ppm peak belongs to a Co (III) CpCo compound although it is not [CpCo(COMe)(PMe_2Ph)I] as the spectrum lacks two doublets in the sp^3 region. The ^{13}C n.m.r. spectrum suggests the solution from ACM 191 contains two or three n.m.r. active compounds. We know from the infrared that [$Co(CO)_2(PMe_2Ph)_2I$] is in solution and this explains the multiplet at δ 20.28 ppm. The infrared spectrum also contains a terminal carbonyl absorption at 2053 cm^{-1}, this may be due to the Cp compound [$CpCo(CO)I_2$]. This monocarbonyl may be the origin of the peak at 92.19 ppm. An alternative explanation is that the 92.19 ppm peak is due to a complex without carbonyl ligands such as [$CpCo(PMe_2Ph)I_2$] which may be formed from [$CpCo(PMe_2Ph)I]^-$, a likely product of $[COMe]^+$ loss from [CpCo(COMe)(PMe_2Ph)I], this would be expected to give rise to a doublet and we could assign this species to the peak 19.80 ppm, as it would be expected to have a doublet at ~ 20 ppm.

From the work thus far it is possible to assign the infrared absorption at 1915-17 cm^{-1} to [$Co(CO)_2(PMe_2Ph)_2I$], the assignment of the other infrared stretches observed in solution are based on studies of spectra involving [$CpCo(CO)_2$] and [$Cp^*Co(CO)_2$], these are detailed in later sections.

DIAGRAM 36: ^{13}C N.m.r. of the Solution from ACM 191 in CD_3OD.

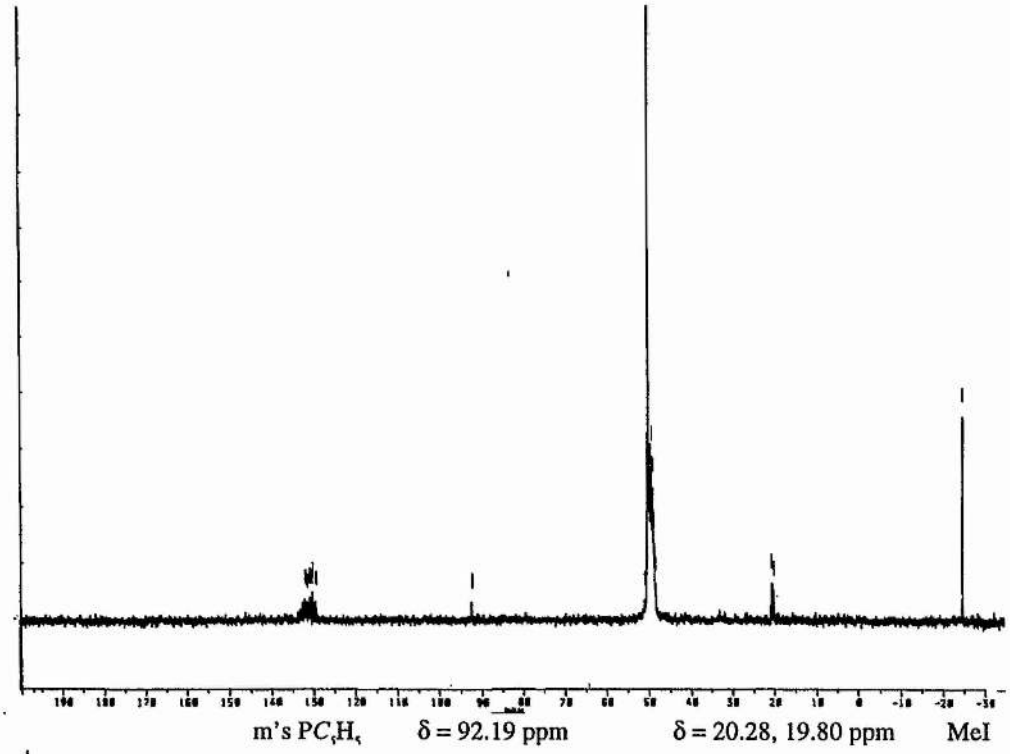

m's PC_5H_5 $\delta = 92.19$ ppm $\delta = 20.28, 19.80$ ppm MeI

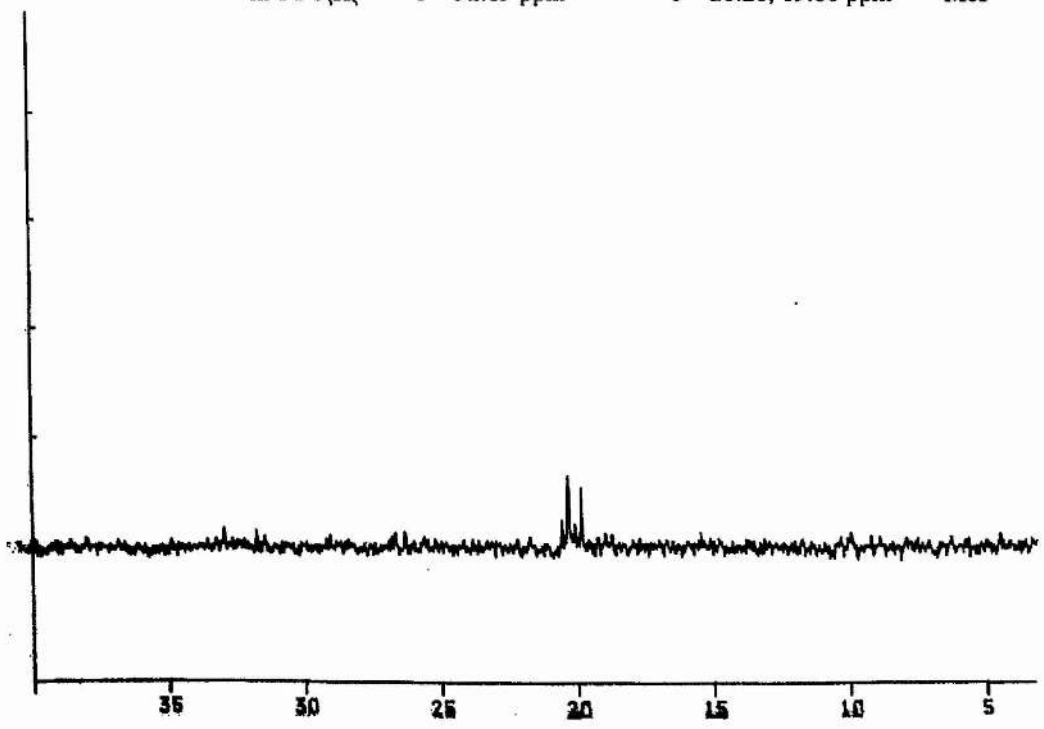

$\delta = 20.28$ ppm, 19.80 ppm

TABLE 3.4: Assignment of ν_{CO} for $CpCo(CO)PMe_2Ph$ *in situ* Infrared Studies.

ν_{CO} / cm^{-1}	Experiment observed	Assignment
1915 - 1917	84, 124	$[Co(CO)_2(PMe_2Ph)_2I]$
1981 - 1984	84 122 124 191	unknown and unstable not detected in the n.m.r.
2024, 2033	84	[CpCo(COMe)(CO)I]
2053	191	$CpCo(CO)I_2$

These assignments are tentative as the compounds, with the exception of $[Co(CO)_2(PMe_2Ph)_2I]$, were unstable in methanol and could not be isolated. R.B King prepared $[CpCo(CO)I_2]$ by oxidatively adding iodine to $[CpCo(CO)_2]$, in KBr ν_{CO} was at 2045 cm^{-1}. [13]

3.2c. Related Experiments.

3.2c i.. Batch Autoclaves [CpCo(CO)P] + Additive. See Table 3.5

We were interested in the effect of various additives on the catalytic activity. The aim of these experiments was to see if the addition of a carefully chosen promoter could greatly increase the rate of carbonylation. All experiments were carried out with the external temperature of the autoclave maintained at 100 °C. When almost one equivalent of free phosphine was added to the catalyst precursor $[CpCo(CO)PEt_3]$ the activity was very successfully enhanced (ACM 32), this experiment was run with only 40 bar CO at room temperature but the system carbonylated methanol at a rate that was more than twice that of $[CpCo(CO)PEt_3]$ alone pressurised with CO (60 bar) (ACM 37). It may be that the addition of free phosphine increases the concentration of $[Co(CO)_2(PEt_3)_2I]$ in solution. To determine the effect of the $[MePEt_3I]$ formed by the reaction of free phosphine and MeI experiment ACM 79 was carried out with $[CpCo(CO)PEt_3]$ + $[MePEt_3I]$ as the catalyst precursor; at 80 bar loading pressure the rate did not approach that measured in ACM 32 although the rate was higher than that measured in ACM 37. We were interested if the effect of the added inorganic iodide involved in the addition of free phosphine to our catalysts and so we tested if LiI was a promoter for carbonylation catalysed by $[CpCo(CO)PMe_2Ph]$. Comparing ACM 80 and ACM 54 (for the catalyst in the absence of

TABLE 3.5: Batch Autoclaves of CpCo(CO)P + Additive as Catalyst in Methanol:

Catalyst + Additive (expressed as molar equivalents)	[Co] / mol dm^{-3}	Expt. No.	Autoclave S = Steel H = Hastelloy	Temp. / °C E=External I = Internal	P / bar RO = Room temp. RE = Reaction Temp.	MeOH / g	MeI / g	Volume / cm^3	Run Time / hr	[MeOAc] / mol dm^{-3}	Rate / mol dm^{-3} hr^{-1}	Rate / turnover hr^{-1}
$CpCo(CO)PEt_3$ + 0.89 PEt_3	0.797	ACM 32	S. 250 cm^3	100 E	40 RO	3.16	2.28	4.8	4	1.700	0.425	0.53
$CpCo(CO)PEt_3$ + 2.70 $MePEt_2I$	0.124	ACM 79	S. 250 cm^3	100 E	80 RO	3.16	1.37	4.60	4	0.145	0.036	0.29
$CpCo(CO)PMe_2Ph$ + 8.70LiI	0.154	ACM 80	S. 250 cm^3	100 E	80 RO	3.16	1.03	4.45	4	0.124	0.031	0.20

promoter) we can see that the conditions of high inorganic iodide and higher CO pressure employed in ACM 80 led to a lower rate of carbonylation.

3.2c ii. The Catalytic Activity of $[Co(CO)_2(PMe_2Ph)_2I]$ see section 2.8b ii.:

The Catalytic activity of the complex was tested in a hastelloy autoclave for a low concentration of catalyst and a 1:4 molar ratio of methyl iodide to methanol. At 100°C and CO (60 bar) loading pressure at room temperature, the catalyst turned over almost 35 times in 24 hours i.e. 1.45 times per hour.

It must be noted that both in turnover frequency and in product identity this system differs from the dicobalt octacarbonyl system. It would appear to be a novel catalytic system. J. Rankin *et al* [14] found that the catalytic precursor $[(PEt_3)_2Rh(Cl)CO]$ was a highly efficient catalyst for the carbonylation of methanol being more active than $[RhI_2(CO)_2]^-$ under comparable conditions.

3.3. DISCUSSION OF RESULTS FROM [CpCo(CO)P] EXPERIMENTS.

3.3a The Batch Autoclaves.

The batch autoclave runs enabled us to recognise the activity of [CpCo(CO)P] systems and compare their selectivity with $[Co_2(CO)_8]$, highlighting the low 1,1-dimethoxyethane production. The results do not warrant any detailed analysis as they were not repeatable. One reason for this was the build up of iodides in the stainless steel reaction vessels, this is avoided by working in hastelloy autoclaves. Another reason for this is the complex decomposition pathways occurring in the reaction solution. These were studied by *in situ* infrared spectroscopy.

3.3b. $[CpCo(CO)PPhMe_2]$ + MeI Under a CO Atmosphere:

All the experiments revealed that the major product of the decomposition of $[CpCo(CO)PPhMe_2]$ in the presence of MeI and CO has a terminal stretching frequency just above 1980 cm^{-1}. It was not possible to isolate and characterise this solid. Solids with similar infrared spectra were obtained throughout the project and are discussed in chapters 4 and 5.

3.3b i. ACM 84: [CpCo(CO)PPhMe$_2$] + MeI in Dichloromethane, Under a CO (60 bar).

When [CpCo(COMe)(PMe$_2$Ph)I] is warmed in dichloromethane and methyl iodide in a CO atmosphere it decomposes to a mixture of complexes. The identity of these compounds is suggested in table 3.4.p96 We believe that there are two side reactions in competition with cleavage of the Co-COMe bond,

i. the cleavage of the Co-PMe$_2$Ph bond,

ii. the displacement of Cp by PMe$_2$Ph.

We believe that the cleavage of the cobalt to phosphorus bond leads to the formation of [CpCo(COMe)(CO)I] and assign the infrared absorptions at 2033 and 2024 cm^{-1} to this species, this spectrum is very similar to that observed for [Cp*Co(COMe)(CO)I] isolated by Haynes *et al.*[15] The displacement of Cp can lead to the formation of small quantities of [Co(CO)$_2$(PMe$_2$Ph)$_2$I]. The mechanism of formation may involve the release of free phosphine followed by subsequent co-ordination to a Co-PMe$_2$Ph complex or it may involve a bimetallic intramolecular exchange of ligands. This type of mechanism has been suggested before by Bergman *et al.* They reported that [CpCo(Me)$_2$PPh$_3$] and [CpCo(CO)$_2$] react to give [CpCo(Me)(μ-CO)]$_2$, and suggested a mechanism involving a dative metal-metal bond to explain this, their mechanism is contained in diagram 37.[16]

DIAGRAM 37: The Rearrangement of $[CpCo(Me)_2PPh_3]$ and $[CpCo(CO)_2]$in to $[CpCo(Me)(\mu\text{-}CO)]_2$ L = PPh_3.

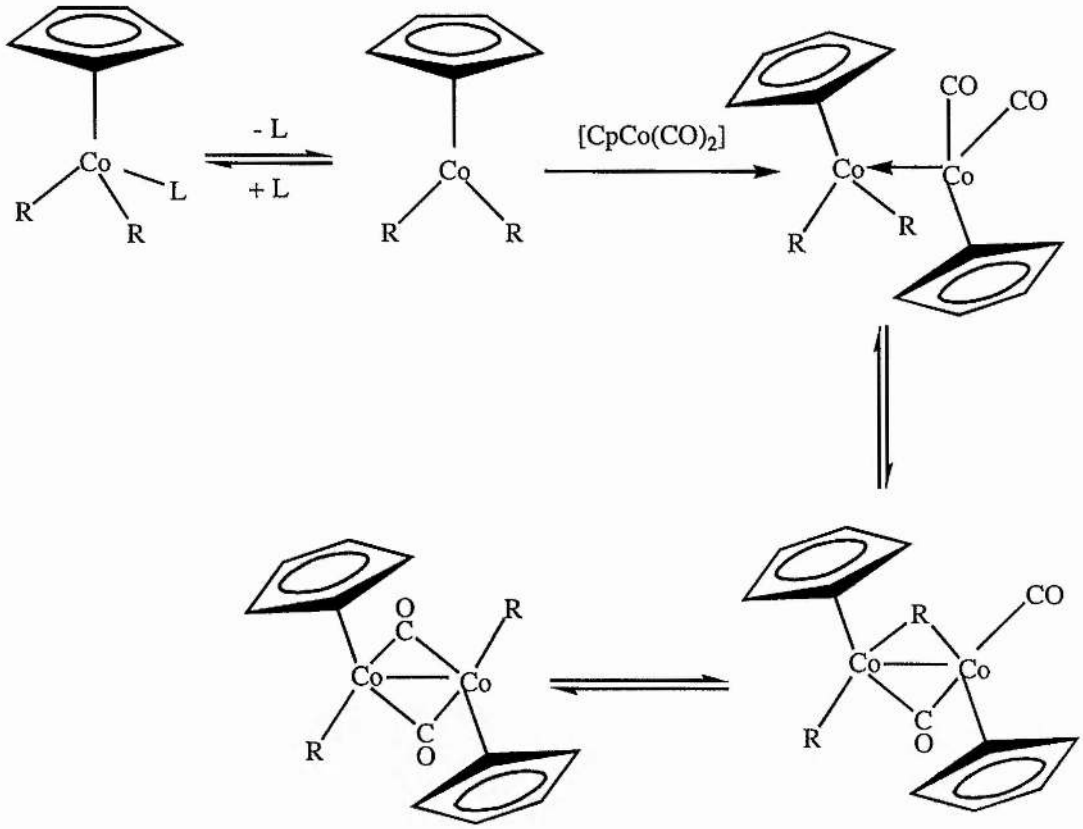

3.3b ii. $[CpCo(CO)PPhMe_2]$ + MeI in Methanol Under a CO Atmosphere:

In methanol the main features of the reaction are the same. The major species in solution is the unknown with ν_{CO} at 1986 cm^{-1}, in addition two other species are detected.

i. In the experiment with CO (60 bar) loading pressure a species is detected with an infrared absorption at 2053 cm^{-1}, this may be $[CpCo(CO)I_2]$. $[CpCo(CO)I_2]$ is formally the product of oxidative addition of iodine to $[CpCo(CO)_2]$ but could be formed from the reaction of [CpCo(CO)] with two equivalents of HI. [CpCo(CO)] is the product of reductive elimination of acetyl iodide from [CpCo(COMe)(CO)I]. An interesting comparison can be drawn between this and the rhodium or iridium catalysed water-gas shift reaction (see sections 1.3e ii. diagram 15 and 1.4c ii. diagram 18). One of the major intermediates in this process, $[M(CO)_2I_4]^-$, has gained two iodide ligands relative to $[M(CO)_2I_2]^-$, the starting material. In the absence of appreciable amounts of water this cobalt (III) compound would be quite stable relative to $[CpCo(CO)_2]$.

ii. In the experiment with loading pressure 10 bar CO more $[Co(CO)_2(PMe_2Ph)_2I]$ was

observed with an infrared absorption at ~ 1915 cm^{-1}. The absence of this absorption at CO (60 bar) in methanol could be explained in a couple of ways. Firstly higher pressures of CO may help to stabilise the CpCo bond by providing alternative reaction pathways i.e. substitution of PMe_2Ph by CO may occur at a faster rate than Cp dissociation by phosphine therefore removing the threat of Cp loss. Secondly the rearrangement of $[CpCo(COMe)(PMe_2Ph)I]$ to $[Co(CO)_2(PMe_2Ph)_2I]$ may occur followed by rapid phosphine loss to yield a monophosphine or cobalt carbonyl. As there was no evidence in the infrared for the formation of tricarbonyl of tetracarbonyl cobalt species the former explanation is more likely.

3.3c Summary.

Although [CpCo(CO)P] compounds can act as catalyst precursors for the catalytic carbonylation of methanol they are unstable under carbonylation conditions.
In most of the catalytic runs very poor rates of carbonylation were measured.
An interesting observation made during these studies was the apparent promotion when PEt_3 was added to $[CpCo(CO)PEt_3]$, we decided to study whether this effect could also be observed on adding PEt_3 to $[CpCo(CO)_2]$ thus removing the need for prior synthesis of $[CpCo(CO)PEt_3]$.

3.4: RESULTS AND DISCUSSIONS FROM THE $[CpCo(CO)_2]$ + PROMOTER CATALYTIC SYSTEM.

3.4a $CpCo(CO)_2$ + Promoter Batch Autoclave Runs

3.4a i. The Addition of PEt_3, See Table 3.6.

If PEt_3 is added to a solution of $[CpCo(CO)_2]$ in methanol and methyl iodide and the solution is heated under CO pressure methyl acetate is formed. At the first glance at table 3.6 the volume of the reaction solutions would appear to be at odds with the composition of the reaction solution. The reason for this reduction in volume is that a proportion of the liquid reactants involved are converted to dissolved solid. When PEt_3 is added to a solution of methanol and methyl iodide most of it reacts with the methyl iodide to generate $[MePEt_3]I$.

$$MeI + PEt_3 \longrightarrow MePEt_3I$$

This is verified by taking the solution and collecting a ^{31}P n.m.r. spectrum. The volume of the solution is therefore more accurately calculated from the volume of methanol plus the volume of methyl iodide minus the volume expected to react with the phosphine and not as the volume of methanol, methyl iodide and phosphine combined.

From the results in table 3.6 ACM 67 and ACM 164 were the most active systems measured by batch autoclave (ACM 180 is calculated from a measure of CO uptake, see section 3.4b). One equivalent of PEt_3 had no significant promoting effect. When the PEt_3 added was increased we observed a marked increase in the rate of catalysis. . When phosphine was added in large excess, 5-10 times the concentration of cobalt, rates of catalytic methyl acetate formation were attained which were much faster than those observed for the [CpCo(CO)P] catalysts. Experiments ACM 67 and ACM 164 illustrate that higher pressures of CO, 80 bar of loading pressure, are required to attain higher rates. The rate measured in experiment ACM 67 is approximate as the methyl acetate generated was far off the our calibration graph for quantifying methyl acetate by g.c. analysis. We had difficulties reproducing this result and reasoned that this was due to catalyst decomposition. The high average rates observed when the autoclave was stopped after 1 hour instead of 4 seemed to support this hypothesis (experiment ACM 164). A very similar experiment run for 17 hours under the same conditions gave a poor turnover per hour. The g.c. analysis of the resulting solutions revealed that the catalyst produced only traces if any 1,1-dimethoxyethane.

3.4a ii. $[CpCo(CO)_2]$ + Iodides, Batch Autoclaves.

A range of iodides were added to $[CpCo(CO)_2]$ in an attempt to initialise the carbonylation of methanol. See Table 3.7.

TABLE 3.6: Batch Autoclaves of $CpCo(CO)_2 + PEt_3$ in methanol.

Expt. No	[Co] / mol dm^{-3}	mass added [PEt_3] / mol dm^{-3}	Autoclave S = Steel H = Hastelloy	Temp. / °C E=External I = Internal	P / bar RO = Room temp. RE = Reaction Temp.	MeOH / g	MeI / g	Volume / cm^3	Run Time / hr	[MeOAc] / mol dm^{-3}	Rate / mol dm^{-3} hr^{-1}	Rate / turnover hr^{-1}
ACM 63	0.219	1.20 g 2.22	S. 250 cm^3	E 100	RO 60	3.16	2.74	4.57	4	0.22	0.055	0.25
ACM 64	0.148	0.08 0.141	S. 250 cm^3	E 100	RO 60	3.16	1.94	4.81	4	0.02	0.005	0.03
ACM 65	0.173	0.88 1.68	S. 250 cm^3	E 100	RO 40	3.16	2.05	4.44	4	0.22	0.055	0.32
ACM 67	0.173	0.88 1.68	S. 250 cm^3	E 100	RO 80	3.16	2.05	4.44	4	~ 1.9	0.48	2.7
ACM 116	0.137	0.80 1.48	H. 28 cm^3	I 100	RO 81	3.16	2.28	4.58	4	0.41	0.103	0.75
ACM 148	0.105	0.56 1.01	H 28 cm^3	I 125	RO 60	3.16	2.28	4.71	24	0.15	0.006	0.06
ACM 164	0.147	0.80 0.79	H 28 cm^3	I 120	RO 80	6.33	2.28	8.58	1	0.81	0.81	5.5
ACM 166	0.188	0.80 0.79	H 28 cm^3	I 120	RO 80	6.33	2.28	8.58	17	0.51	0.030	0.16
ACM 180	0.149	9.150 0.882	H 300 cm^3	I 120	RE 100	65.090	23.590	87.814	4		0.82	5.5

TABLE 3.7: Batch Autoclaves of $CpCo(CO)_2$ + Iodide in methanol.

Expt. No	[Co] / mol dm^{-3}	Promoter [Promoter] / mol dm^{-3}	Autoclave S = Steel H = Hastelloy	Temp. / °C E=External I = Internal	P / bar RO = Room temp. RE = Reaction Temp.	MeOH / g	MeI / g	Volume / cm^3	Run Time / hr	[MeOAc] / mol dm^{-3}	Rate / mol dm^{-3} hr^{-1}	Rate / turnover hr^{-1}
ACM 66	0.186	$MePEt_3I$ 0.506	S 250 cm^3	E 100	RO 40	3.16	2.17	4.95	4	0.05	0.013	0.07
ACM 70	0.120	LiI 1.946	S 250 cm^3	E 100	RO 60	3.16	1.25	4.55	4	0.25	0.063	0.52
ACM 74	0.061	LiI 0.621	S 250 cm^3	E 100	RO 80	3.16	0.73	4.32	4	0.13	0.032	0.51
ACM 77	0.051	LiI 0.51	S 250 cm^3	E 100	RO 80	3.16	1.25	4.55	4	0.07	0.017	0.32
ACM 87	0.107	SnI_2 0.268	S 250 cm^3	E 100	RO 60	3.16	1.32	4.58	4	0.07	0.018	0.17

DIAGRAM 38: ACM 180 CO Uptake of $[CpCo(CO)_2]$ + PEt_3 Catalysed Methanol Carbonylation.

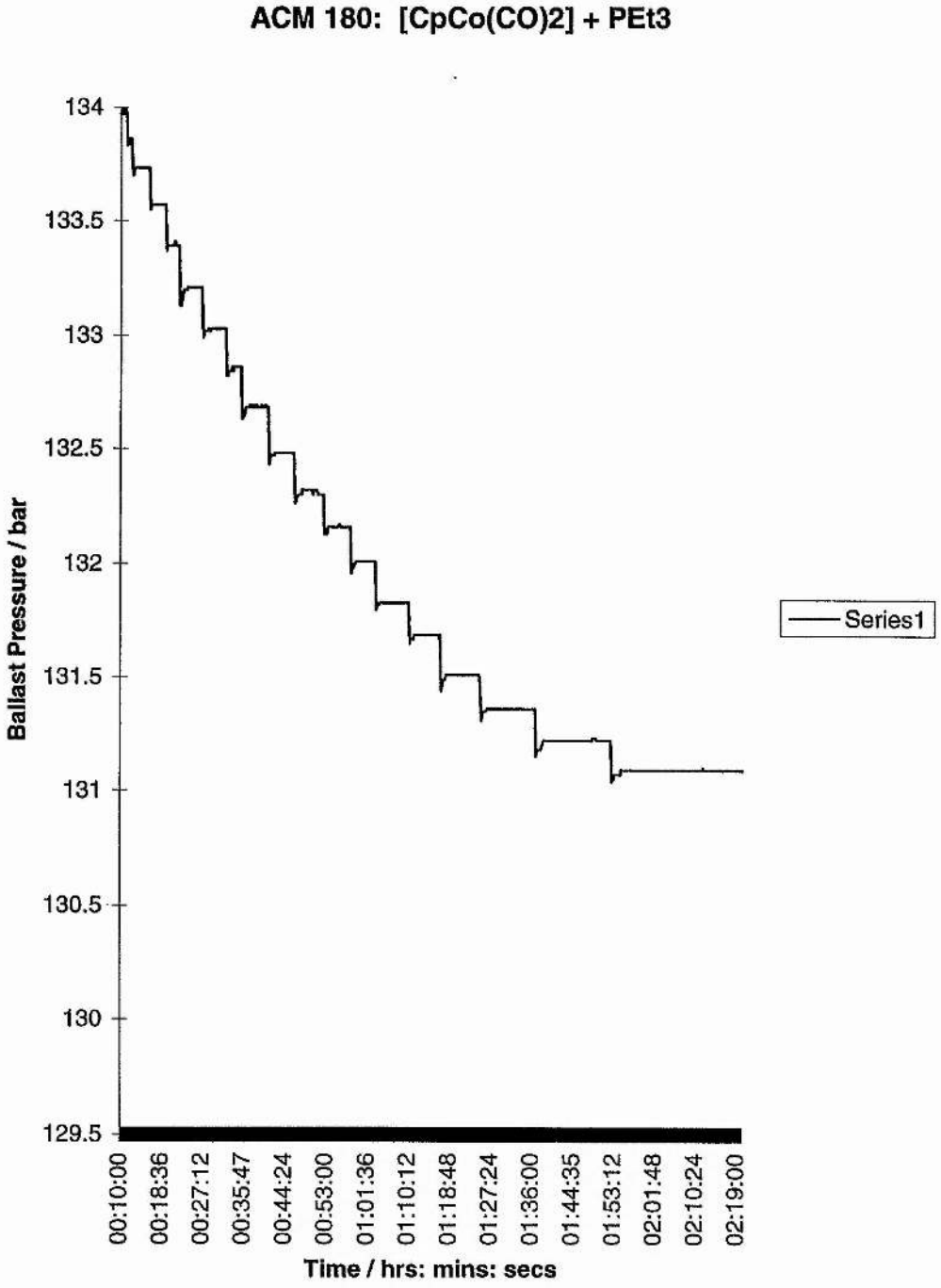

The addition of iodides did initiate catalysis by [$CpCo(CO)_2$]. Particularly effective was the addition of ten equivalents of LiI in ACM 70, 74 and 77. At no time were the kind of rates observed that were observed under similar conditions but in the presence of excess PEt_3, e.g. ACM 67 table 3.6.

The g.c trace from ACM 70 contains essentially no 1,1-dimethoxyethane just dimethyl ether, methanol, methyl iodide, methyl acetate and a trace of a cyclopentadiene breakdown product.

3.4b. Experiment ACM 180, Rate of CO Uptake to a Methanol Solution of [$CpCo(CO)_2$], PEt_3 and MeI.

An experiment to measure the uptake of CO in to the catalytic solution at B.P. Chemicals Hull enabled us to get initial rate data for the reaction ACM 180. The rate observed was similar to that for a one hour batch autoclave experiment. We can see from diagram 38 that the catalyst is dead after 1 hour and 50 minutes.

Comparing the initial rates of carbonylation for [$CpCo(CO)_2$] and [$Co_2(CO)_8$] plus triethyl phosphine (ACM 180 and 181), we see that the rate is slightly higher for the modified [$Co_2(CO)_8$] catalyst. We have already noted the poor stability of [$CpCo(CO)_2$] and conclude that this system needed further improvement.

A detailed analysis of the solution from ACM 180 carried out at B.P. Chemicals Hull will be dealt with in chapter 5.

3.4b Mechanistic Studies on [$CpCo(CO)_2$] + Promoter in Methanol, Methyl Iodide and Under CO.

It was important at this stage to establish what the active species was in the case of the modified [$CpCo(CO)_2$] catalytic systems, and try and determine the slowest step of the catalytic cycle. As before the method we used for this was high pressure infrared spectroscopy.

<u>3.4b i. [$CpCo(CO)_2$] + MeI in Dichloromethane, ACM 85 and 86:</u>

<u>Infrared Spectra 17, 18, 19, 20.</u>

Results:

When [$CpCo(CO)_2$] was heated with methyl iodide in dichloromethane the initial spectrum was that of [$CpCo(CO)_2$], spectrum 17 ν_{CO} 1959, 2024 cm^{-1}. On increasing the

temperature to 60 °C and leaving the autoclave for a few hours two new stretches began to appear as seen in infrared spectrum 18. After a further hour the two new stretches were the only terminal CO stretches in the spectrum (infrared spectrum 19). The position of the stretches were 2043 and 1988 cm^{-1}. On introducing CO, spectrum 20, two major changes occurred. The intensity of the 1988 cm^{-1} peak was reduced and the stretch was shifted to 1985 cm^{-1}. As the 1985 cm^{-1} peak reduced in intensity a new peak grew at 2117 cm^{-1}. The rest of the spectra collected were similar but the terminal carbonyl absorptions reduced in intensity relative to the background noise. The 2117 cm^{-1} absorption decomposed faster than the other stretches. The reduction in relative intensity suggests that the complexes are decomposing and when the autoclave was opened after cooling and degassing a green deposit had formed consistent with the breakdown to Co (II) species.

Discussion:

The peak at 2043 cm^{-1} is at a frequency consistent with a Co (III) complex. The complex could be [CpCo(COMe)(CO)I] or [CpCo(CO)I_2]. In table 3.4 we assigned absorptions in dichloromethane at ν_{co} 2024, 2033 cm^{-1} to [CpCo(COMe)(CO)I] and at ν_{co} 2053 cm^{-1} to [CpCo(CO)I_2]. The absorption at 2043 cm^{-1} is fairly strong in infrared spectrum 19, this spectrum clearly contains an infrared absorption at 1701 cm^{-1}, as do the subsequent spectra 17 and 18, this may be the acyl stretching absorption of [CpCo(COMe)(CO)I]. It seems likely that the 1985 cm^{-1} absorption is the same species observed on decomposing [CpCo(CO)PMe_2Ph] in the presence of MeI. This would suggest that this species does not contain a phosphine ligand. The growth of the peak at 2117 cm^{-1} and the depletion of this peak may suggest that it is a methyl species, this would correlate with its instability towards isolation. From its frequency the species giving rise to the absorption at 2117 cm^{-1} is relatively electron poor and may be cationic. The 2117 cm^{-1} peak may be $[CpCoMe(CO)_2]^+$.but $[CpCo(COMe)(CO)_2]^+$ is also possible. The other carbonyl stretching frequency would be hidden under the broad 2043 cm^{-1} stretch. The analogous species is observed for Cp*.[15] Examining spectrum 20 there does appear to be a shoulder on the high frequency side of the 2043 cm^{-1} absorption which is not evident in spectrum 19.

INFRARED 17: ACM 85 [$CpCo(CO)_2$] + MeI in Dichloromethane, 40 deg.

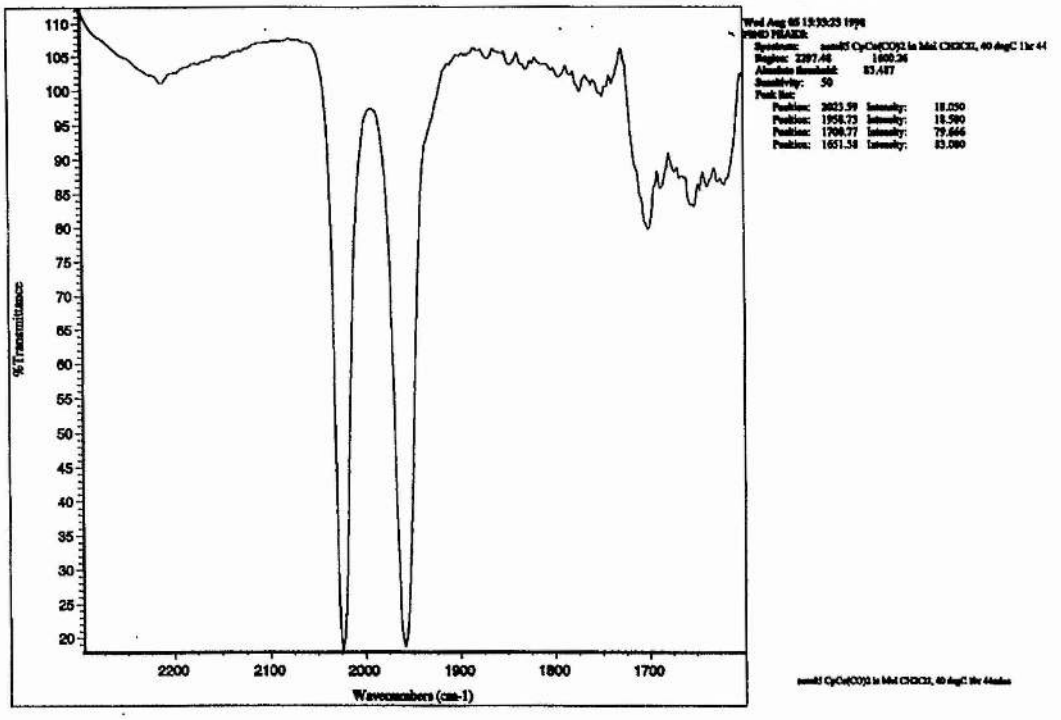

INFRARED 18: ACM 85, 60 degC.

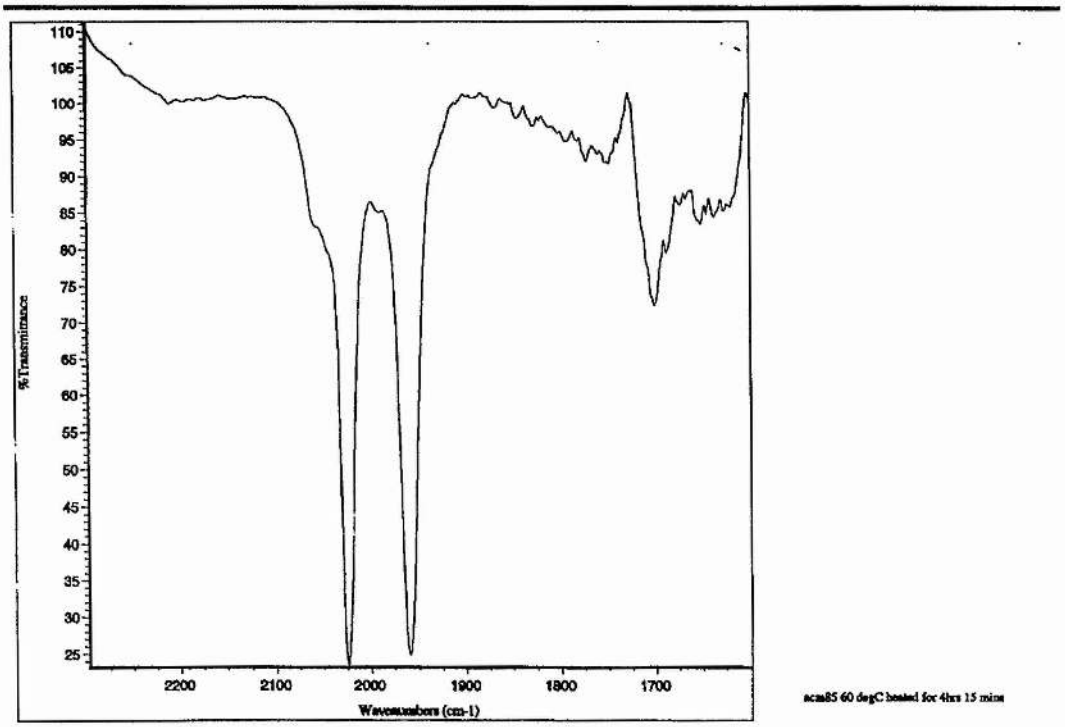

INFRARED 19: ACM 85, 60 degC for 5 hrs. 15 mins.

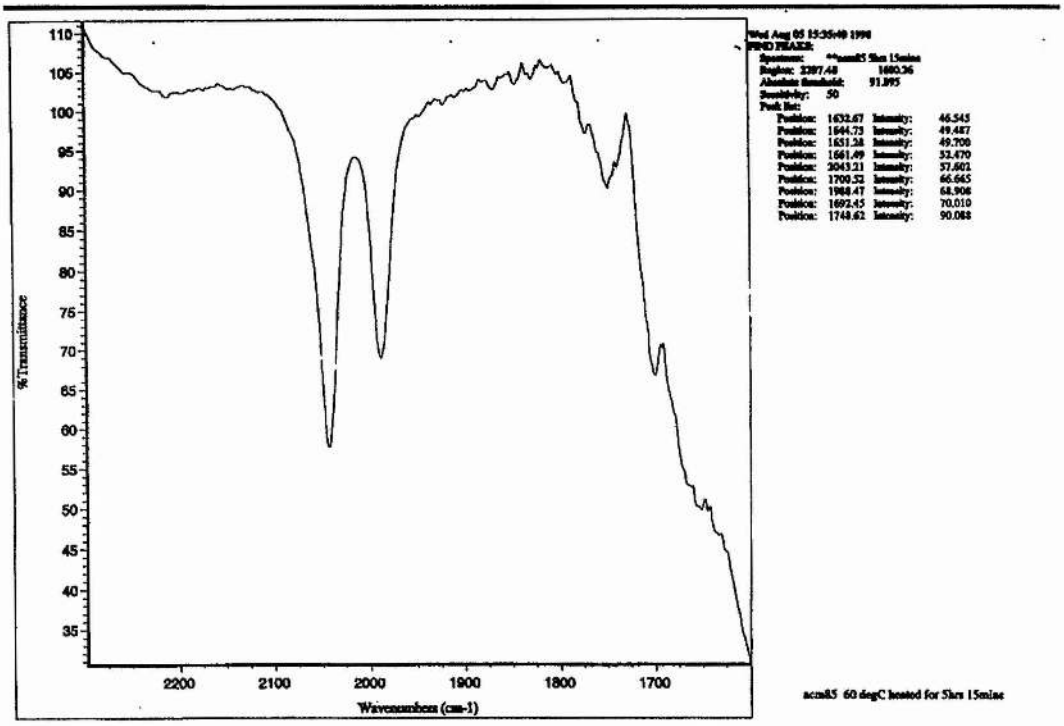

INFRARED 20: ACM 86, ACM 85 + 20 bar CO, room temp.

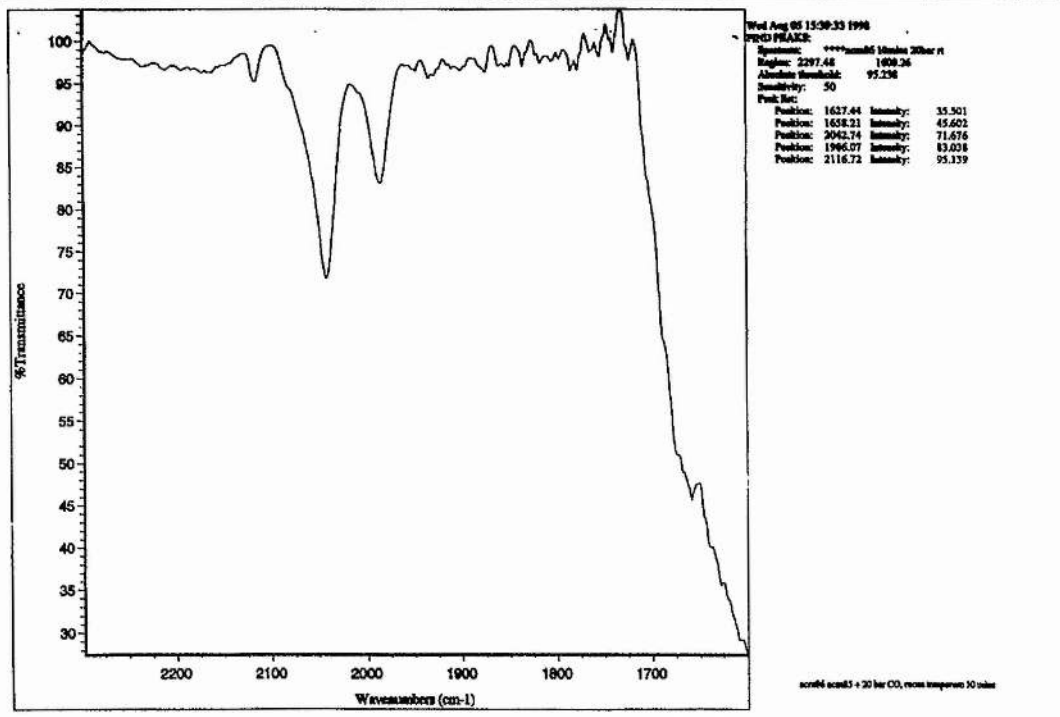

INFRARED 21: ACM 105 $CpCo(CO)_2$ + MeI in Ethanol, room temperature.

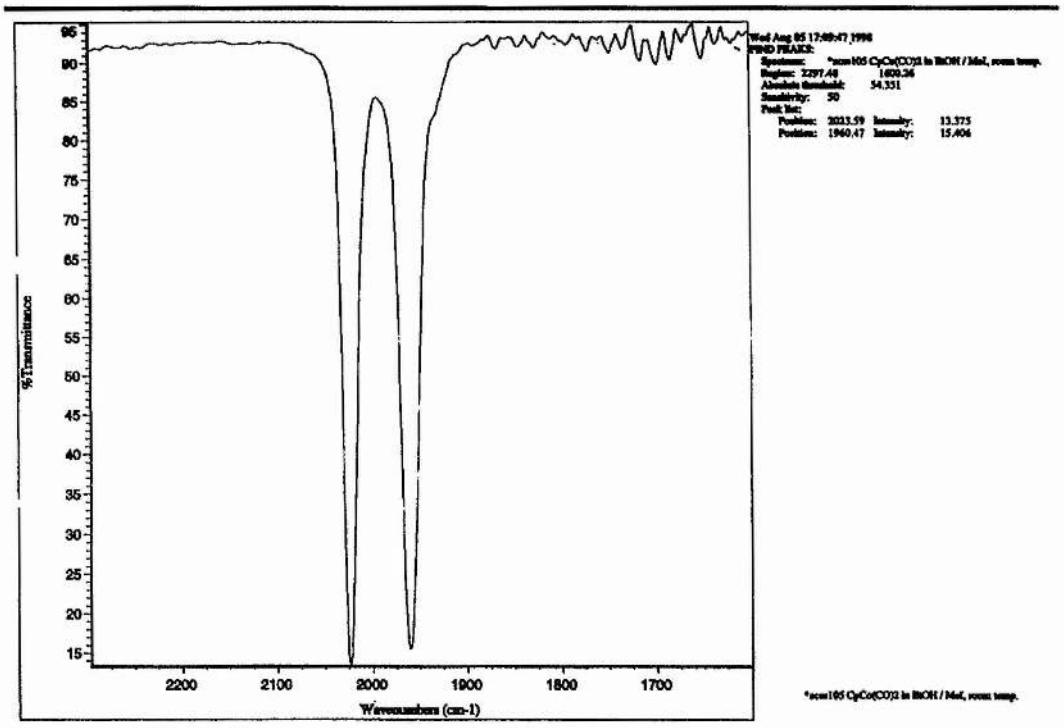

INFRARED 22: ACM 106, ACM 105 + 59 bar CO, 80 degC.

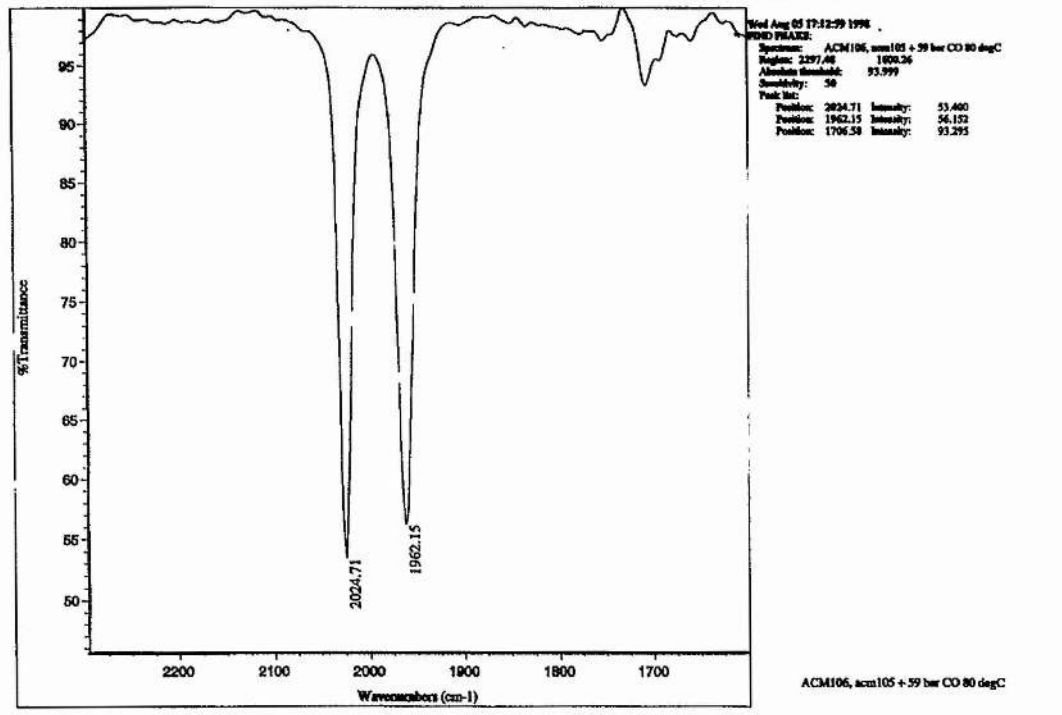

3.4b ii. The Reaction of [$CpCo(CO)_2$] and MeI in Alcohols.

Results.

The Reaction of [$CpCo(CO)_2$] with MeI in Methanol, ACM 133:

[$CpCo(CO)_2$] and MeI were heated slowly to 100 °C in methanol under argon. The terminal carbonyl stretches reduced in intensity as the solution warmed. Once the solution was at 100 °C it was cooled. The red brown solution was transferred to a Schlenk tube under argon and stored at 0 °C. A solid mixture precipitated. An infrared was recorded with a terminal stretch at 1952 cm^{-1}.

The NMR spectrum was consistent with a solid that contained a paramagnetic complex. The solid was re-dissolved in methanol to give a red solution and petrol was added in order to crystallise a solid from the solution, the solution was left in the freezer between -20 and 30°C. After ten weeks a few almost colourless plate and needle crystals had formed. Some of these were removed from the solution. In the absence of methanol the crystals transformed to an opaque green solid, by reintroducing methanol to the atmosphere in the Schlenk tube, (having a methanol pool) the clarity could be restored. The unit cell of these crystals was consistent with a Co (II) centre solvated with methanol, possibly $[Co(MeOH)_6]I_2$, unfortunately the structure could not be solved. [17] This accounts for the paramagnetic n.m.r. spectrum.

[$CpCo(CO)_2$] + MeI in Methanol and Under CO (60 bar), ACM 117:

[$CpCo(CO)_2$] was heated with methyl iodide in methanol under 60 bar of CO. No new terminal carbonyl stretches were observed. The [$CpCo(CO)_2$] stretches disappeared through time.

ACM 119, Attempt to Isolate Products from ACM 117:

The autoclave was cooled and degassed and the brown solution removed and left at 0 °C. After 3 days at 0°C a small quantity of a dark solid had precipitated, more could be collected by cooling the solution to -20°C. Washing the solid with small aliquots of petrol left a red brown solid. The solid was extracted with dichloromethane and an infrared spectrum was recorded. This showed an intense CO stretch at 1951 cm^{-1} not detected in the *in situ* experiment. Stretches were also present at 1694 and 1662 cm^{-1} but only at low intensity. The ^1H n.m.r was recorded of the dark solid in CD_2Cl_2, there was a large peak at 5.36 ppm overlapping with the CD_2Cl_2 peaks. The 1951-1952 cm^{-1} solid observed with or

without CO is probably a decomposition product of [$CpCo(CO)_2$], there is no evidence that it is important in the carbonylation of methanol.

[$CpCo(CO)_2$] + MeI in Ethanol, ACM 105, 106:

Infrared Spectra 21, 22.

The spectra in methanol was very difficult to interpret in the acyl region. In ethanol the spectra were much cleaner: spectra 21, and 22. No novel terminal carbonyl stretches were observed before or after pressurising with CO. There may be a peak around 1707 cm^{-1} in spectrum 22 which may be due the production of a small amount of an acyl species.

Discussion.

From these results it appears that [$CpCo(CO)_2$] does not nucleophilically attack methyl iodide in alcoholic solvents at a significant rate and catalyst decomposition dominates, decomposition is slower in ethanol and may involve protonation of the Cp ring. The lack of nucleophilicity and the instability of [$CpCo(CO)_2$] explains its lack of catalytic activity. In dichloromethane there is some reaction but this is in competition with the decomposition.

3.4b iii. Promotion of Catalysis by PEt_3.

Results.

[$CpCo(CO)_2$] + PEt_3 + MeI in Methanol, ACM 68 and 96:

Infrared Spectra 23, 24, 25, 26, 27.

[$CpCo(CO)_2$] (0.25 cm^3) was dissolved in methanol (8 cm^3) and methyl iodide (2 cm^3) and the solution was cooled in ice. Triethyl phosphine (2 cm^3) was slowly added. The solution was pressurised to 60 bar with CO in the high pressure infrared cell. The experiment was repeated twice, ACM 68 and 96. Experiment ACM 68 did not reveal any new terminal carbonyl stretches just the initiation of catalysis. At 100 °C spectrum 25 may have three terminal CO stretches close to 2000 cm^{-1}. The strong absorption at 1744 cm^{-1} in spectrum 25 is from methyl acetate. In the second experiment the solution was heated more slowly to prevent the swamping of the spectrum by methyl acetate. The resulting spectra infrared spectra 26 and 27 reveal the growth of a stretch at 1985 - 1987 cm^{-1} which is the major species at 82 °C.

Discussion.

There are two major species which are infrared active in the terminal carbonyl region [$CpCo(CO)_2$] and the unknown which absorbs between 1980 and 1990 cm^{-1}. A stretch in this region has been observed for all systems involving Cp ligands. The high concentration of [$CpCo(CO)_2$] terminal carbonyl stretches suggests that methyl iodide oxidative addition is slow and the system may be improved by increasing the electron density and therefore nucleophilicity of the metal centre.

INFRARED 23: ACM 68: $[CpCo(CO)_2]$ + PEt_3 in MeOH / MeI, 60 bar CO, 23 degC.

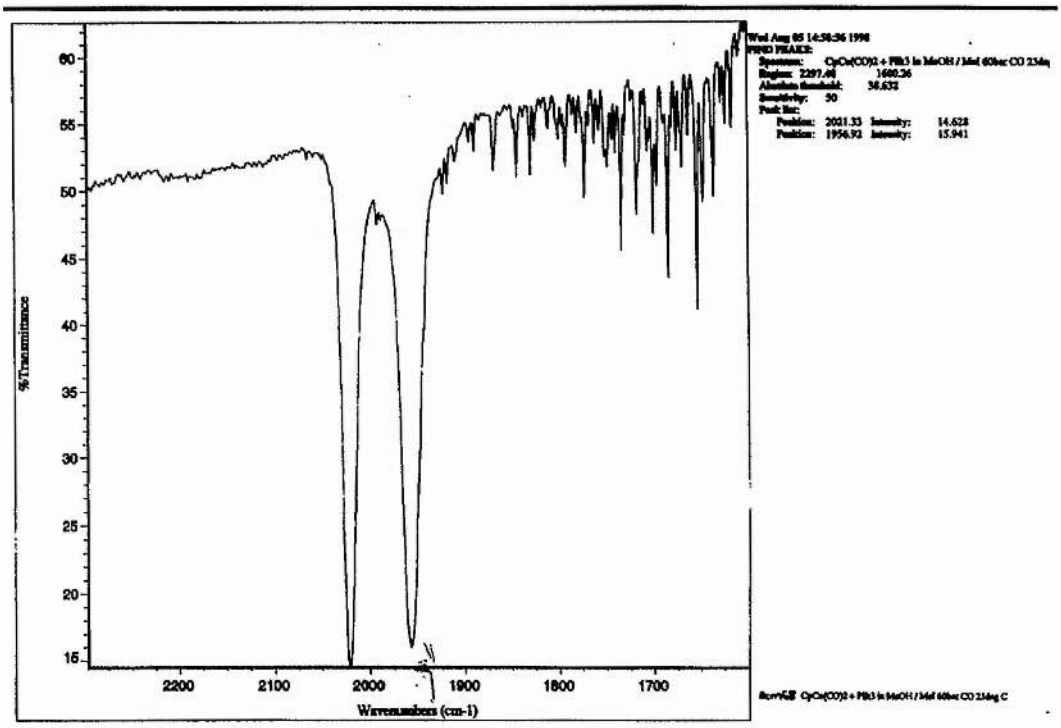

INFRARED 24: ACM 68, 60 degC.

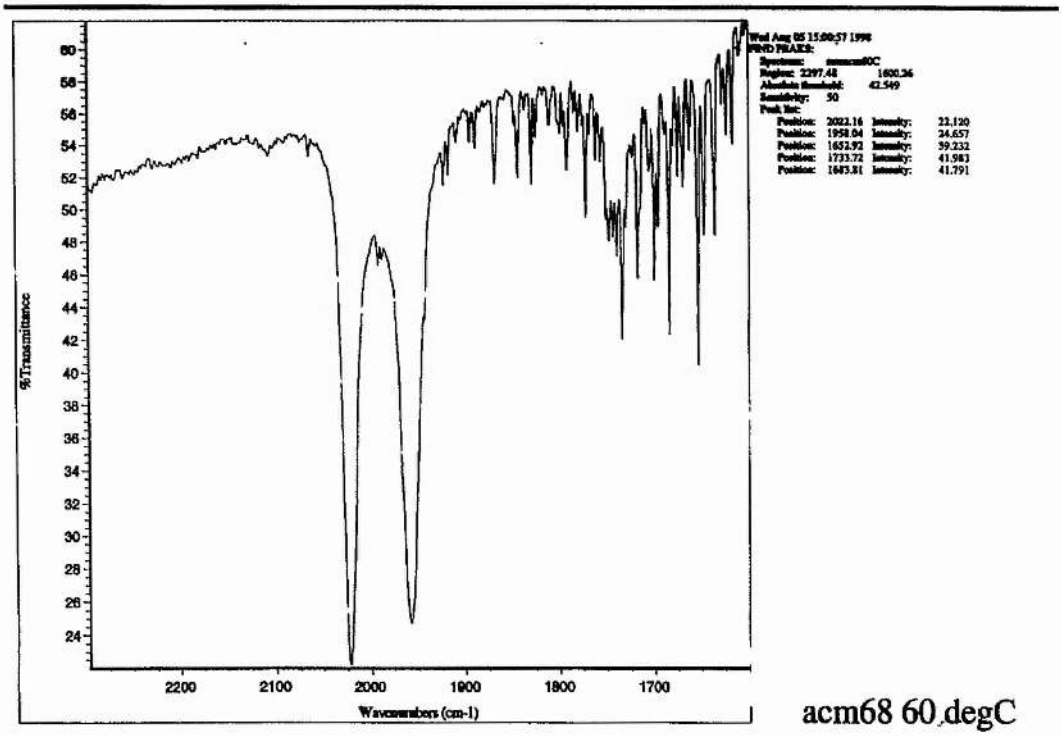

INFRARED 25: ACM 68, 100 °C.

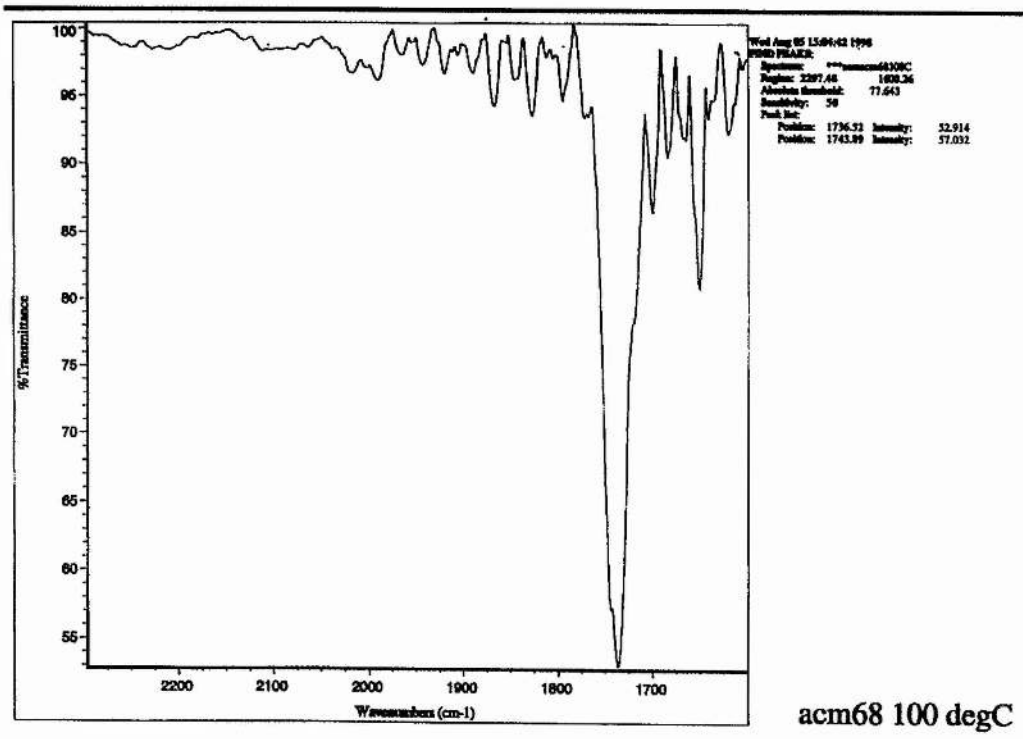

INFRARED 26: ACM 96: $[CpCo(CO)_2]$ + PEt_3 in MeOH / MeI, 60 bar CO, 60 degC.

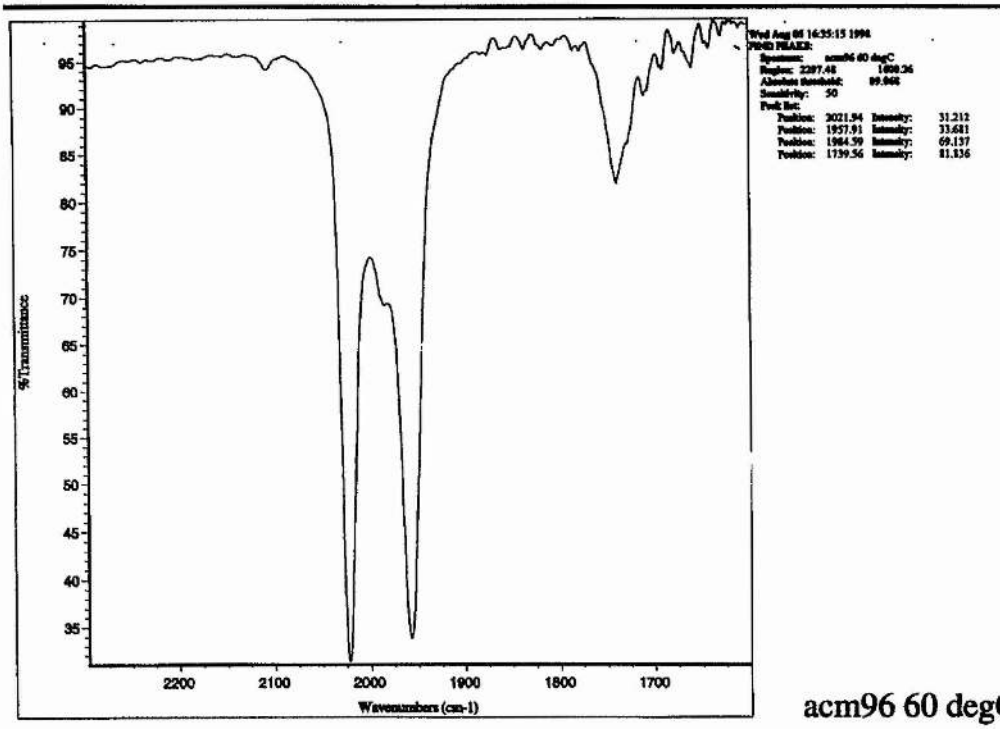

acm96 60 degC

INFRARED 27: ACM 96, 82 degC.

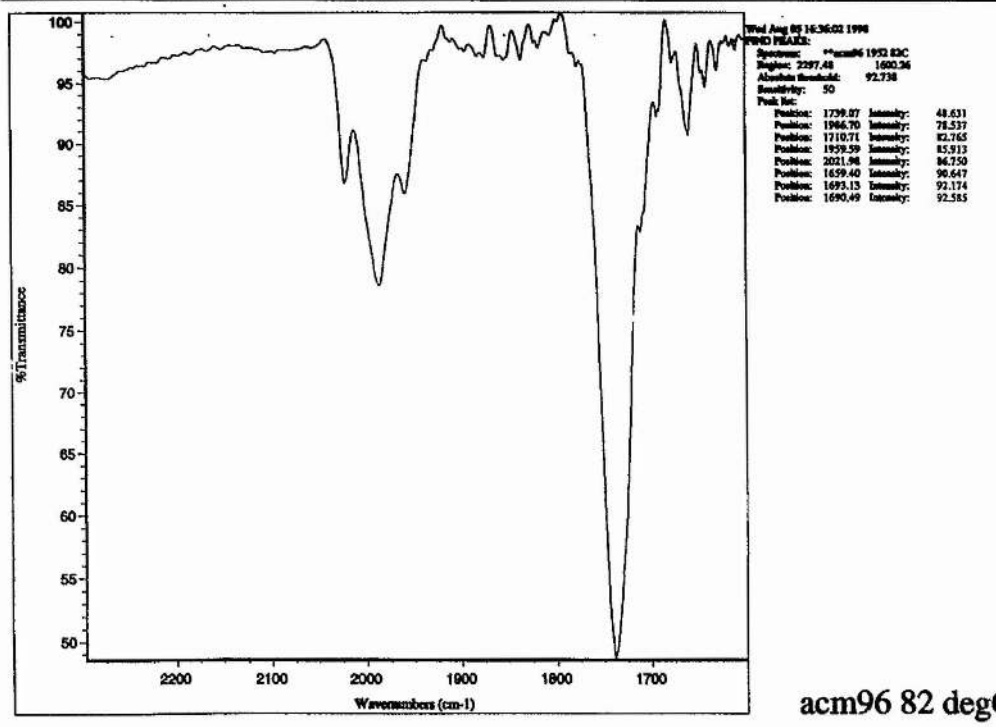

acm96 82 degC

3.4b iv. Promotion of Catalysis by $[MePEt_3]I$.

When triethyl phosphine is added to $[CpCo(CO)_2]$ in methyl iodide and methanol solution a highly exothermic reaction occurs. If the mixture is cooled down then a white solid is observed to form and then re-dissolve. A phosphorus NMR of the catalytic solution reveals only one significant peak at 37.7 ppm indicative of the quaternary phosphonium salt. In order to assess the significance of this compound, we decided to carry out some *in situ* infrared studies on solutions containing the pure compound.

$[CpCo(CO)_2]$ + $[MePEt_3]I$ in Methanol:

$[CpCo(CO)_2]$ + $[MePEt_3]I$ + MeOH + CO (60 bar), ACM 97, Infrared spectrum 28:

$[CpCo(CO)_2]$ and $[MePEt_3]I$ were dissolved in methanol and the solution was injected in to the high pressure infrared vessel. The autoclave was pressurised to 60 bar with CO and heated to 110°C over a period of 2hr 15mins. There was no change detected in the terminal carbonyl stretching frequencies. $[MePEt_3]I$ is not an efficient source of MeI and PEt_3 under the reaction conditions.

$CpCo(CO)_2$ + $[MePEt_3]I$ + MeOH + MeI + CO (60 bar), ACM 98:

Infrared Spectra 29 and 30

The autoclave from the previous experiment was cooled and degassed and methyl iodide was added. As before the autoclave was pressurised with CO and heated. This time there was a gradual increase of a peak at 1735 cm^{-1} indicative of the formation of methyl acetate. The production of methyl acetate was accompanied by the appearance of a very broad weak peak in the 1650 cm^{-1} region. At 104°C there was a significant peak in the acyl region at 1655 cm^{-1} with a lesser peak at 1638 cm^{-1}. Maintaining the temperature above 100°C led to the carbonyl stretches being swamped by organics; just before this happened, a spectrum was recorded which showed the acyl carbonyls at much higher relative intensity than those of $[CpCo(CO)_2]$, infrared spectrum 30.

An organic analysis by g.c. revealed dimethyl ether, methanol, methyl iodide, methyl acetate and a very small concentration of 1,1-dimethoxyethane.

In order to see the cobalt complexes more clearly and give us a greater insight in to the catalytic species, we decided to change the solvent system so that the organics would not grow so rapidly. heptanoic acid, propanol-2-ol and THF do not dissolve significant amounts of $[MePEt_3]I$ so we decided to use ethanol.

INFRARED 28: ACM 97, $[CpCo(CO)_2]$ + $MePEt_3I$ in MeOH, 60 bar CO, 110 degC.

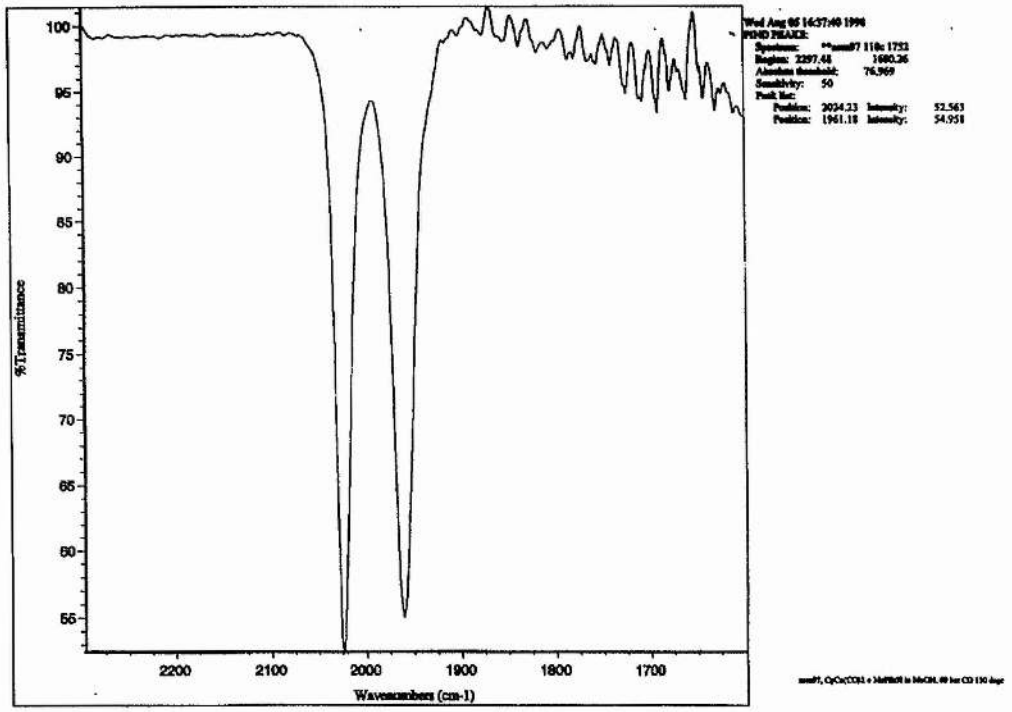

INFRARED 29: ACM 98, ACM 97 + MeI, 60 bar CO, 80 degC.

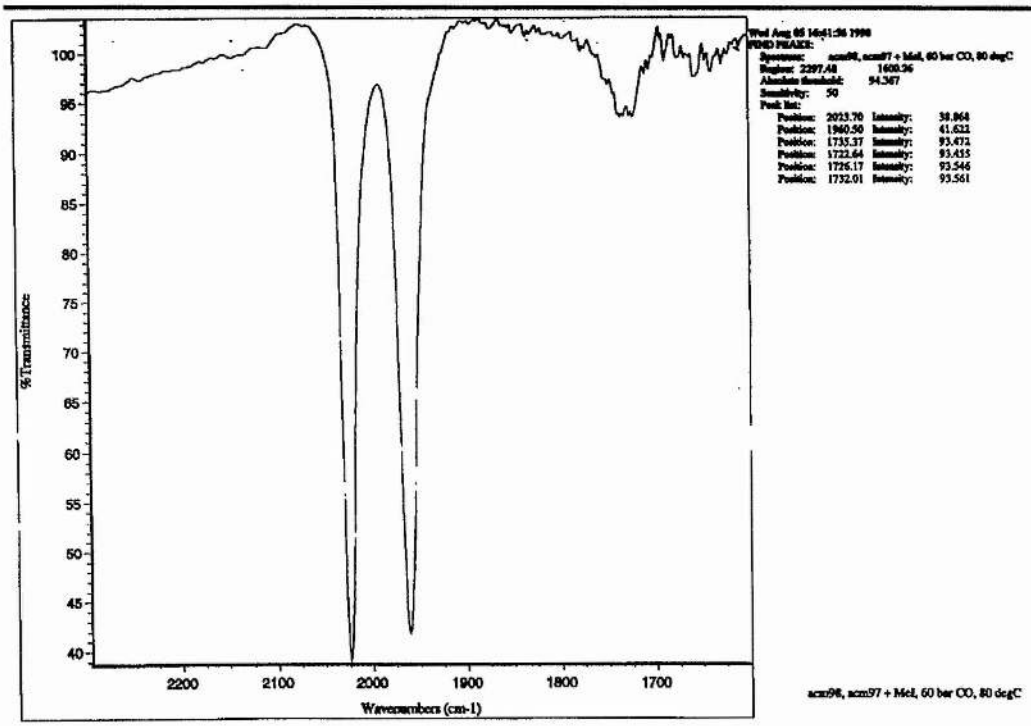

INFRARED 30: ACM 98, 60 bar CO, 104 degC.

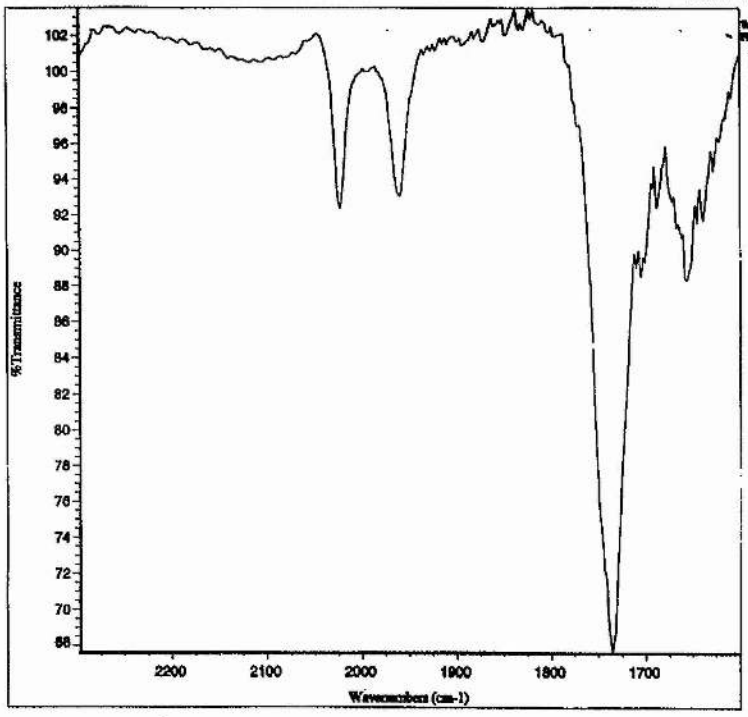

acm98 104 degC

INFRARED 31: ACM 108, [$CpCo(CO)_2$ + $MePEt_3I$ in EtOH / MeI, 58 bar CO, 71 degC for 1 hour.

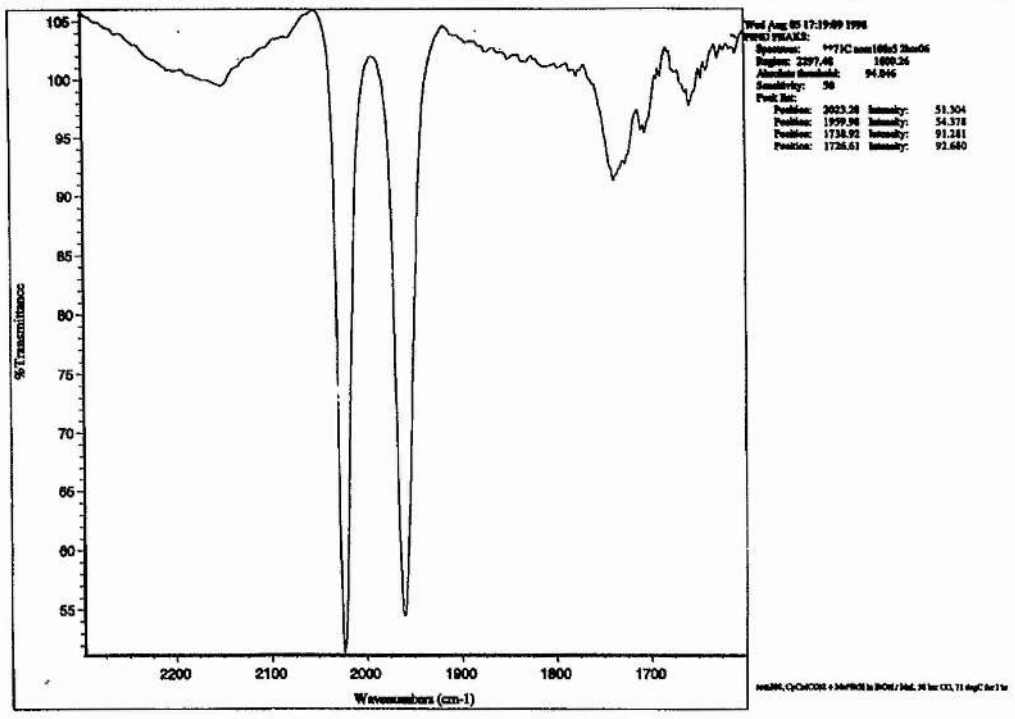

INFRARED 32: ACM 108, 93 degC.

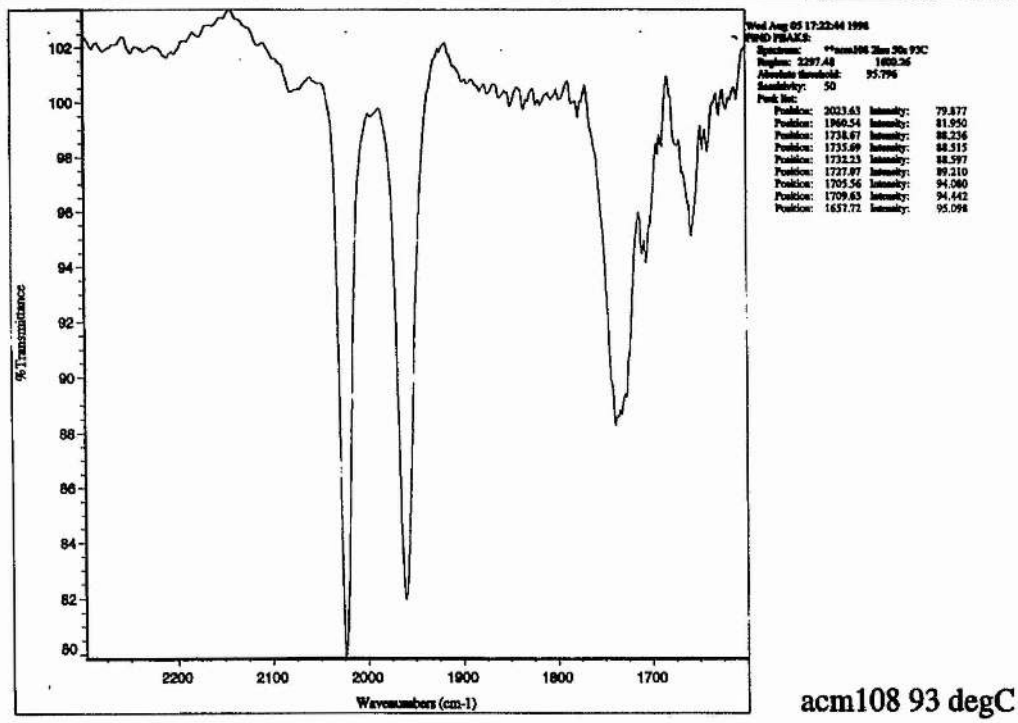

INFRARED 33: ACM 108, 100 degC.

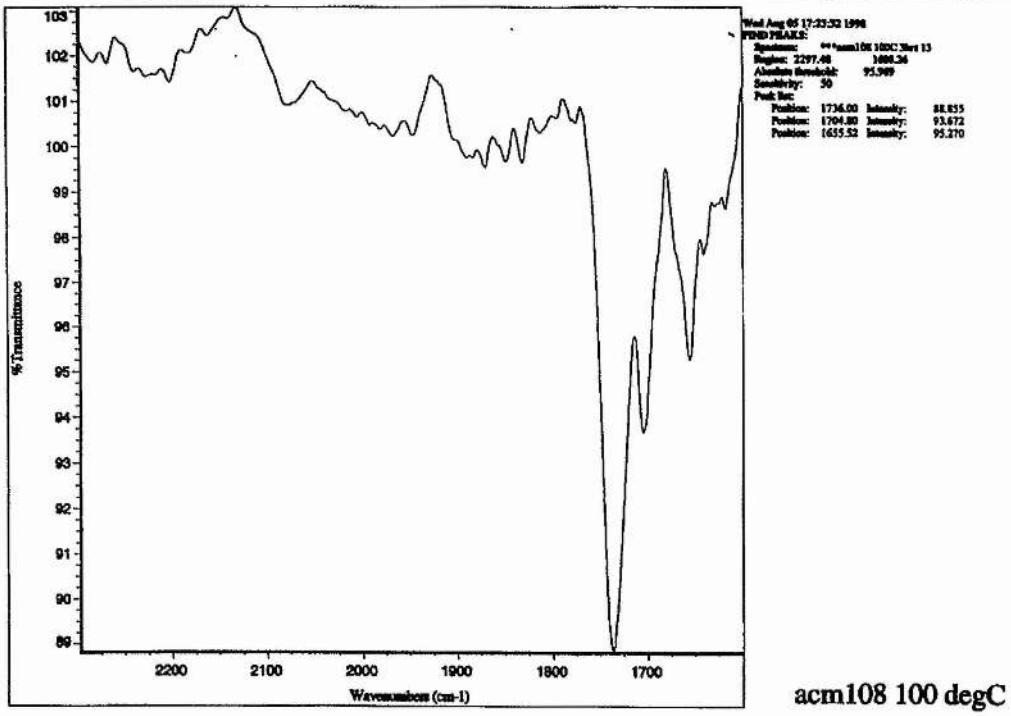

INFRARED 34: ACM 118, [$CpCo(CO)_2$] + LiI in MeOH / MeI, 61 bar CO, 22 degC.

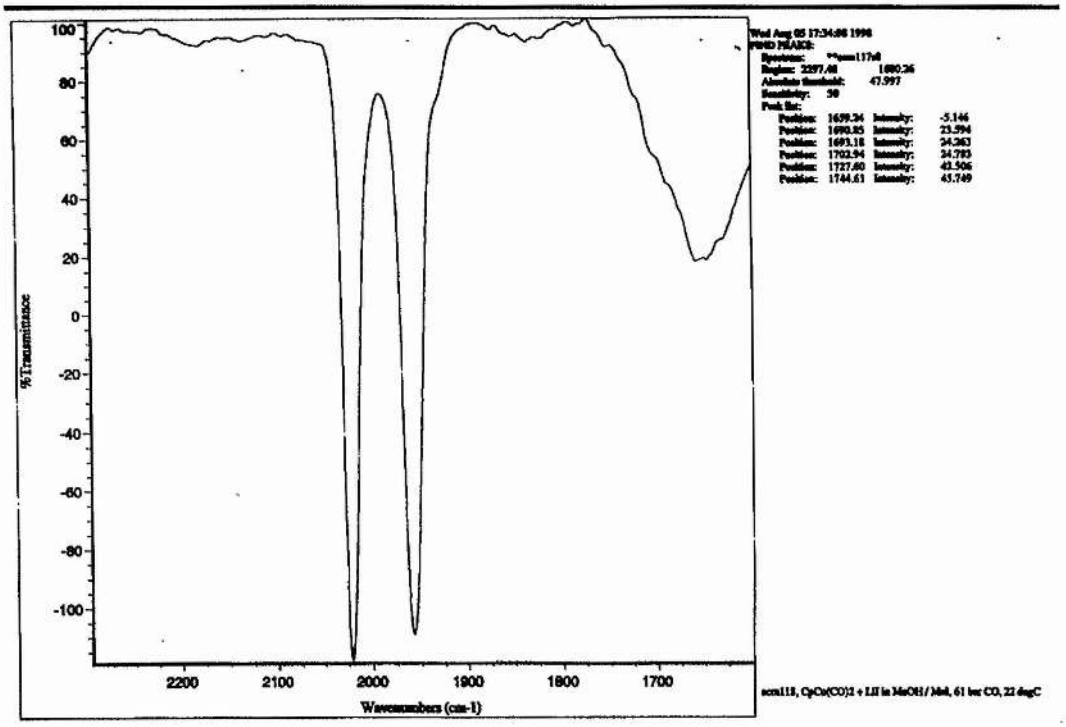

INFRARED 35: ACM 118, 73 degC.

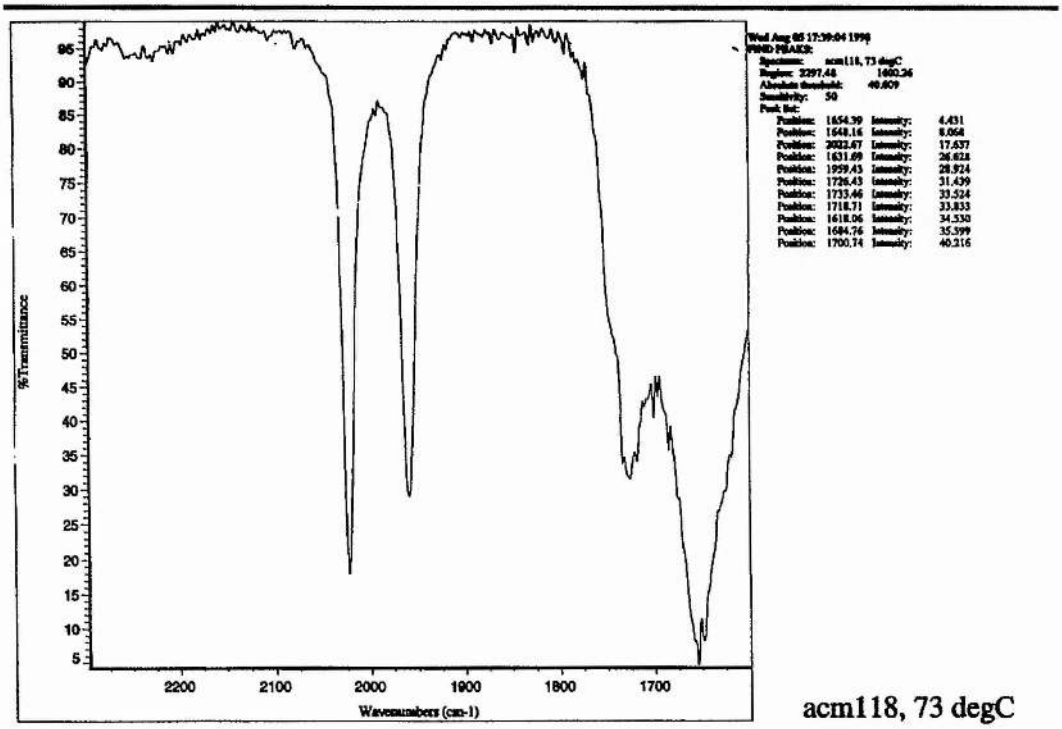

INFRARED 36: ACM 118, 86 degC.

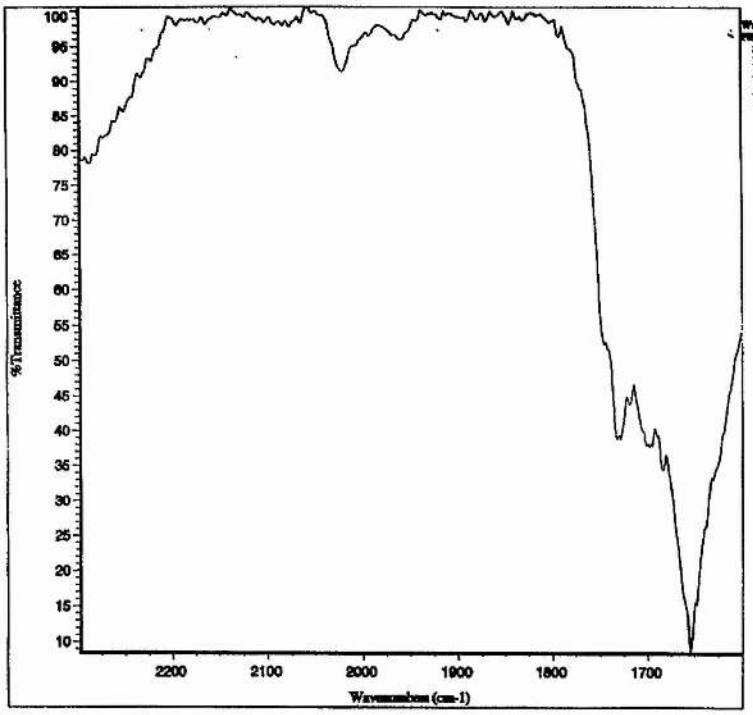

acm118, 86 degC

[$CpCo(CO)_2$] + [$MePEt_3$]I in Ethanol: The Role of Iodide continued.

[$CpCo(CO)_2$] + MeI + EtOH + [$MePEt_3$]I + 58 bar CO, ACM 108:

Infrared Spectra 31, 32 and 33.

[$CpCo(CO)_2$] and [$MePEt_3$]I were dissolved in ethanol and methyl iodide and the solution was injected in to the high pressure infrared vessel. The autoclave was pressurised to 58 bar with CO and heated. On heating to 71 °C, infrared spectrum 31, a peak began to grow at 1739 cm^{-1} indicating the formation of organic acetates. The only terminal stretches were due to [$CpCo(CO)_2$] at 1960 and 2023 cm^{-1}. At 100°C (infrared spectrum 32) peaks were evident at 1656 cm^{-1} and at 1705 cm^{-1}in the acyl region. The peaks due to [$CpCo(CO)_2$] are not obvious in the final spectrum, spectrum 33, which is swamped with ethyl acetate.

Discussion.

This study revealed that the vital components to catalytic activity are [$CpCo(CO)_2$], [$MePEt_3$]I and MeI, free phosphine is not required to generate methyl acetate. The slowest step would appear to be the oxidative addition of methyl iodide. The species with ν_{CO} 1980-90 cm^{-1} was not observed.

3.4b v. Promotion of Catalysis by LiI. Infrared Spectra 34, 35 and 36, ACM 118.

In order to establish whether the [$CpCo(CO)_2$] + [$MePEt_3$]I system is operating as [$CpCo(CO)_2$] + inorganic iodide an *in situ* infrared study was performed on [$CpCo(CO)_2$] + LiI.

[$CpCo(CO)_2$] + MeOH + MeI + LiI, 61 bar CO, ACM 118:

Infrared spectra 35, 36, 37.

Lithium iodide was chosen as it has a high solubility in alcoholic solvents. [$CpCo(CO)_2$] and LiI were dissolved in methanol and methyl iodide and the solution were injected into the high pressure infra red vessel. The autoclave was pressurised to 61 bar with CO and heated. The results obtained were very similar to those obtained with the quaternary phosphonium salt.

Discussion.

$[CpCo(CO)_2]$ + LiI operates as a carbonylation catalyst in a similar way to $[CpCo(CO)_2]$ + $[MePEt_3]I$.

3.4c Discussion of Results

3.4c i. $[CpCo(CO)_2]$:

$[CpCo(CO)_2]$ is not a catalyst for the catalytic carbonylation of methanol as it decomposes faster than it reacts with methyl iodide.

3.4c ii. $[CpCo(CO)_2]$ + Inorganic Iodide:

$[CpCo(CO)_2]$ + inorganic iodide is active for the catalytic carbonylation of methanol. The slowest step is the reaction with methyl iodide as the only terminal carbonyl stretching frequencies detected in the infrared are those associated with $[CpCo(CO)_2]$. In order to increase the rate of carbonylation, iodide must be facilitating the reaction between $[CpCo(CO)_2]$ and methyl iodide. One way in which this promotion may be achieved is via the formation of a highly reactive cobalt intermediate formed by displacement of CO by I^-. 18 electron $[CpCo(CO)I]^-$ would be expected to nucleophilically attack MeI readily. It is very simple to propose a catalytic cycle involving $[CpCo(CO)I]^-$, diagram 39.

DIAGRAM 39: Proposed Mechanism for the $[CpCo(CO)_2] + I^-$ Catalytic Carbonylation of Methanol.

$[CpCo(CO)_2]$ and $[CpCo(CO)I]^-$ may be in equilibrium.

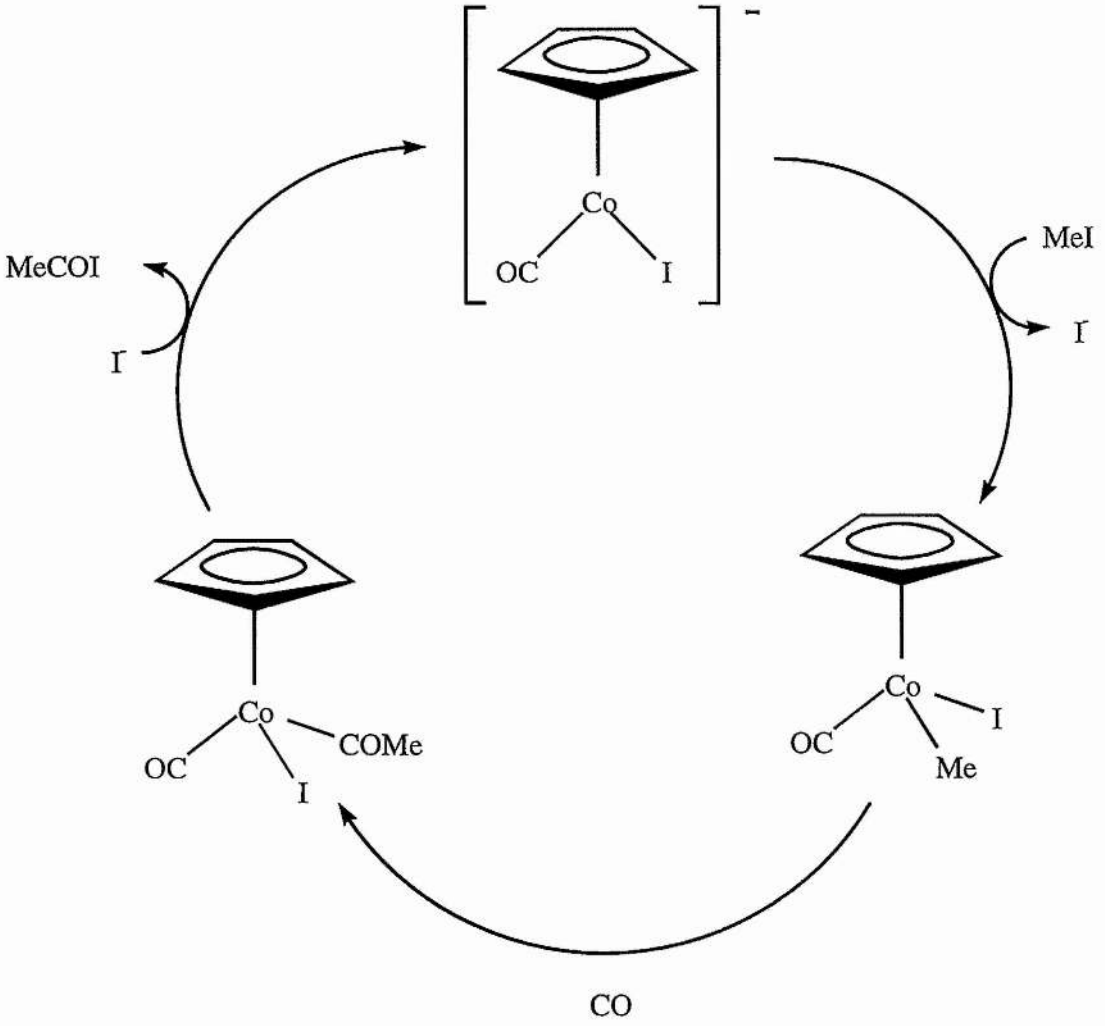

DIAGRAM 40: Possible Equilibrium Between $[CpCo(CO)_2]$ and $[CpCo(CO)I]^-$.

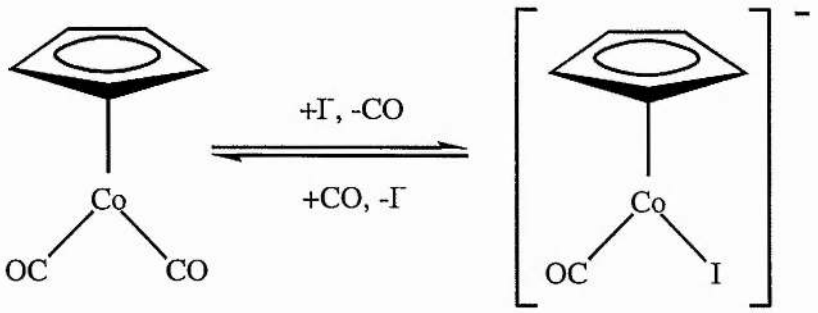

If this equilibrium exists it lies towards $[CpCo(CO)_2]$ under the conditions chosen for the HPIR studies, changes in conditions which increase the concentration of the anion would increase the rate of carbonylation.

3.4c iii. $[CpCo(CO)_2] + PEt_3$:

PEt_3 is the most successful promoter of $[CpCo(CO)_2]$. The high pressure infrared spectra reveal that there are at least two cobalt carbonyl species in solution. The first of these is $[CpCo(CO)_2]$ and this suggests that a $[CpCo(CO)_2]$ + inorganic iodide catalytic system operates. The second is associated with terminal CO stretching frequency ~1985 cm^{-1}. This absorption may be due to the presence of $[CpCo(CO)I]^-$, this would be consistent with the observation of a similar absorption when MeI and $[CpCo(CO)_2]$ were reacted together in dichloromethane ACM 85. The terminal carbonyl stretching absorption of this species may be expected to occur at a lower frequency due to the high electron density on the metal centre and this is only a tentative assignement. This reactive anion may be a result of the rearrangement of [CpCo(COMe)(P)I]. Once formed most of the $[CpCo(CO)I]^-$ would be expected to be converted to inactive $[CpCo(CO)_2]$ due to the equilibrium suggested in diagram 40 p126, this would lead to a reduction in rate. This trend was observed in ACM 180 p105.

3.4c iv. Further Work:

The study of cyclopentadienyl cobalt carbonyl compounds as catalyst precursors has unearthed two new classes of carbonylation catalyst, those involving $[CpCo(CO)_2]$ + inorganic iodide and those involving $[Co(CO)_2(P)_2I]$ catalysts, both are selective catalysts for methanol carbonylation.

As there are no reliable synthetic routes to electron rich compounds of general formula $[Co(CO)_2(P)_2I]$ we decided to develop the cyclopentadienyl cobalt carbonyl chemistry. The major problems with $[CpCo(CO)_2]$ as a catalyst for the carbonylation of methanol are its slow reaction with MeI and its facile decomposition; we hoped to solve both these problems by employing $[Cp^*Co(CO)_2]$ as the catalyst precursor. Pentamethyl cyclopentadienyl is a more basic ligand than cyclopentadienyl and should bond more strongly to cobalt, furthermore its increased basicity should enhance the nucleophilicity of the cobalt centre.

CHAPTER 4: IMPROVING CYCLOPENTADIENYL COBALT CARBONYL CATALYSTS.

4.1 INTRODUCTION.

4.1a. The Pentamethyl Cyclopentadienyl ligand.

The η^5 ligands cyclopentadienyl and pentamethyl cyclopentadienyl have been compared by P.M. Maitis. [1] The Cp* metal complexes are found to be more stable towards ring loss than their Cp analogues. Maitlis attributed the increased stability to the increase in bond strength derived from the greater electron donor power of the ligand and to the increased steric hindrance around the ring which hinders attack at it. The electronic effect is more marked for metals in higher oxidation states. The stability of the compound will also depend on the properties of the particular complex, Maitlis expressed concerns over the stability of the cyclopentadienyl to cobalt bond as Co (II) is a good leaving group.

4.1b Pentamethyl Cyclopentadienyl Cobalt Dicarbonyl, [Cp*Co(CO)$_2$]:

[Cp*Co(CO)$_2$] is easily prepared from [Co$_2$(CO)$_8$]. [2] It is a red brown solid which is stable in air over a few days, this contrasts with [CpCo(CO)$_2$] which is a highly air sensitive dark red oil and illustrates the differences in stability conferred by the two ligands.

4.1c. [Cp*Co(CO)$_2$] + Methyl Iodide.

Considering the desirable stability of the cobalt carbonyl [Cp*Co(CO)$_2$] it is surprising that there is little or no literature on the reaction of [Cp*Co(CO)$_2$] with methyl iodide. Recently A. Haynes *et al* completed a comprehensive study of this reaction the results of which are, as yet, unpublished. [3] They followed the reaction of [Cp*Co(CO)$_2$] and MeI in the infrared by monitoring the changes in the CO absorptions. The reaction proceeds by a mechanism similar to that proposed for [CpCo(CO)P] thus confirming the increased nucleophilicity of [Cp*Co(CO)$_2$] relative to [CpCo(CO)$_2$], diagram 41.

DIAGRAM 41: [Cp*Co(CO)$_2$] + Methyl Iodide:

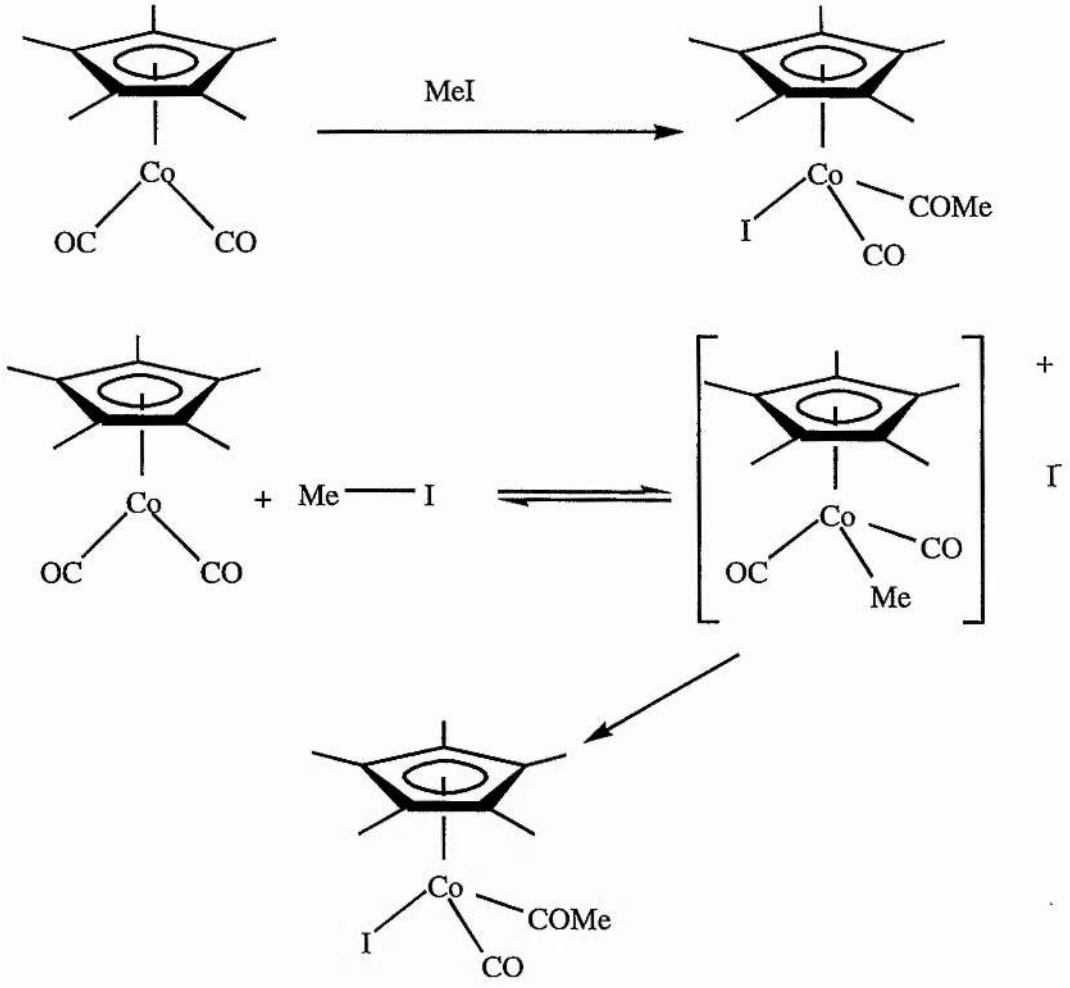

The migration step is rapid and the product observed was [Cp*Co(COMe)(CO)I]. In MeCN and CH_2Cl_2 the reaction is first order in [Cp*Co(CO)$_2$] and MeI suggesting that MeI reductive elimination is not significant. Haynes *et al* followed the reaction of [Cp*Co(CO)$_2$] and [Cp*Rh(CO)$_2$] with MeI in the infrared. They observed the presence of the rhodium intermediate [Cp*Rh(Me)(CO)$_2$]$^+$ when the reaction was carried out in CH_2Cl_2 or MeCN with a relatively high concentration of MeI, the cobalt analogue was not observed suggesting that methyl migration is faster in the cobalt case.

The rhodium and cobalt intermediates [Cp*M(Me)(CO)$_2$]$^+$ were prepared by Haynes *et al* by halide abstraction from [Cp*M(COMe)(CO)I], see diagram 42.

DIAGRAM 42: Synthesis of $[Cp^*M(Me)(CO)_2]^+$

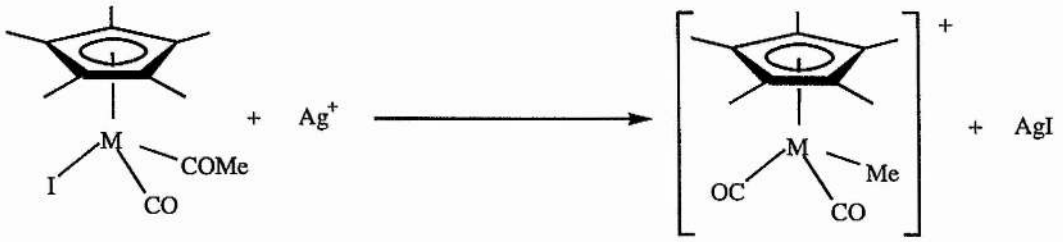

TABLE 4.1: The Infrared Assignments of A. Haynes *et al*:

Complex	Solvent	ν_{CO} / cm^{-1}
$[Cp^*Co(CO)_2]$	CH_2Cl_2, MeCN	1999, 1935
$[Cp^*Co(CO)_2]$	hexane	2008, 1948
$[Cp^*Co(Me)(CO)_2]^+$	CH_2Cl_2	2106, 2076
$[Cp^*Co(COMe)(CO)I]$	CH_2Cl_2	2037, 1668
$[Cp^*Co(COMe)(CO)I]$	MeCN	2035, 1668
$[Cp^*Co(COMe)(CO)I]$	hexane	2043, 1682 (2018, 1697)*

*A Haynes observed two further peaks 2018, 1697 cm^{-1} and suggested they were due to conformational isomers, two sets of absorptions were also observed for the rhodium analogue. The isomers differ in the orientation of COMe relative to the other ligands. The facile reaction between $[Cp^*Co(CO)_2]$ and methyl iodide illustrates the increased electron density on the metal centre compared with $[CpCo(CO)_2]$ which does not react at a significant rate.

4.1d. $[Cp^*Co(CO)_2]$ as a Methanol Carbonylation Catalyst?

The increased reactivity towards methyl iodide and reduction in the rate of decomposition of $[Cp^*Co(CO)_2]$ relative to $[CpCo(CO)_2]$ should make it a more efficient methanol carbonylation catalyst. The facile migratory insertion reaction should further increase rates and may enable this catalyst to operate under conditions that do not tolerate ionic intermediates such as the supercritical carbon dioxide / methanol solvent system.

4.2. RESULTS AND DISCUSSIONS FROM EXPERIMENTS EMPLOYING [$Cp^*Co(CO)_2$] AS A CATALYST PRECURSOR.

4.2a. Batch Autoclaves involving [$Cp^*Co(CO)_2$].

4.2a i. Autoclaves involving just [$Cp^*Co(CO)_2$] as the Catalyst Precursor. Table 4.2.

The results from batch autoclave runs carried out in methanol and methyl iodide are collected in table 4.2.

ACM 150, 151, 24 Hour Run.

The first experiment, ACM 150, involving just [$Cp^*Co(CO)_2$] as a catalyst was carried out for 24 hours at 130 °C in methanol at CO (60 bar) loading pressure in order to establish whether the catalyst was stable. The resulting solution, (~ 2 cm^3) was separated in to two layers an organic layer and an aqueous layer. The main constituents in the liquid fractions were methyl acetate and acetic acid. A g.c. / m.s. analysis suggested that a trace of acetaldehyde had formed.

The conversion of methanol to methyl acetate, water and dimethyl ether had led to the separation of two phases reducing the accuracy of the rate estimate. The high concentration of carbonylated products suggested the catalyst was active for a long period. A similar autoclave was run with dicobalt octacarbonyl as the catalyst precursor. A biphasic product of reduced volume was obtained as before. This time 1,1-dimethoxyethane and acetaldehyde were detected in the product liquor.

ACM 152, 153, [$Cp^*Co(CO)_2$] The Effect of Temperature.

The selectivity of the [$Cp^*Co(CO)_2$] catalytic system was very poor at 100 °C [MeOAc] / [1,1-dimethoxyethane] = 22 . As the temperature was raised the selectivity towards methyl acetate improved [MeOAc] / [1,1-dimethoxyethane] = 79.

The rate however was reduced by increasing the temperature which suggests that the catalyst may be becoming inactive.

TABLE 4.2: Batch Autoclaves of [$Cp^*Co(CO)_2$] in Methanol / Methyl Iodide and Comparison with [$Co_2(CO)_8$].

Expt. No	[Co] / mol dm^{-3}	Autoclave S = Steel H = Hastelloy	Temp. / °C E=External I = Internal	P / bar RO = Room temp. RE = Reaction Temp.	MeOH / g	MeI / g	Volume / cm^3	Run Time / hr	[MeOAc] / mol dm^{-3}	[1,1-dimethoxy ethane] / mol dm^{-3}	Rate / mol dm^{-3} hr^{-1}	Rate / turnover hr^{-1}
ACM 150	0.037	H. 28 cm^3	130-133 I	60 RO	3.16	2.28	5.0	24	3.22	0	0.134	3.6
ACM 152	0.097	H.P.I.R. cell	100-103 I	60 RO 72 RE	6.33	4.56	10.0	1	0.345	0.0155	0.345	3.6
ACM 153	0.031	H. 28 cm^3	140 I	60 RO 85 RE	3.16	2.28	5.0	1	0.055	0.0007	0.055	1.8
ACM 154	0.029	H. 28 cm^3	140 I	60 RO 84 RE	3.56	1.14	5.0	1	0.051	trace	0.051	1.8
ACM 162	0.030	H. 28 cm^3	140 I	80 RO 108 RE	3.16	2.28	5.0	1	0.079	0.0008	0.079`	2.6
[$Co_2(CO)_8$]												
ACM 151	0.045	H. 28 cm^3	140 I	60 RO	3.16	2.28	5.0	24	2.46	0.0015	0.103	2.3

TABLE 4.3 and 4.4: The Composition of the Reactant Solutions and Initial Rate of Carbonylation.

TABLE 4.3: Methanol Based Reaction Solutions. Run at 120 °C and 100 bar at Reaction Temperature.

Expt. No.	Catalyst	Initial [Catalyst] / mol dm^{-3}	Methanol Added/ g	Methyl Iodide Added/ g	Triethyl Phosphine Added/ g	Total Volume/ cm^3	Total Mass/ g	Rate / mol $dm^{-3}hr^{-1}$	Rate/ turnover/ hr
ACM176	$Cp^*Co(CO)_2$	0.088	40.463	1.079	0	51.62	43.65	0.32	3.6
ACM178	$Cp^*Co(CO)_2 + PEt_3$	0.148	32.545	11.730	4.153	44.10	50.06	18.3, 1.06	123, 7.1
ACM179	$Co_2(CO)_8 + PEt_3$	0.148	66.09	23.50	9.28	88.96	101.12	1.36	9.2
ACM180	$CpCo(CO)_2 + PEt_3$	0.149	65.090	23.590	9.150	87.81	100.20	0.82	5.5
ACM181	$Co_2(CO)_8$	0.148	28.877	17.354	0	44.12	47.35	0.64	4.3

TABLE 4.4: Acetic Acid Based Reaction Solutions. Run at 140 °C and 100 bar at Reaction Temperature.

Expt. No.	Catalyst	Initial [catalyst]/ mol dm^{-3}	AcOH Added/ g	MeOAc Added/ g	H_2O Added/ g	MeI Added/ g	Total Volume/ cm^{-3}	Total Mass/ g	Rate/ mol $dm^{-3}hr^{-1}$	Rate/ turnover/ hr
ACM177	$Cp^*Co(CO)_2$	0.133	32.030	7.501	3.525	7.017	45.19	51.58	0.19	1.4
ACM182	$Co_2(CO)_8$	0.134	32.006	7.150	3.553	7.532	45.28	51.28	0.5	3.7

ACM 153, 154, Reducing the [MeI]:

Halving the concentration of methyl iodide in solution appeared to have no effect on the rate. This suggests that under these conditions oxidative addition is not the rate determining step in this system. This means that the rate determining step will involve the reaction of a species with a Co-C bond and is consistent with the production of measurable quantities of 1,1-dimethoxyethane.

ACM 153, 162, Increasing the Concentration of CO:

Increasing the initial pressure of CO enabled us to increase the rate of carbonylation with the increased selectivity associated with the increased temperature.
Getting the CO pressure right for a particular temperature is very important for cobalt catalysed carbonylations as it maximises the concentration of active cobalt carbonyls.

ACM 153, Gaseous Products:

After experiment ACM 153 the autoclave was degassed through toluene and the toluene was analysed by g.c. / m.s. The gas consisted of carbon monoxide, dimethyl ether and traces of carbon dioxide, no methane was detected.

4.2b. Measuring the Rate of CO Uptake.

Experiments ACM 176 and ACM 177 were carried out at B.P. Chemicals, Salt End, Hull in collaboration with Evert Ditzel, technical assistance was given by David Serero. The catalyst, methanol and methyl iodide were all combined and injected in to the autoclave and the autoclave was pressurised to 60 bar with CO and heated to the desired temperature. At temperature the pressure was increased to 100 bar and gas was fed from the ballast to the reaction vessel in order to keep the reaction vessel at constant pressure. A graph was plotted of ballast vessel pressure against time. The composition of the starting solutions and the initial rate results from the experiments conducted at B.P. Hull are contained in tables 4.3 and 4.4. Experiment ACM 180 will be discussed in the next section.

DIAGRAM 43: ACM 176: CO Uptake from a Methanol Solution of [Cp*Co(CO)$_2$] and MeI.

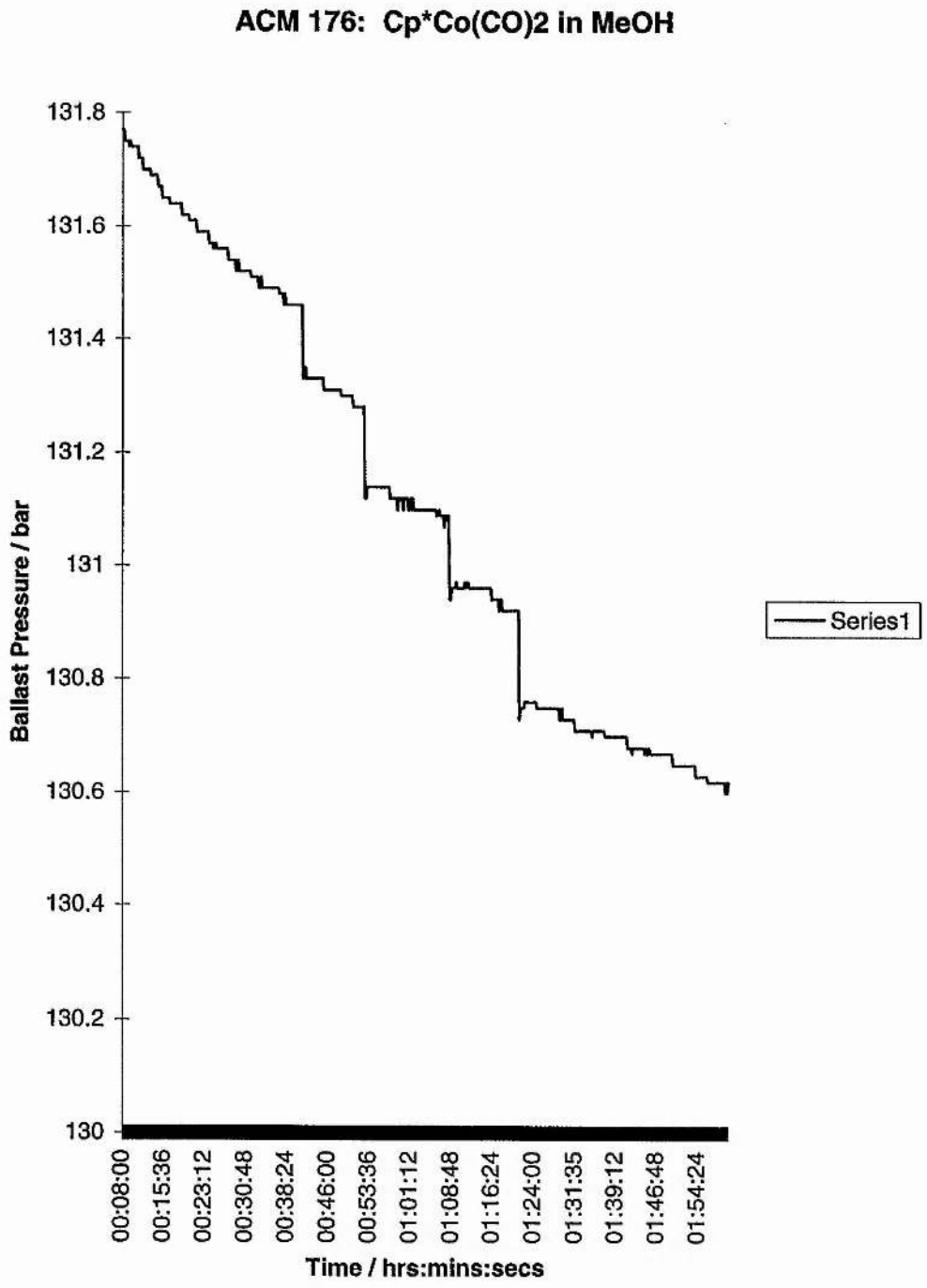

DIAGRAM 44: [$Cp^*Co(CO)_2$] in Low Water Acetic Acid Solvent, Ballast Pressure vs. Time ACM 177.

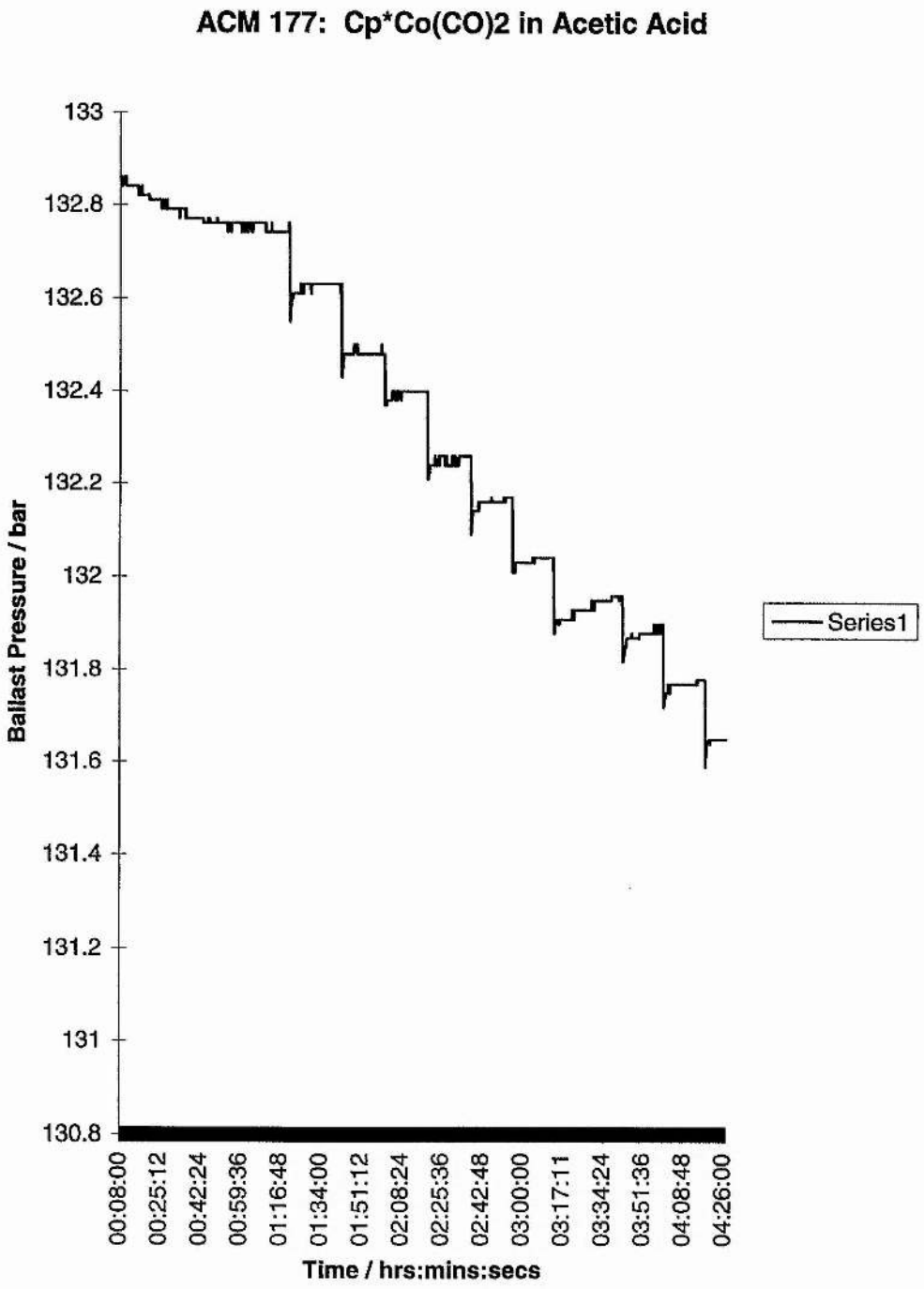

4.2b i. Carbonylation of Methanol in Methanol Solvent, Diagram 43, table 4.3.

This experiment was conducted at 120 °C. The graph of ballast pressure against time is diagram 43. The slowest step under batch autoclave conditions was thought to be reductive elimination as 1,1-dimethoxyethane was formed as a side product, (as in the $[Co_2(CO)_8]$ case, chapter 2). It was hoped that a reduction in the concentration of methyl iodide would improve selectivity. The Co : MeI ratio in this reaction is 1 : 1.6. A rate of 3.6 turnovers per hour was obtained, the initial rate is very similar to the average rates measured during the batch autoclave runs. It is difficult to draw conclusions from pressure rate graph because of its erratic shape, this is the result of the opening and closing of the valve between the ballast and reaction vessels. It seems that the rate has decayed slightly over the one and a half hours, this may be the effect of a reduction in [methanol] and increase in [methyl acetate]. The rate may depend on [methanol].

4.2b ii. ACM 177 Catalysis in Acetic Acid, Diagram 44, table 4.4.

The industrial solvent for methanol carbonylation consists of a mixture of acetic acid, methyl acetate, water and methyl iodide. The methanol is tied up in the form of methyl acetate and the methyl acetate reacts with HI to generate MeI, the active species. The Monsanto catalyst requires relatively high concentrations of water, > 15 % w/w in order to prevent it from being reduced to inactive Rh (III) but these high concentrations of water are expensive to remove from the product mixture. We therefore decided to test our catalysts in a low water acetic acid solvent to see if they presented any advantages over rhodium catalysts.

This experiment was conducted at 140 °C. The rates of carbonylation were very poor and the ballast vessel pressure against time graphs were correspondingly poor as the apparatus had problems regulating such a slow rate of CO flow, see diagram 44. The rate of carbonylation in this solvent system (1.4 turnovers per hour) was lower than the rate in pure methanol. The rate in low water acetic acid is fairly constant throughout the catalytic run. This suggests that the catalyst is stable for four hours at 140 °C at 100 bar. The conditions change very little throughout the run as the rate of carbonylation is so low. The reduction in rate compared with ACM 176, run in methanol may be due to the decrease in the concentration of methanol.

4.2c. Mechanistic Studies on [Cp*Co(CO)$_2$] as a catalyst for Methanol Carbonylation.

The rate data obtained for [Cp*Co(CO)$_2$] as a catalyst precursor for methanol carbonylation were very similar in activity and selectivity to those obtained for [Co$_2$(CO)$_8$] and it was vital to ascertain whether we were observing a novel system or just [Co$_2$(CO)$_8$] . The best technique for investigating the species present during catalytic process is high pressure infrared spectroscopy.

4.2c i. Mechanistic Studies on [Cp*Co(CO)$_2$] + MeI in Dichloromethane, High Pressure Infrared Spectra.

[Cp*Co(CO)$_2$] + MeI in CH_2Cl_2 Under CO, ACM 189:

[Cp*Co(CO)$_2$] was dissolved in methyl iodide and dichloromethane and pressurised to 77 bar with CO. An infrared spectrum was collected, see infrared spectrum 37. The major peaks were 2039 and 2018 cm^{-1}, there was also a small peak at 2117 cm^{-1}. At 70 °C the peak at 2117 cm^{-1} was more obvious and the carbonyl stretches appeared more complex. At 80 °C the complexity was no longer observed and the absorption appeared as one stretch which persisted to 120 °C, the well defined absorptions being at 2052 and 2117 cm^{-1}, infrared spectrum 39. The autoclave was cooled and degassed under argon. The infrared spectrum gave two well defined absorptions at 2053 cm^{-1} and 2118 cm^{-1}, infrared spectrum 40.

Assigning the Spectra, Analysing the Reactant and Product Solutions: Infrared Spectra.

The initial reactant solution ACM 189A:

A sample of the initial reaction solution prior to injecting in to the HPIR autoclave was analysed by infrared spectrum 41, the major terminal absorptions in dichloromethane were 2038 and 2023 cm^{-1}. There were also considerable absorption in the acyl region centred around 1670 cm^{-1}, The n.m.r. spectrum of this solution was also recorded, see below.

INFRARED 37: ACM 189: [Cp*Co(CO)$_2$] + MeI in Dichloromethane, 77 bar CO, 23 °C.

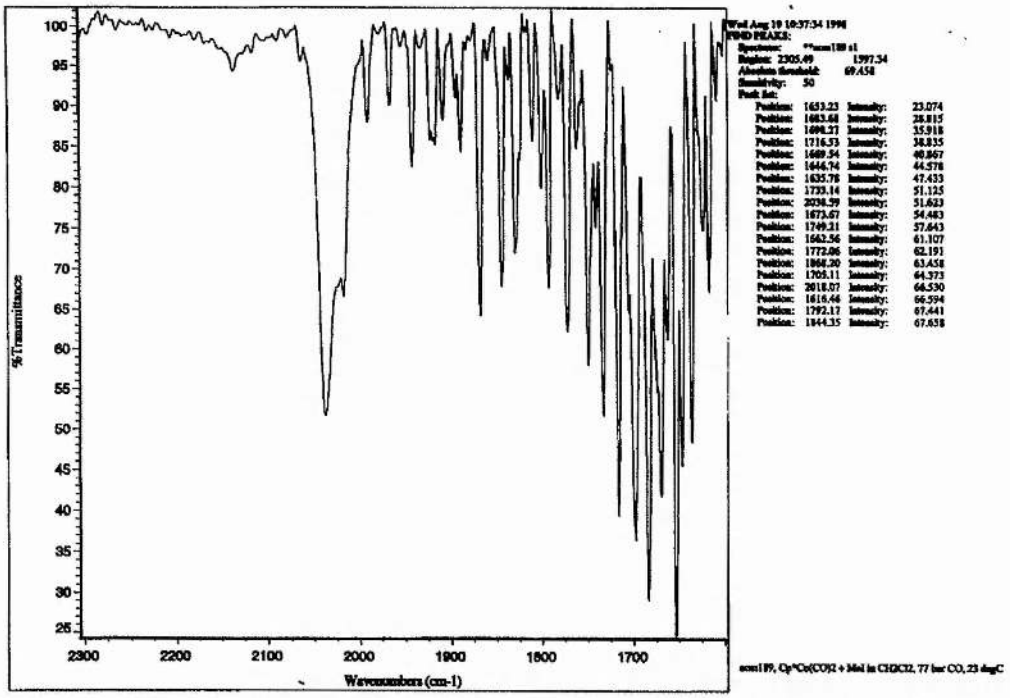

DIAGRAM 38: ACM 189, 70 °C.

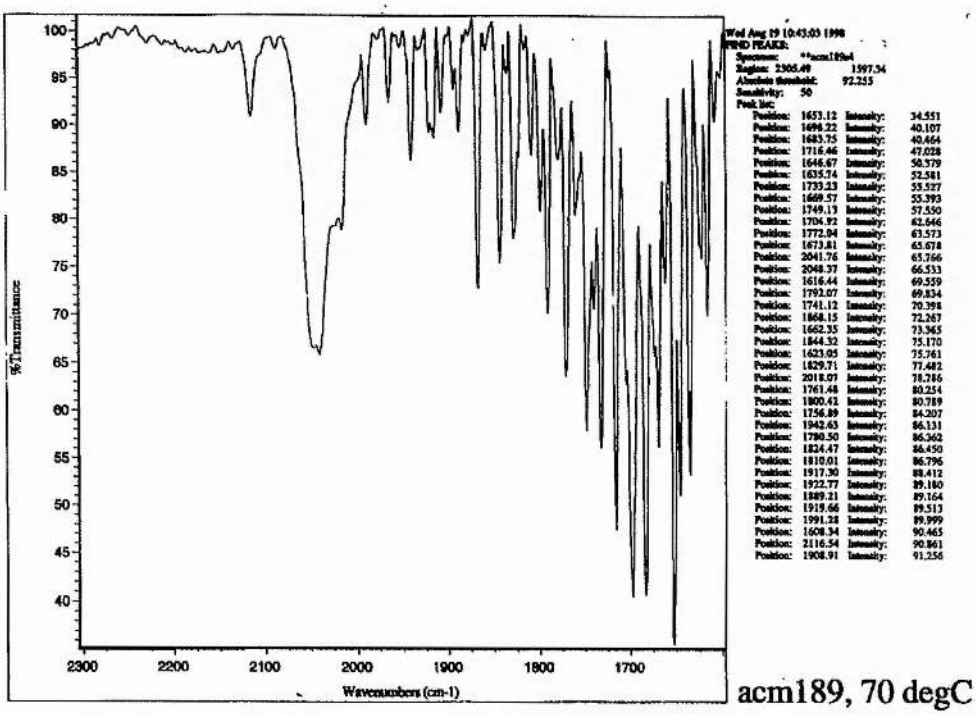

INFRARED 39: ACM 189, 120 °C

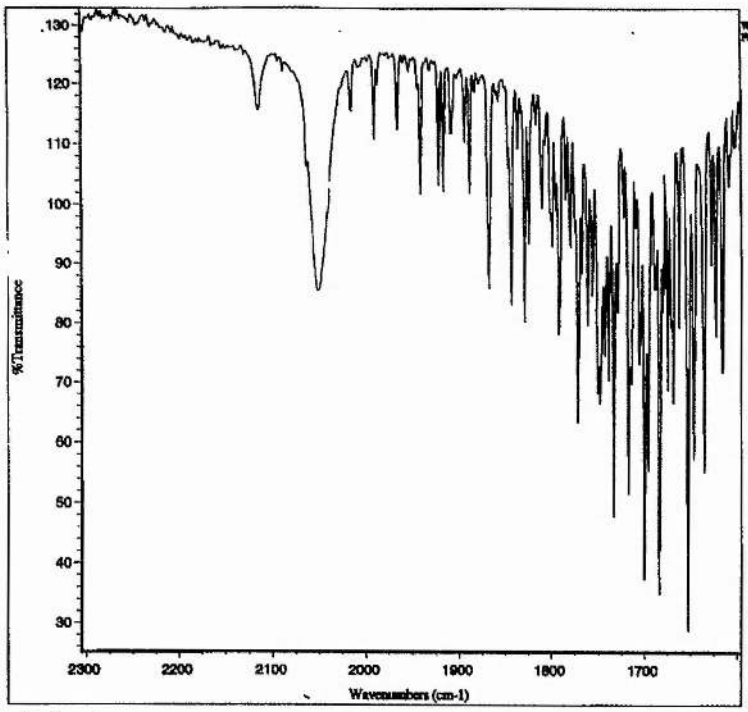

INFRARED 40: ACM 189, Cooled and Degassed.

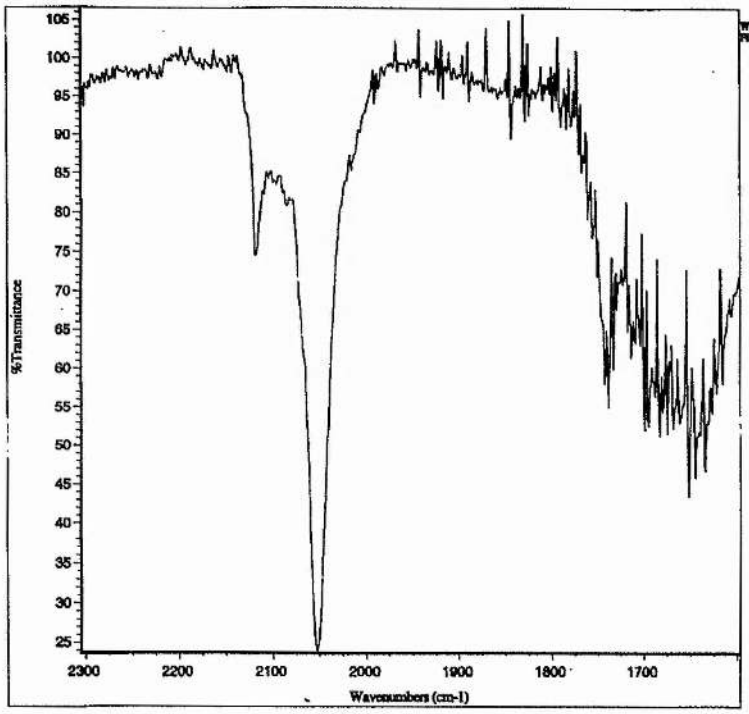

INFRARED 41: ACM 189A in Dichloromethane - Dichloromethane.

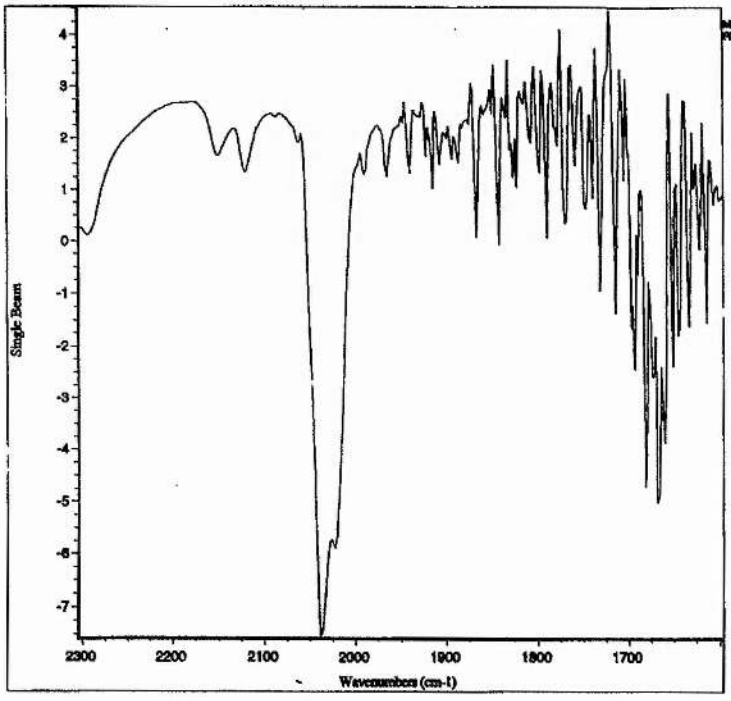

*acm189A diluted - CH2Cl2

INFRARED 42: ACM 189B in Dichloromethane - Dichloromethane.

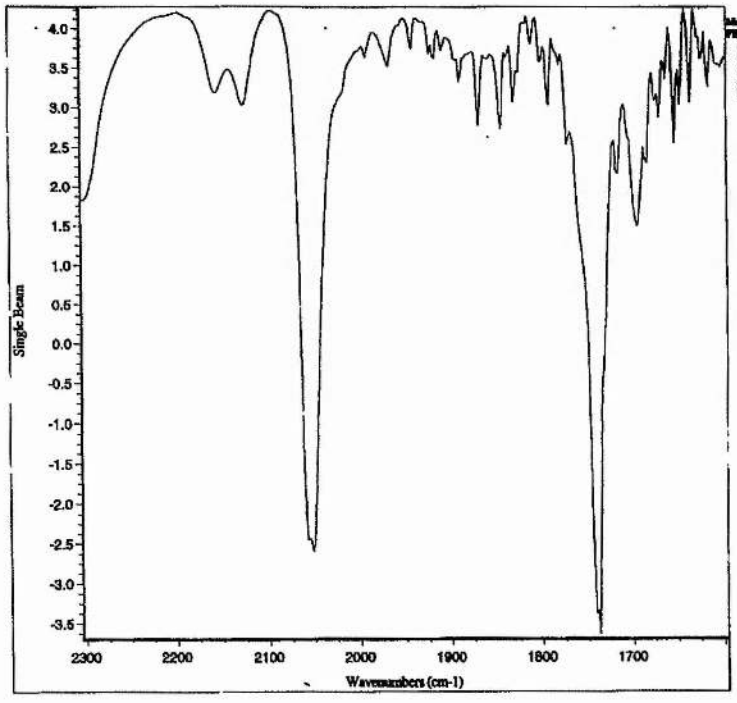

*acm189B diluted with CH2Cl2

The product solution ACM 189B:

The deep red product solution was removed from the autoclave under argon. The solution precipitated a small quantity of a green solid, this was discarded. The solution was stored at 0 °C and some brown red crystals were obtained. The infrared spectrum of these in dichloromethane showed strong absorptions at 1740 and 2055 cm^{-1}, spectrum 42. The 1740 cm^{-1} absorption would appear to indicate that the solid is contaminated with methyl acetate, this may be formed from the reaction of [Cp*Co(COMe)(CO)I] with methanol, methanol and HI can be formed by the reaction of MeI with traces of water in solution. An n.m.r. spectra was recorded (see below). The compound was insoluble in methanol and it was recrystallised from dichloromethane and labelled ACM 192C. The X-Ray crystal structure of ACM 192C was obtained, (see appendix 1). The solid was identified as [Cp*Co(CO)I_2]. The infrared spectrum as a solid gave two peaks, one at 2036 cm^{-1} and one at 2027 cm^{-1}, presumably due to solid state splitting. A microanalysis was also recorded.

n.m.r. Spectra: In CD_2Cl_2

ACM 189A, ^{1}H: The n.m.r. spectrum of this solution in CD_2Cl_2 contained paramagnetic impurities but peaks belonging to Cp*CH_3 at 1.84 ppm and COCH_3 at 2.77 ppm were detected. The other major peak was at 2.17, (CH_3I).

ACM 189A, 13C: This revealed resonances indicative of methyl acetate, verifying the presence of this impurity, methyl iodide and Cp*CH_3 11.00 ppm, $C_5(CH_3)_5$ 102.03 ppm.

ACM 189B,C, [Cp*Co(CO)I_2], 1H: Cp*CH_3 2.23 ppm

ACM 189C, [Cp*Co(CO)I_2], 13C: $C_5(CH_3)_5$ 101.37 ppm

Discussion of ACM 189.

The product of the reaction of [Cp*Co$(CO)_2$] with methyl iodide in dichloromethane at room temperature was [Cp*Co(COMe)(CO)I]. Two terminal carbonyl stretches were detected and these may represent the different confomers of [Cp*Co(COMe)(CO)I].observed by A. Haynes. [3]The n.m.r reveals that [Cp*Co(COMe)(CO)I] was the only major species in solution.

When [Cp*Co(COMe)(CO)I] in methyl iodide and dichloromethane were heated under CO [Cp*Co(CO)I_2] was formed together with a species represented by 2117-2118 cm^{-1}

which was not stable under argon. The infrared spectra suggests that there may be another absorption on the high frequency side of the 2052 cm^{-1} stretch therefore it is possible that the 2118 cm^{-1} absorption is due to $[Cp^*Co(Me)(CO)_2]^+$ or $[Cp^*Co(COMe)(CO)_2]^+$. Haynes *et al* followed the reaction of $[Cp^*Rh(CO)_2]$ with MeI in dichloromethane in the infrared and observed the presence of the rhodium intermediate $[Cp^*Rh(Me)(CO)_2]^+$, ν_{CO} = 2118, 2086 cm^{-1}. [3]

4.2c ii. Mechanistic Studies on $[Cp^*Co(CO)_2]$ + MeI in Methanol.

$[Cp^*Co(CO)_2]$ + MeI in MeOH Under CO, ACM 152, 190:

Infrared Spectra 43, 44, 45, 46.

The infrared spectrum of $[Cp^*Co(CO)_2]$ in methyl iodide and methanol consisted of two major peaks 2038, 2024 cm^{-1} which changed in relative intensity as the sample was heated under CO. At lower temperatures (infrared spectra 43 and 44) 2038 cm^{-1} was the more intense stretch whereas at temperatures close to 100 °C 2024 cm^{-1} was the more intense. At 100 °C there appears to be another absorption at the low frequency side of the 2023 cm^{-1} absorption between 1980 and 1990 cm^{-1}. These absorptions were observed whilst the methyl acetate absorption at ~ 1740 cm^{-1} was growing. The autoclave was heated further and the terminal carbonyl stretches reduced in relative intensity until they were difficult to distinguish from the noise.

ACM 190:

The method was repeated but this time the autoclave was quenched soon after it reached 100 °C and the orange solution was removed. On reducing the solvent volume a translucent solid that wept methanol and turned green was produced indicative of the decomposition of the complexes.

n.m.r. in CD_3OD:

ACM 190A, The Reactant solution, ^1H: The proton spectrum of the solution before pressurising with CO and heating was paramagnetically line broadened, a set of signals was evident at ~ 1.9 ppm.

ACM 190A, 13C: The $^{13}C\{^1H\}$ spectrum contained resonances corresponding with Cp^*CH_3 at 10.28 ppm and $C_5(CH_3)_5$ at 103.03 ppm.

INFRARED 43: ACM 152, [Cp*Co(CO)$_2$] + MeI in Methanol, 60 bar CO, 22 °C.

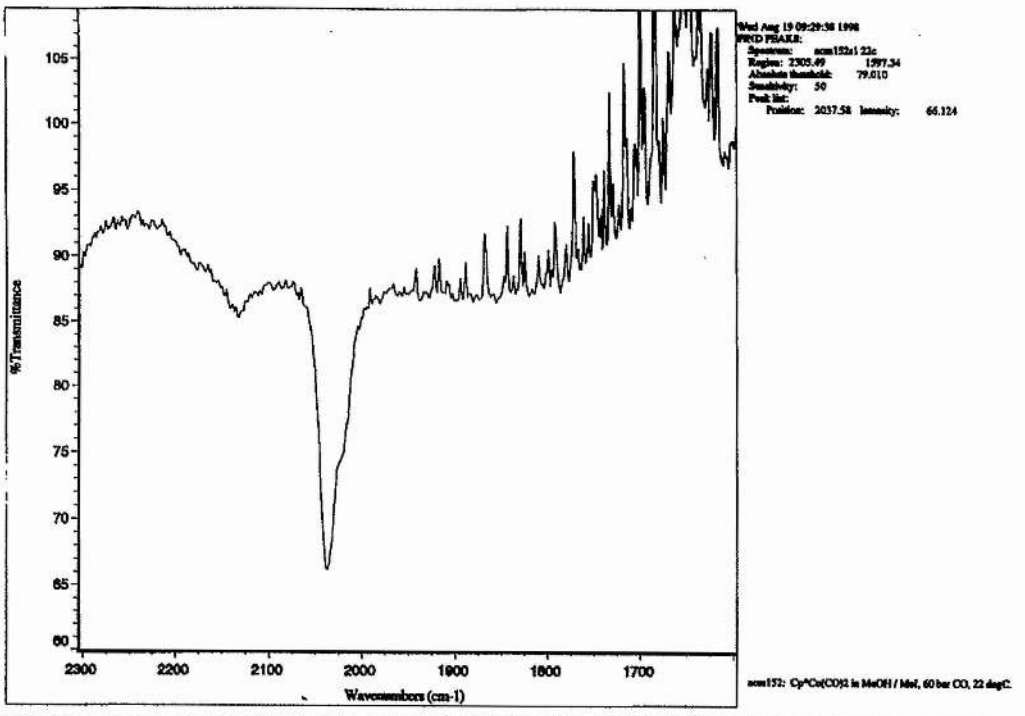

INFRARED 44: ACM 152, 50 °C.

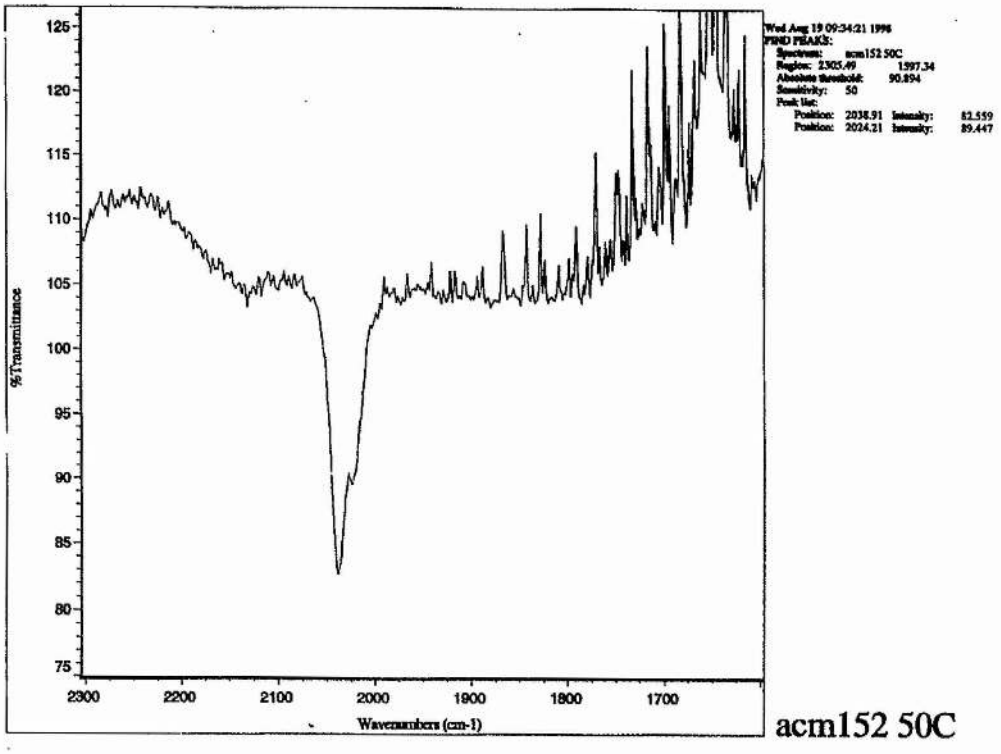

INFRARED 45: ACM 152, 94 °C.

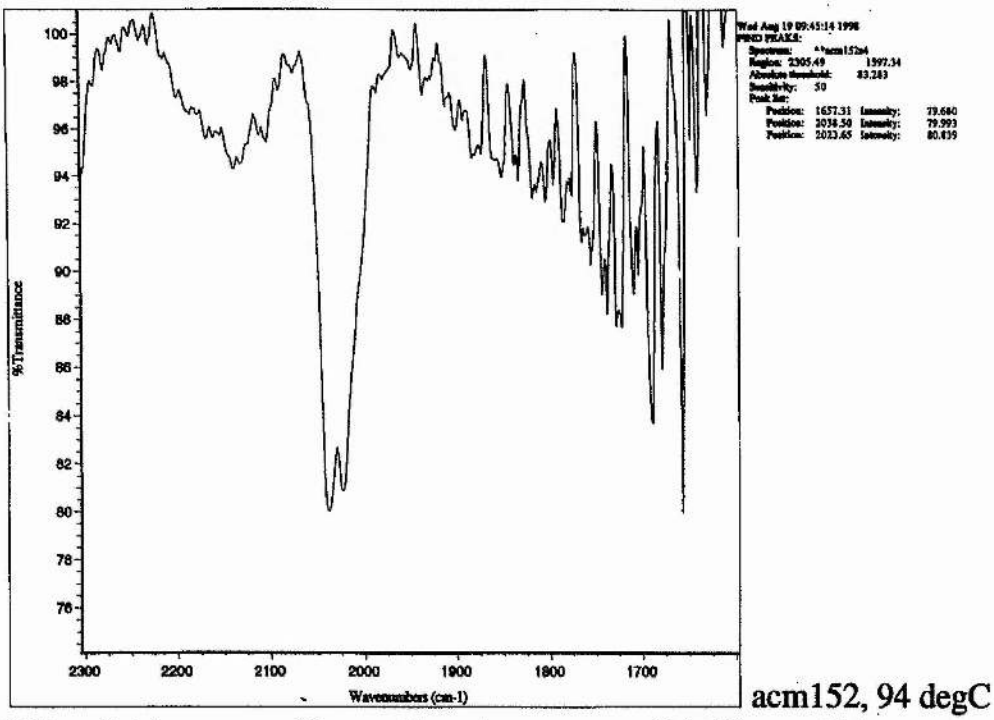

INFRARED 46: ACM 152, 100 °C.

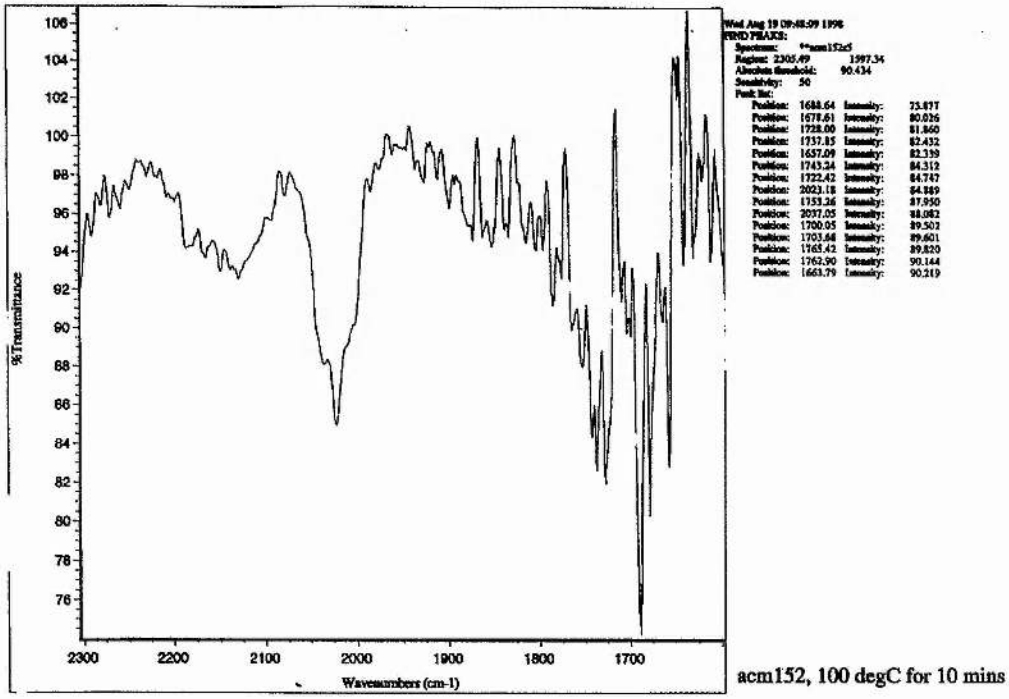

ACM 190B, the product solution, ^{1}H: The proton n.m.r. of the resultant orange solution was highly line broadened, there were two sets of resonances one above and one below 2.0 ppm.

ACM 190B, 13C: The major signals were due to methyl iodide, methyl acetate, and pentamethyl cyclopentadiene (9.62, 10.82, 14.29, 137.11 and 140.26 ppm).

Discussing the Spectra of ACM 152, 190.

The absorption at 2038 cm^{-1} was almost certainly from [Cp*Co(COMe)(CO)I], the n.m.r. of ACM 190A supports the presence of a Cp*-Co bond in the compound. At this point a peak at 2024 cm^{-1} was present also and it may be that this is from the other conformational isomer of [Cp*Co(COMe)(CO)I] as observed by Haynes *et al* in hexane. When this compound was heated to 100 °C under CO (80 bar) and then cooled and degassed it decomposed evolving Cp*H.

4.2d. Conclusions from Mechanistic Studies.

4.2d i. [Cp*Co(CO)$_2$] + MeI.

[Cp*Co(CO)$_2$] + MeI in CH_2Cl_2.

The assignment of the infrared absorptions observed are in table 4.5

TABLE 4.5: Infrared Assignments in ACM 189.

ν_{co} / cm^{-1}	Solvent	Assignment
2018-2023 2038-2039 1667, 1681	CH_2Cl_2	[Cp*Co(COMe)(CO)I] Conformational isomers
2027, 2036	as solid	[Cp*Co(CO)I_2]
2052-2055	CH_2Cl_2	[Cp*Co(CO)I_2]
2117-2118, >2055sh	CH_2Cl_2	[Cp*Co(Me)(CO)$_2$]$^+$ or [Cp*Co(COMe)(CO)$_2$]$^+$

[Cp*Co(CO)$_2$] + MeI in Methanol.

The infrared assignment for experiments 152 and 190 are in table 4.6.

TABLE 4.6: Infrared Assignments in ACM 152, 190.

ν_{CO} / cm^{-1}	Solvent	Assignment
2024, 2038, M-COR Stretches	Methanol	[Cp*Co(COMe)(CO)I] Conformational isomers

Summary.

Some of the possible processes occurring in solution are detailed in diagram 45.

DIAGRAM 45: Major processes Occurring Between $[Cp^*Co(CO)_2]$ and MeI, $[Cp^*Co(Me)(CO)_2]^+ + CO = [Cp^*Co(COMe)(CO)_2]^+$ and cationic cycle omitted:

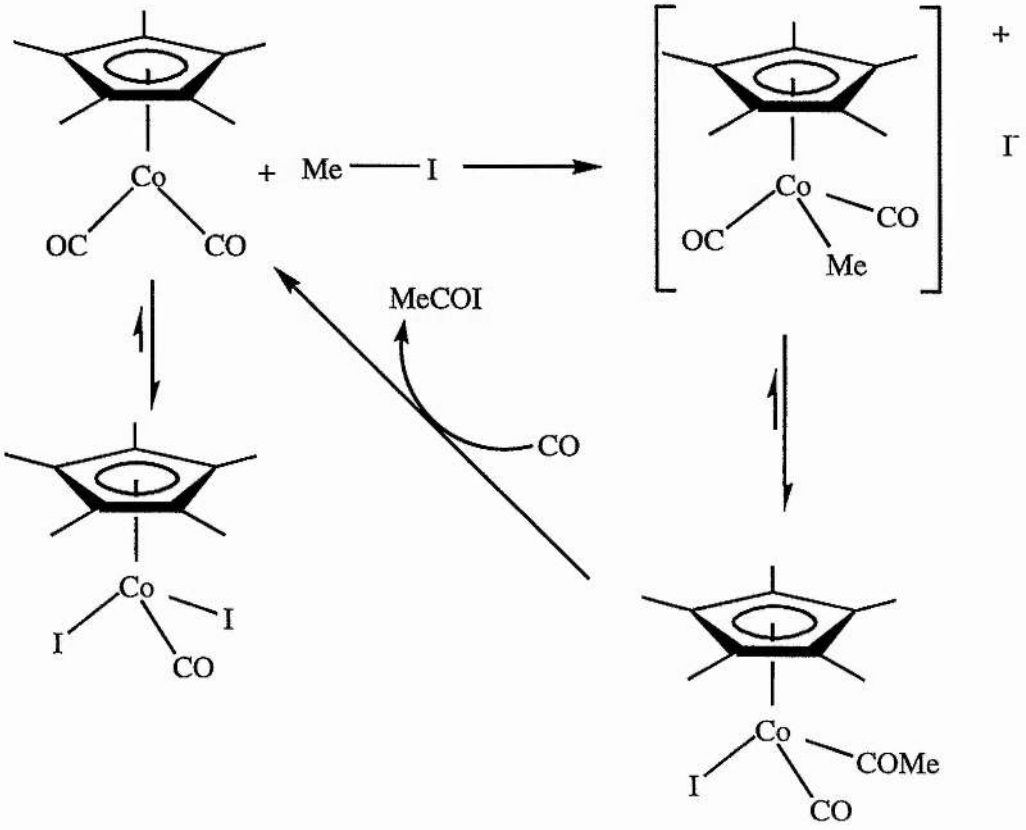

In dichloromethane: the products of reductive elimination undergo a side reaction to generate $[Cp^*Co(CO)I_2]$, this is analogous to compounds derived from the oxidative addition of HI to $[M(CO)_2I_2]^-$ in the iridium and rhodium carbonylation cycles. In the absence of methanol and water there is no facile route back to Co (I) and $[Cp^*Co(CO)I_2]$ builds up as the major product.

In methanol: [Cp*Co(COMe)(CO)I] is the major species detected in solution.
The reduction of [Cp*Co(CO)I_2] to [Cp*Co$(CO)_2$] is facilitated preventing the build up of [Cp*Co(CO)I_2] and the rate of insertion is fast in methanol preventing the build up of the alkyl intermediate.
Under the conditions at which [Cp*Co(COMe)(CO)I] is the major species the slowest step in the cycle is reductive elimination step, this is consistent with production of 1,1-dimethoxyethane as a side product and explains why the behaviour of the system is very similar to that of [$Co_2(CO)_8$]. It also explains why changes in the concentration of methyl iodide had little effect on the rate of carbonylation. At higher temperatures the rate of reductive elimination is expected to increase and it may be that the shoulder on the low frequency side of the [Cp*Co(COMe)(CO)I] infrared absorption represents a build up in the standing concentration of [Cp*Co(CO)I]$^-$ as the temperature increases.
The importance of keeping the pressure of CO high is probably twofold:
Firstly the decomposition pathway of the catalyst may involve loss of CO. This is consistent with the rapid decomposition of the intermediates when the autoclave is degassed. Secondly a high partial pressure of CO will help to recycle cobalt back to the active catalyst and reduce build up of [Cp*Co(CO)I_2], see chapter 5, diagram 57.

4.3 [Cp*Co$(CO)_2$] + PROMOTER FOR CATALYTIC CARBONYLATION OF METHANOL.

4.3a. Batch Autoclaves of [Cp*Co$(CO)_2$] + Promoter.

4.3a i. Batch Autoclaves of [Cp*Co$(CO)_2$] + PEt_3 in MeOH / MeI, Table 4.7.

Table 4.7 contains the results of some autoclave runs carried out with the catalytic precursors [Cp*Co$(CO)_2$] + PEt_3. In general rates were higher than for reactions carried out in the absence of added phosphine.

ACM 167, 168, 173 Repeatability:

The experiments were not repeatable. This suggests that the behaviour in solution is complex. This is substantiated by the decrease in average turnover frequency when the experiment is run for two hours instead of one.

TABLE 4.7: Batch Autoclaves Containing [Cp*Co(CO)$_2$] + PEt$_3$ in Methanol / Methyl Iodide and Comparison with [CpCo(CO)$_2$] and [Co$_2$(CO)$_8$].

Expt. No	[Co] / mol dm^{-3}	[PEt$_3$] / mol dm^{-3}	Autoclave S = Steel H = Hastelloy	Temp. / °C E=External I = Internal	P / bar RO = Room temp. RE = Reaction Temp.	MeOH / g	MeI / g	Volume / cm^3	Run Time / hr	[MeOAc] / mol dm^{-3}	[1,1-dimethoxy ethane] / moldm^{-3}	Rate / mol dm^{-3} hr^{-1}	Rate / turnover hr^{-1}
ACM 159	0.036	0.35	H. 28 cm^3	140 I	60 RO	3.16	2.28	4.89	1	0.068	trace	0.068	1.9
ACM 167	0.147	0.79	H. 28 cm^3	120 I	80 RO	3.80	1.37	5.15	1	1.441	0.0029	1.441	9.8
ACM 168	0.145	0.79	H. 28 cm^3	120 I	80 RO	3.80	1.37	5.15	1	0.846	0.0013	0.846	5.9
ACM 169	0.150	0.79	H. 28 cm^3	150 I	80 RO	3.80	1.37	5.15	2	0.800	0.0012	0.400	2.7
ACM 173	0.149	0.79	H. 28 cm^3	120 I	80 RO	3.80	1.37	5.15	2	0.925	0.0030	0.463	3.1

[CpCo(CO)$_2$] + PEt$_3$ Autoclaves:

ACM 148	0.105	1.01	H. 28 cm^3	125 I	60 RO	3.16	2.28	4.71	24	0.153	0	0.006	0.1
ACM 164	0.147	0.79	H. 28 cm^3	120 I	80 RO	6.33	2.28	8.58	1	0.808	0.0012	0.81	5.5
ACM 166	0.188	0.79	H. 28 cm^3	120 I	80 RO	6.33	2.28	8.58	17	0.51	trace	0.030	0.2

[Co$_2$(CO)$_8$] + PEt$_3$ Autoclaves:

ACM 160	0.036	0.35	H. 28 cm^3	140 I	60 RO	3.16	2.28	4.90	1	0.064	trace	0.064	1.8
ACM 170	0.147	0.79	H. 28 cm^3	150 I	80 RO	3.80	1.37	5.15	2	2.163	0.0051	1.082	7.3

TABLE 4.8: Batch Autoclaves of $[Cp^*Co(CO)_2]$ + Additive in Methanol.

Expt. No	[Co] / mol dm^{-3}	Additive [Additive] / mol dm^{-3}	Autoclave S = Steel H = Hastelloy	Temp. / °C E=External I = Internal	P / bar RO = Room temp. RE = Reaction Temp.	MeOH / g	MeI / g	Volume / cm^3	Run Time / hr	[MeOAc] / mol dm^{-3}	[1,1-dimethoxy ethane] / $moldm^{-3}$	Rate / mol dm^{-3} hr^{-1}	Rate / turnover hr^{-1}
ACM 172	0.128	LiI 0.662	H. 28 cm^3	120 I	80 RO	4.47	0.80	6.00	2	0.288	0.0022	0.144	1.1
ACM 174	0.148	$MePEt_3I$ 0.794	H. 28 cm^3	120 I	80 RO	3.80	0.80	5.15	2	0.409	0.0017	0.205	1.4
ACM 175	0.029	$[Ru(CO)_3Cl_2]_2$ 0.031	H. 28 cm^3	120 I	80 RO	3.16	2.28	5.00	2	0.117	0.0007	0.059	2.0

ACM 159, 167, 168, 169 and 173:

Despite the poor repeatability it was clear that the best conditions for high rates of carbonylation were 120 °C and CO (80 bar) at room temperature. Deviations from this led to a reduction in rate.

Selectivity:

In most cases 1,1-dimethoxyethane was detected in small quantities. In ACM 167, the most successful catalytic run, [MeOAc] / [1,1-dimethoxyethane] = 497, a considerable improvement from the catalytic runs carried out without phosphine. In ACM 162 operated with just $[Cp^*Co(CO)_2]$ as a catalyst the ratio was [MeOAc] / [1,1-dimethoxyethane] = 99, see table 4.2

Comparison With Other Systems, $[Co_2(CO)_8]$:

The batch autoclave runs carried out in the presence of added free phosphine have presented the most promising results, these are reviewed in table 4.6. $[CpCo(CO)_2]$ + PEt_3, represented by batch autoclaves ACM 148, ACM 164 and ACM 166 is a selective but not very active catalytic system. In addition to this systems inferior activity our kinetic experiment suggests that the catalyst is unstable. $[Co_2(CO)_8]$ represented by experiments ACM 160 and ACM 170 has a very similar activity and selectivity to $[Cp^*Co(CO)_2]$ at 140 °C and CO (60 bar) loading pressure, compare ACM 159 and ACM 160. At 150 °C and CO (80 bar) loading pressure, ACM 169 and 170, $[Co_2(CO)_8]$ performs substantially better than $[Cp^*Co(CO)_2]$. The best conditions tested for $[Cp^*Co(CO)_2]$ + PEt_3 are 120 °C and CO (80 bar) loading pressure. These conditions were chosen for measuring the initial rate of CO uptake, see section 4.3 b.

<u>4.3a ii. Batch Autoclaves of $[Cp^*Co(CO)_2]$ + Additives Other than PEt_3 in MeOH / MeI.</u>

LiI, $MePEt_3I$ and $[Ru(CO)_3Cl_2]_2$ were added to $[Cp^*Co(CO)_2]$, the experimental conditions and results are collected in table 4.8. We were unable to achieve the sorts of rates attainable with the $[Cp^*Co(CO)_2]$ + PEt_3 catalytic system.

4.3 b. The Initial Rate Data.

4.3b i. ACM 178, 180 and 181 Catalyst + PEt_3, Table 4.3.

These experiments were conducted at B.P. Chemicals Hull as detailed in section 4.2b. When we compare the initial rates of carbonylation for $[CpCo(CO)_2]$ or $[Co_2(CO)_8]$ with added PEt_3 (ACM 180 and 181), we note that the rate is slightly higher for the modified $[Co_2(CO)_8]$ catalyst. We have already identified the poor stability of $[CpCo(CO)_2]$ and conclude that this system does not warrant further study. The $[Cp^*Co(CO)_2] + PEt_3$ system is quite different as there are two distinct regions of the ballast vessel pressure versus time graph see diagram 46. The first region represents a very efficient and short lived catalyst which carbonylates methanol at a rate of approximately 120 turnovers per hour and evolves methyl acetate at 18 mol $dm^{-3} hr^{-1}$. This rate is very high, especially when we consider that the temperature is only 120 °C! The highly unstable 'supercatalyst' rearranges and there is a period without gas intake before carbonylation sets off once more at a more modest rate of 7 turnovers hr^{-1}, this rate is between that for the modified $[CpCo(CO)_2]$ and $[Co_2(CO)_8]$ catalytic systems.

The initial drop in ballast pressure is not due to filling the vessel as this has been cut out for clarity. Between the two regions of activity there is an apparent halt in carbonylation. The initial period of catalytic activity is short lived suggesting the catalyst is very unstable at 120 °C and 100 bar but the rate is staggering, greater than 10 times more than any other catalyst measured! The rate of the second regime is consistent with a modified $[Cp^*Co(CO)_2]$ catalyst as estimated in the batch autoclave runs. This region shows zero order kinetics followed by a first order decay in rate, this may be due to the decrease in methanol concentration.

DIAGRAM 46: [Cp*Co(CO)$_2$] + PEt$_3$, Ballast Vessel Pressure vs. Time ACM 178.

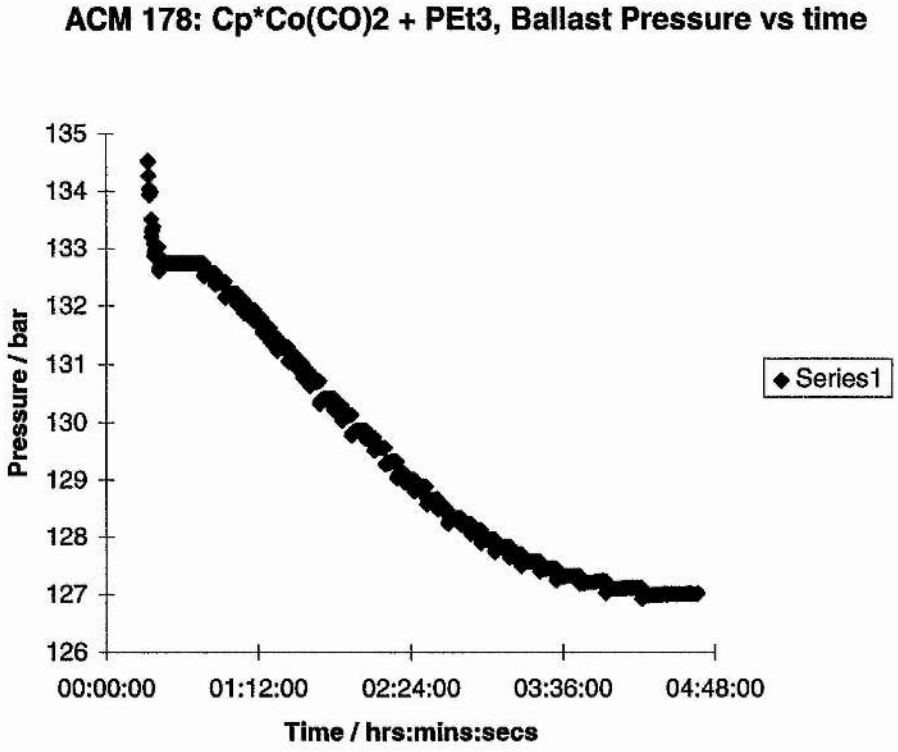

4.3c. The Selectivity of the Cobalt Carbonylation Catalysts.

After the catalytic runs conducted at B.P Chemicals ACM 176, 178, 179, 180, 181, 177 and 182 (see table 4.2 and 4.3) the solutions were analysed by the B.P. Chemicals analytical section.

Now that we have discussed all our data collected at B.P. Chemicals we can contrast the selectivities of the different catalytic systems. In the following discussion the selectivity towards the products (methyl acetate or acetic acid) is expressed as no. moles of product: no. moles side products. This is convenient as the side products of the solutions take many different forms involving different numbers of moles of methanol. Usually only one equivalent is irretrievably consumed, e.g. Methyl acetate production involves two equivalents of methanol but can react with water to return one equivalent, 1,1-dimethoxyethane requires three but can react with water to yield two equivalents.

4.3c i. The Selectivity of Catalysts Operated in Methanol.

The product distribution for the various catalysts operated in methanol is detailed in table 4.10.

ACM 176.

When we compare this result with the results of the batch autoclave runs in table 4.2 we can see that reducing the concentration of MeI has vastly increased the selectivity of $[Cp^*Co(CO)_2]$, the ratio of desired products: side products is 698:1. The only detected side product is acetaldehyde.

ACM 178 and 179.

$[Co_2(CO)_8] + PEt_3$ and $[Cp^*Co(CO)_2] + PEt_3$ have carbonylated methanol to a similar extent and so we can compare the product composition. In the case of $[Co_2(CO)_8]$ the ratio of desired products to side products is 96:1, the ratio for $[Cp^*Co(CO)_2]$ is higher 177:1 mainly due to a fourfold reduction in propanoic acid production, the major side product in both cases.

TABLE 4.9 4.10, 4.11: The Product Composition:

TABLE 4.9: Conc. In Parts Per Million w / w, As Supplied by B.P. Chemicals Analytical Laboratory, Salt End, Hull.

Expt.	Catalyst	CH3CH2COOH	CH3CHO	ACETONE	ETI	ETOAc	PropI	Ethylidene diacetate
ACM176	$Cp^*Co(CO)_2$	<10	40	<10	<10	<10	<10	<10
ACM177	$Cp^*Co(CO)_2$ Hull solvent	108	<15	33	1901	2220	<10	480
ACM178	$Cp^*Co(CO)_2 + PEt_3$	740	<15	<10	<10	380	10	164
ACM179	$Co_2(CO)_8 + PEt_3$	2899	<15	<10	<10	18	<10	<10
ACM180	$CpCo(CO)_2 + PEt_3$	135	<15	<10	<10	<10	<10	713
ACM181	$Co_2(CO)_8$	713	<15	24	<10	<10	<10	110
ACM182	$Co_2(CO)_8$ Hull Solvent	3822	<15	29	1724	<10	<10	<10

TABLE 4.10: Product Composition in Methanol Solvent.

Expt. No.	Catalyst	CH_3COOCH_3 / mol dm^{-3}	CH_3CH_2COOH / mol dm^{-3}	CH_3CHO / mol dm^{-3}	Acetone / mol dm^{-3}	EtOAc / mol dm^{-3}	PropI / mol dm^{-3}	Ethylidene diacetate / mol dm^{-3}
ACM176	$Cp^*Co(CO)_2$	0.538		0.00077				
ACM178	$Cp^*Co(CO)_2$ + PEt_3	3.446	0.01232			0.00532	0.00007	0.00177
ACM179	$Co_2(CO)_8$ + PEt_3	4.803	0.04982			0.00026		
ACM180	$CpCo(CO)_2$ + PEt_3	0.781	0.00212					0.00726
ACM181	$Co_2(CO)_8$	0.808	0.01055		0.045			0.00106

TABLE 4.11: Product Composition in Low Water Acetic Acid Solvent.

Expt. No.	Catalyst	CH_3COOH /mol dm^{-3}	CH_3CH_2COOH /mol dm^{-3}	ACETONE /mol dm^{-3}	EtI /mol dm^{-3}	EtOAc /mol dm^{-3}	Ethylidene Diacetate
ACM177	$Cp^*Co(CO)_2$	0.632	0.00169	0.00066	0.01413	0.02921	0.00488
ACM182	$Co_2(CO)_8$	0.636	0.05936	0.00057	0.01275		

ACM 180 and 181.

$[CpCo(CO)_2]$ + PEt_3 and $[Co_2(CO)_8]$ have carbonylated methanol to a similar extent and we can prepare their product distribution.

The selectivity of $[Co_2(CO)_8]$ is poor, as expected from the batch autoclave experiments giving only 14:1 methyl acetate to side products. The selectivity of $[CpCo(CO)_2]$ + PEt_3 is far better. Methyl acetate: side products is 83:1.

4.3c ii. The Selectivity of Catalysts Operated in Acetic Acid. Table 4.11

ACM 177 and 182.

The selectivities of $[Cp^*Co(CO)_2]$ and $[Co_2(CO)_8]$ operated in this solvent system were poorer than the selectivities in pure methanol. Methyl acetate: side products 13:1 in the case of $[Cp^*Co(CO)_2]$ and 9:1 in the case of $[Co_2(CO)_8]$.

4.3c iii. Summarising the Observed Selectivites:

Numerically the side product distribution is as follows:

TABLE 4.12: Selectivities of Cobalt Carbonylation Catalysts:

Catalyst	Solvent System	MeOAc : Side Products
$[Cp^*Co(CO)_2]$	Methanol, low MeI	700:1
$[Cp^*Co(CO)_2]$ + PEt_3	Methanol	180:1
$[Co_2(CO)_8]$ + PEt_3	Methanol	100:1
$[CpCo(CO)_2]$ + PEt_3	Methanol	80:1
$[Co_2(CO)_8]$	Methanol	10:1
$[Cp^*Co(CO)_2]$	Acetic Acid	10:1
$[Co_2(CO)_8]$	Acetic Acid	10:1

All molar ratios of greater than 100:1 correspond with selectivities of greater than 99 %. The selectivity is greatest for $[Cp^*Co(CO)_2]$ operating at low [MeI], a selectivity for methanol conversion of greater than 99.8 %. The only side product produced was acetaldehyde and at a very low concentration. It seems that the low concentration of MeI has prevented the production of large quantities of acetaldehyde. This may be because the rate determining step has been changed to oxidative addition and there are no longer high concentrations of acyl cobalt intermediates available in solution to be intercepted by HI, H_2 or $[CoH(CO)_4]$.

$[Co_2(CO)_8]$ + PEt_3 and $[Cp^*Co(CO)_2]$ + PEt_3 have very good selectivity and improved activity. PEt_3 modified $[Co_2(CO)_8]$ and $[Cp^*Co(CO)_2]$ have selectivities close to 99 %. The improved selectivity afforded by adding PEt_3 to the catalytic precursors may arise because of the increased concentration of inorganic iodide. One effect $[MePEt_3]I$ can have is to intercept COMe as MeCOI, speeding up the reductive elimination step and thereby reducing the concentration of acyl cobalt complexes in solution.
The poor selectivity in the absence of phosphine and the presence of considerable quantities of methyl iodide is illustrated by the unmodified $[Cp^*Co(CO)_2]$ in acetic acid and unmodified $[Co_2(CO)_8]$ in acetic acid and methanol runs, ACM 177, 182 and 181 respectively, all three catalytic runs showed selectivities of around 90 %.

4.3c iv. Rationalising the Products Observed:

Most of the side products detected result from acetaldehyde production from acyl cobalt species in solution, see diagram 47.

DIAGRAM 47: The Production of Acetaldehyde Related Side Products.

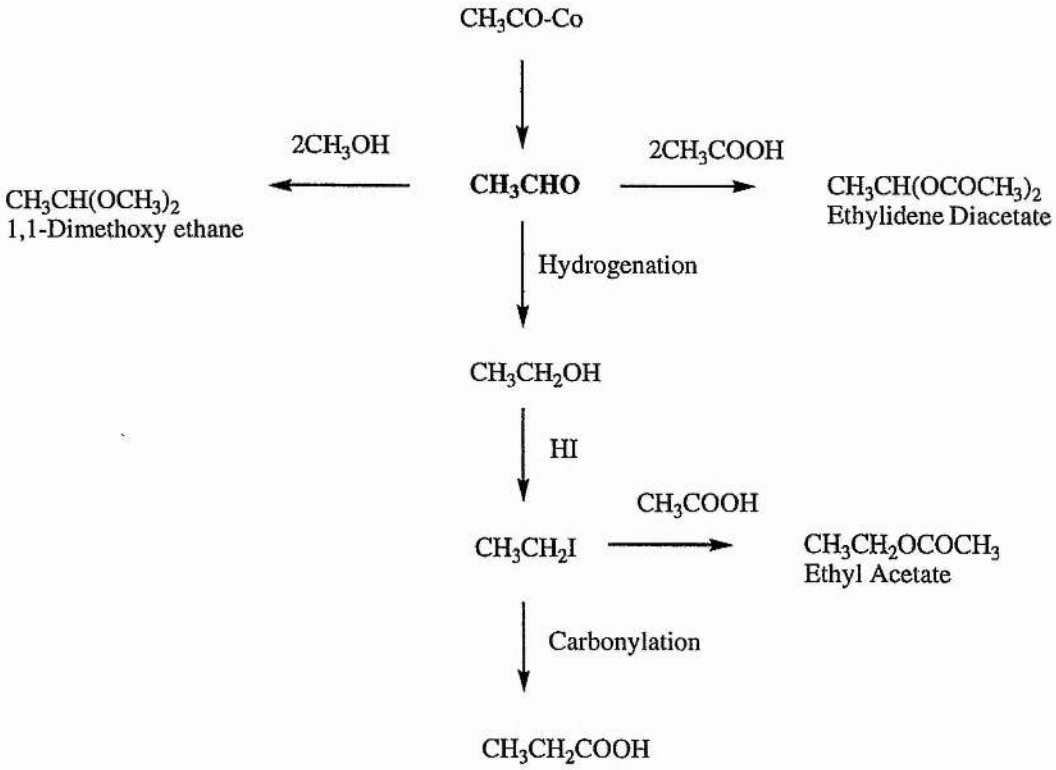

It is unlikely that acetone is produced in this way. Acetone may be produced when alkyl and acyl cobalt intermediates react together.[4]

$CH_3CO\text{-}CoL_4 + CH_3\text{-}CoL_4 \longrightarrow CH_3COCH_3 + 2CoL_4$

The pathway to all the major side products of cobalt catalysed carbonylation of methanol involve reaction of the acyl cobalt intermediate, this is why we reason that a reduction in the standing concentration of this species leads to an increased selectivity. The best selectivities are achieved by ensuring that methyl iodide oxidative addition is rate limiting. This can be achieved by slowing down the rate of oxidative addition or by increasing the rate of reductive elimination, as faster rates are desirable the later option is favoured.

4.3 d. Kinetics Experiments with CATS Catalyst Testing Unit at St. Andrews.

4.3 d. i. Aim of Catalyst Testing.

The preliminary tests carried out at B.P Chemicals had verified the novel nature of our catalytic systems and in particular that of the $[Cp^*Co(CO)_2] + PEt_3$ system. We decided that some further testing on $[Cp^*Co(CO)_2]$ was warranted, we particularly wanted to find if we could generate acetic acid in low water acetic acid solvents.

The tests were carried out in conjunction with the catalyst testing facility at The University of St. Andrews C.A.T.S., technical assistance was given by Gary Schwarz.

4.3d ii. Catalyst Testing in Low Water Acetic Acid, Results. Table 4.13

The solvent and catalyst concentration used were the same as experiments ACM 177 and 182. The conditions chosen were 120 °C and 100 bar at temperature to coincide with the work carried out in methanol.

Methyl iodide was injected at temperature and pressure in order to obtain an instantaneous rate.

ACM 198 $[Cp^*Co(CO)_2]$.

No carbonylation activity was observed for $[Cp^*Co(CO)_2]$ under these conditions. The autoclave was cooled and degassed and then opened. A large quantity of dark brown needles had crystallised from the solution. An infrared spectrum and microanalysis of this compound revealed it to be $[Cp^*Co(CO)I_2]$, the X-Ray crystal structure is in appendix 1.

TABLE 4.13. Experiments with C.A.T.S. In Methanol / Water, ACM 200, 201.

Expt. No.	Catalyst	Initial [Catalyst] / mol dm^{-3}	Methanol Added/ g	Methyl Iodide Added/ g	Triethyl Phosphine Added/ g	Water Added	Total Volume/ cm^3	Rate / $moldm^{-3}$ hr^{-1}	Rate/ turnover/ hr
ACM 200	$Cp^*Co(CO)_2$ + PEt_3	0.1400	3.0494	1.0841	0.7166	0.35 ml	4.30	43.90 2.51	313.6 18.0
ACM 201	$Cp^*Co(CO)_2$ + PEt_3	0.1392	3.0650	1.0709	0.7158	0.3604	4.33	- 3.41	- 24.6

We conclude that the lower temperatures employed in this catalytic run (120 °C compared with 140 °C in ACM 177) were not severe enough to reduce $[Cp^*Co(CO)I_2]$ back to the Co (I) catalytic system $[Cp^*Co(CO)_2]$ and $[Cp^*Co(CO)I]^-$.
Increasing the concentration of water from 7 % to approximately 15 % may also help recycle Co (I).

ACM 199, $[Cp^*Co(CO)_2]$ + LiI.

In the Monsanto system the reduction of Rh (III) to Rh (I) under low water conditions is facilitated by the addition of LiI (see section 1.3 f). The addition of a high concentration of LiI to $[Cp^*Co(CO)_2]$ did not initiate catalytic activity.

ACM 197, $[Cp^*Co(CO)_2]$ + PEt_3.

The addition of PEt_3 instead of LiI also failed to initiate catalytic activity at 120 °C and 100 bar operating pressure.

4.3d iii. Conclusions.

None of our novel catalytic systems operate in low water acetic acid at 120 °C and 100 bar at 7 % w / w water despite considerable rates of reaction in pure methanol under the same conditions. The most likely explanation for this is that the rate is dependent on the concentration of methanol in solution, this is supported by the decay in rate as the reaction proceeds in pure methanol. One possible reason for this is that the high concentration of methanol facilitates the reduction of $[Cp^*Co(CO)I_2]$ to Co (I). In this case the catalytic systems should be operated at low conversion, unfortunately this leads to high concentrations of methyl acetate and dimethyl ether.
The build up of $[Cp^*Co(CO)I_2]$ observed in the absence of catalytic activity, (in acetic acid and dichloromethane) suggests that the catalytic activity is low because there is a low concentration of Co (I) in solution. The mechanism of $[Cp^*M(CO)I_2]$ formation and how M (I) can be maximised will be discussed in section 5.3c.

4.3d iv. Catalyst Testing in Methanol and Water.

In order to test the catalysts sensitivity to water the $[Cp^*Co(CO)_2]$ + PEt_3 catalytic system was operated in methanol + water as a solvent. The concentrations of $[Cp^*Co(CO)_2]$ and PEt_3 and the conditions were kept constant from experiment ACM 197 so that the only change was the replacement of acetic acid and methyl acetate by methanol.

4.3d v. The Ballast Pressure Against Time Graphs. Diagrams 48 and 49.

The results obtained were very encouraging, see table 4.13, diagrams 48 and 49. The composition of the solution in the two catalytic runs were very similar in order to get some idea of experimental error. Clearly the valve between the ballast and reaction vessels was working far better in the case of ACM 200 and these results should be considered as a closer representation of the catalytic activity.

Comparing the graphs of the catalytic systems with and without water we see that they are very similar (diagrams 46 and 48). In the experiment in the absence of water, the catalyst was heated up in the presence of all the substrates and therefore the rate measurement was underestimated. In experiment ACM 200 methyl iodide was injected and this gives a proper measure of the initial rate of about 300 turnovers per hour. This rate is far in excess of any other rates measured for cobalt catalysts. As in the absence of water the first catalytic system suddenly stops carbonylating and a slower rate takes over. The rate of carbonylation for this system is still good ~ 20 turnovers per hour and better than the measurement made in the absence of water. This could be because water helps maintain a high concentration of the active catalyst as in the case of the Monsanto system.

Once again the second region of carbonylation shows a first order decay. We suggest that the second catalytic system shows a first order dependence on the concentration of methanol. The duration of the two experiments ACM 178 and ACM 200 is very similar and it is clear that the tailing evident in the absence of water is not occurring. This is further evidence that water helps maintain the concentration of active catalyst in solution.

DIAGRAM 48 and 49: $[Cp^*Co(CO)_2]$ + PEt_3 in Methanol / Water, Ballast Pressure vs. Time.

DIAGRAM 48: ACM 200.

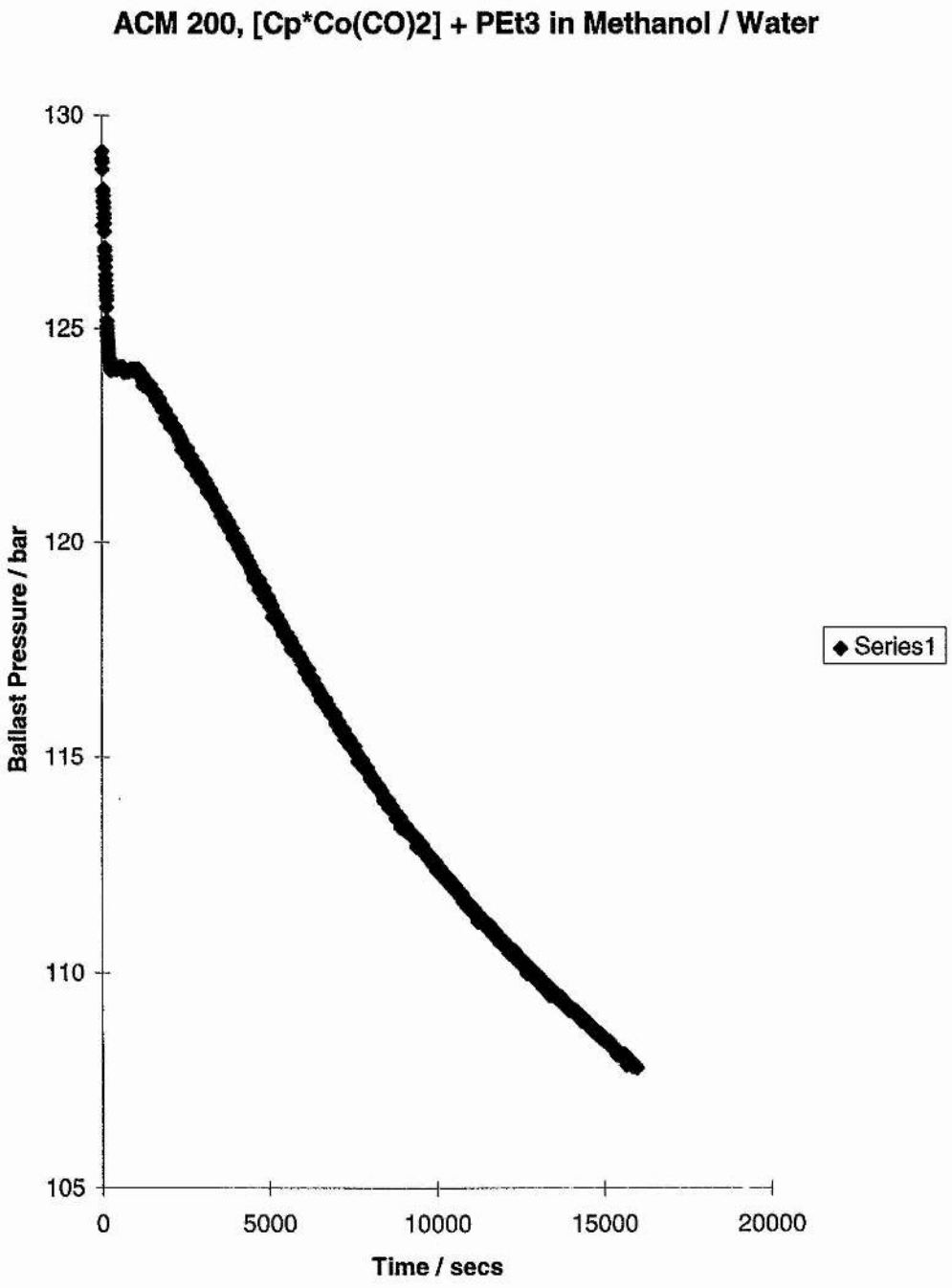

DIAGRAM 49, ACM 201.

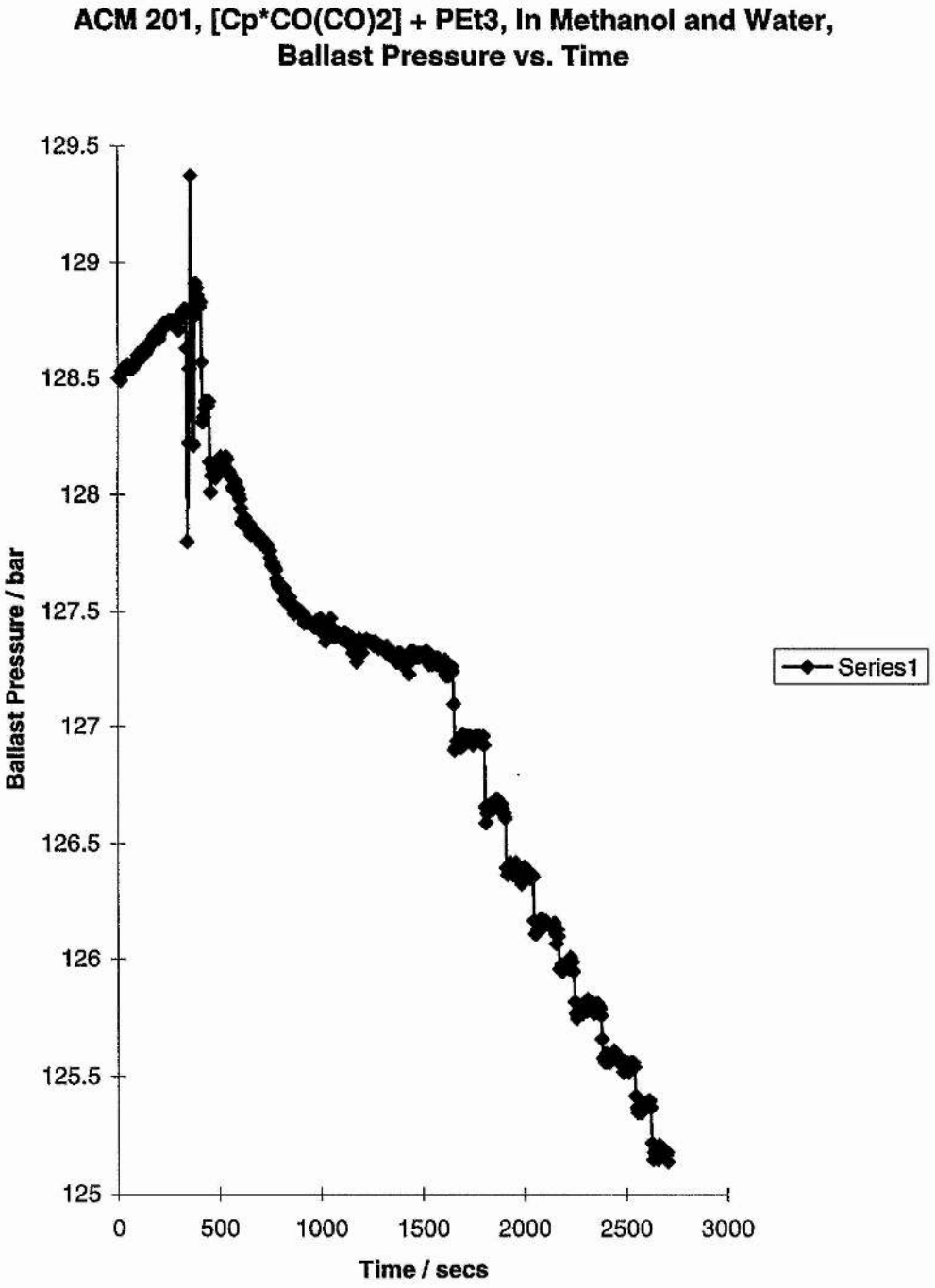

4.3d vi. The Product Composition.

ACM 200, [Cp*Co(CO)$_2$] + PEt$_3$ in MeOH and Water, Diagram 48.

Experiment ACM 200 was run for over 4 hours at 115 - 116 °C and 100 bar operating pressure. The products detected by g.c. analysis were methyl acetate 1.83 mol dm^{-3}, acetic acid and a tiny quantity of 1,1-dimethoxyethane 1.2 x 10^{-3} mol dm^{-3}. From the total CO uptake 8.87 mol dm^{-3} carbonylated products were produced. We estimate that the initial solution contained 22.1 mol dm^{-3} methanol. The selectivity was > 99.9% towards acetates.

The g.c. / m.s. revealed that triethyl phosphine, triethyl phosphine oxide and pentamethyl cyclopentadiene were also in solution.

ACM 201 Compounds Present in Solution.

This experiment was conducted for a shorter time period in order to obtain infrared spectra of the active complexes in solution after cooling and degassing of the autoclave.

The g.c. and g.c. / m.s. analysis: The g.c. / m.s. revealed that, compared with ACM 200, the resultant solution contained more methanol, ~ 45 % less methyl acetate, ~ 95 % less acetic acid, more than four times as much triethyl phosphine, ~ 25 % less triethyl phosphine oxide and, most interestingly, about the same concentration of pentamethyl cyclopentadiene. The solution also contained a trace of 1,1-dimethoxyethane.

The infrared: The solution was removed, it was orange. Using a 0.05 mm pathlength CaF_2 solution cell the infrared of the solution was recorded immediately. The largest metal carbonyl stretching absorption in solution was at 1989 cm^{-1}, there was another, lesser absorption at 1908 cm^{-1}, infrared spectrum 61.

4.3d vii. Discussion of Results.

The [Cp*Co(CO)$_2$] + PEt$_3$ catalytic system operates very well in methanol and water with two regions of activity. The first catalytic species carbonylates at a very rapid rate and then rearranges to a more stable catalyst. The resultant solutions contain the desired products almost exclusively.

When catalysis was quenched during the second period of catalytic activity the resulting solution contained high concentrations of the 1989 cm^{-1} unknown. Similar absorptions have coincided with catalytic activity throughout our work and the complex responsible may be the active catalyst [Cp*Co(CO)I]$^-$. [Co(CO)$_2$(PEt$_3$)$_2$I] was also in solution (the

1908 cm^{-1} absorption, see section 4.3e), this is consistent with the detection of free phosphine and pentamethyl cyclopentadiene in solution. When the solution was analysed much later the concentration of Cp*H had not increased and this suggests that there is no further Cp*-Co bond cleavage after 45 minutes. The active species in the second period of catalytic activity may be $[Cp^*Co(CO)I]^-$ and $[Co(CO)_2(PEt_3)_2I]$. The catalyst responsible for the remarkable activity during the first period have not been characterised. It is likely that the active catalyst contains one or more phosphine ligands as there is free phosphine available at its highest concentration at this period, a likely catalyst is $[Cp^*Co(CO)(PEt_3)]$. The presence of $[Cp^*Co(COMe)(PEt_3)I]$, the product of oxidative addition of MeI to $[Cp^*Co(CO)(PEt_3)]$ would explain the rearrangement evolving Cp*H and the production of $[Co(CO)_2(PEt_3)_2I]$, this idea is developed further in the next section.

4.3e. Mechanistic Studies on $[Cp^*Co(CO)_2] + PEt_3$.

4.3e i. Mechanistic Studies on $[Cp^*Co(CO)_2]$ + Phosphine in MeI in Methanol.

$[Cp^*Co(CO)_2] + PEt_3$ + MeI + MeOH Under CO, ACM 187:

ACM 187A, Infrared Spectrum 47.

PEt_3 was added to a solution of $[Cp^*Co(CO)_2]$ in methanol and methyl iodide. An infrared spectrum was recorded of the solution, it had two peaks in the terminal carbonyl region, 2037 and 2025 cm^{-1} and absorption in the acyl stretching region at 1666 cm^{-1} indicative of $[Cp^*Co(COMe)(CO)I]$.[3]

ACM 187B, Infrared Spectra 48, 49, 50, 51 and 52.

The solution was injected in to the H.P.I.R. cell and pressurised with CO. At room temperature there were three peaks 1938, 2000 and 2034 cm^{-1}, (spectrum 48). These are assigned to $[Cp^*Co(CO)_2]$ (1938 and 2000 cm^{-1}see chapter 6) and $[Cp^*Co(COMe)(CO)I]$ (2034 cm^{-1}, shoulder on low frequency side). At 70 °C there were three major peaks 1984, 2024 cm^{-1} and a shoulder on the high frequency side of the 2024 cm^{-1} peak (spectrum 49). These peaks persisted (spectrum 50), but resolution was lost at 100 °C (spectrum 51). As the initial solution is heated from room temperature infrared 48 to 70 °C, two absorptions grow in the acyl region. The absorption at 1738 cm^{-1} is due to methyl acetate but there is also an absorption at 1700 cm^{-1}

INFRARED 47: ACM 187A in Dichloromethane - Dichloromethane.

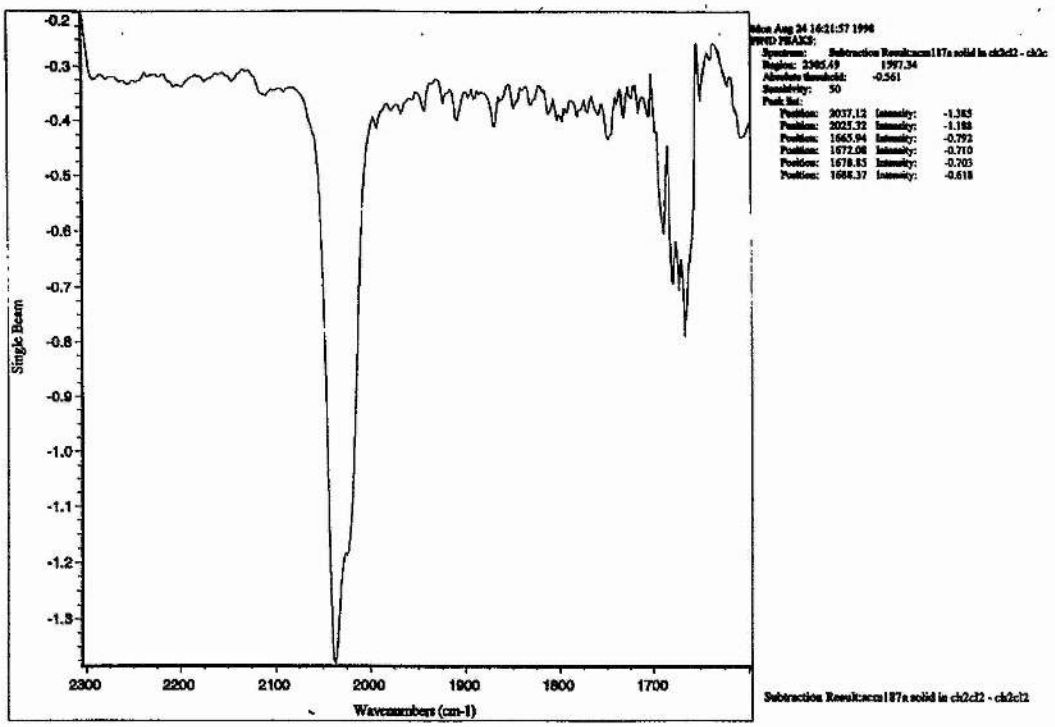

INFRARED 48: ACM 187, $[Cp^*Co(CO)_2]$ + PEt_3 in MeOH and MeI, 77 bar CO, 23 °C.

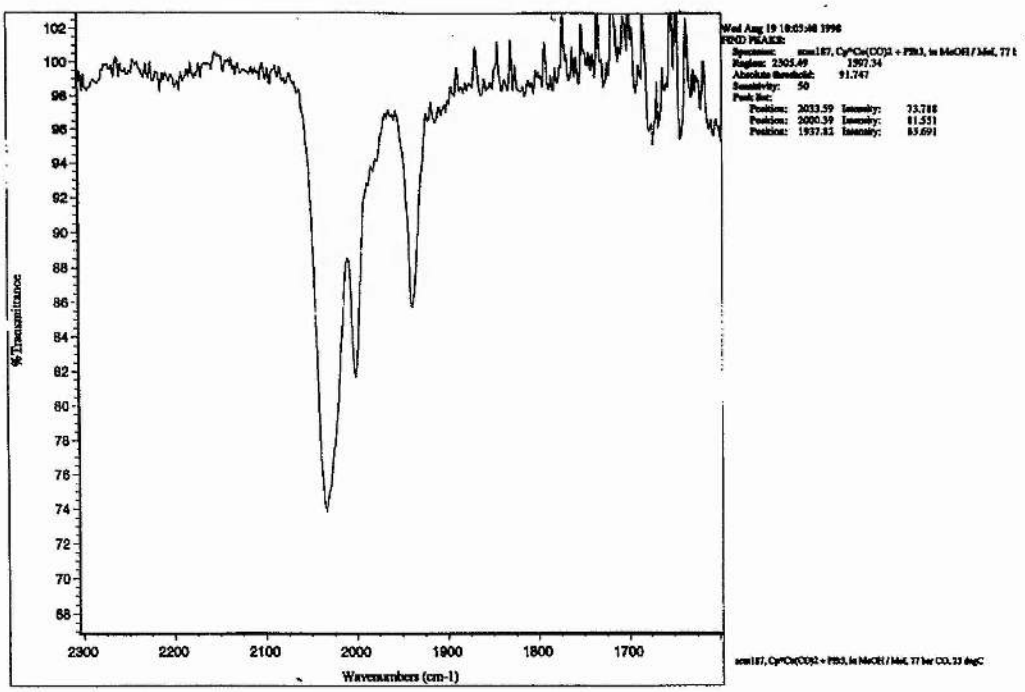

INFRARED 49: ACM 187, 70 °C.

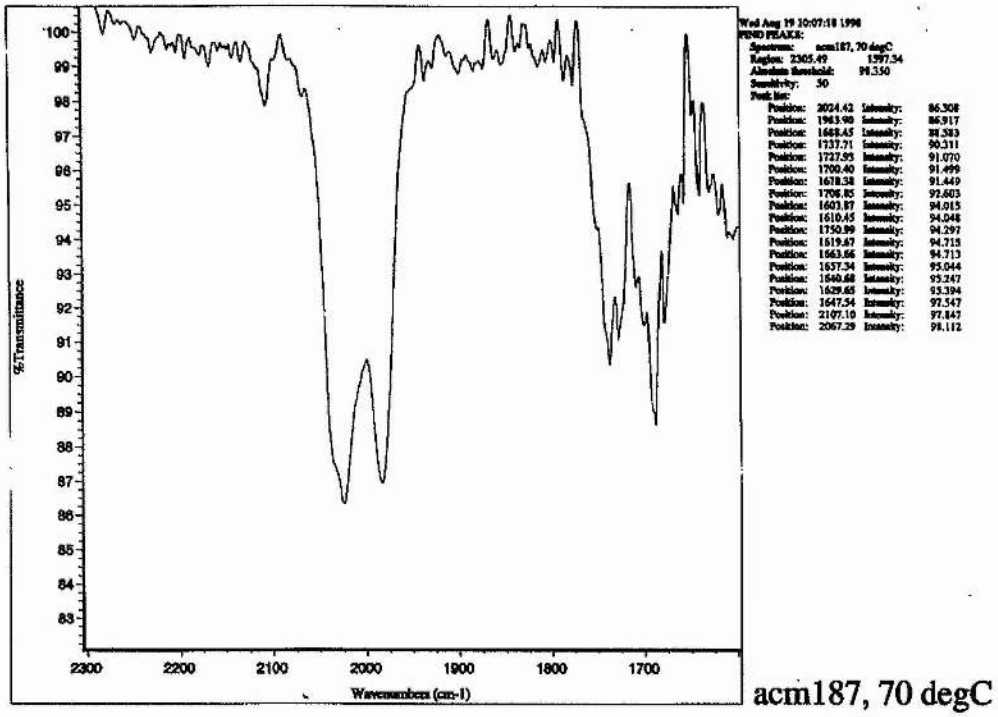

INFRARED 50: ACM 187, 80 °C.

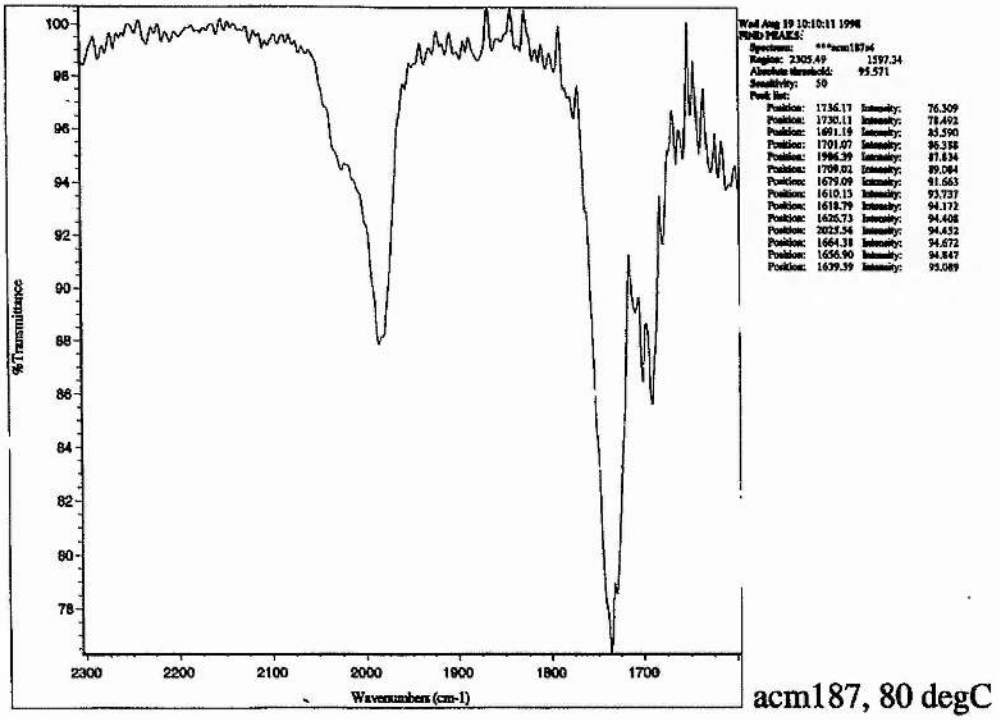

INFRARED 51: ACM 187, 100 °C.

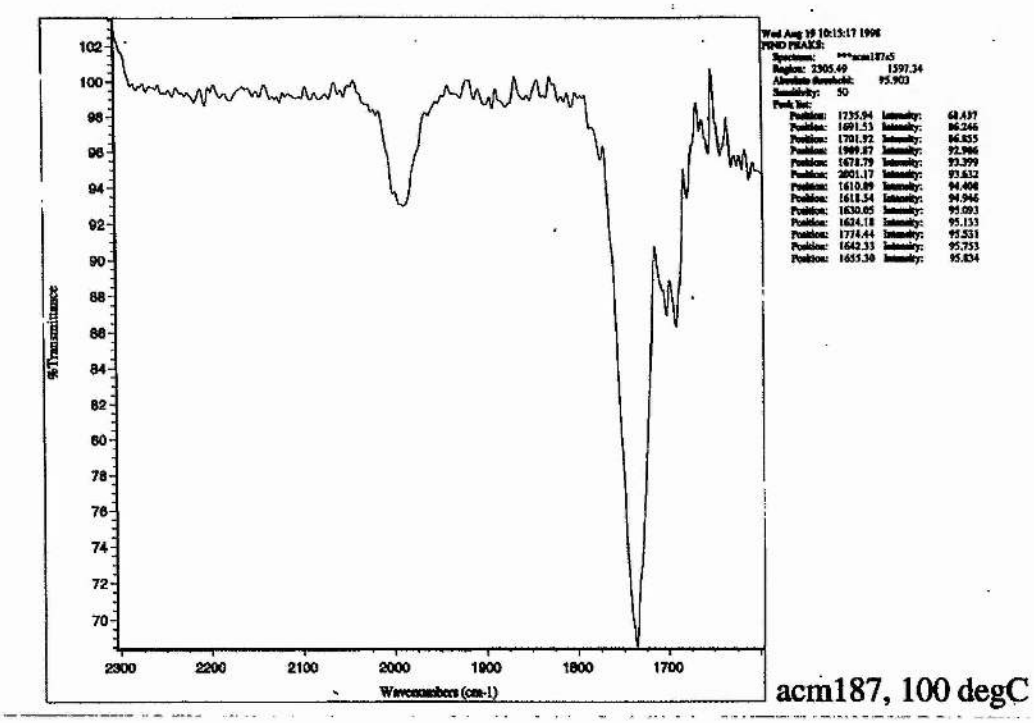

INFRARED 52: ACM 187, Cooled and Degassed.

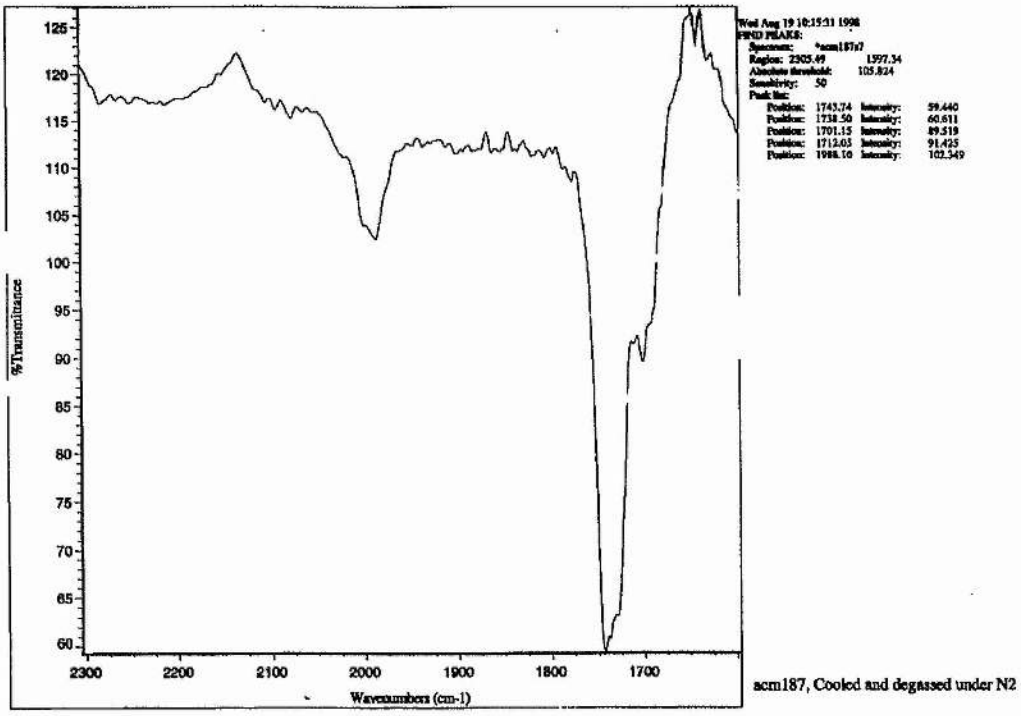

INFRARED 53: ACM 188, $[Cp^*Co(CO)_2]$ + PEt_3 in EtOH and MeI, 76 bar CO, 23 °C.

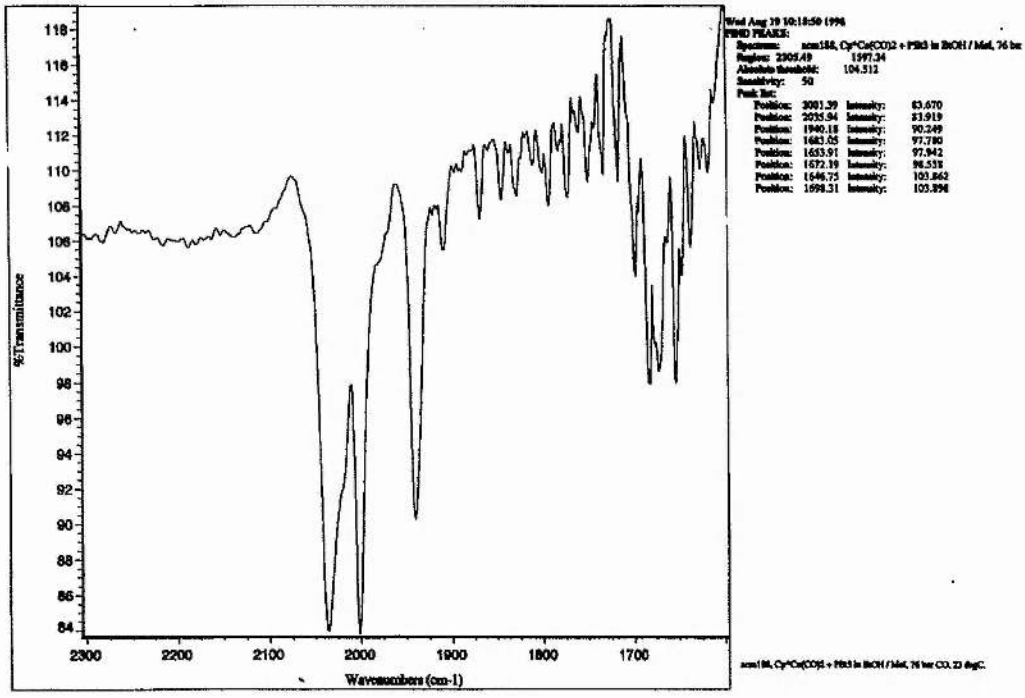

INFRARED 54: ACM 188, 70 °C.

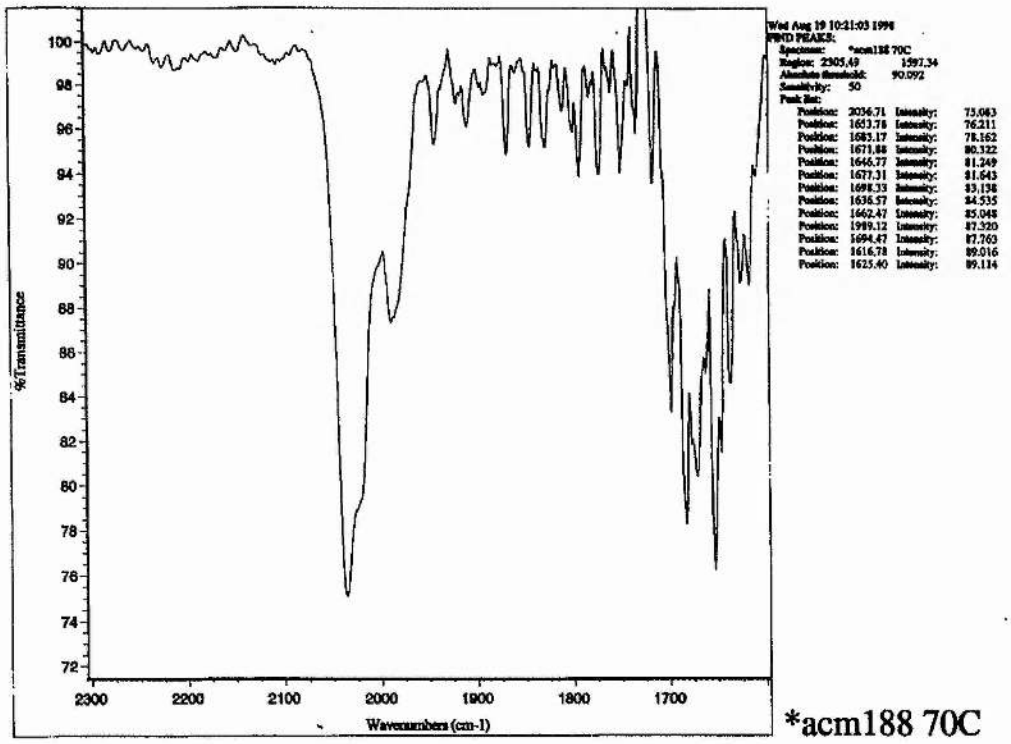

INFRARED 55: ACM 188, 100 °C.

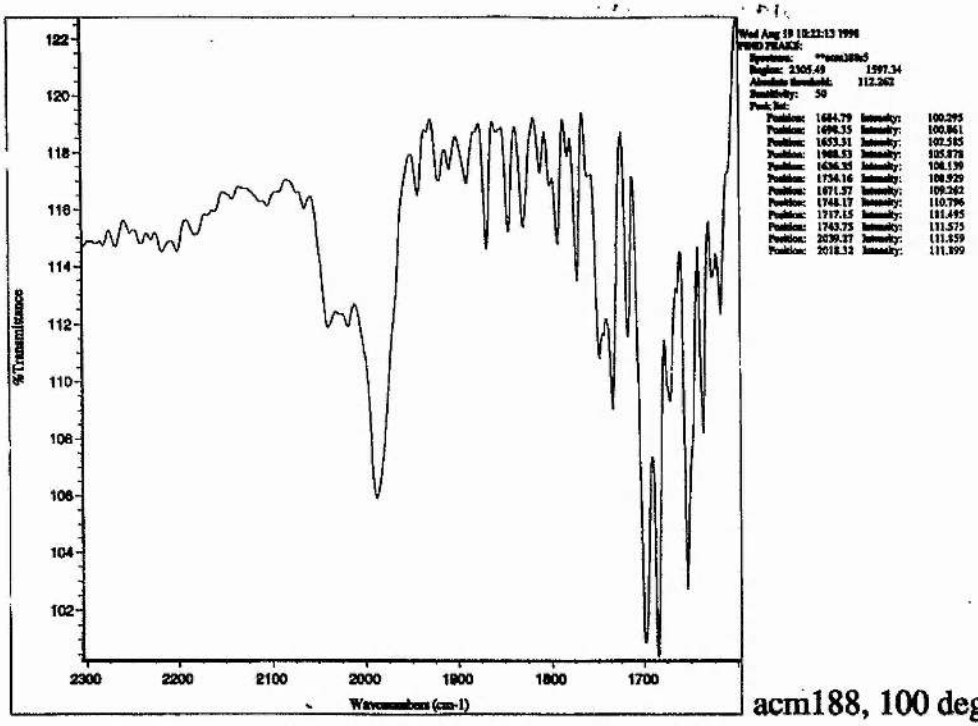

INFRARED 56: ACM 188, 120 °C.

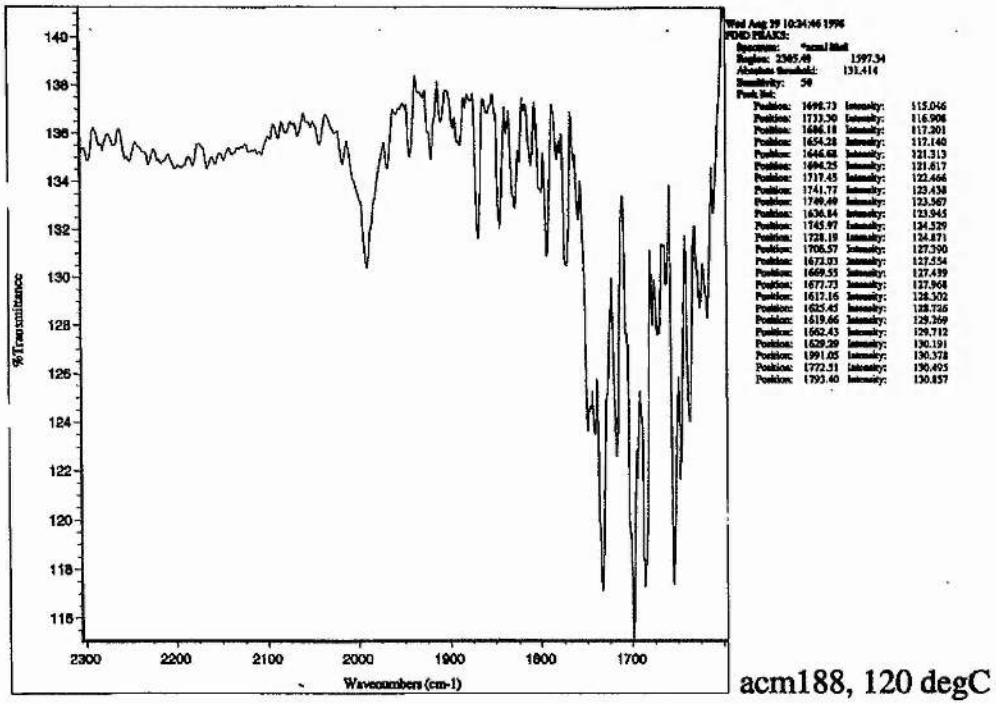

INFRARED 57: ACM 188, Cooled and Degassed.

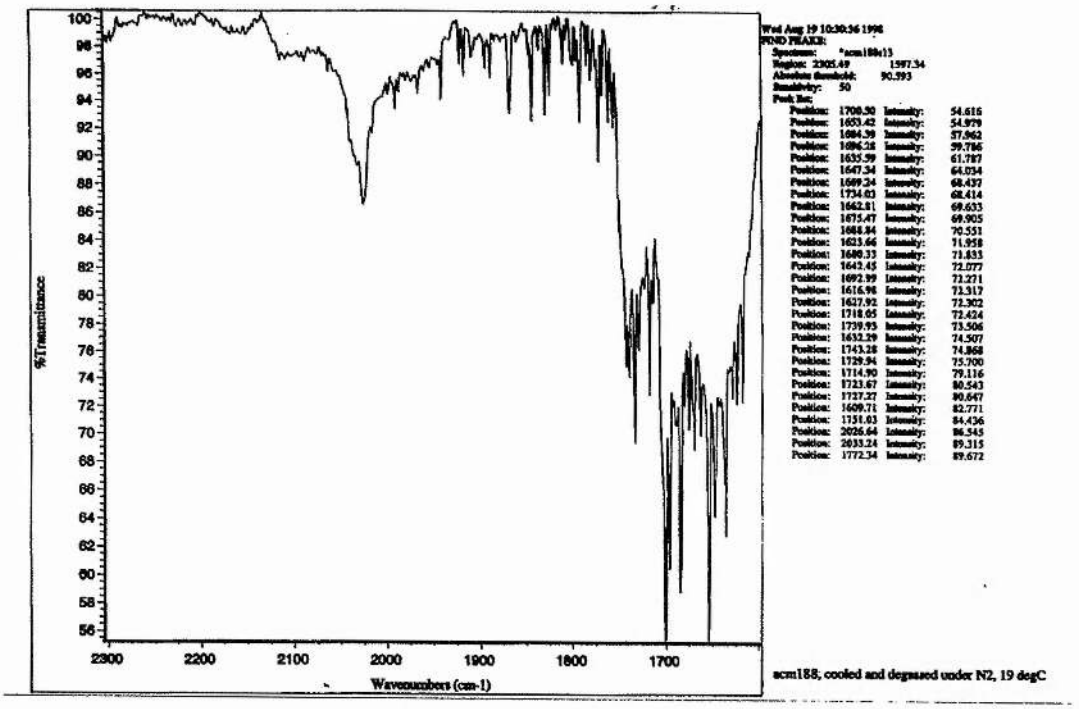

INFRARED 58: ACM 184, $[Cp^*Co(CO)_2]$ + PEt_3 in MeOH and MeI, heated in CO and Cooled.

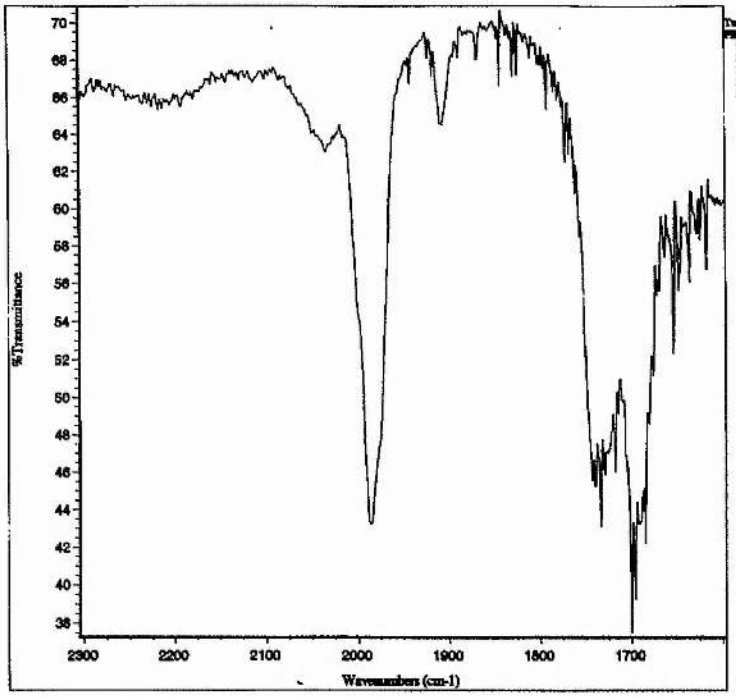

INFRARED 59: Solid Isolated from ACM 184 in CH_2Cl_2 - CH_2Cl_2.

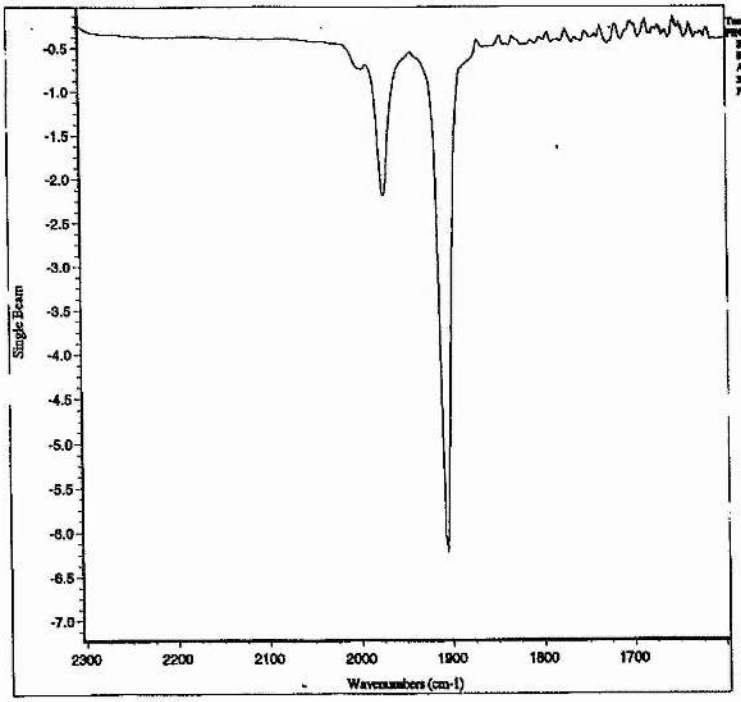

INFRARED 60: ACM 201, The Product Solution Under Argon.

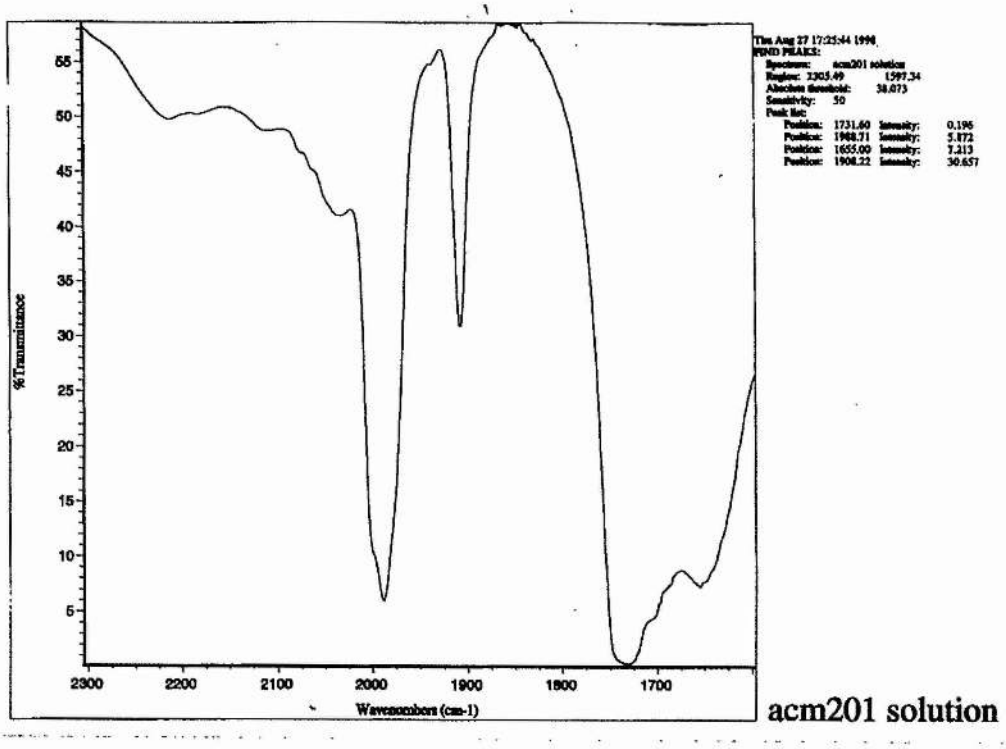

The autoclave was cooled and degassed under nitrogen and another spectrum taken, (spectrum 52) this had peaks at ~ 2024 cm^{-1} and 1988 cm^{-1}, product stretches at 1744 cm^{-1} and also an absorption at 1701 cm^{-1}.

n.m.r.

ACM 187A, The Reactant Solution.

A sample of the reactant solution separated prior to pressurising and heating was cooled until the solids precipitated. There was a dark solid and a white solid. The n.m.r. of these solids was recorded in CD_2Cl_2.

ACM 187A, 1H: The spectrum consisted of peaks of $[MePEt_3]I$ and two more resonances at 1.80 ppm, (Cp^*CH_3Co) and at 2.88 ppm (CH_3COCo), relative intensities ~ 5:1.

ACM 187A, 13C: There were peaks due to $[MePEt_3]I$ (see chapter 6) and $[Cp^*CH_3Co]$ 9.73 ppm.

ACM 187B, The product Solution.

After cooling and degassing the autoclave the orange solution was removed under nitrogen and n.m.r. spectra recorded in CD_3OD.

ACM 187B, 1H: The proton spectrum was paramagnetically line broadened and unintelligible.

ACM 187B, 13C: Only resonances due to $[MePEt_3I]$ were well resolved, although there were at least two peaks around 10 and one around 20 ppm.

Assigning the Spectra.

When PEt_3 was added to a solution of $[Cp^*Co(CO)_2]$ in methanol and methyl iodide the terminal carbonyl region of the infrared spectrum produced can be assigned to $[Cp^*Co(COMe)(CO)I]$. When this solution was pressurised with CO $[Cp^*Co(CO)_2]$ was detected. As the solution was heated up the infrared absorptions due to $[Cp^*Co(COMe)(CO)I]$ persisted, (2024, 2034 cm^{-1}) and those due to $[Cp^*Co(CO)_2]$ were consumed. A new CO stretching frequency at 1988 cm^{-1} was generated and this was a major species. There was considerable activity also in the acyl region of the infrared with the growth of an absorption at 1700 cm^{-1} that was more intense at 70 °C than the absorption due to methyl acetate and almost as intense as the terminal carbonyl

absorptions!, this may be [Cp*Co(COMe)(PEt_3)I] as the relative intensity of this absorptions was far in excess of that expected for [Cp*Co(COMe)(CO)I] alone.

[Cp*Co(CO)$_2$] + PEt_3 in MeI / Ethanol, ACM 188:

Infrared Spectra 53, 54, 55, 56 and 57.

In order to suppress the growth of organics and observe the spectrum for longer the experiment was rerun in ethanol. At room temperature and under CO pressure the spectrum was similar to that obtained in methanol (spectrum 53). As the temperature was increased to 70 °C the CO stretches at 2037, 1989 could be clearly seen (spectrum 54). Between 70 °C and 100 °C there was considerable growth in the acyl region between 1680 and 1700 cm^{-1}. In the terminal carbonyl region at 100 °C the stretch at 1989 cm^{-1} dominated and this persisted to 120 °C (spectrum 56), the product peaks were also strong ν_{co} = 1742 cm^{-1}. The autoclave was cooled and degassed under nitrogen and another spectrum taken (spectrum 57). The stretches at 2027 and 2033 cm^{-1} replaced 1989 cm^{-1} as the major absorptions in the terminal carbonyl region.

n.m.r. Spectra.

ACM 188B: The Resultant Solution in CD_3OD.

ACM 188B, 1H: The spectrum was paramagnetically line broadened.

ACM 188B, 13C: All the major peaks could be explained by the presence of EtOH, EtOAc, [$MePEt_3$]I and Cp*H.

Assigning the Infrared Spectra.

The reaction of [Cp*Co(CO)$_2$], MeI and PEt_3 was very similar in EtOH and MeOH, [Cp*Co(COMe)(CO)I] was the first product detected in solution. In methanol [Cp*Co(COMe)(CO)I] and [Cp*Co(CO)$_2$] were detected when the solution was pressurised with CO. The stretches due to the initial product [Cp*Co(COMe)(CO)I] gave way to the 1989 cm^{-1} absorption as the solution was heated under CO. When cooled and degassed the infrared spectrum returned to the spectrum for [Cp*Co(COMe)(CO)I] ν_{co} 2027, 2033 cm^{-1}. The compounds present break down in solution in the absence of CO to evolving Cp*H. The replacement of 1989 cm^{-1} by 2027 and 2033 cm^{-1} on cooling and degassing suggests that these compounds are related. An alternative explanation is that the 1989 cm^{-1} compound has decomposed, this does not explain the high relative intensity of the 2027 and 2033 cm^{-1} stretches in spectrum 57.

The changes in the acyl carbonyl stretching region were also very interesting. In infrared spectra 55, 56, 57 and 58 there were very strong absorptions in near 1700 cm^{-1} which were not due to methyl acetate. The intensity of these absorptions was greater than that of the absorptions in the terminal carbonyl region and this suggests that they were not due to any of the complexes with terminal carbonyl ligands. We assign this ν_{CO} to [Cp*Co(COMe)(PEt_3)I].

Attempts to Isolate the Compound with ν_{CO} 1989 cm^{-1}.

In all the infrared studies involving added PEt_3 a peak just below 1990 cm^{-1} had been observed during active carbonylation. Previous experiments suggested that this species contains a Cp* ligand and is part of a cycle involving [Cp*Co(COMe)(CO)I]. All attempts to isolate it have failed.

[Cp*Co$(CO)_2$] + PEt_3 in Methanol / Methyl Iodide, short run, ACM 184:

The 1989 cm^{-1} peak is a major product of heating [Cp*Co$(CO)_2$], MeI and PEt_3 together in an alcohol, an experiment was conducted in which these compounds were injected in to an autoclave, loaded with CO (80 bar) at room temperature and slowly heated to 100 °C. At 100 °C the autoclave was quenched in ice and cooled and degassed in a CO_2 / MeOH bath. The brown solution was removed under argon, residual solid turned green on exposure to air. The solution was syringed in to the high pressure infrared cell and a spectrum taken. The dominant peak was 1986 cm^{-1} although there were peaks at 2035 [Cp*Co(COMe)(CO)I] and 1908 cm^{-1} (infrared spectrum 58), peaks from MeOAc were also in evidence. The [$MePEt_3$]I was removed by successive reduction of volume, cooling and filtering. The dark red solution was left cooled at -20 °C. After over a month a solid was collected, this consisted of Co (II) and some red brown plate crystals. The red brown crystals had some impurities on their surface and were cleaned by extracting the impurities with petrol. The compound was short lived in dichloromethane decomposing to a green solid, before it decomposed an infrared spectrum was collected, (infrared spectrum 59). The resulting infrared had peaks at 1906 and 1974 cm^{-1}, indicative of a dicarbonyl compound. The ^1H n.m.r. in CD_2Cl_2 contained two multiplets at 1.20 and 2.14 ppm ratio of areas ~ 6:9, suggesting the presence of PEt_3, no signals due to Cp* were detected. The crystals were submitted for an X-Ray crystal structure, the X-Ray structure of this compound, identified as [Co$(CO)_2(PEt_3)_2$I], see appendix 1. The

product trans $[Co(CO)_2(PEt_3)_2I]$ was analogous to $[Co(CO)_2(PMe_2Ph)_2I]$ isolated from the reaction of $[CpCo(CO)PMe_2Ph]$ and MeI under CO in methanol. Once again we were unable to identify the source of the 1986 cm^{-1} peak.

4.3e ii. Conclusions from the Mechanistic Studies.

ACM 187, 188: $[Cp^*Co(CO)_2]$ + MeI and PEt_3 in Alcohols.

The infrared assignments from experiments 187 and 188 are in table 4.14.

TABLE 4.14: The Infrared Assignment of Experiments ACM 187 and ACM 188.

ν_{co} / cm^{-1}	Solvent	Assignment
1938, 2000	Methanol	$[Cp^*Co(CO)_2]$
1940, 2001	Ethanol	$[Cp^*Co(CO)_2]$
1984-1988	Methanol	Unknown
1989	Ethanol	Unknown
~ 1700	Methanol, Ethanol	$[Cp^*Co(COMe)(PEt_3)I$
2024-2025, 2034-2037 acyl-M stretches	Methanol	$[Cp^*Co(COMe)(CO)I]$
2027, 2033-2037 acyl-M stretches	Ethanol	$[Cp^*Co(COMe)(CO)I]$

The chemistry is essentially the same in methanol and ethanol, in methanol the main product is methyl acetate, in ethanol ethyl acetate. At 100 °C - 120 °C the unknown species dominates and this is the key to understanding the enhanced rates of carbonylation. It is clear that the potential to operate via the a pathway involving intermediates derived from $[Cp^*Co(CO)_2]$ is still there as the cooled and degassed solution contains $[Cp^*Co(COMe)(CO)I]$.

$[Co(CO)_2(PEt_3)_2I]$ was not detected in the *in situ* experiments, this suggests that if it is present, it exists only in a low concentration.

ACM 184: $[Cp^*Co(CO)_2]$ + PEt_3 in Methanol / Methyl Iodide, Short Run.

Attempts to isolate the unknown with ν_{co} ~1986 cm^{-1} unearthed an unexpected substance in the solution. If the solution is frozen and degassed after just reaching 100 °C the solution exhibited absorptions at 1908, 1986 and 2035 cm^{-1}. A solid was isolated from

the solution with absorptions at 1906 and 1974 cm^{-1} in dichloromethane. This did not represent the most intense absorption in the original solution but was significant. This compound was discovered to be $[Co(CO)_2(PEt_3)_2I]$. The infrared assignments are in table 4.15.

TABLE 4.15: The Infrared Assignment of Experiment ACM 184.

ν_{CO} / cm^{-1}	Solvent	Assignment
1908, under 1986	Methanol	$[Co(CO)_2(PEt_3)_2I]$
1906, 1974	Dichloromethane	$[Co(CO)_2(PEt_3)_2I]$
1986	Methanol	Unknown
2035	Methanol	[Cp*Co(COMe)(CO)I]

4.3e ii. Conclusions, the Effect of PEt_3.

PEt_3 as a Ligand.

The isolation of $[Co(CO)_2(PEt_3)_2I]$ leads us to some important conclusions. Firstly it shows that phosphine has taken an active role in the catalytic mixture binding to cobalt and increasing the electron density on the metal. This opens the possibility that $[Cp^*Co(CO)PEt_3]$ exists in solution for a short time. In chapter 3 the rearrangement of $[CpCo(CO)PMe_2Ph]$ in methanol and methyl iodide was observed, this gave rise to $[CpCo(COMe)(PMe_2Ph)I]$ which decomposed in CO to $[Co(CO)_2(PMe_2Ph)_2I]$ and an unknown of ν_{CO} 1981-1984 cm^{-1}. The analogous behaviour could account for the spectrum of the solution observed in ACM 184. Secondly the transition from Cp to Cp* has not strengthened the ring to cobalt bond enough to prevent its displacement by triethyl phosphine. Thirdly we discovered the catalytic activity of $[Co(CO)_2(PMe_2Ph)_2I]$ in chapter 3 and can therefore assume that $[Co(CO)_2(PEt_2)_2I]$ also has catalytic activity in solution, we conclude that the catalytic activity in these solutions is due to at least two catalytic systems.

DIAGRAM 50: $[Cp^*Co(CO)_2] + PEt_3$
Processes Occurring in Solution:

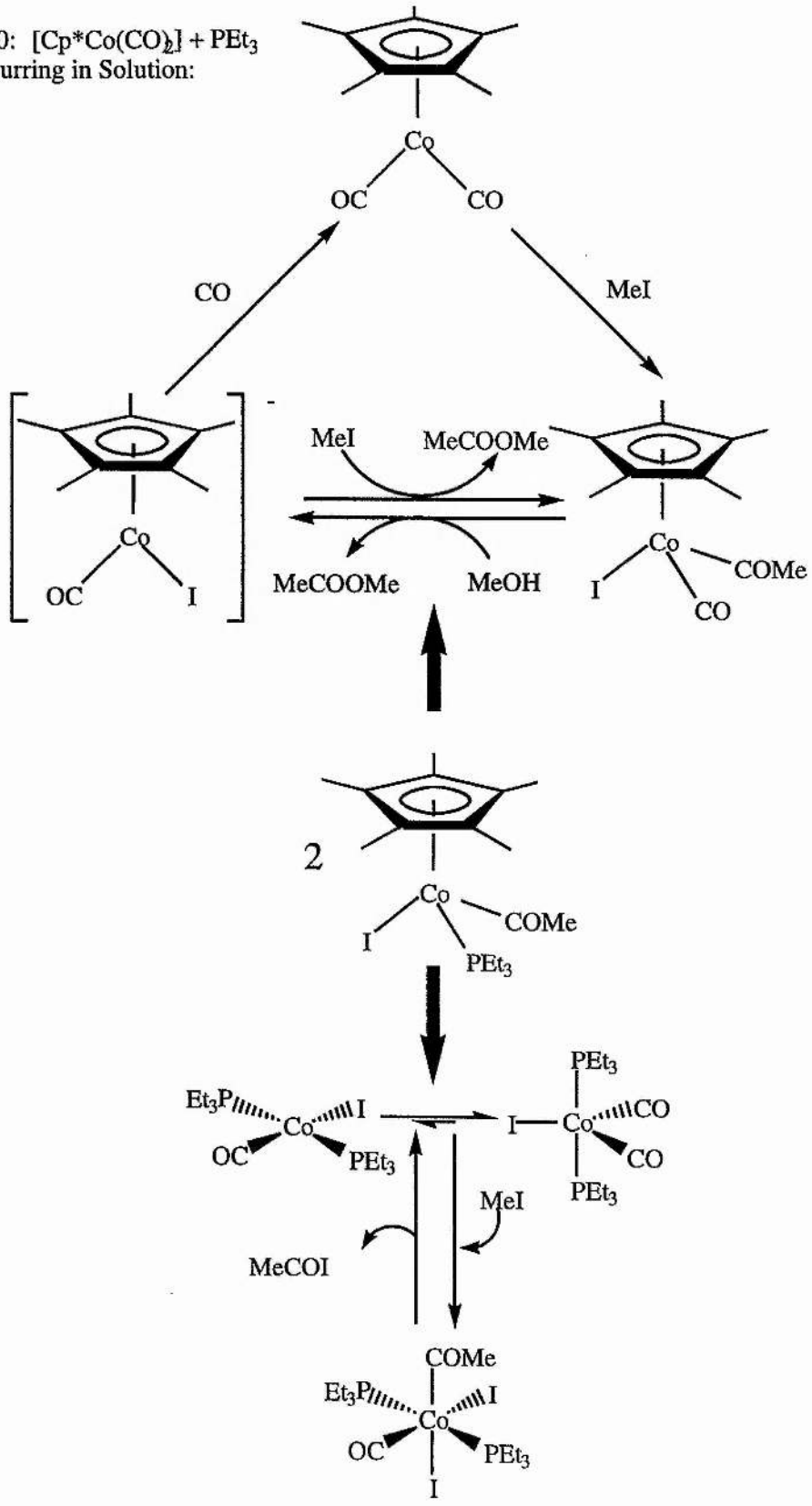

One possible explanation for the activity observed in the kinetics experiments on $[Cp^*Co(CO)_2] + PEt_3$ is detailed in diagram 50, this suggestion is consistent with our HPIR experiments. $[Cp^*Co(COMe)(PEt_3)I]$ from the reaction of a Cp* intermediate with PEt_3 decomposes to $[Co(CO)_2(PEt_3)_2I]$ and the unknown which we propose is involved in the Cp* cycle. The shape of the ballast vessel versus time graphs obtained for $[Cp^*Co(CO)_2] + PEt_3$ contained three regions, the initial fast rate, a period of no carbonylation and the second, more stable, region of catalytic activity. By evoking Bergman's idea that the mechanism for ligand rearrangement CpCo involves dicobalt intermediates [5] we can suggest a mechanism that explains this observation, diagram 51. The initial period of methanol carbonylation may be due to a $[Cp^*Co(CO)PEt_3]$ derived catalytic system. The product of oxidative addition of MeI to $[Cp^*Co(CO)PEt_3]$ is $[Cp^*Co(COMe)(PEt_3)I]$. If the slowest step in this rapid carbonylation cycle is reductive elimination $[Cp^*Co(COMe)(PEt_3)I]$ will collect and the cycle will not show up in the terminal carbonyl region of the infrared. MeCO removal from $[Cp^*Co(COMe)(PEt_3)I]$ may result in a build up of $[Cp^*Co(PEt_3)I]^-$ which would also not register in the terminal carbonyl region of the infrared. Some of the $[Cp^*Co(PEt_3)I]^-$ may lose PEt_3 and gain a carbonyl ligand to form $[Cp^*Co(CO)I]^-$.

We know that the early catalyst undergoes a rearrangement generating Cp*H, $[Co(CO)_2(PEt_3)_2I]$ and a species with an infrared ν_{CO} at ~ 1986 cm^{-1}, similarly in chapter 3 $[CpCo(COMe)(PMe_2Ph)I]$ was found to undergo a rearrangement to generate $[Co(CO)_2(PMe_2Ph)_2I]$, and it is sensible to suggest that the route to $[Co(CO)_2(PEt_3)_2I]$ is via $[Cp^*Co(COMe)(PEt_3)I]$. Working through our proposed mechanism another likely product of the rearrangement is $[Cp^*Co(CO)I]^-$, this species may be responsible for the infrared absorption at ~ 1986 cm^{-1}. The period of no catalytic activity occurs when most of the metal is tied up as $[Cp^*Co(PEt_3)(I)]^-$ at high phosphine concentration. In the final solution the concentration of $[Cp^*Co(CO)I]^-$ exceeds that of $[Co(CO)_2(PEt_3)_2I]$ because the anion can also be formed by the substitution of PEt_3 by CO in $[Cp^*Co(PEt_3)(I)]^-$. This mechanism also explains the observation that $[CpCo(COMe)(PMe_2Ph)I]$ was found to generate $[Co(CO)_2(PMe_2Ph)_2I]$ under 10 bar of CO but none of the bis phosphine complex was observed at 60 bar of CO. The higher pressure of CO promoted the formation of $[CpCo(CO)I]^-$ from $[CpCo(PMe_2Ph)I]^-$ and prevented the rearrangement reaction which requires $[CpCo(PMe_2Ph)I]^-$ as one of the reactants.

DIAGRAM 51: Possible Mechanism for the formation of $[Co(CO)_2(PEt_3)_2I]$ incuding ν_{co} observed in ACM 184.

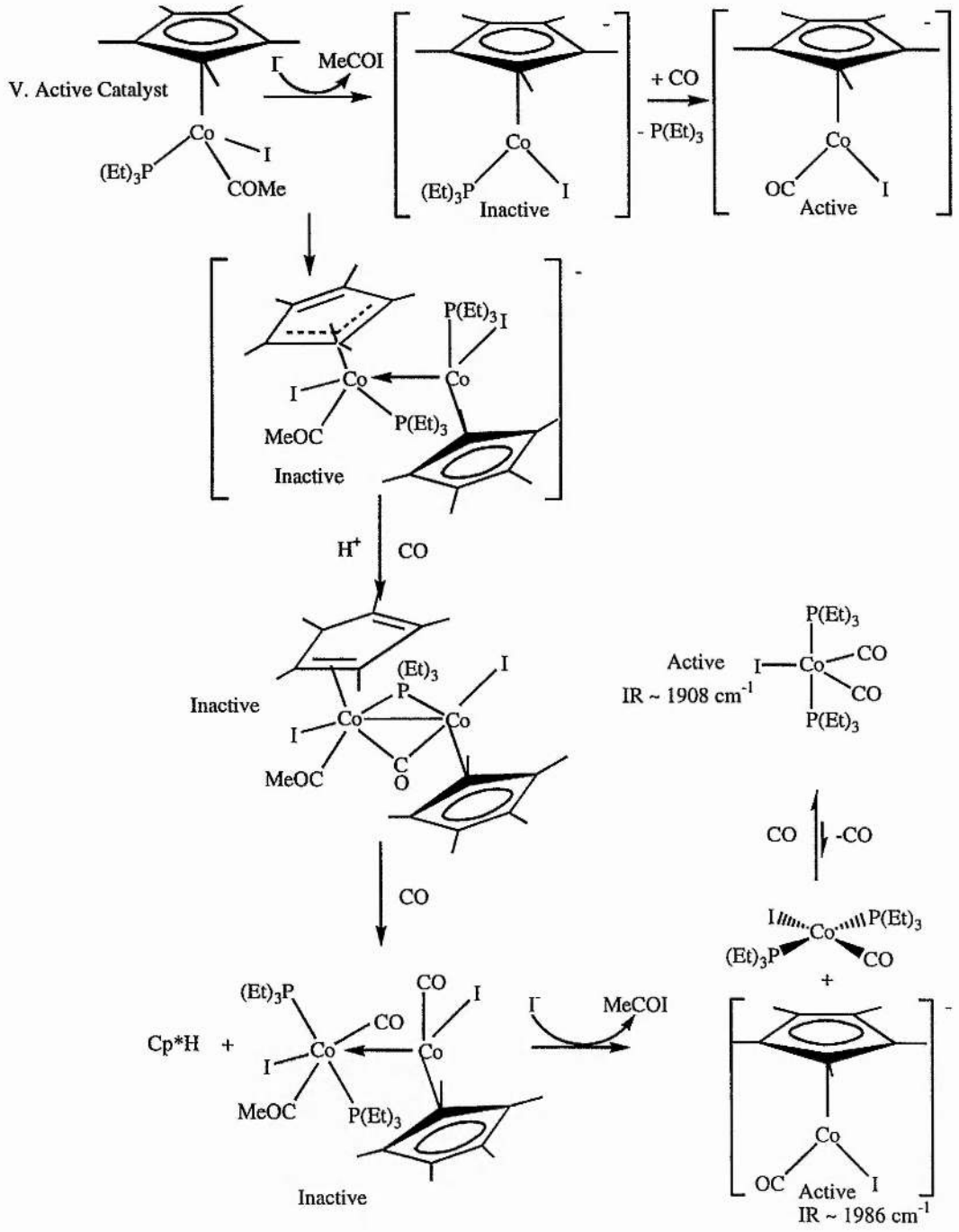

In the presence of excess PEt_3 it is not necessary to propose a dinuclear intermediate to explain the production of $[Co(CO)_2(PEt_3)_2I]$ as this may form as the result of a displacement of Cp* from the metal centre by PEt_3 possibly through a ring slippage mechanism involving cleavage of a η^1 Co-Cp* bond. The possibility of such a

mechanism is suggested by the results obtained for [CpCo(CO)PMe_2Ph].
Although one possible explanation, the mechanisms detailed in diagram's 50 and 51 fail to explain the high concentration of the 1980 – 1990 cm^{-1} absorption in the final solution of ACM 201. $[Cp^*Co(CO)I]^-$ would be expected to be in equilibrium with $[Cp^*Co(CO)_2]$. This equilibrium should lie towards the dicarbonyl species and this species is not observed.

PEt_3 as a Source of Iodide.

PEt_3 reacts with MeI to form $[MePEt_3]I$. The availability of I^- may speed up the reductive elimination of MeCO from [Cp*Co(COMe)(CO)I] and therefore increase the concentration of Co (I) and hence the rate of carbonylation. An increase in the rate of reductive elimination would account for the improved selectivity on adding phosphine to the system. Increased I^- may also increase the concentration of $[Cp^*Co(CO)I]^-$.

4.4. FURTHER WORK.

The work thus far has revealed that it is possible to produce a highly active and selective cobalt catalyst. In chapter 5 we will propose some likely methanol carbonylation cycles available to cobalt in the systems we have studied, and discuss how the chemistry could be improved in order to further boost activity and improve the stability of the catalysts involved.

CHAPTER 5: DISCUSSION AND FURTHER WORK.

5.1. DISCUSSION.

5.1 a. Cyclopentadienyl Cobalt Carbonyl Phosphines.

The first class of catalyst studied was of the general formula [CpCo(CO)P]. Some catalytic activity was observed but the average turnovers calculated from the batch autoclave results were always very low. *In situ* infrared spectroscopy on these systems revealed that they were prone to rearrangement with loss of the Cp ligand.

The processes occurring in solution may be as summarised in diagram 52.

DIAGRAM 52: The Fate of [CpCo(CO)PR_3] in Solution.

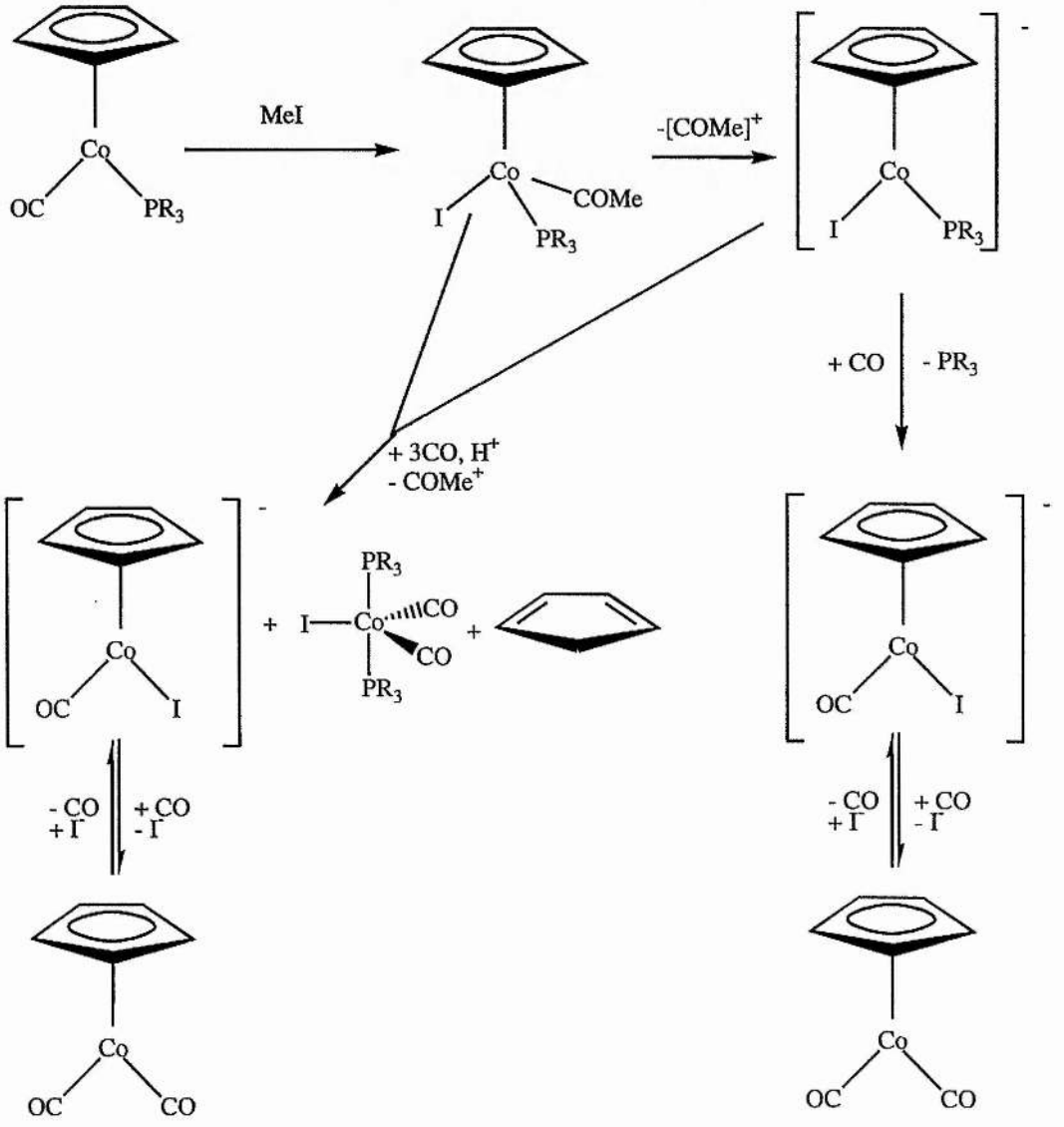

[CpCo(COMe)(P)I] can rearrange to $[Co(CO)_2(P)_2I]$ and $[CpCo(CO)I]^-$. The Co-I bond is labile under CO and the anionic species will be in equilibrium with the $[CpCo(CO)_2]$. This equilibrium lies towards the dicarbonyl complex under catalytic conditions and this explains the low activity of these catalysts as most of the catalytic activity observed is due to a low level of $[Co(CO)_2(P)_2I]$. The rate can be increased by adding free phosphine. Work on these systems was abandoned as the rates were poor.

5.1b. Cyclopentadienyl Cobalt Dicarbonyl.

Batch autoclave testing revealed that the addition of PEt_3, $[MePEt_3]I$ or LiI could initiate catalytic activity for $[CpCo(CO)_2]$. As $[CpCo(CO)_2]$ does not significantly react with MeI it we conclude that the oxidative addition step has been facilitated.

5.1b i. The Addition of Iodide.

The addition of high quantities of iodides is more effective than one equivalent and we propose that the activity is due to the production of $[CpCo(CO)I]^-$ in solution. The increased electron density on the metal centre would be expected to initiate a reaction with MeI. *In situ* infrared spectroscopy revealed that the only terminal metal carbonyls in solution were those of $[CpCo(CO)_2]$, this would suggest that the concentration of $[CpCo(CO)I]^-$ was low under these conditions. The rate of carbonylation could be increased by increasing the concentration of the active species.

5.1b ii. The Addition of PEt_3.

We believe that the addition of PEt_3 has three effects.

The first effect is that of added inorganic iodide as PEt_3 quaternises with MeI to produce $[MePEt_3]I$. The second effect is to facilitate the displacement of the Cp ring and rearrangement to $[Co(CO)_2(PEt_3)_2I]$ this is expected to be an active carbonylation catalyst by analogy with $[Co(CO)_2(PMe_2Ph)_2I]$. The third effect is to increase the concentration of the unknown species with ν_{co} 1980 -1990 cm^{-1} which may be $[CpCo(CO)I]^-$.

$[CpCo(CO)I]^-$ may be formed from the reaction of $[CpCo(PEt_3)I]^-$ with CO and from the rearrangement reaction that also generates $[Co(CO)_2(PEt_3)_2I]$, see section 5.1 a. The existence of two catalysts in solution help to explain why the $[CpCo(CO)_2] + PEt_3$ catalytic precursor was the most active so far. Unfortunately the catalysts were comparatively short lived. We decided to develop this idea, strengthening the cobalt to

ring bond by changing the ligand to the more basic pentamethyl cyclopentadienyl. It was also hoped that the Cp* ligand would enable more of the cobalt in solution to be active as $[Cp^*Co(CO)_2]$ itself reacts with MeI.

5.1c. Catalysts Derived from Pentamethyl Cyclopentadienyl Cobalt Dicarbonyl.

5.1c i. $[Cp^*Co(CO)_2]$.

$[Cp^*Co(CO)_2]$ is an active catalyst for the carbonylation of methanol. We believe that the slowest step in the reaction at temperatures of ~ 100 °C is reductive elimination as $[Cp^*Co(COMe)(CO)I]$ was detected as the major species in our *in situ* studies at this temperature. This is consistent with the production of acetaldehyde related side products detected in the product solutions.

5.1c. ii. $[Cp^*Co(CO)_2] + PEt_3$.

The addition of phosphine to $[Cp^*Co(CO)_2]$ has a very dramatic effect on the activity and this is the most active cobalt carbonylation catalyst precursor studied.

The first effect is that of inorganic iodide. As well as setting up an equilibrium with $[Cp^*Co(CO)I]^-$ the presence of $[MePEt_3]I$ is expected to increase the rate of reductive elimination as it is a nucleophile capable of attacking the carbonyl carbon of the acetyl grouping. This will increase the rate of carbonylation and improve the selectivity. Both effects are observed when PEt_3 is added. As before the free phosphine also displaces some of the rings as Cp* is labile to substitution reactions. One of the products of this rearrangement is $[Co(CO)_2(PEt_3)_2I]$ and is expected to be an active carbonylation catalyst by analogy with $[Co(CO)_2(PMe_2Ph)_2I]$.

There is a further effect of adding PEt_3 not observed in any of the other systems studied, the production of a very highly active carbonylation catalyst during the early part of the reaction. At this point in the reaction the concentration of free phosphine is at its highest and it may be that the mystery catalyst is $[Cp^*Co(CO)(PEt_3)]$. We can explain the absence of such high catalytic activity in the case of $[CpCo(CO)_2] + PEt_3$ as $[CpCo(COMe)(PEt_3)I]$ is expected to lose Cp faster than $[Cp^*Co(COMe)(PEt_3)I]$ due to the improved ligating properties of the pentamethyl cyclopentadienyl ligand. Suggested catalytic cycles are contained in diagrams 53 and 54.

DIAGRAM 53: The $[Cp^*Co(CO)_2]$ Catalytic Cycles.

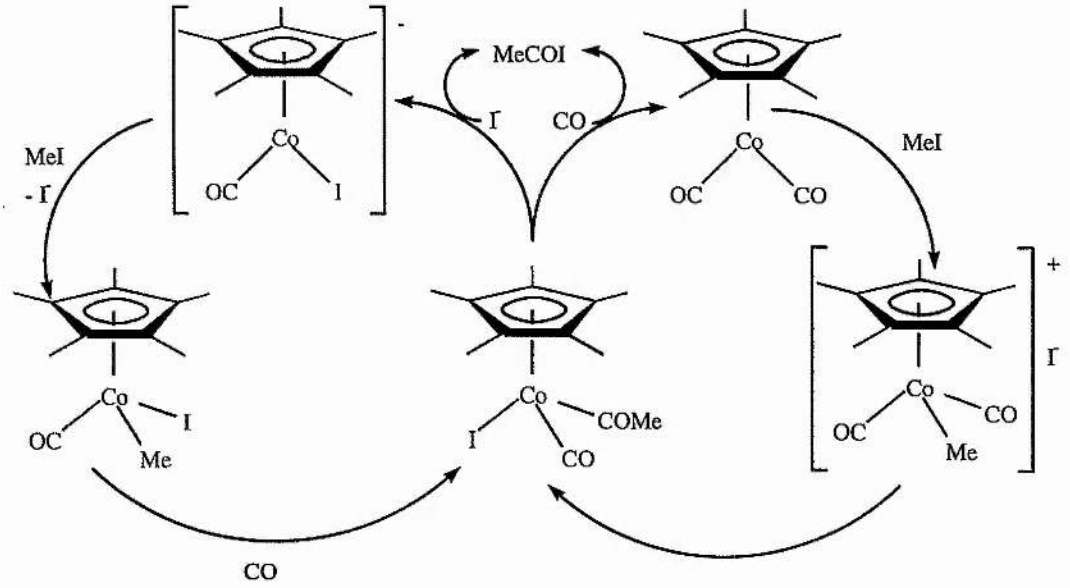

DIAGRAM 54: The $[Co(CO)_2(PEt_3)_2I]$ Catalytic Cycle.

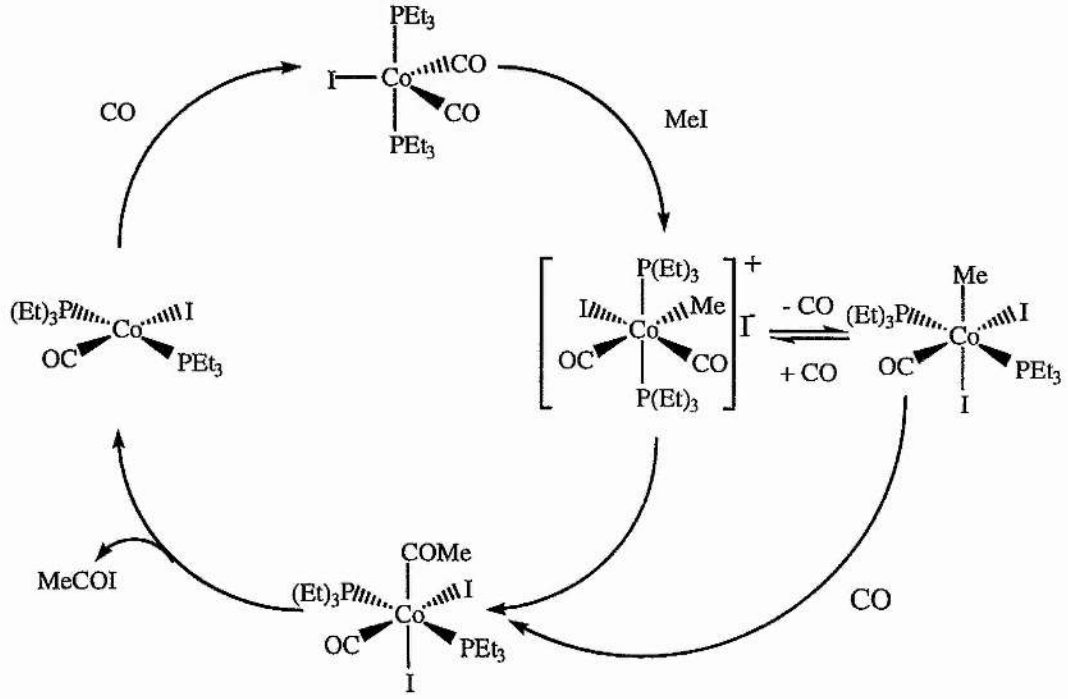

5.2 FURTHER WORK ON NOVEL GROUP 9 CATALYSTS FOR THE CATALYTIC CARBONYLATION OF METHANOL.

5.2a. Cyclopentadienyl Cobalt Carbonyl Catalyst Precursors.

It is clear that the ring to cobalt bond is susceptible to cleavage by good nucleophiles. In the absence of basic phosphines the metal to ring bond would appear to stay in tact. The main focus of further work in to pentamethyl cyclopentadienyl cobalt carbonyl catalysts will be to reproduce the kind of rates observed in the initial period of the $[Cp^*Co(CO)_2]$ + PEt_3 catalytic runs and stabilise the active species. This would give a highly active carbonylation catalyst based on a cheap metal and would represent a significant step forward in methanol carbonylation technology.

In our group David Elias has done some initial studies on phosphine substituted cyclopentadienyl cobalt carbonyl compounds as catalyst precursors for the carbonylation of methanol with exactly this goal in mind [1]. D. Elias did observe the production of small amounts of methyl acetate when $[Cp^*Co(CO)(PEt_3)]$ was employed as a catalyst precursor. An *in situ* infrared study of $[Cp^*Co(CO)PMe_2Ph]$, inactive under the same conditions, pointed to a catalytic cycle which was held up at the $[Cp^*Co(COMe)(PMe_2Ph)I]$ stage. The reductive elimination step is slow as the high electron density in the metal. The addition of iodide should help resolve this problem.

In order to improve the stability of the metal to ring and metal to phosphine linkages chelating cyclopentadienyl ligands could be employed. The use of Cp ligands with a pendant arm attached to a basic phosphine would give the correct geometry for catalytic activity combined with the high electron density provided by the donor ligands and the added stability afforded by the chelate effect. Work on these compounds was begun by D. Elias in collaboration with A. J. Brown and myself [1].

5.2b. Other Cyclopentadienyl Metal 9 Carbonyl Catalyst Precursors.

The decomposition of cyclopentadienyl cobalt compounds occurs by ring displacement. The other two members of group 9 are held together by a stronger metal to ring linkage. [2] It is worthwhile to consider the use of the cyclopentadienyl rhodium and iridium carbonyls:

5.2b i. The Reaction of MeI and $[Cp^{(*)}M(CO)_2]$, M = Ir, Rh.

$[CpRh(CO)_2]$ and $[CpIr(CO)_2]$ are well documented metal bases. [3] These electron rich 18 electron complexes react readily with electrophiles despite their lack of a lone pair of electrons. They are, however, thought to be inert to methyl iodide as the presence of two carbonyl groups attached to these soft metals reduces the electron density on the metal too much. They do undergo reactions with perfluorinated alkyl halides analogous to those of $[CpCo(CO)_2]$.

By moving to the pentamethyl cyclopentadienyl (Cp^*) rhodium and iridium carbonyls the desired reaction with methyl iodide can be induced. The product obtained reflects the tendency of the different metals to promote alkyl migration reactions. [4] At 50°C in benzene $[Cp^*Rh(CO)_2]$ reacts with alkyl halides to form the acyl iodo complex $[Cp^*Rh(COMe)(CO)I]$ in high yield. The mechanism is nucleophilic attack of MeI, followed by nucleophilic attack of I^- and insertion of CO in to the methyl-carbon to rhodium bond.

DIAGRAM 55: The Reaction of $[Cp^*Rh(CO)_2]$ with MeI.

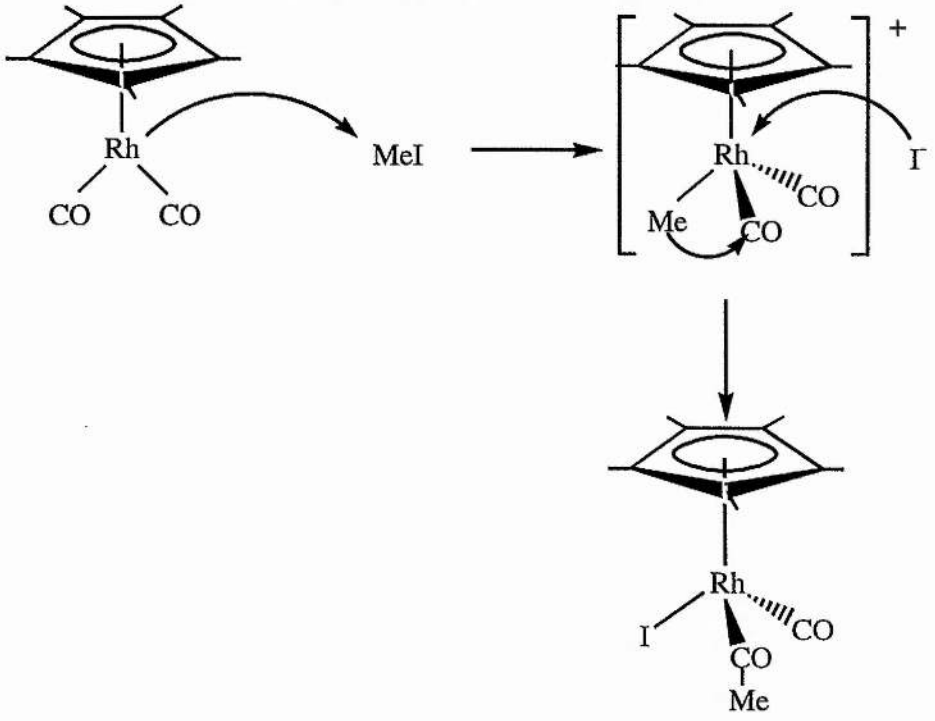

The iridium complex attacks methyl iodide even more readily forming the ionic complex $[Cp^*Ir(CO)_2Me]I$. The rate of migratory insertion is slow and this is as far as the iridium reaction goes. This complex decomposes in air to form $[Cp^*Ir(CO)I_2]$ and reform

[Cp*Ir(CO)$_2$], or in chloroform-*d* to form [Cp*Ir(CO)I$_2$] and [Cp*Ir(CO)Cl$_2$] despite the comparative strength of the iridium- carbon bond. [Cp*Ir(CO)I$_2$] and [Cp*Ir(CO)Cl$_2$] are susceptible to further reversible loss of CO. The decomposition pathway is believed to be:

DIAGRAM 56: The Decomposition Pathway of [Cp*Ir(CO)$_2$Me]I.

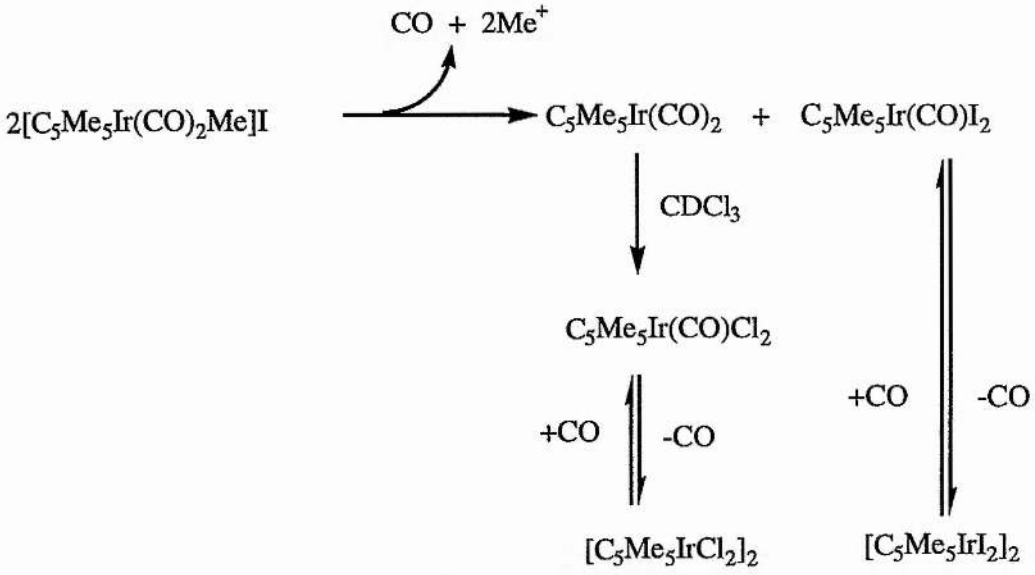

Maitlis *et al* [5] compared the rates of reaction of Cp*Rh(CO)$_2$ and Cp*Ir(CO)$_2$ with methyl iodide. In Dichloromethane the reaction is second order in rhodium. The intermediate methyl complex was not detected by HPIR techniques. The product of the iridium reaction [Cp*Ir(CO)$_2$Me]I is in equilibrium with the reactants and therefore although first order in both reactants, the kinetics of this process are more complicated. Under comparable conditions the iridium complex was found to react approximately four times faster.

From these results it would seem that Cp*Rh(CO)$_2$ is the most likely candidate for a Cp metal dicarbonyl carbonylation catalyst.

5.2c. [Cp*Rh(CO)$_2$] as a Catalyst for Methanol Carbonylation.

5.2c i. Batch Autoclave Runs in Methanol.

See table 5.1. The results were very promising, the rates of reaction were very high. Comparison of the two results suggested that there was an initial period of induction before the rate reached its highest value.

TABLE 5.1: Batch Autoclaves with [Cp*Rh(CO)$_2$]:

Expt. No	[Rh] / mol dm^{-3}	Autoclave S = Steel H = Hastelloy	Temp. / °C E=External I = Internal	P / bar RO = Room temp. RE = Reaction Temp.	MeOH / g	MeI / g	Volume / cm^3	Run Time / hr	[MeOAc] / mol dm^{-3}	Rate / mol dm^{-3} hr^{-1}	Rate / turnover hr^{-1}
ACM 144	0.0010	H. 28 cm^{-3}	135 I	62 RO	3.16	2.28	5.0	4	3.23	0.808	808
ACM 157	0.0012	H. 28 cm^3	140 I	60 RO	3.16	2.28	5.0	1	0.51	0.510	441

5.2c ii. High Pressure Infrared Studies.

In order to establish the nature of the active species in solution we carried out an infrared study.

[Cp*Rh(CO)$_2$] + MeI + EtOH + CO, Catalyst Stability, ACM 145:

[Cp*Rh(CO)$_2$] was heated to 110 °C with MeI in ethanol under CO pressure for three hours. The autoclave was cooled and degassed and the deep red solution removed under N_2. The solution contained a high concentration of ethyl acetate. The solvent was removed under reduced pressure. The red brown solid (ν_{CO} 2070 cm^{-1}) produced was unstable in dichloromethane, it was redissolved in a small quantity of methanol and diethyl ether was added. An infrared was taken in the solution cell. There was one terminal carbonyl stretching absorption at 2061 cm^{-1}, spectrum 61. This infrared spectrum is similar to that of [Cp*Rh(CO)I$_2$] discussed below.

[Cp*Rh(CO)$_2$] + MeI + MeOH, ACM 192A:

[Cp*Rh(CO)$_2$] and methyl iodide were combined in methanol and syringed in to the high pressure infrared autoclave. An FTIR was recorded at room temperature, spectrum 62. A sample of this solution ACM 192A was taken and the solvent removed under vacuum. The infrared of the resulting solid had one major terminal carbonyl stretch at 2035 cm^{-1} in deuterated dichloromethane and a few absorptions in the acyl region, the largest of which were at 1679 and 1690 cm^{-1}, spectrum 63. A ^{1}H and ^{13}C n.m.r. spectra were recorded in CD_2Cl_2. Some crystals were recovered from the solution and their structure was solved as [Cp*Rh(COMe)(CO)I] by X-ray crystallography, the data is contained in appendix 1. The spectra of the ACM 192A solution were compared with the spectra of the isolated compounds [Cp*Rh(COMe)(CO)I] and [Cp*Rh(CO)I$_2$] (isolated as ACM 192C, see below) and assigned according to table 5.2.

Assignment of ACM 192.

TABLE 5.2: The Spectra of ACM 192A:

Spectrum	Peak / Stretch	Solvent	Assignment
Infrared	2032 cm^{-1}	MeOH / MeI	Cp*Rh(COMe)(CO)I
Infrared	2035 cm^{-1} ν_{CO} in acyl region	CD_2Cl_2	Cp*Rh(COMe)(CO)I
^1H n.m.r.	1.95 ppm	CD_2Cl_2	$C_5(CH_3)_5Rh(COMe)(CO)I$
^1H n.m.r.	2.76 ppm	CD_2Cl_2	$C_5(CH_3)_5Rh(COCH_3)(CO)I$
^1H n.m.r.	2.23 ppm	CD_2Cl_2	$C_5(CH_3)_5Rh(CO)I_2$
^{13}C n.m.r.	10.19 ppm	CD_2Cl_2	$C_5(CH_3)_5Rh(COCH_3)(CO)I$

The infrared spectrum of [Cp*Rh(COMe)(CO)I] in CD_2Cl_2 correlates well with the findings of A. Haynes *et al* [6] (ν_{CO} 2034, 1684 cm^{-1} in CH_2Cl_2). In some spectra there was a shoulder on the high frequency side of the strong absorption corresponding with the pattern of terminal carbonyl absorptions observed by Haynes *et al* in hexane (ν_{CO} 2030 (vs), 2052 (m)).

The ^1H n.m.r. spectrum of [Cp*Rh(COMe)(CO)I] correlates well with the findings of P. Maitlis *et al* [4]. δ_H 1.95 ppm, 2.79 ppm (in $CDCl_3$).

The ratio of Cp* due to the acyl product and Cp* due to [Cp*Rh(CO)I_2] was 3.5:1. The infrared stretching frequency of the diiodo Rh (III) compound comes just above that of [Cp*Rh(COMe)(CO)I] and is therefore part of the 2043 cm^{-1} absorption in methanol.

[Cp*Rh(CO)$_2$] + MeI + MeOH Heating Under CO, ACM 192:

The rest of ACM 192A was now heated under CO. The first spectrum under CO revealed two stretches from the 2043 cm^{-1} absorption 2043 and 2047 cm^{-1} see spectrum 64. As the temperature was increased the absorption at 2047 cm^{-1} increased in relative intensity and was shifted to a higher frequency and another absorption grew at 1985 cm^{-1}, see spectrum 65. At 80 degrees, (spectrum 66) these were the two largest absorptions although [Cp*Rh(COMe)(CO)I] is still in evidence ν_{CO} 2033 cm^{-1}. The spectrum at 97 °C is noisy as there is now considerable methyl acetate in solution (spectrum 67). The terminal carbonyl stretches assigned to the acyl intermediate are now small. The absorption at approximately 1986 cm^{-1} appears fragmented and the largest

absorption has shifted up in frequency to 2059 cm^{-1}. At 150 °C, spectrum 69, the only detected peak is 2067 cm^{-1}. Cooling the autoclave and degassing shifts this down to 2062 cm^{-1}, (spectrum 70).

When the autoclave was opened a large quantity of red brown needles has crystallised from solution. The needles were labelled ACM 192C. The deep red solution ACM 192 was cooled to -20 °C and some more ACM 192C was obtained.

Analysis of the Resultant Solution and Collection of the Trace Solid ACM 192B.

After the first batch of ACM 192C (later identified as $[Cp^*Rh(CO)I_2]$ was removed by filtration the solution was diluted with CD_3OD and a proton n.m.r. collected. The solution contained two peaks which can be assigned to rhodium species. The largest peak at approximately six times the intensity of the other peak was at 2.16 ppm. The lesser peak was at 2.00 ppm.

Once all the $[Cp^*Rh(CO)I_2]$ had crystallised the remaining solution was reduced to dryness giving a small quantity of a dark amorphous solid ACM192B. This solid was extracted with dichloromethane and an infrared was recorded. The infrared of this trace solid was 2083 cm^{-1}, there was not enough of this to get any other spectroscopic data but this may be the species responsible for the 2.00 ppm peak in the n.m.r. The remainder of the solid was extracted with toluene. The infrared spectrum of this solution did not contain any obvious terminal carbonyl stretching absorptions.

ACM 192C, $[Cp^*Rh(CO)I_2]$.

The infrared of the ACM 192C needles was carried out in dichloromethane. The spectrum contained a single ν_{co} at 2068 cm^{-1}, spectrum 71. Deposited as a solid the infrared consisted of two absorptions 2050 and 2039 cm^{-1}, spectrum 72.

The ^1H and ^{13}C n.m.r. spectra of ACM 192C were collected in CD_2Cl_2.

The ^1H spectrum contained one peak at 2.23 ppm. The carbon spectrum contained two at 11.42 and 105.61 ppm. A microanalysis of the compound revealed it to be $[Cp^*Rh(CO)I_2]$.

INFRARED 61: ACM 145, Solid from a [Cp*Rh(CO)$_2$] Autoclave.

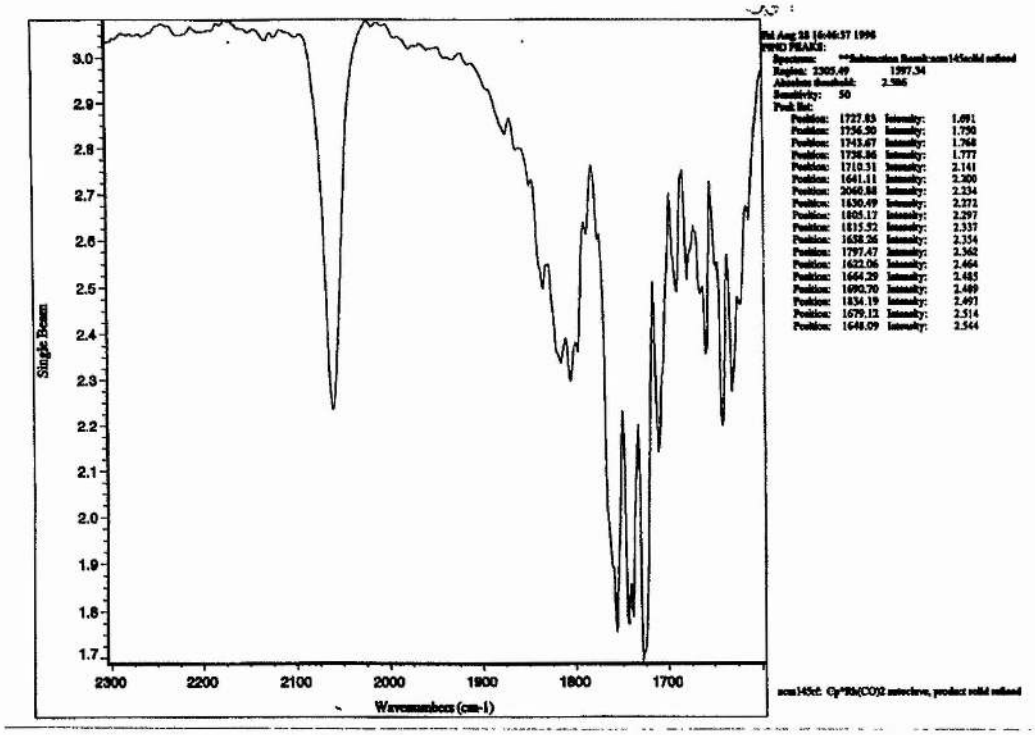

INFRARED 62: ACM 192, [Cp*Rh(CO)] + MeI + MeOH, 19 °C.

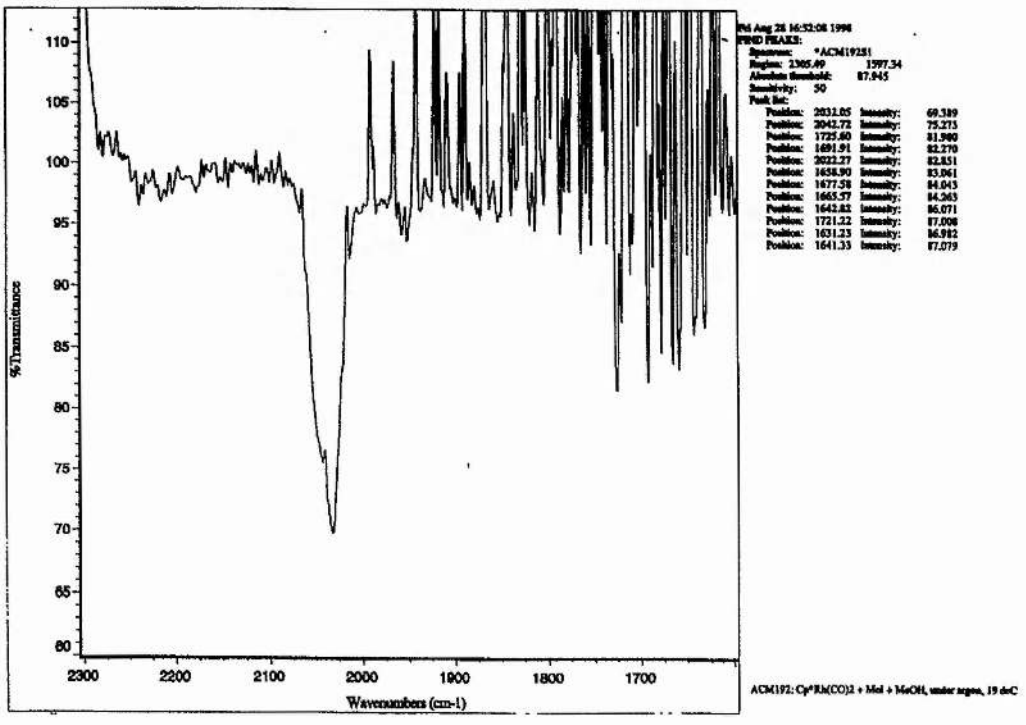

INFRARED 63: ACM 192A in CH_2Cl_2 - CH_2Cl_2.

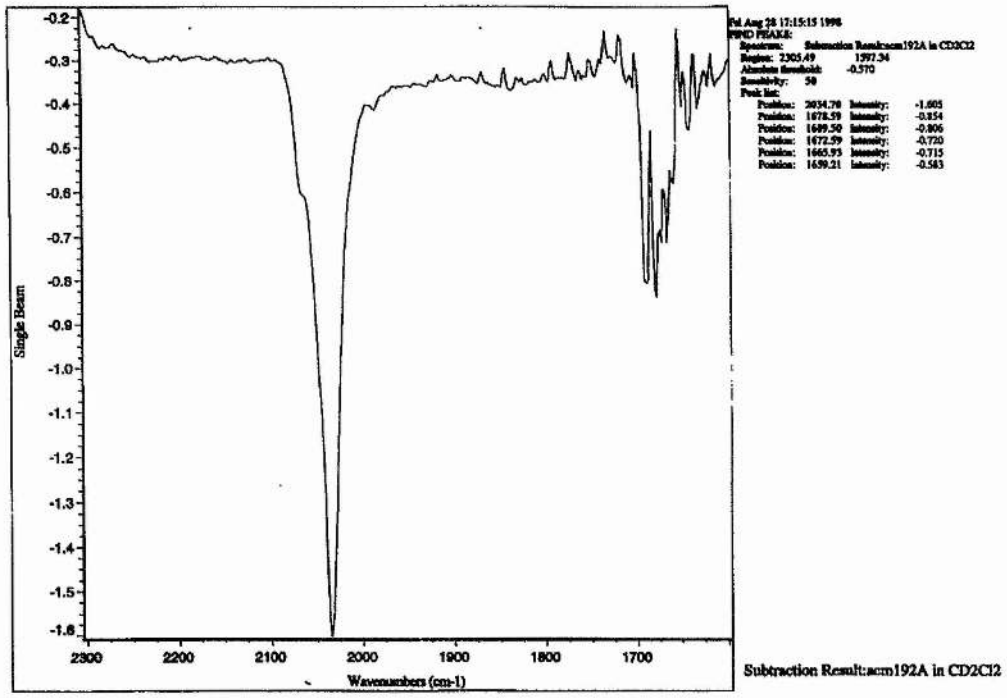

INFRARED 64: ACM 192, 20 bar CO, 19 °C.

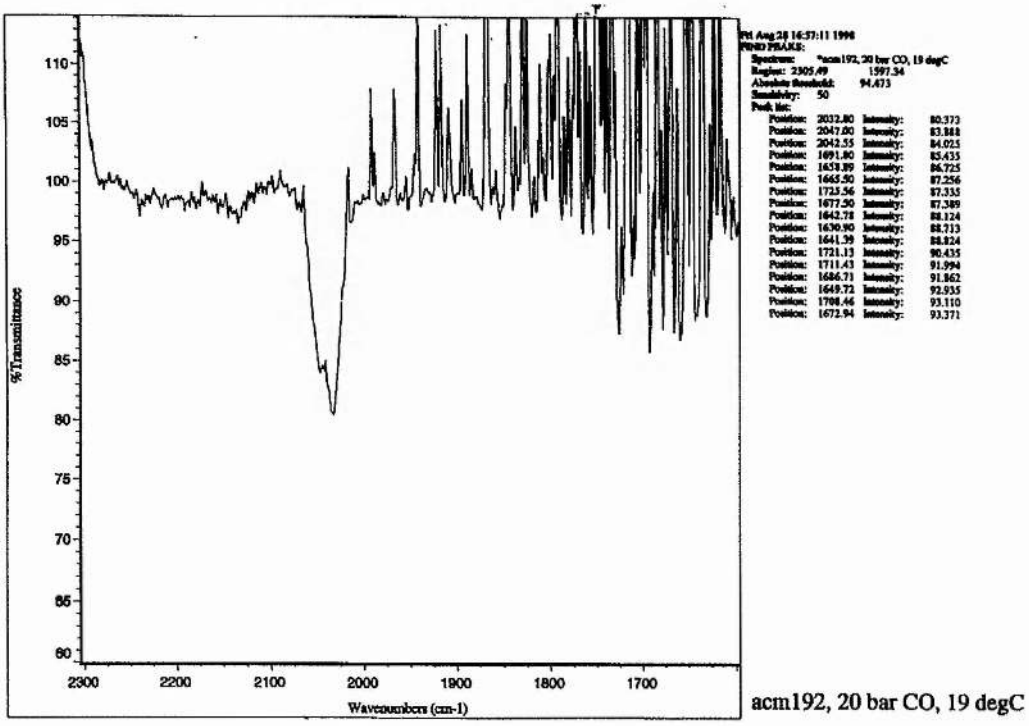

INFRARED 65: ACM 192, 69 °C.

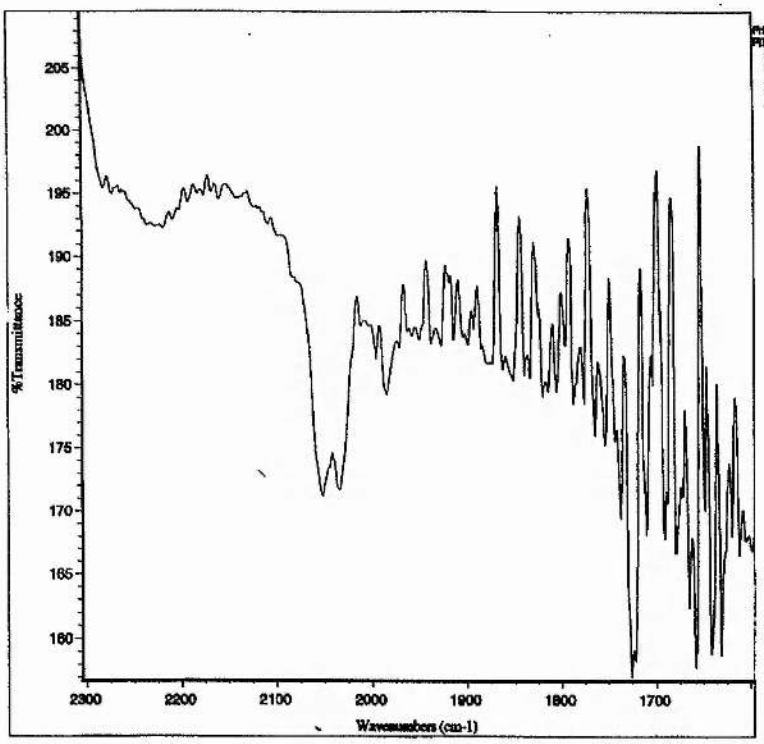

INFRARED 66: ACM 192, 80 °C.

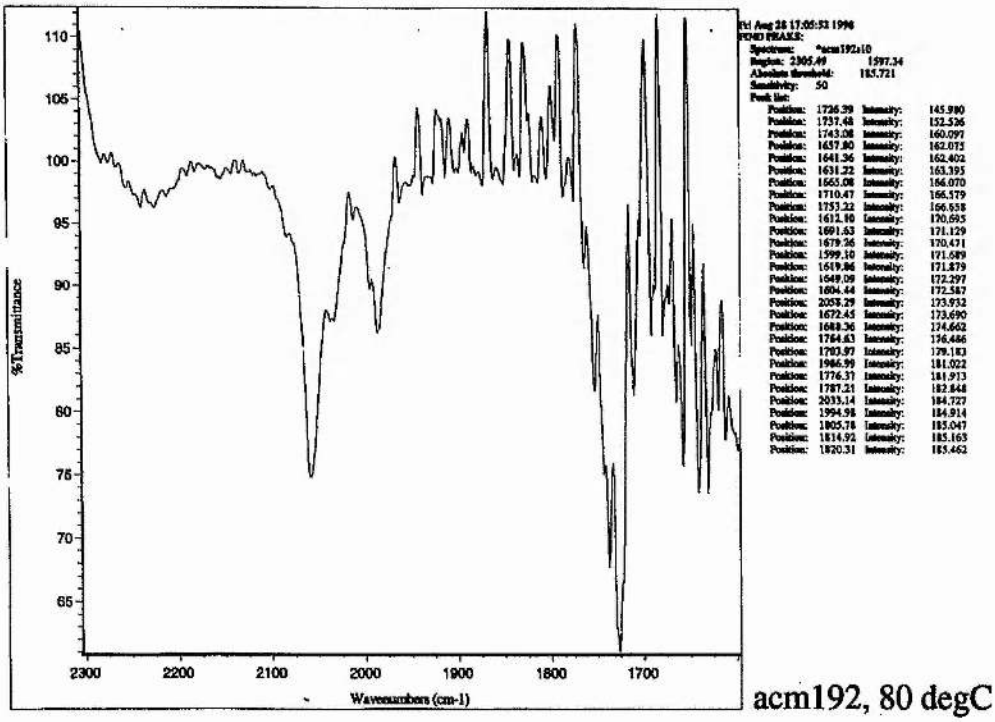

INFRARED 67: ACM 192, 90 °C.

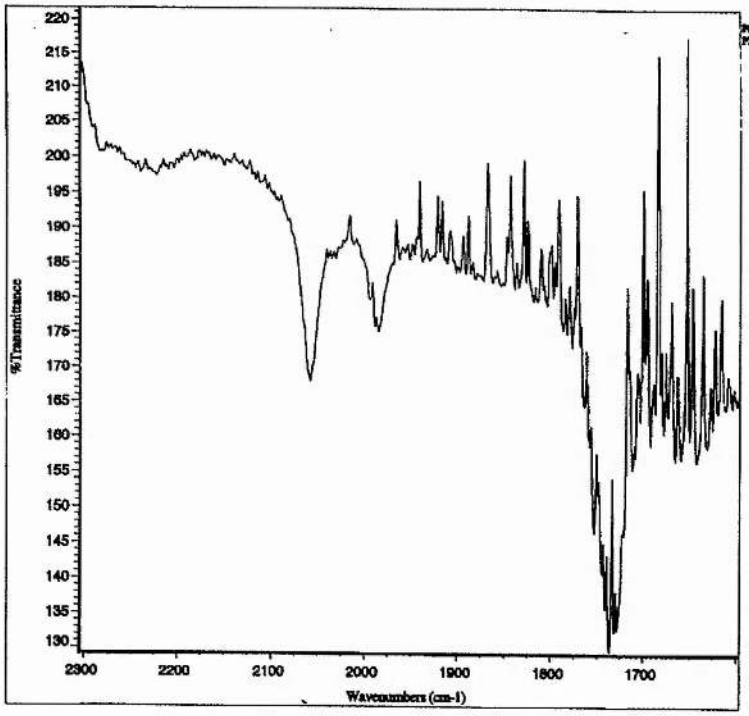

acm192, 97 degC

INFRARED 68: ACM 192, 140 °C.

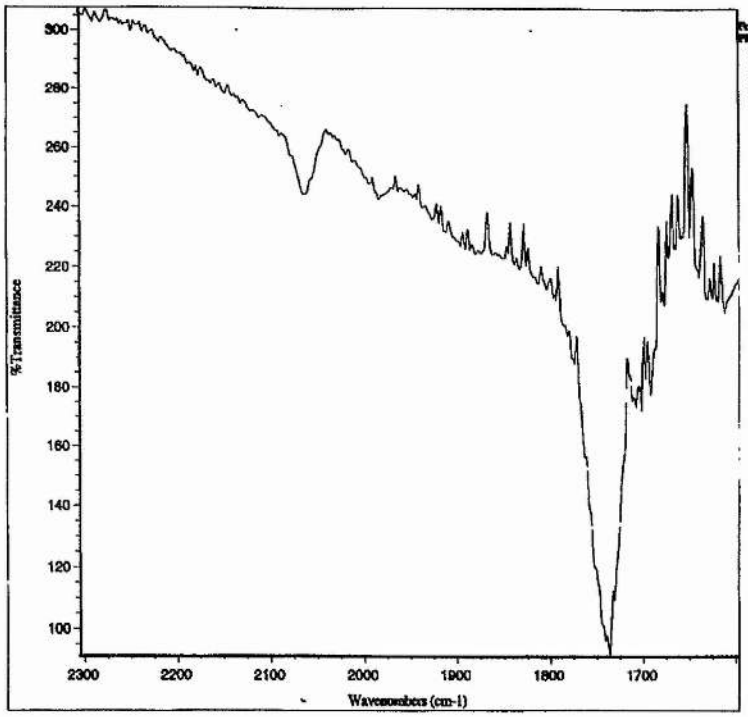

acm192, 140 degC

INFRARED 69: ACM 192, 150 °C.

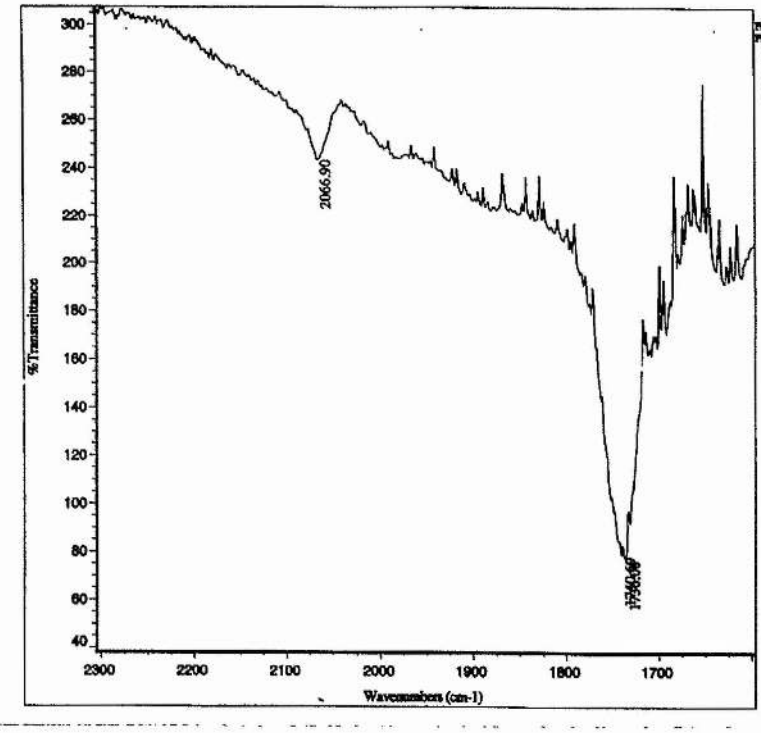

acm192, 150 degC

INFRARED 70: ACM 192, Cooled and Degassed.

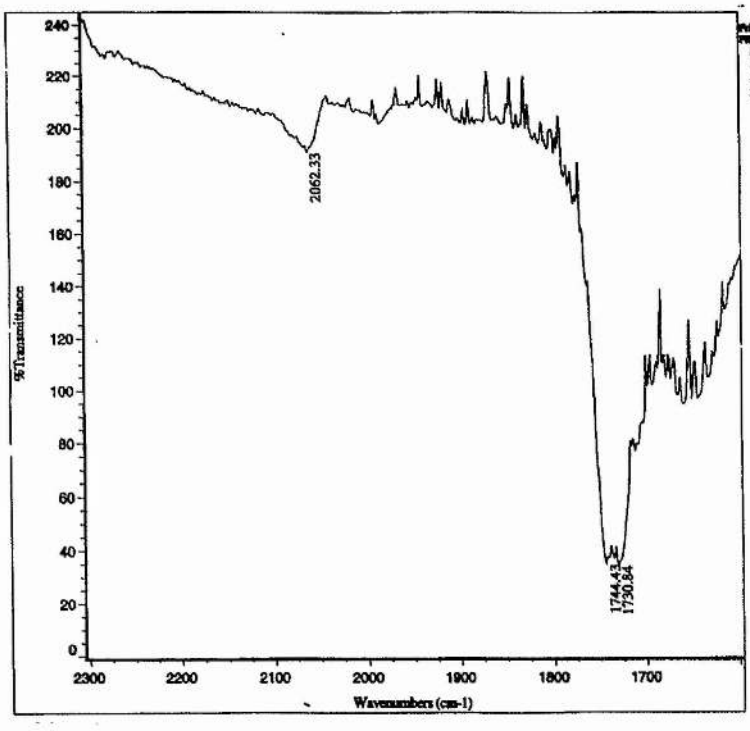

acm192, cooled and degassed.

INFRARED 71: ACM 192C in CH_2Cl_2 - CH_2Cl_2.

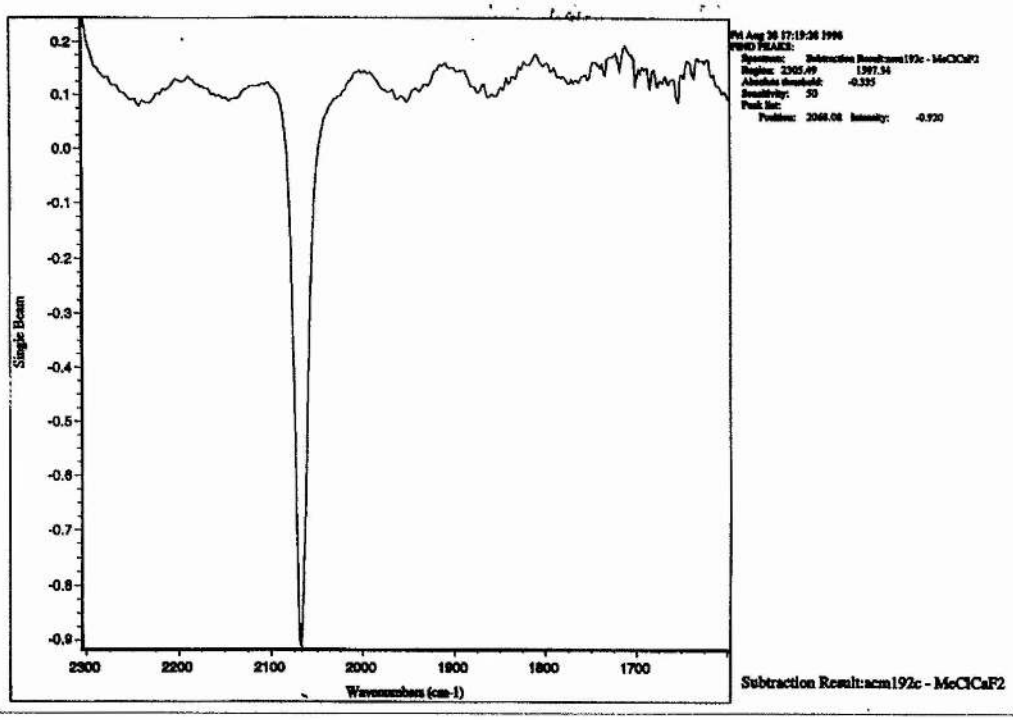

INFRARED 72: ACM 192C As a Solid.

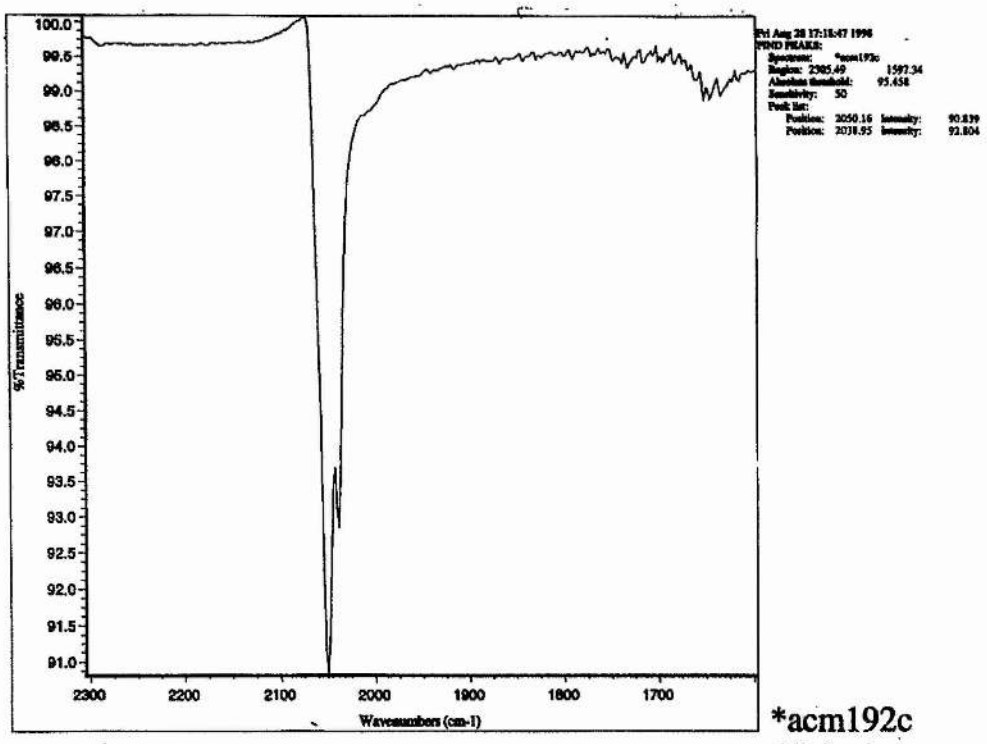

Assignment and Conclusions.

TABLE 5.3: Assigning the Spectra of ACM 192C.

Spectrum	Peak / Stretch	Solvent	Assignment
Infrared	2068 cm^{-1}	CH_2Cl_2	[Cp*Rh(CO)I_2]
Infrared	2050, 2039 cm^{-1}	Solid	[Cp*Rh(CO)I_2]
^{1}H n.m.r.	2.23 ppm	CD_2Cl_2	$C_5(CH_3)_5Rh(CO)I_2$
^{13}C n.m.r.	11.42 ppm	CD_2Cl_2	$C_5(CH_3)_5Rh(CO)I_2$
^{13}C n.m.r.	105.61 ppm	CD_2Cl_2	$C_5(CH_3)_5Rh(CO)I_2$

TABLE 5.4: Assigning Spectra from Experiments in Methanol.

Spectrum	Conditions / °C	Peak / Stretch	Solvent	Assignment
Infrared	19	2032, 2043 cm^{-1}	MeOH / MeI	[Cp*Rh(COMe)(CO)I]
Infrared	19	2047	MeOH / MeI	[Cp*Rh(CO)I_2]
Infrared	97	1985-6 cm^{-1}	MeOH / MeI	Unknown
Infrared	150	2062-2066 cm^{-1}	MeOH / MeI	[Cp*Rh(CO)I_2]
^{1}H n.m.r.	Room temp.	2.16 ppm	MeOH / MeI CD_3OD	$C_5(CH_3)_5Rh(CO)I_2$
^{1}H n.m.r.	Room temp.	2.00 ppm	MeOH / MeI CD_3OD	Unknown

We suggest that the initial product of the reaction between [Cp*Rh$(CO)_2$] and methyl iodide in methanol is [Cp*Rh(COMe)(CO)I], when this species is heated under CO it releases methyl acetate and the concentration of [Cp*Rh(CO)I_2] increases. As the temperature is increased the concentration of Rh (I), represented by the 1986 cm^{-1} (this may be [Cp*Rh(CO)$I]^-$) increases. At 150 °C the main carbonyl stretching absorption is at 2068 cm^{-1}, on cooling this is reduced to 2062 cm^{-1}. The cooled solution has crystallised large quantiites of [Cp*Rh(CO)I_2].

We have assigned a wide range of absorptions to [Cp*Rh(CO)I_2]. Examining the spectra 65-71 helps to explain why we have done this. As the temperature is increased you can observe the infrared absorption due to the acyl intermediate and that due to the [Cp*Rh(CO)I_2] as they change in relative intensity. As the [Cp*Rh(CO)I_2] absorption increases and the temperature is raised there is a gradual shift to higher frequency. At no

point do we see the decay of the stretch due to this species and emergence of another at higher frequency. Comparison of these results with those in table 5.3 reveal that the infrared of [Cp*Rh(CO)I_2] varies widely depending on the conditions. The value in dichloromethane is close to that observed at the end of the experiment whereas the value in the solid state is similar to that observed before heating. One explanation for these observations is that [Cp*Rh(CO)I_2] becomes increasingly solvated as the temperature is increased and on cooling this solvation sphere is still in tact. This type of effect was observed by Polliakoff *et al* for [Cp*Ir(CO)$_2$] dissolved in a hydrocarbon solvent. [7] They observed a shift in the carbonyl stretching frequencies when a small quantity of a perfluorinated alcohol was added, see table 5.5. They explained the effect as a hydrogen bonding interaction between the proton of the alcohol and the metal centre.

TABLE 5.5: ν_{co} of [Cp*Ir(CO)$_2$].

Solvent	ν_{co}	ν_{co}
n-heptane	2019.2	1953.1
n-heptane + $(C_3F_7)(CF_3)_2COH$	2031.0	1970.5
n-heptane + $(CF_3)_2CHOH$	2027.8	1964.8

5.2c iii. Conclusions from HPIR, The Carbonylation of Methanol by [Cp*Rh(CO)$_2$].

The reaction of [Cp*Rh(CO)$_2$] with MeI occurs at room temperature to form [Cp*Rh(COMe)(CO)I]. This species loses methyl acetate, the mechanism of this may be reductive elimination or nucleophilic attack by iodide followed by alcoholysis.
This is analogous to the cobalt catalysed process discussed in chapter 4. The [Cp*Rh(CO)$_2$] cycle differs as the Rh (III) species [Cp*Rh(CO)I_2] is an important component of the reaction mixture in methanol whereas [Cp*Co(CO)I_2] is only formed in high concentrations in acetic acid and dichloromethane. There are two possible mechanisms for the formation of M (III). The first mechanism is detailed in diagram 56, section 5.2b and involves the reacting together of two moles of [Cp*M(Me)(CO)$_2$]I this is unlikely when the metal M is rhodium or cobalt as the insertion process is fast. [6] A more likely explanation is the existence of a water-gas shift cycle, see diagram 57.

DIAGRAM 57: The Water / Gas Shift Reaction For $[Cp^*M(CO)_2]$

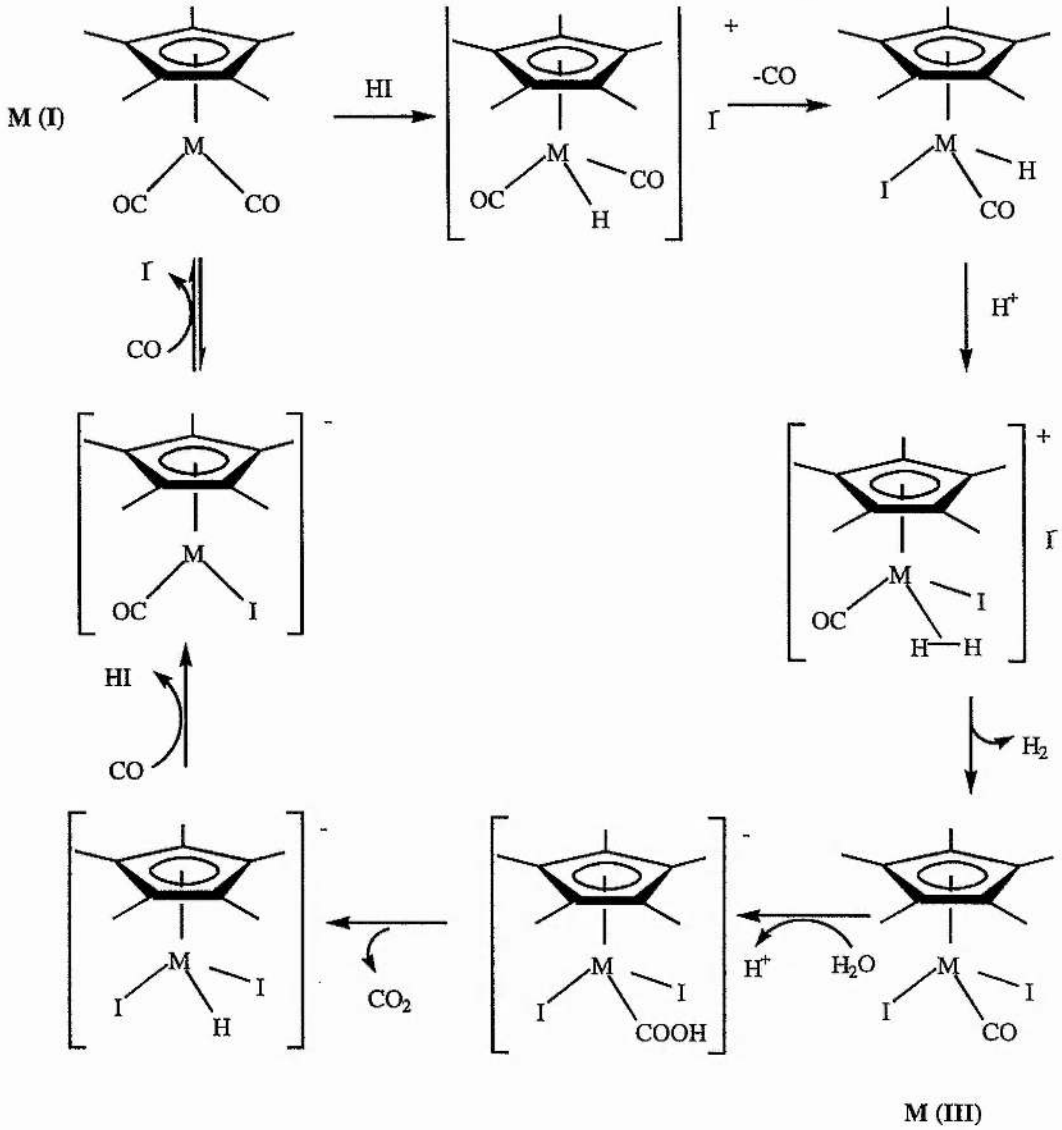

We suggest that when [Cp*Rh(COMe)(CO)I] is heated under CO it reductively eliminates acetyl iodide which is converted to methyl acetate. The rhodium product is $[Cp^*Rh(CO)_2]$ or $[Cp^*Rh(CO)I]^{\cdot}$, most of the Rh (I) is immediately caught up in the water / gas shift cycle and transformed in to $[Cp^*Rh(CO)I_2]$. As the temperature is increased and the concentration of water builds, (due to $2MeOH + CO = MeOAc + H_2O$) the rate of reduction to Rh (III) increases and Rh (I) is observed in solution (at 1986 cm^{-1}). Cooling the reaction causes precipitation of Rh (III) as $[Cp^*Rh(CO)I_2]$ driving the oxidation to completion.

The major problem in the catalytic cycle is the slow reduction of Rh (III) to Rh (I) under these conditions, this substantially lowers the rate by reducing the concentration of active rhodium, the rate should be enhanced by conditions which favour Rh (I).

5.2c iii. Measuring the Rate of CO Uptake.

The Initial Rate of Carbonylation, see table 5.6, Diagrams 58 and 59.

The rate of reaction was measured by measuring the rate of CO uptake in to solution from a ballast vessel as detailed in chapter 4. The same experiment was conducted on equipment at B.P. Chemicals and at St. Andrews in collaboration with the CATS catalyst testing unit in order to compare the results obtained from the two sets of apparatus.
In experiment ACM 183 the catalyst, methyl iodide, methyl acetate, water and acetic acid were injected in to the autoclave then it was pressurised with 8 bar of CO and heated to temperature. At temperature the pressure of CO was increased to 28 bar and the gas uptake from the ballast vessel monitored. In ACM 196 the method was similar except methyl iodide in solution was injected at temperature to initiate the reaction and get a true initial rate.
Comparing the initial rates obtained they are fairly similar and the average rate is 1.4 +/- 0.1 mol dm^{-3} hr^{-1}, 330 turnovers per hour.
After approximately one hour the pressure of reaction ACM 183 was increased to 40 bar in order to see if this increased the rate, the new initial rate was 2.55 mol dm^{-3} hr^{-1} , 604 turnovers per hour. This indicates a dependence on the pressure of CO which is not observed for the Monsanto catalyst. The increase in CO pressure may be increasing the concentration of active catalyst in solution. This is consistent with the water gas shift mechanism proposed in diagram 57 as the oxidation involves the loss of CO and the reduction step by which the active catalyst is recycled involves uptake of CO.

Selectivity, MeOH Conversion and Stability.

A detailed analysis of the products produced from the carbonylation of methanol catalysed by [Cp*$Rh(CO)_2$] was conducted by the analytical department at B.P. Chemicals, the concentration of the side products obtained are quoted in table 5.7. The acetic acid production is calculated from the total uptake of CO. Comparing this with the initial concentration of methyl acetate (the substrate) reveals that within experimental error the substrate is 100 % converted.
Some other products are detected in the product mixture, The approximate ratio of desired to side products is 135:1 and acetic acid is approximately 99.3 mole % of the carbonylated product mixture.

TABLE 5.6: [Cp*Rh(CO)$_2$] For Methanol Carbonylation in Low Water Acetic Acid.

Expt. No.	Catalyst	Initial [catalyst]/ mol dm^{-3}	Temp. inside reactor. / °C	Pressure at reaction Temp.	AcOH Added/ g	MeOAc Added/ g	H_2O Added/ g	MeI Added/ g	Total Volume/ cm^{-3}	Total Mass/ g	Rate/ mol dm^{-3} hr^{-1}	Rate/ turnover/ hr
ACM183	Cp*Rh(CO)$_2$	4.22x10^{-3}	185	28	64.018	15.002	7.009	13.996	90.27	100.137	1.46	345
ACM 196	Cp*Rh(CO)$_2$	4.22x10^{-3}	185	28	3.200	0.750	0.350	0.695	4.51	4.995	1.28	304

TABLE 5.7: Products from [Cp*Rh(CO)$_2$] Catalysed Carbonylation of Methanol Operated in Low Water Acetic Acid at B.P Hull.

Expt. No.	Catalyst	Initial [MeOAc] / M	CH_3COOH /mol dm^{-3}	EtCOOH /mol dm^{-3}	ACETONE /mol dm^{-3}	EtI /mol dm^{-3}	EtOAc /mol dm^{-3}	EDAc /mol dm^{-3}
ACM183	Cp*Rh(CO)$_2$	2.240	2.265	0.00068	0.01002	0.00120	0.00434	0.00026

TABLE 5.8: Methyl Acetate Carbonylation.

Expt. No.	Catalyst	Initial [catalyst]/ mol dm^{-3}	Temp. inside reactor. / °C	Pressure at reaction Temp. / bar	AcOH Added/ g	MeOAc Added/ g	AcOAc Added/ g	MeI Added/ g	LiI Added / g	Total Volume / cm^{-3}	Rate/ mol dm^{-3} hr^{-1}	Rate/ turnover/ hr
ACM194	$Cp^*Rh(CO)_2$	0.0065	189	36	3.100	1.529	0.032	0.912	0.7314	5.4	6.90	1062
ACM 195	$Cp^*Rh(CO)I_2$	0.0065	189	36	3.100	1.529	0.032	0.912	0.7308	5.4	1.19	182

DIAGRAM 58: ACM 183, $Cp^*Rh(CO)_2$ Measured at B.P Chemicals Hull.

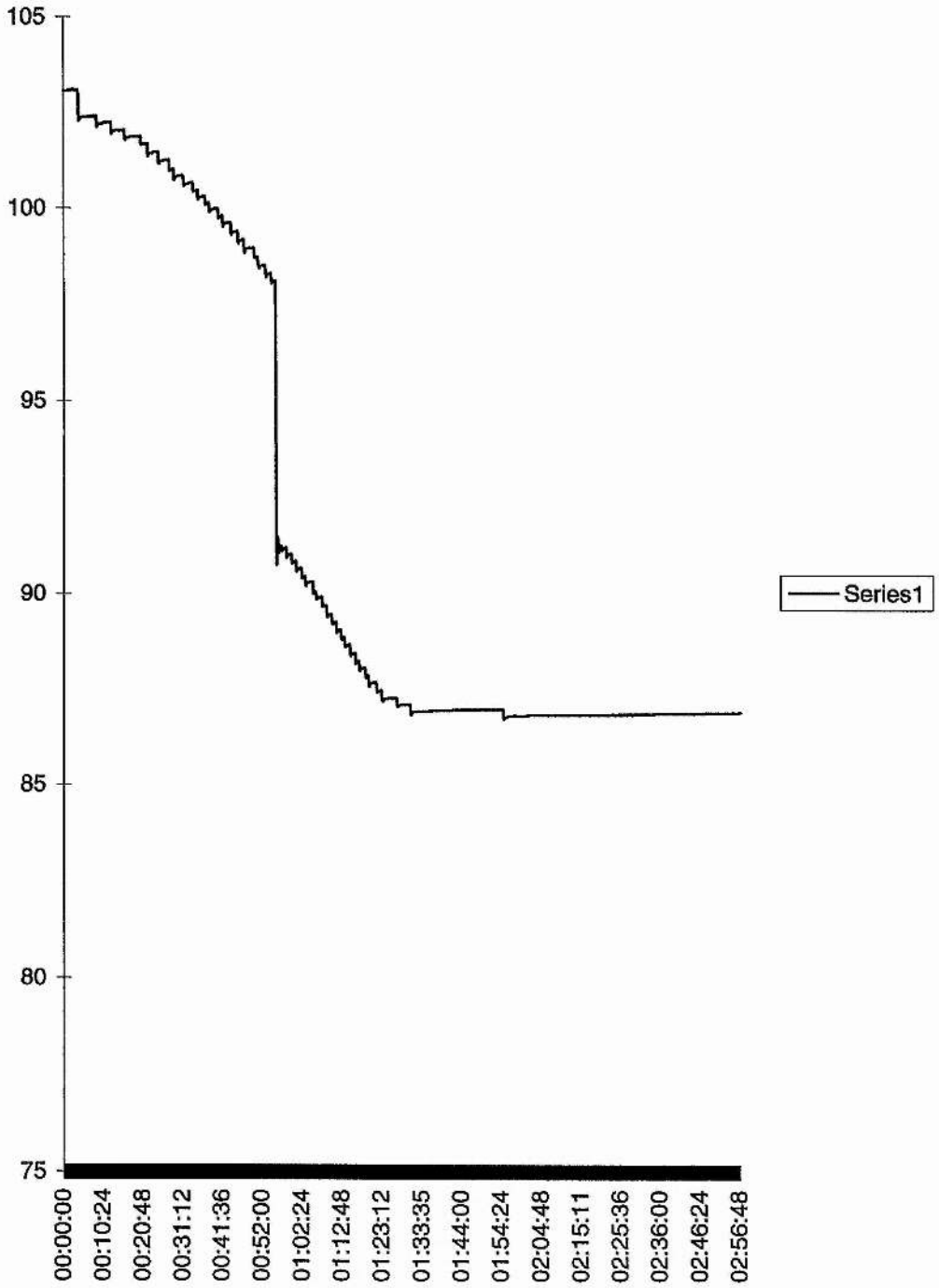

DIAGRAM 59: ACM 196, $Cp^*Rh(CO)_2$, measured in St. Andrews.

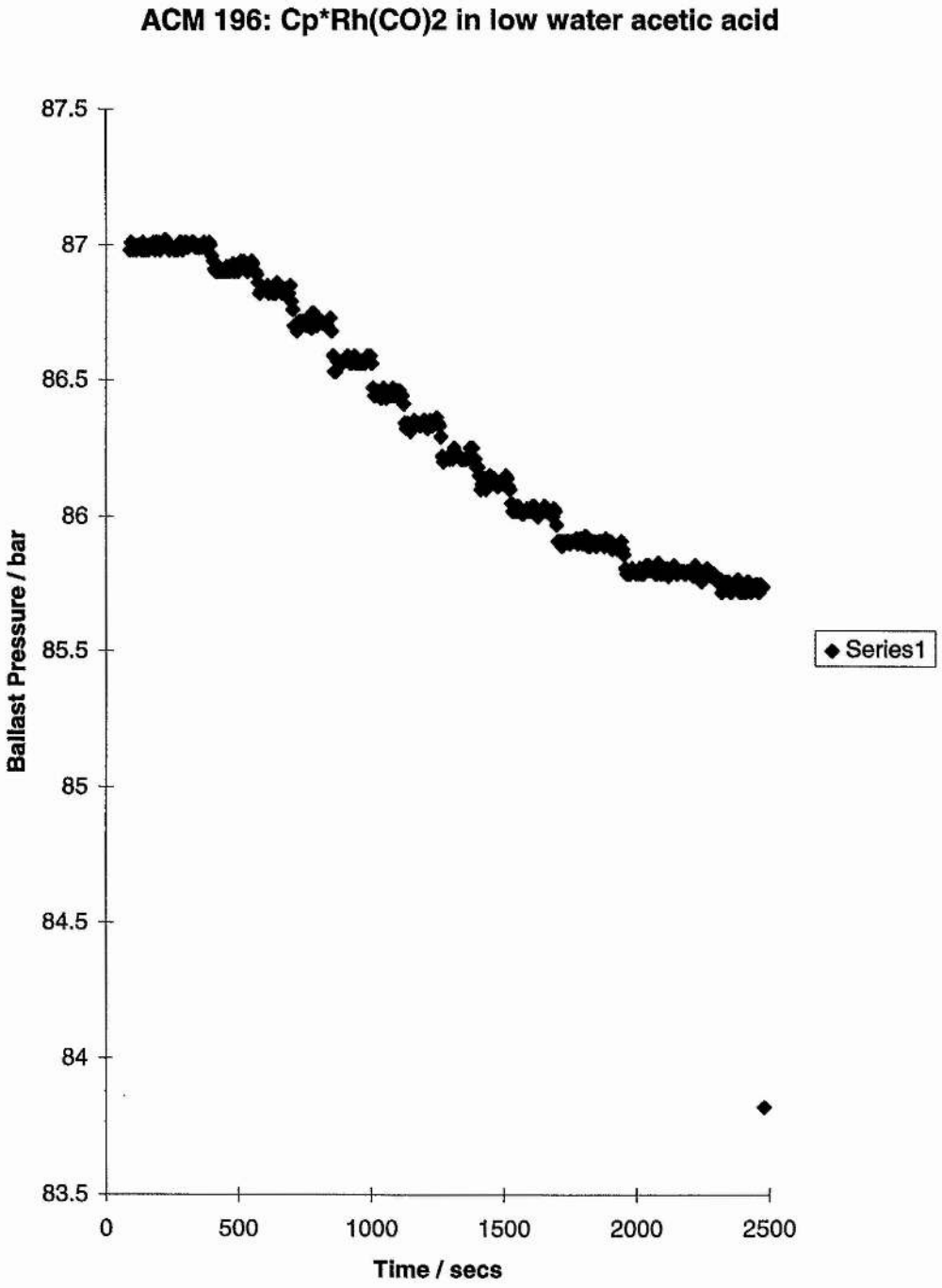

Comparison With the Monsanto Catalyst.

Under standard Monsanto conditions rates approach 10 mol/l/hr with a rhodium concentration of 400 ppm.

5.2d. [Cp*Rh(CO)$_2$] As a Catalyst for Methyl Acetate Carbonylation: Anhydrous Chemistry.

5.2d i. Introduction to Methyl Acetate Carbonylation.

When all the water is excluded from the reaction mixture conventional rhodium carbonylation catalysts carbonylate methyl acetate to acetic anhydride. [8] The Rh / MeI / CO catalytic system has a long induction period and a low rate for this process. LiI and hydrogen are employed as promoters to improve the rate and reduce the length of the induction period.

Hydrogen reverses the oxidation to Rh (III) which results from operating with no water unfortunately it is also detrimental to the selectivity of the process. Side products include ethylidene diacetate, acetone, carbon dioxide, methane and polyester polyketones. Promoter salts such as LiI are also employed to enhance the rate of carbonylation. The effect of these are summarised in Zoeller's mechanism, diagram 60.

DIAGRAM 60: The Mechanism of Methyl Acetate Carbonylation.

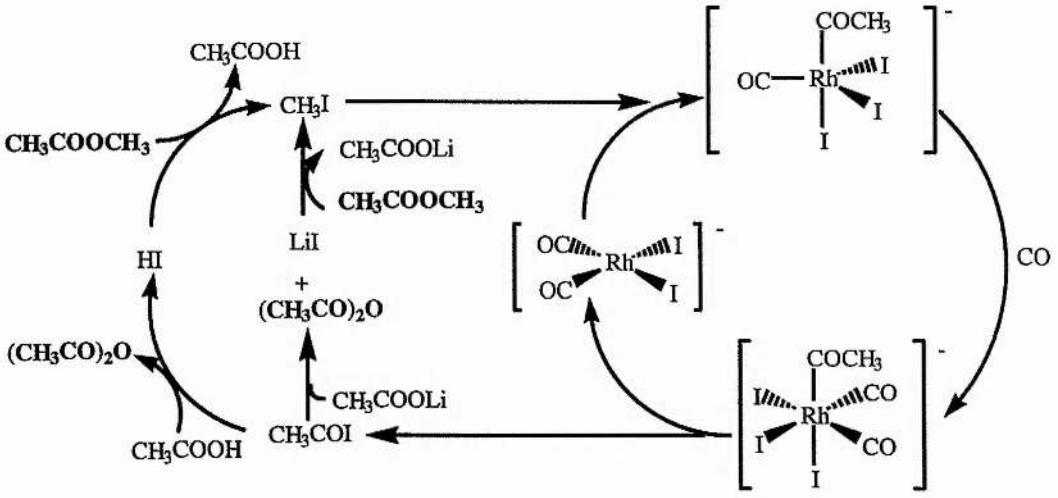

The chemistry is very similar to that of methanol carbonylation and this explains why the Monsanto catalyst is poor as it requires water for efficient methanol carbonylation. Rh (III) collects in solution as $[Rh(CO)_2I_4]^-$ and is vulnerable to decomposition and precipitation as $[RhI_3]$. The stability of $[Cp^*Rh(CO)_2]$ may be higher in the absence of water as the Cp* to metal bond in $[Cp^*Rh(CO)I_2]$ may protect this complex from further

decomposition.

5.2d ii. Results.

Rates:

The initial rates of methyl acetate carbonylation by [Cp*Rh(CO)$_2$] and [Cp*Rh(CO)I$_2$] were measured at St. Andrews in collaboration with the CATS testing facility. The conditions of the experiments and initial rates observed are detailed in table 5.8, the ballast pressure, time graphs are in, diagrams 61 and 62. We can see that the rate is quite high for [Cp*Rh(CO)$_2$] but considerably less for [Cp*Rh(CO)I$_2$], this illustrates that not all the Rh (III) is being recycled to Rh (I).

In the absence of hydrogen a rate of approximately 7 mol dm^{-3} hr^{-1} is very respectable. For conventional rhodium catalysts under the same conditions approximately 0.06 w/w % Rh (these experiments were at 0.057 w/w %) gives a rate of 8 mol dm^{-3} hr^{-1} when under 35 bar CO and 0.5 bar H_2. If the H_2 is excluded the rate reduces significantly[9]

Product Composition.

The original solution contained 3.82 mol dm^{-3} methyl acetate, (the substrate). From the CO uptake the concentration of carbonylated products in the final solution was 2.20 mol dm^{-3} for [Cp*Rh(CO)$_2$] as a catalyst and 1.49 mol dm^{-3} for [Cp*Rh(CO)I$_2$], 58 and 39 % conversion respectively. A g.c. / m.s. of the ACM 194 solution revealed that there were no major side products.

Catalyst Stability and Further Work.

The high activity obtained for the [Cp*Rh(CO)$_2$] catalysed carbonylation of methyl acetate is very promising. 58 % of the methyl acetate is converted over one hour. The rate undergoes a period of zero order kinetics followed by a decay in activity. The loss of activity may be due to the build up of [Cp*Rh(CO)I$_2$] as well as a rate dependence on methyl acetate concentration. When [Cp*Rh(CO)I$_2$] is used as the catalyst precursor the rate is considerably lower showing that there is a high concentration of inactive species in solution. The decay in carbonylation rate is less for this system, this is consistent with the suggestion that [Cp*Rh(CO)$_2$] is losing activity because the concentration of [Cp*Rh(CO)I$_2$] in solution is rising.

This novel catalytic system is much less vulnerable to decomposition under conditions of

DIAGRAM 61: ACM 194 Ballast Pressure Against Time Graph.

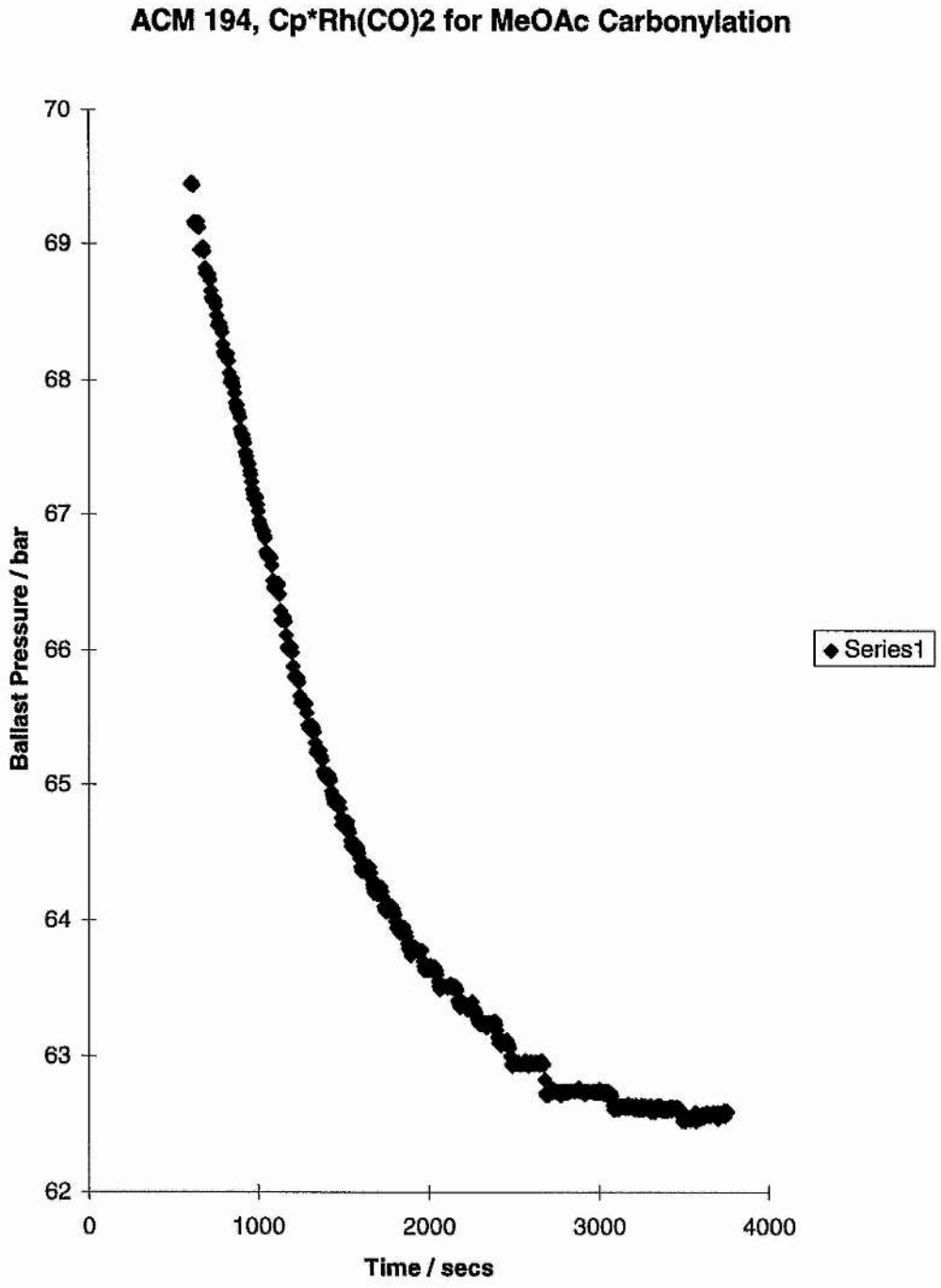

DIAGRAM 62: ACM 195 $Cp^*Rh(CO)I_2$.

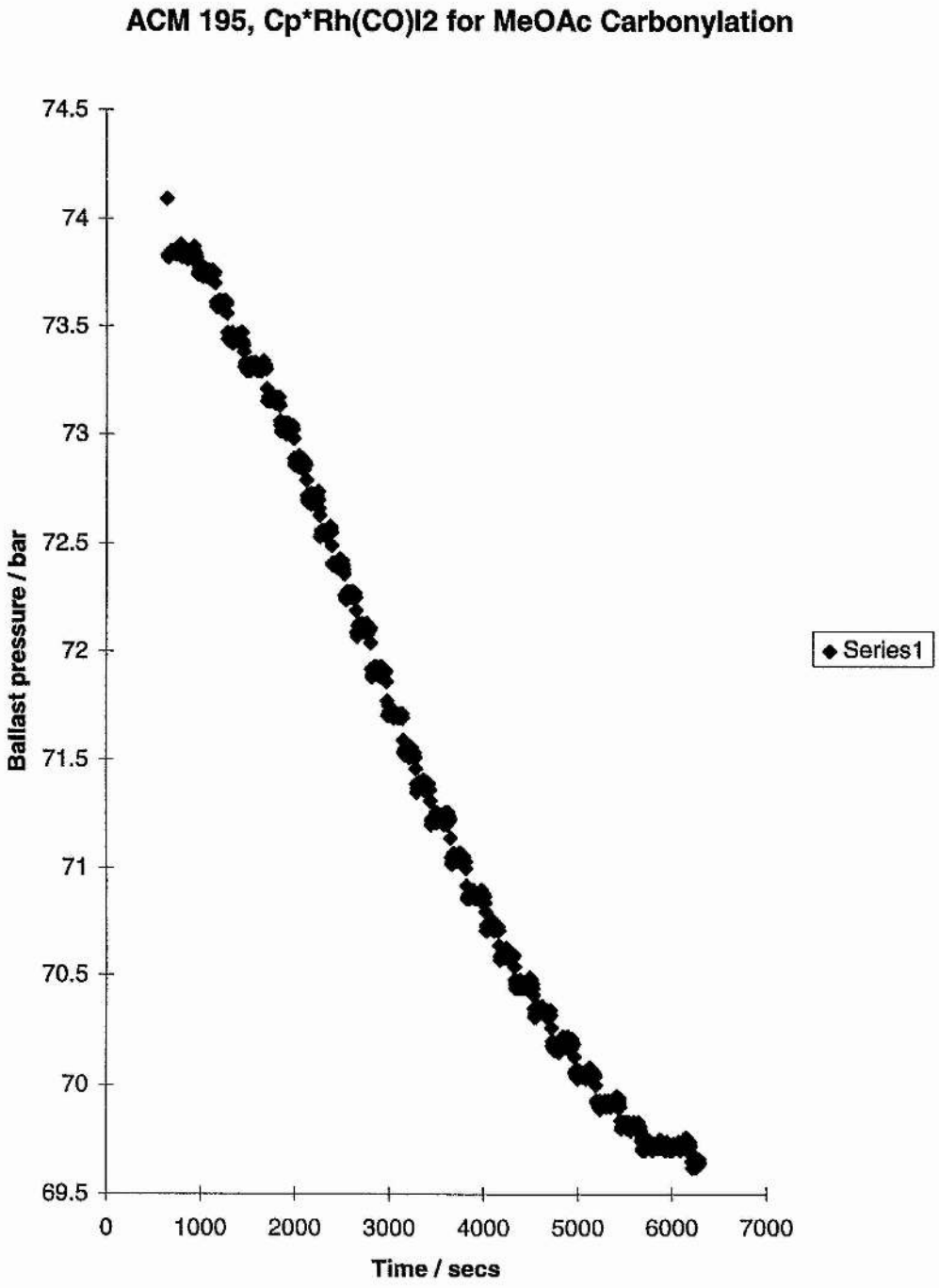

low and no water than the traditional Monsanto catalyst and may find future application under these conditions.

5.3 COBALT CATALYSTS WITH CARBONYL AND PHOSPHINE.

5.3a. A New Class of Cobalt Catalysts.

Attaching two basic phosphines to a Co (I) centre makes it a catalyst for methanol carbonylation. The catalytic activity of $[Co(CO)_2(PMe_2Ph)_2I]$ has been observed under mild conditions. When $[Cp^*Co(CO)_2]$ and PEt_3 were tested at 120 °C and 100 bar in methanol and water the catalytic system produced was a very efficient methanol carbonylation catalyst, ACM 200 and 201. This system illustrated both very high activity and good catalyst stability. The first regime probably represents a catalytic species involving a Cp* ligand but the solution responsible for the second region of activity contains $[Co(CO)_2(PEt_3)_2I]$ (the crystal structure of this compound is in appendix 1). It is likely that this compound contributes to the overall catalytic activity of the system which is approximately 3 mol dm^{-3} hr^{-1}. The relative stability of the second catalytic system can be clearly seen from the ballast pressure temperature graph of ACM 200 p163, this, and the isolation and crystallisation suggests that $[Co(CO)(PEt_3)_2I]$ does not undergo rapid decomposition under these conditions.

Designing New Catalysts

Considering the general formula $[Co(I)(P)_2(CO)_2]$ it is easy to see that there are many ways in which these systems could be improved in order to achieve the perfect balance of activity and stability. One such improvement would be to incorporate chelating diphosphine ligands in order to protect against cobalt phosphorus bond cleavage.
We have begun work on this with G. Schwarz. The problem with preparing compounds of this sort is the lack of good synthetic strategies.

The main strategy we employed was:

$$CoI_2 + 2P \longrightarrow CoI_2P_2 \xrightarrow{2CO} Co(CO)_2(P)_2I + I^-$$

This is based on work by Bordignon *et al*[10] For $P_2 = (Me)_2P(CH_2)_2P(Me)_2$ we obtained the cobalt (III) bis diphosphine complex $[Co\{(Me)_2P(CH_2)_2P(Me)_2\}_2I_2]I$. The complex was crystallised from dichloromethane and an X-Ray crystal structure was determined (see appendix 1). So far we have not successfully prepared an active carbonylation catalyst of this type.

5.4. CATALYSTS IN SUPERCRITICAL FLUIDS.

It is hoped that the application of catalysts with predominantly neutral catalytic cycles, i.e. cycles in which the main intermediates are uncharged, will facilitate the carbonylation of methanol in supercritical carbon dioxide. To this end $[Co_2(CO)_8]$ was introduced to CO_2 / methanol as the catalyst precursor but the selectivity towards acetate production was poor.

The catalysts of the general formula $[Cp^*M(CO)_2]$ may find application in supercritical fluids for four reasons. Firstly compounds of this type are known to be soluble in supercritical fluids.[7] Secondly the electron density on the metal centre is achieved without the application of iodide ligands which often result in ionic intermediates. Thirdly the rhodium and cobalt compounds undergo rapid migratory insertion of CO and therefore the main species in solution are likely to be $[Cp^*M(COMe)(CO)I]$ and $[Cp^*M(CO)_2]$, both of which are 18 electron neutral intermediates, this may help to keep the catalyst in solution. Lastly in order to avoid the problems of solubilising large quantities of water it is advantageous to work with a catalyst which can tolerate high methanol and low water conditions. Our novel $[Cp^*M(CO)_2]$ catalysts work under such conditions.

ACM 156.

We tested $[Cp^*Rh(CO)_2]$, working with I. Bach. $[Cp^*Rh(CO)_2]$ (0.0087g) was dissolved in MeOH (1 cm^3) and MeI (1 cm^3) to give a red solution and injected in to a small (28 cm^3) hastelloy autoclave. The autoclave was pressurised to 20 bar with CO and then up to 90 bar with CO_2. The autoclave was heated between 80 °C and 90 °C for one hour. The resulting solution contained 0.063 mol dm^{-3} methyl acetate, that is it carbonylated methanol at a rate of 0.063 mol dm^{-3} hr^{-1}. These conditions are very mild and it is not surprising that the rate of carbonylation is slow. The result does however illustrate that methanol carbonylation in CO_2 / methanol is possible. The mobility of CO within the phase may help to obtain higher rates of carbonylation.

CHAPTER 6: EXPERIMENTAL.

6.1. GENERAL PROCEDURE.

6.1a. Laboratory Reagents.

All experiments were carried out under a dry nitrogen / argon atmosphere, dried through a Cr (II) / silica packed glass column. Reactions were carried out on vacuum lines. Liquids were transferred under inert atmosphere by syringe or catheter through suba seals. Solids were transferred directly from one Schlenk tube to another or weighed out in a glove box under argon.

Carbon monoxide was purchased from BOC gases. Ethanol was distilled from magnesium ethoxide, methanol was distilled from magnesium methoxide, both were handled under nitrogen and stored under nitrogen / argon over molecular sieves. Cyclohexane and hexane were stored over sodium. Water was distilled and stored under nitrogen / argon. Petroleum ether (boiling range 40-60 °C) and diethyl ether were distilled over sodium diphenylketyl. Dichloromethane was distilled over calcium hydride. Toluene was distilled over sodium. Methyl iodide (Aldrich Chemicals) was stored at 3 °C under nitrogen / argon. Deuterated solvents (Cambridge Isotope Laboratories) were stored under nitrogen / argon. All alkyl phosphines were bought from Strem Chemicals under argon and stored under an inert atmosphere. Pentamethyl cyclopentadiene (Aldrich), 1,3-cyclohexadiene (Aldrich), dicyclopentadiene (Aldrich), methyl acetate (Aldrich), acetic anhydride (Aldrich) and hexamethyl dewar benzene (Aldrich) were stored under nitrogen / argon. All solvents that were not stored under an inert atmosphere such as acetic acid (Fisons) were degassed immediately prior to use.

Dicobalt octacarbonyl (Strem) was stored at 3 °C and with the exclusion of light in a carbon monoxide atmosphere. Most of the solids used were stored under nitrogen / argon including cyclopentadienyl cobalt dicarbonyl (Strem), lithium iodide (Aldrich), tin (II) iodide (Aldrich), cobalt (II) iodide (Aldrich), [$RhCl_3.3H_2O$] (Avocado) was stored in a desiccator over silica gel.

6.1b. Analytical Techniques.

Infrared spectra were obtained using a Nicolet Protege 460 with CsI optics. The infrared

spectrometer was interfaced to a personal computer via the OMNIC operating system. G.C. analyses were carried out at 12 °C using a Phillips PU 4000 fitted with a 100% dimethyl siloxane column.

G.C. M.S. were carried out using a Hewlett Packard 5890 G.C. with an Incos quadrupole mass spectrometer fitted with a SGE BP1 column and a Hewlett Packard HP6890 G.C. with a 5973 mass selective detector fitted with a 5 % phenyl methyl siloxane capillary column.

Carbon and proton n.m.r. spectra were recorded on a Bruker AM 300 n.m.r. spectrometer. Phosphorus n.m.r. spectra were recorded on a Varian 300 n.m.r. spectrometer. Broad band decoupling was used for ^{13}C and ^{31}P spectra. ^{1}H and ^{13}C n.m.r. spectra were referenced internally to deuterated solvents: CD_2Cl_2: ^{1}H, δ, 5.35 ppm, ^{13}C, δ, 53.8 ppm. CD_3OD: ^{1}H, δ, 3.35 ppm, ^{13}C, δ, 49.0 ppm. ^{31}P n.m.r. were referenced externally to phosphoric acid 85 % H_3PO_4.

CHN microanalysis was carried out on a Carlo Erba Model 1106.

6.2. SYNTHESIS.

6.2a. Cobalt Complexes.

6.2a i. ACM 14 The Synthesis of $[Co_2(CO)_6(PEt_3)_2]$. [1]

PEt_3 (2.3 cm^3, 0.016 moles) was syringed on to $[Co_2(CO)_8]$ (2.5953g, 0.0076 moles) in toluene (70 cm^3). The solution was refluxed for 6 hours under nitrogen. The solvents were removed under vacuum and the product was extracted with warm petroleum ether (25 cm^3) and left to recrystallise. The product was unstable in solution but a small quantity of a red powder was recovered.

The powder was $[Co_2(CO)_6(PEt_3)_2]$ ν_{CO} 1924 cm^{-1} (s) , 1963 cm^{-1} (vs, vw) (in KBr). (lit. ν_{CO} 1953, 1971 cm^{-1} in benzene).

CHN analysis: C 41.47 %, H 5.97 %, N 0 %, (theoretical C 41.40 %, H 5.79 %, N 0 %).

6.2a ii. ACM 35. The Synthesis of $[CpCo(CO)PMe_3]$. [3]

PMe_3 (1.4 cm^3, 13.8 mmoles) was syringed on to $[CpCo(CO)_2]$ (0.5 cm^3, 3.9 mmoles) under nitrogen. After stirring for one and an half hours the excess phosphine was removed under vacuum to give the product as a dark red oil.

N.m.r. in CD_2Cl_2: ^{31}P, δ 19.30 ppm, contaminated with Me_3PO δ 36.65 ppm.
Infrared in hexane: ν_{CO} 1929 cm^{-1} (vs).

6.2a iii. ACM 128. The Synthesis of Pure [CpCo(CO)PEt_3].

The method of Spencer *et al* [3] can be modified in order to reduce the excess of triethyl phosphine employed and obtain pure [CpCo(CO)PEt_3] as a red oil.
PEt_3 (1.5 cm^3, 10.2 mmoles) was syringed on to [CpCo$(CO)_2$] (1.0 cm^3, 7.8 mmoles) under argon. The mixture was stirred vigorously for 19 hours and the excess phosphine was removed under vacuum. [CpCo(CO)PEt_3] was distilled as a red oil at 0.02 mmHg, boiling point ~70 °C.
N.m.r. in CD_2Cl_2: ^1H, δ 1.10 ppm, [CpCo(CO)$P(CH_2CH_3)_3$, dt, $^3J_{H-H}$ = 7.6 Hz, $^2J_{H-P}$ = 15.7 Hz], 1.61 ppm, [CpCo(CO)$P(CH_2CH_3)_3$, dq, $^2J_{H-P}$ = 7.8 Hz, $^3J_{H-H}$ = 7.6 Hz], 4.78 ppm, [C_5H_5Co(CO)$P(CH_2CH_3)_3$, s]. ^{13}C, δ 8.21 ppm, [C_5H_5Co(CO)$P(CH_2CH_3)_3$ s], 21.58 ppm, [C_5H_5Co(CO)$P(CH_2CH_3)_3$, d, $^1J_{C-P}$ = 72.3 Hz], 81.27 ppm, [C_5H_5Co(CO)$P(CH_2CH_3)_3$ s].
Infrared in hexane: ν_{CO} 1928 cm^{-1} (vs).

6.2a iv. ACM 50, 56, 138. The Synthesis of [CpCo(CO)PMe_2Ph]. [4]

[CpCo(CO)PMe_2Ph] can be prepared by the general procedure of Hart - Davis and Graham.
PMe_2Ph (0.8 cm^3, 8.8 mmoles) and [CpCo$(CO)_2$] (1.251 g, 6.95 mmoles) were refluxed in cyclohexane (50 cm^3) under nitrogen for 3 hours. The solvent and unreacted phosphine were removed under vacuum. The resulting dark red oil was dissolved in the smallest quantity of diethyl ether (~ 2 cm^3) and cooled in CO_2 (s) to crystallise. Yield 1.5g of dark red solid, 75 %.
N.m.r. in CD_3OD: ^1H, δ, 1.72 ppm, [C_5H_5Co(CO)PCH_3Ph, d, $^2J_{H-P}$ = 9.0 Hz], 4.75 ppm, [C_5H_5Co(CO)PCH_3Ph, s], 7.44 ppm, [C_5H_5Co(CO)PCH_3Ph, m, 3H], 7.83 ppm, [C_5H_5Co(CO)PCH_3Ph, m, 2H], ^{13}C, δ, 21.18 ppm, [C_5H_5Co(CO)PCH_3Ph, d, $^1J_{C-P}$ = 125.1 Hz], 82.67 ppm, [C_5H_5Co(CO)PCH_3Ph, s], 129.07, 129.20, 130.32, 130.33, 131.51, 131.66 ppm, [C_5H_5Co(CO)PCH_3Ph, 5C]
Infrared in hexane: ν_{CO} 1932 cm^{-1} (vs) (lit. ν_{CO} 1934 cm^{-1} in hexane).
CHN analysis: C 57.15 %, H 5.39 %, N 0 %, (theoretical C 57.95 %, H 5.56 %, N 0 %).

6.2a v. ACM 51. The Synthesis of [CpCo(CO)PMePh$_2$]. [4]

[CpCo(CO)PMePh$_2$] can be prepared by the general procedure of Hart - Davis and Graham.

PMePh$_2$ (1.1 cm^3, 5.9 mmoles) and [CpCo(CO)$_2$] (0.5 cm^3, 3.9 mmoles) were refluxed for 6 hours in cyclohexane (40 cm^3), under nitrogen. The solution was cooled in ice, the product precipitated as a brown solid.

Infrared in hexane: ν_{co} 1933 cm^{-1} (vs) (lit. ν_{co} 1934 cm^{-1} in hexane).

CHN analysis: C 61.82 %, H 5.05 %, N 0 %, (theoretical C 64.78 %, H 5.15 %, N 0 %).

6.2a vi. ACM 45. The Synthesis of [CpCo(CO)PPh$_3$]. [4]

[CpCo(CO)PPh$_3$] can be prepared by the general procedure of Hart - Davis and Graham.

PPh$_3$ (1.5533 g, 5.9 mmoles) and [CpCo(CO)$_2$] (0.9891 g, 5.5 mmoles) were refluxed in cyclohexane (50 cm^3) for 17.5 hours. On cooling to room temperature the red brown solid product precipitated.

Infrared in hexane: ν_{co} 1938 cm^{-1} (vs), (lit. ν_{co} 1937 cm^{-1} in hexane).

CHN analysis: C 68.32 %, H 4.81 %, N 0 %, (theoretical C 69.57 %, H 4.87 %, N 0 %).

6.2a vii. ACM 82. The Synthesis of [CpCo(COMe)(PMe$_2$Ph)I]. [4]

[CpCo(CO)PMe$_2$Ph] (0.325g, 1.1 mmoles) and MeI (2 cm^3, 32.1 mmoles) were stirred in dichloromethane (3 cm^3) for 20 minutes. The solvent and unreacted MeI were removed under vacuum and the product was recrystallised from dichloromethane-hexane at 0 °C. The dark red brown plates were obtained in an isolated yield of ~100 %.

N.m.r. in CD_2Cl_2: ^{1}H, δ, 1.88 ppm, [$C_5H_5Co(COCH_3)(P(CH_3)_2Ph)I$, d, $^2J_{H\text{-}P}$ = 9 Hz], 1.92 ppm, [$C_5H_5Co(COCH_3)(P(CH_3)_2Ph)I$, d, $^2J_{H\text{-}P}$ = 9-10 Hz], 3.36 ppm [$C_5H_5Co(COCH_3)(P(CH_3)_2Ph)I$, s], 4.74 ppm, [$C_5H_5Co(COCH_3)(P(CH_3)_2Ph)I$, s], 7.47 ppm [$C_5H_5Co(COCH_3)(P(CH_3)_2Ph)I$, m, 3H], 7.95 ppm, [$C_5H_5Co(COCH_3)(P(CH_3)_2Ph)I$, m, 2H]. ^{13}C, δ, 15.40 ppm, [$C_5H_5Co(COCH_3)(P(CH_3)_2Ph)I$, d, $^1J_{C\text{-}P}$ = 31.9 Hz], 19.19 ppm, [$C_5H_5Co(COCH_3)(P(CH_3)_2Ph)I$, d, $^1J_{C\text{-}P}$ = 34.3 Hz], [$C_5H_5Co(COCH_3)(P(CH_3)_2Ph)I$, s], 128.98, 129.10, 130.64, 131.38, 131.48 ppm, [$C_5H_5Co(COCH_3)(P(CH_3)_2Ph)I$].

Infrared in cyclohexane: ν_{co} 1658 cm^{-1} (s), (lit. ν_{co} 1650 cm^{-1} (s), 1629 (sh) cm^{-1} in dichloromethane).

6.2a viii. ACM 139, 171. The Synthesis of $[Cp^*Co(CO)_2]$. [2]

$[Co_2(CO)_8]$ (5.54 g, 16.2 mmoles) was dissolved in dichloromethane (50 cm^3). Pentamethylcyclopentadiene (2.8 cm^3, 17.9 mmoles) and 1,3-cyclohexadiene (2.4 cm^3, 25.2 mmoles) were added and the solution was gently refluxed under argon for 45 minutes. A further aliquot of Cp*H (2.2 cm^3, 14.0 mmoles) was added and the solution was refluxed for a further 1 hour and 45 minutes. The solution was left cooling and stirring overnight. A sample of the solution was taken and diluted with dichloromethane in order to take an infrared spectrum. The spectrum revealed that the major species in solution was $[Cp^*Co(CO)_2]$, if the reaction has not gone to completion a further aliquot of Cp*H can be added and the solution refluxed for a further period. The liquids were removed under vacuum and the product extracted from the soft oily product with petroleum ether (50 cm^3). The dark extract was reduced in volume to 20 cm^3 under vacuum and left at -20 °C to crystallise the product. The yield of dark red brown crystals is 79 %.

N.m.r. in CD_2Cl_2: ^1H, δ, 1.93 ppm, $[C_5(CH_3)_5Co(CO)_2]$, ^{13}C, δ, 10.66 ppm, $[C_5(CH_3)_5Co(CO)_2]$, 97.25 ppm $[C_5(CH_3)_5Co(CO)_2]$.

Infrared, in petroleum ether: ν_{CO} 2008 (s) cm-1, 1949 cm^{-1}(s), in KBr: ν_{CO} 1988 cm^{-1} (s), 1925 cm^{-1} (s), (lit. ν_{CO} 1999, 1935 cm^{-1} in dichloromethane).

CHN analysis: C 57.78 %, H 5.86 %, N 0 %, (theoretical C 57.61 %, H 6.04 %, N, 0 %).

6.2a ix. ACM 132. The Synthesis of $[Co(CO)_2(PMe_2Ph)_2I]$.

A small quantity of $[Co(CO)_2(PMe_2Ph)_2I]$ was isolated from the reaction of $[CpCo(CO)PMe_2Ph]$ and MeI at 40 °C in methanol under 10 bar of CO. The details of the experiment are given in section 6.4c xvi.

N.m.r. in CD_3OD: ^1H, δ, 2.18, 2.19, 2.21 ppm, $[Co(CO)_2(P(CH_3)_2Ph)_2I$, $H_6PP'H'_6$ $^5J_{PH}$ + $J_{PH'}$ = 8.2 Hz], 7.51 ppm, $[Co(CO)_2(P(CH_3)_2Ph)_2I$, m], 7.91 ppm, $[Co(CO)_2(P(CH_3)_2Ph)_2I$, m]. ^{13}C, δ, 20.18, 20.42, 20.66 ppm, $[Co(CO)_2(P(CH_3)_2Ph)_2I$, m, AXX', $^1J_{C-P}$+ $^1J_{C-P'}$ = 144.9 Hz], 129.43, 129.49, 129.55, 131.48, 132.11, 132.17 ppm, $[Co(CO)_2(P(CH_3)_2Ph)_2I]$.

Infrared in Dichloromethane: ν_{CO} 1916 cm^{-1} (vs), 1982 cm^{-1} (m).

The crystal structure is in appendix 1.

6.2a x. ACM 184. The Synthesis of $[Co(CO)_2(PEt_3)_2I]$.

A few crystals of $[Co(CO)_2(PEt_3)_2I]$ were isolated from the reaction of $[Cp^*Co(CO)_2]$, PEt_3 and MeI in methanol at 100 °C under CO (80 bar). The full procedure is detailed in section 6.4c.

N.m.r. in CD_2Cl_2: δ, ^1H, 1.20 ppm, $[Co(CO)_2(P(CH_2CH_3)_3)_2I$, m], ^{13}C, 2.14 ppm, $[Co(CO)_2(P(CH_2CH_3)_3)_2I$, m].

Infrared in dichloromethane: ν_{CO} 1906 cm^{-1} (vs), 1974 cm^{-1} (m).

The X-ray crystal structure is in appendix 1.

6.2a xi. ACM 189, 198. The Synthesis of $[Cp^*Co(CO)I_2]$.

$[Cp^*Co(CO)I_2]$ has been isolated as the major product from the reaction of $[Cp^*Co(CO)_2]$ and MeI in dichloromethane under CO (80 bar) (at room temperature) heated to 120 °C ACM 189. $[Cp^*Co(CO)I_2]$ has also been isolated from a mixture of $[Cp^*Co(CO)_2$, MeI, acetic acid, methyl acetate and water heated to 120 °C under CO pressure at 100 bar ACM 198. The full procedure to experiments ACM 189 and 198 are in section 6.4c xii.

N.m.r. in CD_2Cl_2: ^1H, δ, 2.23 ppm, $[C_5(CH_3)_5Co(CO)I_2]$, ^{13}C, 11.72 ppm, $[C_5(CH_3)_5Co(CO)I_2]$, 101.37 ppm, $[C_5(CH_3)_5Co(CO)I_2]$.

Infrared: In dichloromethane, ν_{CO} 2055 cm^{-1} (vs), as a solid, ν_{CO} 2027 cm^{-1} (vs), 2035 cm^{-1} (s), (lit. ν_{CO} 2060 cm^{-1} in dichloromethane [8]).

CHN analysis: ACM 189, C 28.96 %, H 3.29 %, N 0 %, ACM 198, C 26.29 %, 2.84 %, N 0 %, (theoretical C 27.76 %, H 3.18 %, N 0 %).

The X-ray crystal structure of $[Cp^*Co(CO)I_2]$ is in appendix 1.

6.2b. Synthesis Of Non-Cobalt Solids.

6.2b i. ACM 101. The Synthesis of $[MePEt_3I]$.

Under nitrogen PEt_3 (20 cm^3, 0.135 moles) was dropped very slowly on to MeI (20 cm^3, 0.321 moles) in MeOH (50 cm^3) cooled in an ice bath. The solution was stirred in ice untill the exothermic reaction subsided. Still in ice the volume of the solution was reduced under vacuum until the white product began to precipitate and the flask was then cooled to - 20 °C. The yield was 34.3g, 97 %.

N.m.r. in CD_2Cl_2: δ, ^1H, 1.30 ppm, $[CH_3P(CH_2CH_3)_3I$, dt, $^3J_{H\text{-}P}$ = 18.7 Hz, $^2J_{C\text{-}P}$ = 7.7 Hz],

2.04 ppm, [C*H*$_3$P(CH$_2$CH$_3$)$_3$I, d, 13.3 Hz], 2.47 ppm, [CH$_3$P(C*H*$_2$CH$_3$)$_3$I, dq, $^2J_{H\text{-}P}$ = 13.0 Hz, $^2J_{C\text{-}P}$ = 7.7 Hz], ^{13}C, 4.33 ppm, [*C*H$_3$P(Et)$_3$I, d, $^1J_{C\text{-}P}$ 208.7 Hz], 5.98 ppm, [CH$_3$P(CH$_2$*C*H$_3$)$_3$I, s], 14.04 ppm, [CH$_3$P(*C*H$_2$CH$_3$)$_3$I, d, $^1J_{C\text{-}P}$ 199.9 Hz], ^{31}P, δ, 37.53 cm^{-1}.

6.2b ii. ACM 165. [Cp*Rh(CO)$_2$]. [6,7]

[Cp*Rh(CO)$_2$] was prepared by a modification of the method of Maitlis *et al.* To avoid subliming the product we replaced this purifying step by extracting and recrystallising in petroleum ether. The sublimation of [Cp*Rh(CO)$_2$] was avoided as it led to partial decomposition and we found it difficult to separate [Cp*Rh(CO)$_2$] and hexamethyl benzene produced in this way.

[Cp*RhCl$_2$]$_2$ was prepared by the literature procedure. [6] [Cp*RhCl$_2$]$_2$ (1.60g, 2.59 mmoles) was dissolved in methanol (80 cm^3). Zinc dust (0.53g, 8.11 mmoles) was added and CO was bubbled through the solution for 1.5 hours. The solution was heated under gentle reflux for 3 hours with CO bubbling through. The brown solution was filtered from the residual solid and the solvent was removed under vacuum. The product was extracted from the solid with 2x20 cm^3 of petroleum ether giving a red solution. Petroleum ether was removed until the solid was at the point of crystallising and the product was redissolved using hand heat. The solution was stored at 0 °C to encourage the solid to crystallise. The product was obtained as pure red crystals.

N.m.r. in CD$_3$OD: ^{1}H, δ, 2.10 ppm, [C$_5$(C*H*$_3$)$_5$Rh(CO)$_2$], ^{13}C, δ, 11.03 ppm, [C$_5$(*C*H$_3$)$_5$Rh(CO)$_2$], in CD$_2$Cl$_2$: ^{1}H, δ, 2.07 ppm, [C$_5$(C*H*$_3$)$_5$Rh(CO)$_2$], ^{13}C, δ, 11.02 ppm, [C$_5$(*C*H$_3$)$_5$Rh(CO)$_2$].

Infrared in petroleum ether: ν_{CO} 1964 cm^{-1} (s), 2026 cm^{-1} (s), (lit. ν_{CO} 1950, 2000 cm^{-1} as a solid).

CHN analysis: C 48.97 %, H 5.13 %, N 0 %, (theoretical C 49.00 %, H 5.13 %, N 0 %).

6.2b iii. ACM 192. The Synthesis of [Cp*Rh(COMe)(CO)I].

[Cp*Rh(COMe)(CO)I] is the product of the reaction of [Cp*Rh(CO)$_2$] and MeI in methanol. The details of the experiment are in section 6.4c xviii.

N.m.r. in CD$_2$Cl$_2$: ^{1}H, δ, 1.95 ppm, [C$_5$(C*H*$_3$)$_5$Rh(COMe)(CO)I], 2.76 ppm, [C$_5$(CH$_3$)$_5$Rh(COC*H*$_3$)(CO)I], ^{13}C, δ, 10.19 ppm, [C$_5$(*C*H$_3$)$_5$Rh(COMe)(CO)I].

Infrared in CD$_2$Cl$_2$: ν_{CO} 2035 cm^{-1} (vs) + shoulder at ~ 2050 cm^{-1}, ν_{CO} 1679, 1690, 1673, 1666, 1659 cm^{-1} (m).

6.2b iv. ACM 192. The Synthesis of [Cp*Rh(CO)I_2].

The [Cp*Rh(COMe)(CO)I] containing solution from ACM 192 was pressurised with 20 bar of CO and heated to 150 °C, [Cp*Rh(CO)I_2] was isolated from the resultant solution. The full procedure is detailed in section 6.4c xviii.

N.m.r. in CD_2Cl_2: ^1H, δ, 2.23 ppm, [$C_5(CH_3)_5$Rh(CO)I_2], ^{13}C, δ, 11.42 ppm, [$C_5(CH_3)_5$Rh(CO)I_2], 105.61 ppm, [$C_5(CH_3)_5$Rh(CO)I_2].

Infrared: in dichloromethane, ν_{co} 2068 cm^{-1}, in the solid state ν_{co} 2039 cm^{-1} (s), 2050 cm^{-1} (vs).

CHN analysis: C 26.02 %, H 2.67 %, N 0 %, (theoretical C 25.41 %, H 2.91 %, N 0 %).

6.3.BATCH AUTOCLAVE RUNS.

6.3a. General Considerations.

The equipment used for high pressure work varied throughout the project, leading to changes in the scale of the reactions carried out. Throughout the procedure was very similar for all the experiments and differed mainly in the ratio of reactants and identity of the catalytic system. For the batch autoclave runs the reactant solution details are given in the appropriate table contained within chapters 2,3,4 and 5.

6.3b. 250 cm^3 Stainless Steel Autoclaves.

The 250 cm^3 stainless steel autoclave consisted of a 250 cm^3 stainless steel bomb with a screw top head sealed with a viton O ring. The head was fitted with an injection port sealed with a screw cap and a side arm fitted with a Hoke tap for controlling inflow and outflow of gases. A glass liner was fitted in to the base of the vessel for holding the reaction solution. The solution was stirred by a magnetic follower which contained holes to help pull gas in to the reactant solution. The autoclave was placed on the magnetic stirrer and heated by a metal heating jacket connected to a temperature controller.

The disadvantages of this set up were the lack of provision for a pressure transducer and thermocouple inside the reaction vessel, consequently the conditions of reaction are quoted as pressure at room temperature and temperature of the heat band, (external temperature, this will be 10 - 20 °C more than the internal temperature).

6.3b i. Batch Autoclave Experiments Without Free Phosphine.

The results are in the following tables: TABLE 2.1: ACM 43, 72; TABLE 2.2: ACM 15; TABLE 2.4: ACM 28, 75; TABLE 3.2: ACM 40, 36, 37, 41, 47, 49, 52, 53, 54, 62; TABLE 3.3: ACM 79, 80; TABLE 3.6: 66, 70, 74, 77, 87.

All operations were carried out under argon or nitrogen.

The stainless steel autoclave was sealed and attached to a vacuum line then evacuated and flushed with nitrogen or argon three times. With the inert gas flowing in to the autoclave the cap was removed from the injection port.

The catalyst and promoter (if required) were weighed out in to a Schlenk tube. Methanol and methyl iodide were injected on top of the catalyst using degassed syringes through a suba seal. Once the solids were dissolved the solution was injected in to the autoclave. The autoclave was sealed and attached to the CO cylinder. The connection between the autoclave and cylinder was degassed and the autoclave was pressurised to with CO. The sealed autoclave was then stirred vigorously (~ 850 rpm). The autoclave was heated to temperature at 20 °C min^{-1}. The time of reaction was started after ten minutes of beginning heating. After the reaction time the autoclave was plunged in to ice to quench the reaction. After approximately one hour the autoclave was degassed slowly. The autoclave was taken out of the ice bath and opened. The resultant solution was syringed in to a sample vial and analysed by g.c. The internal standard for g.c. analysis was tetrahydropyran (Aldrich), 1 cm^3 of sample solution + 0.04 cm^3 of tetrahydropyran at 12 °C ensured good separation. If metal complex analysis was required the solution was cathetered through a suba seal in the injection port in to a Schlenk tube under an inert atmosphere.

6.3b ii. Batch Autoclave Experiments Catalyst+ PEt_3.

The results are in the following tables: TABLE 3.3: ACM 32; TABLE 3.5: ACM 63, 64, 65, 67.

The procedure for running the autoclave reaction was the same as in section 4.3b i. The reactant solution was made up as follows. The catalyst was weighed in to a Schlenk. Methanol and methyl iodide were syringed on top and the solution was cooled in an ice bath. PEt_3 was dropped on to the solution slowly by syringe through a suba seal. Once all the PEt_3 was transferred the solution was allowed to warm back to room temperature before injecting it in to the autoclave.

6.3c. 28 cm^3 Hastelloy Autoclave.

This 28 cm^3 Hastelloy autoclave consists of a 28 cm^3 vessel which screws in to a fixed head with attached mechanical stirrer, pressure transducer, internal thermometer, injection port and gassing / degassing side arm fitted with a tap to control flow. The autoclave and head screw together and are sealed using a teflon O ring, since these studies it has been discovered that viton will give a more reliable seal.
The autoclave was heated by a heating jacket attached to a temperature controller.

6.3c i. Batch Autoclave Experiments Without Free Phosphine.

The results are in the following tables: TABLE 2.1: ACM 113, 151; TABLE 2.7: ACM 158; TABLE 4.4: ACM 172, 174, 175; TABLE 5.1: ACM 144, 157.
All operations were carried out under argon or nitrogen.
The autoclave was attached to an argon cylinder and flushed with argon through the open injection port for at least 30 minutes.
The catalyst and promoter (if required) were weighed out in to a Schlenk tube. Methanol and methyl iodide were injected on top of the catalyst using degassed syringes through a suba seal. Once the solids were dissolved the solution was injected in to the autoclave. The autoclave was sealed and attached to the CO cylinder. The connection between the autoclave and cylinder was degassed and the autoclave was pressurised to with CO. The sealed autoclave was then stirred vigorously. The autoclave was heated to temperature at 20 °C min^{-1}, temperature was monitored inside the vessel. The time of reaction was started after ten minutes of starting heating. After the reaction time the autoclave was plunged in to ice to quench the reaction. After approximately one hour the autoclave was degassed slowly. The ice bath was removed and the autoclave was opened. The resultant solution was analysed as discussed in section 6.3b i If metal complex analysis was required the solution was cathetered through a suba seal in the injection port in to a Schlenk tube under an inert atmosphere.

6.3c ii. Batch Autoclave Experiments Catalyst + PEt_3.

The results are in the following tables: TABLE 2.4: ACM 160, 170; TABLE 3.5: ACM 116, 148, 164, 166; ACM 159, 167, 168, 169.

The autoclave procedure was as 6.3c i. the solution was made up as 6.3b ii.

6.3c iii. Batch Autoclave Experiments Catalyst + PEt_3.

TABLE 4.3: ACM 173.

$[Cp^*Co(CO)_2]$ (0.1918g, 0.767 mmoles) was weighed in to Schlenk under argon. MeOH (4.8 cm^3, 118.50 mmoles) was syringed on top followed by PEt_3 (0.6 cm^3, 4.06 mmoles). The solution was cooled in ice and MeI (0.6 cm^3, 9.64 mmoles) was syringed slowly onto the solution. The Schlenk was allowed to warm back to room temperature and the solution was injected in to the autoclave. The rest of the procedure was as section 6.3c ii.

6.3d. Batch Autoclaves in CO_2.

TABLE 2.6: ACM 114; CHAPTER 5: ACM 156.

These reactions were carried out in a 28 cm^3 Hastelloy autoclave. The CO_2 was compressed by an H.P.L.C. pump and pumped in to the reaction vessel to the right pressure.

6.3d i. ACM 114: $[Co_2(CO)_8]$ + MeOH + MeI.

The autoclave was degassed with CO_2. The $[Co_2(CO)_8]$ (0.0513g, 0.150 mmoles), methanol (2.0 cm^3) and methyl iodide (0.35 cm^3) were injected in to the autoclave under the CO_2 flow. The autoclave was sealed and the stirrer was switched on. The pressure in the vessel was 14 bar at 20 °C. The CO cylinder was attached and degassed then CO was introduced to the reaction vessel to a total pressure of 56 bar at 23 °C. CO_2 was pumped in to the autoclave up to a total pressure of 91.2 bar. Once equilibrated the vessel was heated to 100 °C internal temperature. Once the reaction mixture had reached 95 °C the timer was started for the 4 hour run (17 minutes). After 4 hours the autoclave was cooled to -5 °C and degassed. The autoclave was opened and the orange solution syringed out and analysed.

6.3d ii. ACM 156: $[Cp^*Rh(CO)_2]$ + MeOH + MeI.

The autoclave was degassed with CO_2. A solution of $[Cp^*Rh(CO)_2]$ (0.0087g, 0.0296 mmoles) in MeOH (1.0 cm^3) and MeI (1.0 cm^3) was injected in to the autoclave under the CO_2 flow. The autoclave was sealed. The CO cylinder was attached and the vessel was pressurised to 20 bar with CO at room temperature. CO_2 was pumped in to the autoclave up to a total pressure of 90 bar. The autoclave was and heated to 90 °C internal temperature. Once the reaction mixture had reached 80 °C (15 minutes) the timer was started for the 1 hour run. After 1 hour the autoclave was cooled and degassed. The autoclave was opened and the solution was syringed out and analysed.

6.4. HIGH PRESSURE INFRARED STUDIES.

6.4a. Apparatus.

The details of the infrared equipment used are in section 6.1. The high pressure infrared autoclave consists of a Parr high pressure vessel with a single crystal silicon rod passing through it. The autoclave allows *in situ* pressure and temperature readings, catalyst injection and pressurising / depressurising through a tap. The autoclave was stirred mechanically from above. The silicon rod bathes in the reaction solution. The apparatus lies in the infrared beam which is focussed on the pointed end of the silicon rod which protrudes out of the vessel. The optics are optimised by making small adjustments to the autoclave position relative to the beam. The infrared spectrometer is set for ATR correction. Once optimised the beam will pass into the rod, reflect along the inside of the crystal and pass out of the other end in to the infrared detector. At the surface of the rod the solution absorbs energy from the beam and the resultant beam which emerges is deficient in the specific frequencies absorbed by the species in solution. Heating is effected by heating rods which pass in to holes in the base of the Parr vessel.

6.4b. General Procedure.

CO was ommited when it was not required, (see chapters 2,3,4 and 5).

The autoclave was degassed by passing argon or nitrogen in to the gassing / degassing side arm and out of the open injection port. The reaction solvents were injected in to the vessel and the autoclave was sealed. The vessel was pressurised to the required pressure

with CO and tested for leaks. If sealed the autoclave was fixed in to the infrared beam and the optics were optimised. Background spectra were recorded at regular intervals as the autoclave was heated and saved on the hard disk of a p.c.
The autoclave was now cooled, emptied, cleaned and degassed and the reactant solution was injected under an inert atmosphere. The autoclave was pressurised with CO. Again the vessel was placed between the beam and the optics were optimised. The relevant background file was chosen from the hard disk and spectra were collected as the autoclave was heated up displaying them in terms of transmittance. The backgrounds of the spectra were corrected manually using the OMNIC package.

6.4c. Mechanistic Studies and Experiments Using the H.P.I.R. Apparatus.

Detailed in this section are the methods used for the mechanistic studies performed. The appropriate *in situ* spectra are contained in chapters 2,3,4 and 5, the spectroscopic properties of the solids prepared and isolated are in section 6.2.

6.4c i. ACM 73: $[Co_2(CO)_8]$ in MeOH and MeI, Under CO.

Spectra were recorded using a background of MeOH (8.0 cm^3) and MeI (2.0 cm^3) under CO (60 bar).
$[Co_2(CO)_8]$ (0.2718g, 0.795 mmoles), MeOH (8.0 cm^3) and MeI (2.0 cm^3) were injected in to the autoclave under argon. The autoclave was pressurised to 60 bar with CO and spectra were recorded according to the procedure detailed in section 6.4b.. The autoclave was cooled and degassed and the orange solution was removed from the autoclave. Analysis by g.c. revealed that the solution contained dimethyl ether, a trace of acetaldehyde, methanol, methyl iodide, methyl acetate and 1,1-dimethoxyethane. The spectra collected are contained in section 3.2b i.

6.4c ii. ACM 83 and 84: $[CpCo(CO)PMe_2Ph]$ in CH_2Cl_2 and MeI.

Spectra were recorded using a background of CH_2Cl_2 (8.0 cm^3) and MeI (2 cm^3).
$[CpCo(CO)PMe_2Ph]$ (0.464g 1.60 mmoles) was dissolved in CH_2Cl_2 (8 cm^3) and MeI (2 cm^3). The solution was injected in to the autoclave under argon. An infrared spectrum was recorded without heating. The autoclave was pressurised to 60 bar with CO. Spectra were recorded as the autoclave was warmed to 40 °C. The autoclave was held at this temperature for 22 hours as further spectra were recorded.

The spectra collected are contained in section 3.2b i.

6.4c iii. ACM 122 and 191: [CpCo(CO)PMe_2Ph] in MeOH and MeI Under CO (60 bar).

Spectra were recorded using a background of MeOH (8.0 cm^3) and MeI (2.0 cm^3) under CO (60 bar).

ACM 122:

[CpCo(CO)PMe_2Ph] was dissolved in MeOH (8 cm^3) and MeI (2 cm^3). The solution was warmed to dissolve all the solid and injected in to the autoclave under nitrogen. The autoclave was pressurised to 60 bar with CO. Spectra were recorded as the autoclave was warmed to 50 °C, the autoclave was degassed under nitrogen and another spectrum ran at 40 °C. The solution was cathetered out of the autoclave under nitrogen and the solvents were removed under vacuum giving an amorphous green solid.

ACM 191.

[CpCo(CO)PMe_2Ph] (0.3930g 1.354 mmoles) was dissolved in MeOH (8.0 cm^3) and MeI (2.0 cm^3). The solution was injected in to the autoclave under nitrogen. The autoclave was pressurised to 60 bar with CO and left for 2 hours. Spectra were recorded as the autoclave was heated to 40 °C. The temperature was maintained at 41-42 °C until the 1986 cm^{-1} absorption stopped growing, total heating time 45 minutes. The autoclave was cooled and degassed in ice water and another spectrum recorded. The red / brown solution was cathetered from the autoclave under nitrogen and stored at 0 °C, ^1H and ^{13}C n.m.r. spectra were recorded by adding CD_3OD to this solution. No useful solid could be precipitated.

The spectra collected are contained in section 3.2b i.

6.4c iv. ACM 124 and 132: [CpCo(CO)PMe_2Ph] in MeOH and MeI Under 13 bar CO, Including Isolation of [$Co(CO)_2(PMe_2Ph)_2I$].

All manipulations were carried out under an inert atmosphere.

ACM 124.

A saturated solution of [CpCo(CO)PMe_2Ph] was prepared by stirring the solid in MeOH (8 cm^3) and MeI (2 cm^3) for 1 hour 30 minutes. The solution was injected in to the autoclave under nitrogen. The autoclave was pressurised with 13 bar of CO and spectra were recorded as the autoclave was warmed to 40 °C and held at that temperature for 1 hour. The autoclave was cooled and degassed and the solution cathetered from the

autoclave under nitrogen.

The spectra collected are contained in section 3.2b i.

ACM 132, Isolating $[Co(CO)_2(PMe_2Ph)_2I]$.

Argon was bubbled through the deep red solution to drive off the MeI. The solution was cooled in a CO_2 / EtOH bath until crystals began to form. The solution was then stored in solid CO_2 overnight. There was not enough solid to collect so the volume of the solution was reduced under vacuum slowly whilst cooling in a CO_2 / EtOH bath. Light brown needles crystallised from the solution, these were separated by filtration. The solid was recrystallised in methanol by dissolving the sample then cooling and reducing the volume as before until the solid began to crystallise, n.m.r. and infrared spectra were recorded. Crystals of better quality could be obtained by cooling the methanol solution to 0 ° C for a few days but this also led to partial decomposition of the solid, the X-ray crystal structure of the red platelets obtained in this way (see appendix 1).

The spectra of $[Co(CO)_2(PMe_2Ph)_2I]$ are assigned in section 6.2a xi.

6.4c v. ACM 85 and 86: $[CpCo(CO)_2]$ in CH_2Cl_2 and MeI.

ACM 85.

Spectra were recorded using a background of CH_2Cl_2 (8.0 cm^3) and MeI (2 cm^3). $[CpCo(CO)_2]$ (0.53g, 2.9mmoles), CH_2Cl_2 (8.0 cm^3) and MeI (2.0 cm^3) were combined. The solution was injected in to the autoclave under argon. The autoclave was slowly heated to 60 °C. After 7 hours total heating the autoclave was cooled.

ACM 86.

The autoclave was pressurised to 20 bar with CO and heated to 60 °C. The autoclave was cooled, degassed and opened, a green solid had precipitated.

The spectra collected are contained in section 3.4b ii.

6.4c v. ACM 133: $[CpCo(CO)_2]$ in MeOH and MeI.

Spectra were recorded using a background of MeOH (8.0 cm^3) and MeI (2 cm^3). $[CpCo(CO)_2]$ (0.5 cm^3), MeOH (8.0 cm^3) and MeI (2.0 cm^3) were combined. The solution was injected in to the autoclave under argon. The autoclave was heated to 95 °C. After 4 hours 20 minutes of total heating the autoclave was cooled. The red / brown solution was cathetered from the autoclave.

The spectra collected are contained in section 3.4b ii.

6.4c vi. ACM 117, 119 [$CpCo(CO)_2$] in MeOH and MeI Under CO (60 bar).

Spectra were recorded using a background of MeOH (8.0 cm^3) and MeI (2.0 cm^3) under CO (60 bar).

[$CpCo(CO)_2$] (0.25 cm^3), MeOH (6.5 cm^3) and MeI (1.5 cm^3) were injected in to the HPIR autoclave and pressurised to 60 bar with CO. The autoclave was heated to 100 °C and spectra were recorded. The autoclave was then cooled to room temperature and an infrared spectrum was recorded. The autoclave was degassed under nitrogen and another spectrum was recorded.

The spectra collected are contained in section 3.4b ii.

6.4c vii. ACM 105, 106 [$CpCo(CO)_2$] in EtOH and MeI Under CO (60 bar).

Spectra were recorded using a background of EtOH (8.0 cm^3) and MeI (2.0 cm^3) pressurised to 58 bar with CO.

[$CpCo(CO)_2$] (0.25 cm^3), EtOH (6.5 cm^3) and MeI (0.5 cm^3) were injected in to the autoclave under nitrogen. Spectra were recorded as the apparatus was heated to 105 °C. The autoclave was pressurised to 59 bar with CO and another spectrum recorded at 80 °C.

The spectra collected are contained in section 3.4b ii.

6.4c viii. ACM 68, 96 [$CpCo(CO)_2$] + PEt_3 in MeOH and MeI Under CO (60 bar).

Spectra were recorded using a background of MeOH (8.0 cm^3) and MeI (1.0 cm^3) pressurised to 60 bar with CO.

ACM 68.

[$CpCo(CO)_2$] (0.25 cm^3), MeOH (8.0 cm^3) and MeI (2.0 cm^3) were combined under argon. PEt_3 (2.0 cm^3) was slowly added using a syringe. The solution was injected in to the autoclave and the autoclave was pressurised to 60 bar with CO. Spectra were recorded as the apparatus was heated to 100 °C. The temperature was maintained at 83 °C overnight and then increased back to 100 °C, some more spectra were recorded. The autoclave was cooled and another spectrum was taken. The pressure had reduced to 53 bar. The autoclave was degassed and the dark brown solution analysed by g.c. The solution contained dimethyl ether, methanol, methanol, methyl acetate and acetic acid.

ACM 96. Gentle Heating.

$[CpCo(CO)_2]$ (0.25 cm^3), MeOH (8.0 cm^3) and MeI (2.0 cm^3) were combined under argon. PEt_3 (2.0 cm^3) was slowly added using a syringe. The solution was injected in to the autoclave and the autoclave was pressurised to 60 bar with CO. Infrared spectra were recorded as the autoclave was warmed slowly to 82 °C over two hours.
The spectra collected are contained in section 3.4b iii.

6.4c ix. ACM 97, 98, $[CpCo(CO)_2]$ + $[MePEt_3I]$ in MeOH Under CO (60 bar).

ACM 97.

Spectra were recorded using a background of MeOH (10 cm^3) under CO (60 bar). $[CpCo(CO)_2]$ (0.25 cm^3, 1.95 mmoles), $[MePEt_3I]$ (0.9023g, 4.38 mmoles) and MeOH (10 cm^3) were injected in to the HPIR autoclave under argon. The autoclave was pressurised to 60 bar with CO. Spectra were recorded as the apparatus was heated to 114 °C. The autoclave was cooled and degassed under argon.

ACM 98.

MeI (1.0 cm^3) was added to the autoclave from ACM 97 under argon. The autoclave was repressurised to 60 bar and infrared spectra were recorded as the autoclave was heated up to 100 °C. The autoclave was cooled and degassed. The dark red solution was removed and analysed by g.c. its main constituents were dimethyl ether, methanol, methyl iodide and methyl acetate. The metal complexes in solution decomposed in air, turning green.
The spectra collected are contained in section 3.4b iv.

6.4c x. ACM 108, $[CpCo(CO)_2]$ + $[MePEt_3I]$ in EtOH Under CO (60 bar).

Spectra were recorded using a background of EtOH (8.0 cm^3) and MeI (2.0 cm^3) pressurised to 58 bar with CO.

$[MePEt_3I]$ (2.4363g, 9.367 mmoles) was warmed in EtOH (8.0 cm^3) and MeI (2.0 cm^3) in order to dissolve the solid. Once cooled $[CpCo(CO)_2]$ (0.25 cm^3, 1.95 mmoles) was added and the solution was injected in to the autoclave under nitrogen. The autoclave was pressurised to 58 bar with CO. Spectra were recorded as the apparatus was heated to 100 °C. The autoclave was cooled and degassed, a green solution was removed.
The spectra collected are contained in section 3.4b iv.

6.4c xi. ACM 118, $[CpCo(CO)_2]$ + LiI in MeOH Under CO (60 bar).

Spectra were recorded with a background of MeOH (8.0 cm^3) and MeI (2.0 cm^3) under CO (60 bar).

LiI (2.4829g, 18.55 mmoles) was dissolved in MeOH (8.0 cm^3) and MeI (2.0 cm^3). $[CpCo(CO)_2]$ (0.25 cm^3, 1.95 mmoles) was added and the solution was injected in to the HPIR autoclave under nitrogen. The autoclave was pressurised to 60 bar with CO and infrared were recorded as the autoclave was slowly heated to 86 °C over 2 hours. The autoclave was cooled and degassed and a g.c. run on the red solution, it was found to contain dimethyl ether, methanol, methyl iodide, methyl acetate and a trace of 1,1-dimethoxyethane.

The spectra collected are contained in section 3.4b v.

6.4c xii. ACM 189, $[Cp^*Co(CO)_2]$ in CH_2Cl_2 and MeI Under CO (80 bar), Including Isolation of $[Cp^*Co(CO)I_2]$.

Spectra were collected with a background of CH_2Cl_2 (8.0 cm^3), MeI (2.0 cm^3) under CO (60 bar).

$[Cp^*Co(CO)_2]$ (0.2738g, 1.094 mmoles) was dissolved in CH_2Cl_2 (8.0 cm^3) and MeI (2.0 cm^3). A sample of the solution ACM 189A was diluted with CH_2Cl_2 and an infrared spectrum was run in a KBr solution cell. Another sample of ACM 189A was diluted with CD_2Cl_2 and ^1H and ^{13}C n.m.r. spectra recorded.

The solution was injected in to the HPIR autoclave under nitrogen. The autoclave was pressurised to 80 bar with CO. Spectra were recorded as the apparatus was heated to 120 °C. After 1 hour at 120 °C the autoclave was cooled to room temperature and another infrared spectrum was recorded. The autoclave was degassed under nitrogen and another spectrum recorded. The deep red / brown solution was cathetered out of the autoclave, some green breakdown product was detected. A sample of the solution ACM 198B was diluted with CH_2Cl_2 and an infrared spectrum was recorded in a KBr solution cell. Another sample of the solution was diluted with CD_2Cl_2 and ^1H and ^{13}C n.m.r. spectra were recorded.

Isolating $[Cp^*Co(CO)I_2]$.

After storing the solution for 3 days at 0 °C in a suba seal topped Schlenk tube the CH_2Cl_2 had been absorbed in to the suba seal. The result was a dark crystalline solid and oily green breakdown product. The dark crystalline solid was $[Cp^*Co(CO)I_2]$. An infrared

was collected of the dark crystalline solid in CH_2Cl_2 in a 0.05mm pathlegnth CaF_2 solution cell. The solid was recrystallised by dissolving it in a small volume of CH_2Cl_2 and leaving it in a suba seal topped Schlenk at 0 °C giving dark red brown plates ACM 189C. The solid is not air sensitive in the short term. The X-Ray crystal structure was determined (see appendix 1). The ^1H and ^{13}C n.m.r. spectra of this solid were recorded in CD_2Cl_2, a solid state infrared was recorded by depositing a thin layer of the solid on to a CaF_2 plate in CH_2Cl_2 solution and letting the CH_2Cl_2 evaporate (the solution was purple). A micranalysis was performed (see section 6.2a xi). The spectra of $[Cp^*Co(CO)I_2$ are assigned in section 6.2a xi).

6.4c xiii. ACM 152, 190, $[Cp^*Co(CO)_2]$ in MeOH and MeI Under CO (80 bar).

ACM 152, Average Rate Data.

Spectra were recorded with MeOH (8.0 cm^3) and MeI (2.0 cm^3) under CO (60 bar) as a background.

$[Cp^*Co(CO)_2]$ (0.2430g, 0.971 mmoles), MeOH (8.0 cm^3) and MeI (2.0 cm^3) were combined under argon and injected in to the autoclave. The autoclave was pressurised to 60 bar with CO. Spectra were recorded as the apparatus was heated to 100 °C. After 1 hour 10 minutes total heating time and 1 hour at 100 °C the autoclave was cooled. The autoclave was degassed and the orange solution cathetered out under argon. A sample was analysed by g.c and g.c. / m.s. The solution contained dimethyl ether, methanol, methanol, methyl acetate and 1,1-dimethoxyethane.

ACM 190.

Spectra were collected with a background of MeOH (8.0 cm^3) and MeI (2.0 cm^3) under CO (80 bar).

$[Cp^*Co(CO)_2]$ (0.3174g, 1.269 mmoles) was dissolved in MeOH (8.0 cm^3) and MeI (2.0 cm^3). A sample of ACM 190A was diluted with CD_3OD and ^1H and ^{13}C n.m.r. spectra recorded.

The rest of the solution was injected in to the HPIR autoclave under nitrogen. The autoclave was pressurised to 80 bar with CO. Spectra were recorded as the apparatus was slowly heated to 100 °C over 1 hour 20 minutes. Once the autoclave had reached 100 °C the autoclave was cooled to room temperature and another infrared spectrum was recorded. The autoclave was degassed under nitrogen and another spectrum recorded. The orange solution was cathetered out of the autoclave. A sample of the solution ACM

190B was diluted with CD_3OD and ^1H and ^{13}C n.m.r. spectra were recorded.
The details of the spectra recorded are in section 4.2c ii.

6.4c xiv. ACM 187, $[Cp^*Co(CO)_2]$ + PEt_3 in MeOH and MeI Under CO (80 bar). Early Phase.

Spectra were recorded with MeOH (8.0 cm^3) and MeI (2.0 cm^3) under CO (80 bar) as a background.

MeOH (8.0 cm^3) was added to $[Cp^*Co(CO)_2]$ (0.3201g, 1.279 mmoles) to give a red solution. Complete dissolution and darkening of the solution was affected by adding MeI (1.0 cm^3). The solution was cooled in ice and PEt_3 (1.0 cm^3, 6.8 mmoles) was slowly dropped in. Once warmed to room temperature a sample of the dark brown solution ACM 187A was analysed by ^1H and ^{13}C n.m.r. in CD_3OD. The rest of the solution was injected in to the HPIR autoclave under nitrogen. The autoclave was pressurised to 80 bar with CO. Infrared spectra were recorded as the autoclave was quickly heated to 100 °C. The autoclave was cooled and another spectrum was taken. The autoclave was degassed and another spectrum taken. The orange solution was cathetered out of the autoclave under nitrogen. An infrared spectrum of the solution ACM 187B was recorded in a 0.05mm pathlength CaF_2 solution cell. The ^1H and ^{13}C n.m.r. spectra of a sample of ACM 187B in CD_3OD were recorded.
The details of the spectra recorded are in section 4.3e i.

6.4c xv. ACM 188, $[Cp^*Co(CO)_2]$ + PEt_3 in EtOH and MeI Under CO (80 bar). Late Phase.

Spectra were recorded using backgrounds of EtOH (8.0 cm^3) and MeI (2.0 cm^3) Under 58 bar CO.

$[CpCo(CO)_2]$ (0.3178g, 1.270 mmoles) was dissolved in EtOH (8.0 cm^3) and MeI (1.0 cm^3) and the solution was cooled in ice. PEt_3 (1.0 cm^3, 6.8 mmoles) was dropped slowly on to the cooled solution. The solution was allowed to warm to room temperature and was injected in to HPIR autoclave. The autoclave was pressurised to 80 bar with CO and infrared spectra were collected as it was heated to 120 °C. The autoclave was cooled in ice water and another spectrum was recorded. It was then degassed under nitrogen and another spectrum recorded. The solution ACM 188B was removed by catheter under pressure of nitrogen, it was dark green. CD_3OD was added to a sample of this solution

and ^{1}H and ^{13}C n.m.r. spectra were recorded. The remainder of the solution was stored at -20 °C under an inert atmosphere, it turned purple suggesting the presence of $[Cp^*Co(CO)I_2]$.

The details of the spectra collected are in section 4.3e i.

6.4c xvi. ACM 184, $[Cp^*Co(CO)_2]$ + PEt_3 in MeOH and MeI Under CO (80 bar), Isolating $[Co(CO)_2(PEt_3)_2I]$.

$[Cp^*Co(CO)_2]$ (0.5657g, 2.261 mmoles) was dissolved in MeOH (8.0 cm^3) and MeI (1.0 cm^3). The solution was cooled in ice and PEt_3 (1.0 cm^3, 6.8 mmoles) was dropped slowly in. The solution was injected in to a 250 cm^3 hastelloy autoclave lined with a glass liner. The autoclave was pressurised to 80 bar with CO and heated to 100 °C (internal temperature) with a heating jacket. The autoclave took 17 minutes to reach 80 °C and spent 23 minutes at 80 - 100 °C before being quenched in ice, then cooled in a CO_2 / methanol bath. The autoclave, still standing in the CO_2 / methanol bath, was degassed under argon. It was then removed from the bath and the reaction solution was removed in to a Schlenk using a catheter under argon pressure. The solution was red / brown, some $[MePEt_3I]$ had precipitated, it was discarded. A g.c.analysis of the solution revealed methyl acetate and 1,1-dimethoxyethane had been produced. The solution was syringed in to the HPIR cell under argon and an infrared spectrum was recorded. The solution was diluted with MeOH (10 cm^3) and cooled in CO_2 / acetone to precipitate $[MePEt_3I]$. The solution was filtered off from the $[MePEt_3I]$ which was discarded. The solution was cooled in CO_2 / acetone and reduced in volume under vacuum until more $[MePEt_3I]$ crystallised. This was discarded as before. The reduction and filtration were repeated until the solid precipitating was no longer $[MePEt_3I]$, at this point the solution was allowed to warm to 0 °C and homogenise. The resultant solution formed a few good quality red plate crystals when stored at 0 °C for 1.5 months (as well as some breakdown product). A few of the crystals were dissolved in CD_2Cl_2 and an infrared (in a 0.05 mm CaF_2 solution cell) and ^{1}H n.m.r. were recorded before the solid decomposed. The X-ray crystal structure of the solid was determined, it was identified as $[Co(CO)_2(PEt_3)_2I]$ (see appendix 1).

The details of the infrared spectra recorded are in section 4.3e i. The spectra of $[Co(CO)_2(PEt_3)_2I]$ are assigned in section 6.2a x.

6.4c xvii. ACM 145, [Cp*Rh(CO)$_2$] in EtOH and MeI Under CO (58 bar).

Spectra were recorded using backgrounds of EtOH (8.0 cm^3) and MeI (2.0 cm^3) Under 58 bar CO.

[Cp*Rh(CO)$_2$] (0.0175g, 0.0595 mmoles) was weighed in to a Schleck tube and dissolved in EtOH (8.0 cm^3) and MeI (2.0 cm^3). The solution was injected in to the HPIR autoclave under argon. The autoclave was pressurised with 60 bar of CO and left for 1 hour. Spectra were recorded as the apparatus was heated to 100 °C over 45 minutes. The autoclave was kept at 100 °C for 3 hours and then cooled to room temperature. A spectrum was recorded at room temperature under CO and the autoclave was degassed under argon. Another spectrum was collected and then the deep red solution was cathetered out under argon pressure. A g.c. revealed the production of ethyl acetate and a trace of methyl acetate. A sample of the solution was reduced to the solid under vacuum and an infrared spectrum was recorded in diethyl ether in a KBr solution cell ν_{co} 2061 cm^{-1}.

6.4c xviii. ACM 192, [Cp*Rh(CO)$_2$] in MeOH and MeI Under 20 bar CO, and the isolation of [Cp*Rh(COMe)(CO)I] and [Cp*Rh(CO)I$_2$].

ACM 192A.

[Cp*Rh(CO)$_2$] (0.1204g, 0.4093 mmoles) was dissolved in MeOH (8.0 cm^3) and MeI (2.0 cm^3). A sample of the solution was stored at 0 °C in a Schlenk tube sealed with a suba seal. A dark red solid crystallised from solution and an infrared spectrum of this solid ACM 192A was recorded in CH_2Cl_2. The solid was dissolved in CD_2Cl_2 and ^1H and ^{13}C n.m.r. spectra were recorded. The X-ray crystal structure of this compound is in appendix 1, it was identified as [Cp*Rh(COMe)(CO)I].

The spectra of [Cp*Rh(COMe)(CO)I].are assigned in section 6.2b iv.

ACM 192 and Isolating [Cp*Rh(CO)I_2].

Spectra were recorded with a background of MeOH (8.0 cm^3) and MeI (2.0 cm^3) under CO. The remainder of the [Cp*Rh$(CO)_2$], solution, prepared as above, was injected in to the HPIR autoclave under argon. The autoclave was pressurised to 20 bar with CO and infrared spectra were recorded as the autoclave was heated to 150 °C. The autoclave was quenched in water and another spectrum recorded. It was then degassed under argon and another spectrum recorded. The solution ACM 192B was cathetered out of the autoclave in to a Schlenk tube and the ^1H and ^{13}C n.m.r. spectra were recorded in CD_3OD. The autoclave was opened revealing a large quantity of red needles ACM 192C (unfortunately these were twinned). The ^1H and ^{13}C n.m.r. spectra of this solid were recorded in CD_2Cl_2 and the infrared spectrum was recorded as a solid and in CH_2Cl_2 in a 0.05 mm pathlength CaF_2 solution cell. A microanalysis was also obtained (section 6.2b iv). More solid crystallised from the product solution ACM 192D. Solids ACM 192C and D were identified as [Cp*Rh(CO)I_2]. The remainder of the product solution ACM 192B was reduced to a small quantity of a dark red powder under vacuum. This solid was extracted with CH_2Cl_2. The infrared in a 0.05 mm pathlength CaF_2 solution cell revealed a terminal carbonyl absorption at 2083 cm^{-1}.

The spectra collected are contained in section 5.2c ii. The spectra of [Cp*Rh(CO)I_2] are assigned in section 6.2b iv.

6.5. INITIAL RATE MEASUREMENTS AT B.P. CHEMICALS HULL.

These experiments were conducted in a 300 cm^3 Hastelloy autoclave attached to a 567.1 cm^3 ballast vessel under constant pressure and temperature. The autoclave was fitted with a stirrer, heater and catalyst injector.

6.5a. Reactions in Methanol.

6.5a i. Reactions Without Added Phosphine.

ACM 176, ACM 181.

The catalyst, methanol, methyl iodide and autoclave were handled in a glove bag under a nitrogen atmosphere. The catalyst was weighed into a beaker, methanol and methyl iodide were added and the solution was poured in to the autoclave. The autoclave was sealed and fitted to the ballast vessel open to a CO cylinder. The headspace was flushed with CO and pressurised with CO (60 bar) at room temperature. The autoclave was stirred rapidly and heated to the desired reaction temperature, heating took 5-10 minutes. At temperature the pressure was increased to 100 bar from the ballast vessel and the connection between the ballast vessel and external CO source was closed. Measurements of ballast vessel pressure against time were recorded on an interfaced computer. After the reaction the autoclave was allowed to cool and was degassed. The autoclave was opened in the glove bag and the contents were transferred to a screw top jar.

6.5a ii. Reactions With Added Phosphine.

ACM 178, ACM 179 and ACM 180.

The initial steps of the procedure were identical to those detailed in section 6.5a i. Once the autoclave was sealed it was cooled in solid CO_2 and PEt_3 (weighed into a syringe in the glove bag) was injected in to the autoclave. The autoclave was sealed and fitted to the ballast vessel. The remaining procedure was as detailed in section 6.5a i.

6.5b. Reactions in the Low Water Acetic Acid Solvent.

6.5b i. Cobalt Catalysed Reactions.

ACM 177 and 182.

The catalyst, methyl acetate, acetic acid, water, methyl iodide and autoclave were handled in a glove bag under a nitrogen atmosphere. The catalyst (3 % w/w) was weighed out in

to a beaker, acetic acid (64 % w/w), water (7 % w/w), methyl iodide (14 % w/w) and methyl acetate (15 % w/w) were added and the solution was poured into the autoclave. The autoclave was sealed and fitted to the ballast vessel open to a CO cylinder. The headspace was flushed with CO and pressurised with CO (60 bar) at room temperature. The autoclave was stirred rapidly and heated to 140 °C. At temperature the pressure was increased to 100 bar from the ballast vessel and the connection between the ballast vessel and external CO source was closed. Measurements of ballast vessel pressure against time were recorded on an interfaced computer. After the reaction the autoclave was allowed to cool and was degassed. The autoclave was opened in the glove bag and the contents were transferred to a screw top jar.

6.5b ii. ACM 183: [Cp*Rh(CO)$_2$] Catalysed Reactions.

The catalyst, methyl acetate, acetic acid, water, methyl iodide and autoclave were handled in a glove bag under a nitrogen atmosphere. The catalyst (400 ppm Rh w/w, 0.112g, 0.381 mmoles) was weighed out in to a beaker, acetic acid (64 % w/w, 64.018g), water (7 % w/w, 7.009g) and methyl acetate (15 % w/w, 15.002g) were added and the solution was poured in to the autoclave. The autoclave was sealed and fitted to the ballast vessel open to a CO cylinder. Methyl iodide (14 % w/w, 13.996g) was weighed in to a syringe and injected through the injection port. The headspace was flushed with CO and pressurised with 8 bar CO at room temperature. The autoclave was stirred rapidly and heated to 185 °C. At temperature the pressure was increased to 28 bar from the ballast vessel, the methyl iodide was injected and the connection between the ballast vessel and external CO source was closed. Measurements of ballast vessel pressure against time were recorded on an interfaced computer. After 1 hour the pressure in the reaction vessel was further increased to 40 bar. After the reaction the autoclave was allowed to cool and was degassed. The autoclave was opened in the glove bag and the contents were transferred to a screw top jar.

6.6. INITIAL RATE MEASUREMENTS WITH CATS CATALYST TESTING UNIT.

These experiments were conducted in a 30 cm^3 Hastelloy autoclave attached via a mass flow controller to a 43.5 cm^3 ballast vessel under constant pressure and temperature. The autoclave was fitted with a stirrer, heater, catalyst injector, internal thermocouple and pressure transducer for the autoclave and ballast vessel.

6.6a. Experiments in Low Water Acetic Acid.

A stock solution was prepared containing acetic acid (64.000 g), methyl acetate (15.000 g) and water (7.000 g). The solution was degassed by bubbling argon through it.

6.6a i. ACM 198: $[Cp^*Co(CO)_2]$ in Low Water Acetic Acid.

$[Cp^*Co(CO)_2]$ (0.1506g, 0.602 mmoles) was weighed in to the autoclave under argon. The apparatus was flushed with argon and stock solution (4.000g) was injected in to the autoclave. The autoclave was pressurised to 60 bar with CO and stirred. MeI (0.700g) in stock solution (0.300g) was injected in to the injection port under argon. The autoclave was heated to 120 °C and the pressure was increased to 100 bar with CO. The MeI was injected and the external CO source was closed. Ballast pressure against time readings were recorded on an interfaced computer. After the reaction the autoclave was quenched in water and cooled to room temperature. The autoclave was degassed and opened. A large quantity of dark needles had crystallised. These were collected and identified as $[Cp^*Co(CO)I_2]$.

6.6a ii. ACM 199: $[Cp^*Co(CO)_2]$ + LiI in Low Water Acetic Acid.

$[Cp^*Co(CO)_2]$ (0.1506g, 0.602 mmoles) and LiI (0.8007g, 5.983mmoles) were weighed in to the autoclave under argon. The apparatus was flushed with argon and stock solution (4.0068g) was injected in to the autoclave. The autoclave was pressurised to 60 bar with CO and stirred. MeI (0.7096g) in stock solution (0.3005g) was injected in to the injection port under argon. The autoclave was heated to 120 °C and the pressure was increased to 100 bar with CO. The MeI was injected and the external CO source was closed. Ballast pressure against time readings were recorded on an interfaced computer. After the reaction the autoclave was quenched in water and cooled to room temperature. The

autoclave was degassed.

6.6a iii. ACM 197: [Cp*Co(CO)$_2$] + PEt$_3$ in Low Water Acetic Acid.

[Cp*Co(CO)$_2$] (0.1503g, 0.601 mmoles) was weighed in to the autoclave under argon. The apparatus was flushed with argon. Stock solution (4.3088g) was weighed out in to a Schlenk tube under argon. PEt$_3$ (0.6985g, 5.911 mmoles) was slowly dropped on to the solution from a syringe under argon. The solution was injected in to the autoclave. The autoclave was pressurised to 60 bar with CO and stirred. MeI (1.080g) was injected in to the injection port under argon. The autoclave was heated to 100 °C and the pressure was increased to 90 bar with CO. The MeI was injected and the external CO source was closed. Ballast pressure against time readings were recorded on an interfaced computer. After 1 hour the temperature was increased to 120 °C, after 2 hours the temperature was increased to 140 °C and the pressure to 100 bar. After the reaction the autoclave was quenched in water and cooled to room temperature. The autoclave was degassed.

6.6a iv. ACM 196: [Cp*Rh(CO)$_2$] in Low Water Acetic Acid, Repeat of ACM 183.

This reaction was a scale down of ACM 183 in order to see how reproducible our results were.

[Cp*Rh(CO)$_2$] (0.0056g, 0.0190 mmoles) was dissolved in stock solution (4.000g) under argon. The apparatus was flushed with argon and the solution was injected in to the autoclave. The autoclave was pressurised to 10 bar with CO and stirred. MeI (0.695g) in stock solution (0.300g) was injected in to the injection port under argon. The autoclave was heated to 185 °C and the pressure was increased to 28 bar with CO. The MeI was injected and the external CO source was closed. Ballast pressure against time readings were recorded on an interfaced computer. After the reaction the autoclave was quenched in water and cooled to room temperature. The autoclave was degassed and opened.

6.6b. Experiments in Methanol and Water.

6.6b i. ACM 200: [Cp*Co(CO)$_2$] + PEt$_3$ in Methanol and Water.

This experiment was designed to be equivalent to ACM 197 with the acetic acid and methyl acetate replaced by methanol.

[Cp*Co(CO)$_2$] (0.1507g, 0.602 mmoles) was weighed in to the autoclave under argon. The apparatus was flushed with argon. Methanol (2.0487g), water (0.35 cm^3) and triethyl

phosphine (0.7166g, 6.065 mmoles) were combined and injected in to the autoclave under argon. The autoclave was pressurised to 60 bar with CO and stirred. MeI (1.0841g) in methanol (1.0007g) was injected in to the injection port under argon. The autoclave was heated to 115-116 °C and the pressure was increased to 100 bar with CO. The MeI was injected and the external CO source was closed. Ballast pressure against time readings were recorded on an interfaced computer. After the reaction the autoclave was quenched in water and cooled to room temperature. The autoclave was degassed and an orange solution was syringed out under argon. G.c. and g.c. / m.s. were recorded of the solution.

6.6b i. ACM 201: $[Cp^*Co(CO)_2]$ + PEt_3 in Methanol and Water.

This experiment was carried out to determine the repeatability of ACM 200 and try to establish the catalysts involved in the second step.

$[Cp^*Co(CO)_2]$ (0.1507g, 0.602 mmoles) was weighed in to the autoclave under argon. The apparatus was flushed with argon. Methanol (2.0546g), water (0.3604 g) and triethyl phosphine (0.7158g, 6.058 mmoles) were combined and injected in to the autoclave under argon. The autoclave was pressurised to 60 bar with CO and stirred. MeI (1.0709g) in methanol (1.0104g) was injected in to the injection port under argon. The autoclave was heated to 116-117 °C and the pressure was increased to 100 bar with CO. The MeI was injected and the external CO source was closed. Ballast pressure against time readings were recorded on an interfaced computer. The reaction was stopped by quench cooling in water after enough data points had been collected to measure the rate of the second step. The autoclave was degassed and a dark orange / brown solution was syringed out under argon. An infrared spectrum of the solution was collected immediately in a CaF_2, 0.05 mm pathlength solution cell under argon. G.c. and g.c. / m.s. traces were collected. The results are given in sections 4.3d v and 4.3d vi.

6.6c. The Carbonylation of Methyl Acetate.

A stock solution was prepared containing acetic acid (96.70g), methyl acetate (47.70g), acetic anhydride (1.00g). Argon was bubbled through this solution to degas it.

6.6c i. ACM 194: $[Cp^*Rh(CO)_2]$ Catalysed Carbonylation.

The autoclave was degassed with argon. $[Cp^*Rh(CO)_2]$ (0.0104g, 0.0354 mmoles) and LiI (0.7314g, 5.4647 mmoles) were weighed in to a Schlenk tube under argon. Stock

solution (4.4 cm^3) was added and the dark red solution was injected in to the autoclave. The headspace was flushed and pressurised to 10 bar with CO, the stirrer was set to ~670 rpm. Methyl iodide (0.4 cm^3) in stock solution (0.6 cm^3) was injected in to the injection port under argon. The autoclave was heated to 189 °C. Once at temperature for 10 minutes the MeI solution was injected, the pressure was increased to 36 bar with CO and a ballast pressure time graph was plotted on an integrated p.c. After the reaction time the autoclave was cooled in water, degassed and the deep red solution was syringed out of the autoclave under argon. G.c. and g.c. / m.s. traces were obtained.
The results are quoted in section 5.2d ii.

6.6c ii. ACM 195: [Cp*Rh(CO)I_2] Catalysed Carbonylation.

The conditions employed were very similar to those used in ACM 194.
The autoclave was degassed with argon. [Cp*Rh(CO)I_2] (0.0183g, 0.0352 mmoles) and LiI (0.7308g, 5.4603 mmoles) were weighed in to a Schlenk tube under argon. Stock solution (4.4 cm^3) was added and the dark red solution was injected in to the autoclave. The headspace was flushed and pressurised to 10 bar with CO, the stirrer was set to ~670 rpm. Methyl iodide (0.4 cm^3) in stock solution (0.6 cm^3) was injected in to the injection port under argon. The autoclave was heated to 189 °C. Once at temperature for 10 minutes the MeI solution was injected, the pressure was increased to 36 bar with CO and a ballast pressure time graph was plotted on an integrated p.c. After the reaction time the autoclave was cooled in water, degassed and the deep red solution was syringed out of the autoclave under argon.
The results are quoted in section 5.2d ii.

References: Chapter 1

1. R. Sneeden, in *"Comprehensive Organometallic Chemistry"*, eds. G. Wilkinson, E. Abel and F. G. A. Stone, Pergamon Press, Oxford, 1982, Vol. 8, 20.
2. R. Pearce, W. R. Patterson,*"Catalysis and Chemical processing"*,
3. J. Rankin, PhD thesis university of St Andrews 1997.
4. D. Forster, *The Chemist*, 1981, 7.
5. R. Sneeden, in *"Comprehensive Organometallic Chemistry"*, eds. G. Wilkinson, E. Abel and F. G. A. Stone, Pergamon Press, Oxford, 1982, Vol. 8, 73.
6. H. Hohenschutz, N. von Kutepow and W. Himmele, *Hydrocarbon Processing*, 1996, **45,** 11, 141.
7. V. Galamb and G. Palyi in *Coord. Chem. Rev.*, 1994, **59**, 203.
8. W. R. Pretzer and T. P. Kobylinski, *Annals New York Academy of Sciences*, 1980, **333**, 58.
9. T. W. Dekleva and D. Forster, *Advan. catal.*, 1986, **34**, 81.
10. T. Mizoroki and M. Nakayama, *Bull. Chem. Soc. Jpn.*, 1965, **38**,11, 1876.
11. P. S. Braterman, B. S. Walker and T. H. Robertson, *J. Chem. Soc., Chem. Commun.*, 1977, 651.
12. R.F. Heck and D.S. Breslow, in *"Advances in the Chemistry of the Co - ordination Compounds, 6th International Conference of Co - ordination Chemistry"*, Macmillan, 1961.
13. J. T. Martin and M. C. Baird, *Organometallics,* 1983, **2**, 1073.
14. F. Piacenti and M. Bianchi in *"Organic Synthesis via Metal Carbonyls"*, eds., I. Wender and P. Pino, Wiley, 1977.
15. T. Mizoroki and M. Nakayama, *Bull. Chem. Soc. Jpn.*, 1968, **41**. 1628.

16. G. S. Koermer and W. E. Slinkard, *Ind. Eng. Chem. Prod. Res. Dev.*, 1978, **17**. 231.

17. J. Gauthier-Lafaye, R. Perron and Y. Colleuille, *J. Mol. Catal.* 1982, **17**, 339.

18. M. Röper and H. Lovenich, *J. Organomet. Chem.* 1983, **255**, 95.

19. R. T. Eby and T. C. Singleton, *Appl. Ind. Catal.*, 1983, **1**, 275.

20. D. Forster and T. C. Singleton, *J. Mol. Catal.*, 1982, **17,** 299.

21. W. Reppe, N. von Kutepow and H. Bille, U.S. Pat., 1961, 3014962.

22. T. Mizoroki and M. Nakayama, *Bull. Chem. Soc. Jpn.*, 1966, **39**, 1477.

23. J.R. Zoeller, in *"Acetic Acid and its Derivatives"*, eds., V. H. Agreda and J. R. Zoeller, Marcel Dekker, New York, 1993, Chap. 4.

24. T. Mizoroki, T. Matsumoto and A. Ozaki, *Bull. Chem. Soc. Jpn.*, 1979, **52**. 479.

25. S. D. Aubigne, J. B. Cooper; B. L. Williams, D. J. Watson, BP Chemicals Limited Appl. No.: 276,873, Jul. 18, 1994.

26. H. D. Grove, *Hydrocarbon Processing*, 1972, 76.

27. P. M. Maitlis, A. Haynes, G. L. Sunley and M. J. Howard, *J. Chem. Soc., Dalton Trans.*, 1996, 2187.

28. G. W. Adamson J. J. Daly and D. Forster, *J. Organomet. Chem,* 1974, **71**, C17.

29. D. Forster, *J. Am. Chem. Soc.*, 1975, **97:4**, 951.

30. D. Forster, *J. Am. Chem. Soc.*, 1976, **98:3**, 846.

31. D. Forster, *Annals New York Academy of sciences*, 1977, **295**, 79.

32. H. B. Tinker and D. E. Morris, *The review of scientific instruments*, 1972, **43**, 1024.

33. A. Haynes, B. E. Mann, D. J. Gilliver, G. E. Morris and P.M. Maitlis, *J. Am. Chem. Soc.*, 1991, **113**, 8567.

34. A. Haynes, B. E. Mann, G. E. Morris and P.M. Maitlis, *J. Am. Chem. Soc.*, 1993, **115**, 4093.

35. L. A. Howe and E. E. Bunel, *Polyhedron*, 1995, **14/1**, 167.

36. N. A. Cruise and J. Evans, *J. Chem. Soc. Dalton Trans.* 1995, 3089.

37. A. G. Kent, B. E. Mann and C. P. Manuel, *J. Chem. Soc. Chem. Commun.*, 1985, 728.

38. A. Fulford, C. E. Hickey and P. M. Maitlis, *J. Organomet, Chem.*, 1990, **398**, 311.

39. J. Hjortkjaer and O. R. Jensen, *Ind. Eng. Chem., Prod. Res. Dev.*,1977, **4**, 281.

40. E. C. Baker, D. E. Hendriksen and R. Eisenberg, *J. Am. Chem. Soc.*, 1980, **102**, 1020.

41. B. L. Smith, G. P. Torrence, M. A. Murphy and A. Anguiló, *J. Mol. Catal.*, 1987, **39,** 115.

42. T. Matsumoto, k. Mori, T. Mizoroki and A. Ozaki, *Bull. Chem. Soc. Jpn.*, 1977, **50**, 2337.

43. S. B. Dake and R. V. Chaudhari, *J. Mol. Catal.*, 1984, **26,** 135.

44. M. A. Murphy, B. L. Smith, G. P. Torrence and A. Aguiló, *J. Organomet. Chem.*, 1986, **303**, 257.

45. M. A. Murphy, B. L. Smith, G. P. Torrence and A. Aguiló, *Inorg. Chim. Acta.*, 1985, **101**, L47.

46. M. J. Howard, M. D. Jones, M. S. Roberts and S. A. Taylor, *Catalysis Today*, 1993, **18**, 325.

47. C. E. Hickey and P. M. Maitlis, *J. Chem. Soc. Chem. Commun.*, 1984, 1609.

48. M. Gauβ, A. Seidel, P. Torrenceand P. Heymanns, in "*Applied Homogenous Catalysis with Organometallic Compounds*", eds. B. Cornils, W. A. Hessmann, VCH, 1996, Vol. 1.

49. C. S. Garland, M. F. Giles, J. G. Sunley, European Pat., 1995, 0 643 034 A1.

50. J. G. Sunley, Presentation at "R.S.C Symposium of the Applied Catalysis group" 2/4/98.

51. D. E. Forster, *J. Chem. Soc., Dalton Trans.*, 1979, 1639.

52. T. Ghaffar, A. Haynes, P.M. Maitlis and G. J. Sunley, *11th International Symposium Homogeneous Catalysis*, 1998, P203, J. M. Pearson, A. Haynes, G.E. Morris, G. J. Sunley and P. M. Maitlis, *J. Chem. Soc., Chem. Commun.*, 1995, 1045.

53. T. Ghaffar, H. Adams, P.M. Maitlis, G.J. Sunley, M.J. Baker and A. Haynes, *J. Chem. Soc., Chem. Commun.*, 1998, 1023.

54. P.M. Maitlis, A. Haynes, G.J. Sunley and M.J. Howard, *J. Chem. Soc., Dalton Trans.*, 1996, 2187.

55. M. Bassetti, G.J. Sunley, F.P. Fanizzi and P.M. Maitlis, *J. Chem. Soc., Dalton Trans.*, 1990, 1799.

56. F. Calderazzo, *Angew. Chem. Int. Ed. Engl.*, 1977, **16**, 299.

57. R.G. Pearson and P.E. Figdore, *J. Am. Chem. Soc.*, 1980, **102**, 1541

***References:* CHAPTER 2**

1. D. Nicholls, *Complexes and First - Row Transition Elements"*, Macmillan, 1990, Chap. 16.

2. F.A. Cotton and G. Wilkinson, *"Advanced Inorganic Chemistry"*, 5th edn., Wiley, New York, 1988.

3. T. Mizoroki and N. Nakayama, *Bull. Chem. Soc. Jpn.*, 1968, **41**, 1628.

4. I. Kovacs, F. Ungvary and L. Marko, *Organometallics*, 1986, **5**, 209.

5. J.R. Zoeller, *"Acetic Acid and its Derivatives"*, Marcel Dekker, New York, 1993, Chap. 4.

6. P. S. Braterman, "*Metal Carbonyl Spectra*", Academic Press, London, 1975.

7. K. Watanabe, K. Kudo, N. Sugita, *Bull. Chem. Soc. Jpn.*, 1979, **58**, 2029.

8. W. R. Pretzer and T. P. Kobylinski, *Annals New York Academy of sciences*, 1980, **333**, 58.

9. J. Rankin, A.D Poole, A.C. Benyei and D.J. Cole - Hamilton, *J. Chem. Soc., Chem. Commun.*, 1997, 1835.

10. J. Rankin, PhD thesis university of St Andrews 1997.

References: CHAPTER 3

1. K.P.C. Vollhardt, *Angew. Chem. Int. Ed. Eng.*, **1984**, *23*, 539

2. Ref: S. Frith, J.L. Spencer, J.C. Nicholls, H. Werner, R. Feser, V. Harder, W. Hofmann and H. Neukomm, *Inorganic Synthesis*, **1990**, Vol. 28, 273.

3. D.L. Lichtenbeger, D.C. Calabro and G.E. Kellog, *Organometallics*, 1984, **3**, 1623

4. R.L. Sweany, *"Comprehensive Organometallic Chemistry II, A Review of the Literature 1982 - 1994"*, Pergamon, Oxford, 1995, Vol. 8.

5. D.L. Lichtenberger, C.H. Blevins, R.B. Ortega, *Organometallics*, **1984**, 3, 1614. N.

6. Dudeney, O.N. Kirchner, J.C. Green and P.M. Maitlis, *J. Chem. Soc. Dalton Trans.*, **1984**, p1877.

7. D.A. Brown, H.L. Clarke and N.J. Fitzpatrick, *J. Organomet. Chem.*, 1973, **47**, C11 - C12.

8. F. Basalo, *Polyhedron,* 9.2, **1990**, 1503.

9. R.B. King, P.M. Treichel and F.G.A. Stone, *J. Am. Chem. Soc.*, 1961, **83**, 3593.

10. A. Spencer and H. Werner, *J. Organomet. Chem.*, 1979, **171**, 219.

11. A.J. Hart - Davis and W.AG. Graham, *Inorganic Chemistry*, 1970, **Vol. 9 No. 12**, 2658.

12. Aldrich Library of FT NMR Spectra, Edn 1, Vol 2, 1650, 1993, Aldrich

13. R.B. King, *Inorganic Chem.*, 5, **1966**, 82.

14. J. Rankin, A.D Poole, A.C. Benyei and D.J. Cole - Hamilton, *J. Chem. Soc., Chem. Commun.*, 1997, 1835.

15. A.Haynes, University of Sheffield, Private Communication.

16. N.E Schore, C.S. Ilenda, M.A. White, H.E. Bryndza, M.G. Matturro and R.G. Bergmann, *J.Am.Chem.Soc.*, 1984, **106**, 745.

17. P.Lightfoot, University of St. Andrews Private Communications.

References: CHAPTER 4

1. P.M. Maitlis, *Chem. Soc. Rev.*, 10, **1981**, 1

2. A. Frith, J.L. Spencer, *Inorganic Synthesis*, 28, **1990**, 273.

3. A. Haynes, University of Sheffield, Private Communications.

4. R.F. Heck and D.S. Breslow, *Advances in the Chemistry of the Co-ordination Compounds, 6th International Conference of Co-ordination Chemistry*, Macmillan, 1961.

5. N.E. Schore, C.S. Ilenda, M.A. White, H.E. Bryndza, M.G. Matturro, R.G. Bergman, *J. Am. Chem. Soc.*, **1984**, *106*, 7451.

***References:* CHAPTER 5**

1. David Elias, Honours Project Report, University of St. Andrews, 1998

2. P.M. Maitlis, *Chem. Soc. Rev.*, 10, **1981**,

3. H. Werner, *Angew. Chem. Int. Ed. Engl.*, 1983, **22**, 927. R.S. Dickson, *"Organometallic Chemistry of Rhodium and Iridium"*, Academic Press inc., New York, 1983.

4. J.W. Kang and P.M. Maitlis, *J. Organomet. Chem.*, 1971, **26**, 393.

5. M. Bassetti, D. Monti, A. Haynes, J.M. Pearson, I.A. Stanbridge and P.M. Maitlis, *Gaz. Chim. Ital.*, 1992, **122,** 391.

6. A. Haynes, Private Communication.

7. S.G. Kazarian, P.A. Hamley and M. Poliakoff, *J. Chem. Soc., Chem. Commun.*, 1992, 994.

8. Applied Homogeneous Catalysis with Organometallic Compounds, Edit. Boy Cornils and Wolfgang A. Hermann, Chap 2.1.2.1.3, p116 M. Gauβ, A. Seidel, P. Torrence, P. Heymanns. VCH Weinheim.

9. A. D. Poole, Private Communication.

10. E. Bordignon, U. Croatto, U. Mazzi and A. A. Orio, Inorg. Chem., 1974, **13**, 935.

***References:* CHAPTER 6**

1. A.R. Manning, J. Chem. Soc. (A), 1968, 1135.

2. S. A. Frith and J. L. Spencer, *Inorganic Synthesis*, 1990, **28**, 273.

3. A. Spencer and H. Werner, *J. Organomet. Chem.*, 1979, **171**, 219.

4. A.J. Hart - Davis and W.AG. Graham, *Inorg. Chem.*, 1970, **Vol. 9 No. 12**, 2658.

5. R.K. Harris, *Can. J. Chem.*, 1964, **42**, 2275.

6. J.W. Kang, K. Mosely, P.M. Maitlis, *J. Am. Chem. Soc.*, 1969, **91**, 5970.

7. J.W. Kang, P.M. Maitlis, *J. Organomet. Chem.*, 1971, **26**. 393.

8. R.B. King, A. Efraty and W.M. Douglas, *J. Organomet. Chem.*, 1973, **56**, 345.

APPENDIX I

Crystallographic Data

X-ray Structure Report
Thu Aug 28 1997
acm132b

EXPERIMENTAL DETAILS

Crystal Data
Empirical Formula C 18 H 22 CoIP 2 O 2
Formula Weight 518.16
Crystal Color, Habit brown, plate
Crystal Dimensions 0.50 X 0.40 X 0.10 mm
Crystal System monoclinic
Lattice Type Primitive
No. of Reflections Used for Unit
Cell Determination (2` range) 25 (34.5 - 35.0 ffi)
Omega Scan Peak Width
at Half-height 0.29 ffi
Lattice Parameters a = 12.293(5) š A
b = 11.473(3) š A
c = 15.865(3) š A
fi = 100.65(2) ffi
V = 2199(1) š A 3
Space Group P2 1 /c (#14)
Z value 4
D calc 1.565 g/cm 3
F 000 1024.00
¯(MoKff) 23.37 cm
Radiation MoKff (– = 0.71069 A)
graphite monochromated
Attenuator Zr foil (factor = 8.53)
Take-o
Angle 6.0 ffi
Detector Aperture 9.0 mm horizontal
13.0 mm vertical
Crystal to Detector Distance 235 mm
Temperature 20.0 ffi C
Scan Type !-2`
Scan Rate 16.0 ffi /min (in !) (up to 4 scans)
Scan Width (1.52 + 0.35 tan `) ffi
2` max 50.0 ffi
No. of Reections Measured Total: 4282
Unique: 4083 (R int = 0.032)
Corrections Lorentz-polarization
Absorption
(trans. factors: 0.5120 - 1.0000)
Secondary Extinction
(coecient: 1.52896e-07)

Structure Solution and Renement
Structure Solution Direct Methods (SIR92)
Renement Full-matrix least-squares
Function Minimized w (jFoj 2
Least Squares Weights 1
oe 2 (Fo) = 4Fo 2
oe 2 (Fo 2)
p-factor 0.0040
Anomalous Dispersion All non-hydrogen atoms
No. Observations (I?3.00oe(I)) 3084
No. Variables 218
Reection/Parameter Ratio 14.15 6

Residuals: R; Rw 0.042 ; 0.056
Goodness of Fit Indicator 4.87
Max Shift/Error in Final Cycle 0.00
Maximum peak in Final Diff. Map 1.82 e 3
Minimum peak in Final Diff. Map -0.68 e
Table 1. Atomic coordinates and B iso /B eq
atom x y z B eq
I(1) 0.75374(6) -0.26141(6) 1.33806(4) 4.25(2)
Co(1) 0.71402(10) -0.06134(10) 1.25448(7) 2.65(3)
P(1) 0.6100(2) 0.0007(2) 1.3450(1) 3.10(5)
P(2) 0.8247(2) -0.1177(2) 1.1680(1) 3.43(6)

O(1) 0.8640(6) 0.1287(7) 1.3047(5) 6.2(2)
O(2) 0.5262(6) -0.0574(8) 1.1169(4) 6.7(2)
C(1) 0.4845(8) -0.0817(8) 1.3494(6) 3.4(2)
C(2) 0.3860(9) -0.0502(10) 1.3011(6) 4.7(3)
C(3) 0.2901(9) -0.119(1) 1.3073(8) 7.0(4)
C(4) 0.300(1) -0.215(1) 1.3600(9) 7.0(4)
C(5) 0.395(1) -0.243(1) 1.4052(8) 6.4(4)
C(6) 0.4870(9) -0.1808(9) 1.4005(7) 4.8(3)
C(7) 0.6819(9) 0.0078(10) 1.4568(6) 5.1(3)
C(8) 0.5607(9) 0.1493(8) 1.3237(6) 5.0(3)
C(9) 0.8389(8) -0.0104(8) 1.0873(5) 3.2(2)
C(10) 0.9280(8) 0.0659(9) 1.0946(6) 4.6(3)
C(11) 0.9366(9) 0.1499(9) 1.0337(7) 5.0(3)
C(12) 0.854(1) 0.1594(10) 0.9644(7) 5.3(3)
C(13) 0.7662(9) 0.0864(10) 0.9528(6) 4.8(3)
C(14) 0.7579(8) 0.0006(8) 1.0141(6) 4.2(3)
C(15) 0.781(1) -0.2482(9) 1.1075(6) 6.7(3)
C(16) 0.9664(9) -0.147(1) 1.2211(7) 6.3(3)
C(17) 0.8057(8) 0.0510(8) 1.2874(6) 3.8(2)
C(18) 0.6014(8) -0.0635(9) 1.1725(6) 3.8(2)
8

Table 1. Atomic coordinates and B iso /B eq (continued)
atom x y z B eq
H(1) 0.3807 0.0154 1.2641 5.6423
H(2) 0.2197 -0.0979 1.2749 8.2267
H(3) 0.2359 -0.2611 1.3629 8.3236
H(4) 0.3998 -0.3088 1.4425 7.7378
H(5) 0.5559 -0.2055 1.4334 5.7052
H(6) 0.7115 -0.0666 1.4744 5.9934
H(7) 0.7404 0.0630 1.4619 5.9934
H(8) 0.6313 0.0309 1.4923 5.9934
H(9) 0.6215 0.1994 1.3212 5.9119
H(10) 0.5102 0.1520 1.2705 5.9119
H(11) 0.5240 0.1745 1.3683 5.9119
H(12) 0.9855 0.0603 1.1436 5.4038
H(13) 0.9990 0.2005 1.0405 5.9804
H(14) 0.8586 0.2180 0.9227 6.2750
H(15) 0.7096 0.0935 0.9032 5.7294
H(16) 0.6961 -0.0507 1.0055 4.9734
H(17) 0.7132 -0.2340 1.0695 7.9616
H(18) 0.8360 -0.2698 1.0751 7.9616
H(19) 0.7718 -0.3096 1.1456 7.9616
H(20) 0.9667 -0.2027 1.2653 7.5899
H(21) 1.0080 -0.1754 1.1808 7.5899
H(22) 0.9995 -0.0763 1.2458 7.5899
B eq = 8
3 ß 2 (U 11 (aa 3) 2 + U 22 (bb 3) 2 + U 33 (cc 3) 2 + 2U 12 aa 3 bb 3 cos fl + 2U 13 aa 3 cc 3 cos fi + 2U 23 bb 3 cc 3 cos ff)
9

Table 2. Anisotropic Displacement Parameters
atom U 11 U 22 U 33 U 12 U 13 U 23
I(1) 0.0680(5) 0.0436(4) 0.0521(4) 0.0086(4) 0.0163(3) 0.0107(3)
Co(1) 0.0343(7) 0.0333(7) 0.0338(6) -0.0012(6) 0.0086(5) -0.0017(5)
P(1) 0.042(2) 0.036(1) 0.043(1) -0.001(1) 0.015(1) -0.002(1)
P(2) 0.053(2) 0.040(1) 0.040(1) 0.006(1) 0.017(1) -0.002(1)
O(1) 0.077(6) 0.079(6) 0.086(6) -0.041(5) 0.033(4) -0.031(5)
O(2) 0.051(5) 0.138(8) 0.060(5) 0.000(5) -0.004(4) 0.012(5)
C(1) 0.043(6) 0.046(6) 0.045(5) -0.007(5) 0.023(5) -0.009(4)
C(2) 0.049(7) 0.075(8) 0.060(7) -0.009(6) 0.020(5) -0.002(6)
C(3) 0.038(7) 0.15(1) 0.076(9) -0.016(8) 0.015(6) -0.051(9)
C(4) 0.09(1) 0.09(1) 0.09(1) -0.053(10) 0.055(9) -0.030(9)
C(5) 0.10(1) 0.052(7) 0.11(1) -0.023(8) 0.058(9) -0.010(7)
C(6) 0.072(8) 0.045(6) 0.076(7) -0.003(6) 0.043(6) 0.003(6)
C(7) 0.064(8) 0.082(8) 0.047(6) -0.005(6) 0.015(5) -0.015(6)
C(8) 0.069(8) 0.041(6) 0.082(8) 0.004(6) 0.024(6) 0.003(5)
C(9) 0.046(6) 0.042(5) 0.036(5) 0.005(5) 0.013(4) -0.004(4)
C(10) 0.049(7) 0.065(7) 0.059(7) 0.000(6) 0.009(5) -0.003(6)
C(11) 0.061(8) 0.058(7) 0.075(8) -0.005(6) 0.020(6) 0.009(6)
C(12) 0.083(9) 0.060(7) 0.071(8) 0.013(7) 0.049(7) 0.017(6)
C(13) 0.067(8) 0.074(8) 0.043(6) 0.018(7) 0.016(5) 0.013(6)

C(14) 0.053(7) 0.054(6) 0.054(6) -0.002(5) 0.016(5) -0.006(5)
C(15) 0.16(1) 0.043(6) 0.063(7) 0.000(8) 0.049(8) -0.008(6)
C(16) 0.069(9) 0.094(10) 0.086(8) 0.038(7) 0.037(7) 0.031(7)
C(17) 0.057(7) 0.047(6) 0.048(6) 0.001(5) 0.029(5) -0.005(5)
C(18) 0.041(6) 0.063(7) 0.041(5) -0.006(5) 0.012(5) 0.005(5)
10

Table 2. Anisotropic Displacement Parameters (continued)
atom U 11 U 22 U 33 U 12 U 13 U 23
The general temperature factor expression:
exp(2 (a 32 U 11 h 2 + b 32 U 22 k 2 + c 32 U 33 l 2 + 2a 3 b 3 U 12 hk + 2a 3 c 3 U 13 hl + 2b 3 c 3 U 23 kl))
11

Table 3. Bond Lengths(š A)
atom atom distance atom atom distance
I(1) Co(1) 2.651(1) Co(1) P(1) 2.209(3)
Co(1) P(2) 2.201(3) Co(1) C(17) 1.73(1)
Co(1) C(18) 1.715(9) P(1) C(1) 1.822(9)
P(1) C(7) 1.832(9) P(1) C(8) 1.820(10)
P(2) C(9) 1.808(9) P(2) C(15) 1.80(1)
P(2) C(16) 1.82(1) O(1) C(17) 1.14(1)
O(2) C(18) 1.156(10) C(1) C(2) 1.36(1)
C(1) C(6) 1.39(1) C(2) C(3) 1.44(1)
C(3) C(4) 1.38(2) C(4) C(5) 1.29(2)
C(5) C(6) 1.35(1) C(9) C(10) 1.39(1)
C(9) C(14) 1.39(1) C(10) C(11) 1.38(1)
C(11) C(12) 1.35(1) C(12) C(13) 1.36(1)
C(13) C(14) 1.40(1)
12

Table 4. Bond Lengths(š A)
atom atom distance atom atom distance
C(2) H(1) 0.95 C(3) H(2) 0.95
C(4) H(3) 0.95 C(5) H(4) 0.95
C(6) H(5) 0.95 C(7) H(6) 0.95
C(7) H(7) 0.95 C(7) H(8) 0.95
C(8) H(9) 0.95 C(8) H(10) 0.95
C(8) H(11) 0.95 C(10) H(12) 0.95
C(11) H(13) 0.95 C(12) H(14) 0.95
C(13) H(15) 0.95 C(14) H(16) 0.95
C(15) H(17) 0.95 C(15) H(18) 0.95
C(15) H(19) 0.95 C(16) H(20) 0.95
C(16) H(21) 0.95 C(16) H(22) 0.95
13

Table 5. Bond Angles(ffi)
atom atom atom angle atom atom atom angle
I(1) Co(1) P(1) 91.66(7) I(1) Co(1) P(2) 88.83(8)
I(1) Co(1) C(17) 116.4(3) I(1) Co(1) C(18) 114.5(3)
P(1) Co(1) P(2) 177.1(1) P(1) Co(1) C(17) 89.3(3)
P(1) Co(1) C(18) 90.8(3) P(2) Co(1) C(17) 87.9(3)
P(2) Co(1) C(18) 91.6(3) C(17) Co(1) C(18) 129.0(5)
Co(1) P(1) C(1) 117.0(3) Co(1) P(1) C(7) 114.2(3)
Co(1) P(1) C(8) 113.2(3) C(1) P(1) C(7) 104.2(4)
C(1) P(1) C(8) 103.8(5) C(7) P(1) C(8) 102.8(5)
Co(1) P(2) C(9) 113.2(3) Co(1) P(2) C(15) 114.8(4)
Co(1) P(2) C(16) 114.4(4) C(9) P(2) C(15) 104.3(4)
C(9) P(2) C(16) 104.0(5) C(15) P(2) C(16) 105.0(6)
P(1) C(1) C(2) 120.9(8) P(1) C(1) C(6) 121.2(8)
C(2) C(1) C(6) 117.9(9) C(1) C(2) C(3) 118(1)
C(2) C(3) C(4) 120(1) C(3) C(4) C(5) 120(1)
C(4) C(5) C(6) 121(1) C(1) C(6) C(5) 122(1)
P(2) C(9) C(10) 123.2(7) P(2) C(9) C(14) 120.4(7)
C(10) C(9) C(14) 116.4(8) C(9) C(10) C(11) 122.8(9)
C(10) C(11) C(12) 118(1) C(11) C(12) C(13) 121(1)
C(12) C(13) C(14) 119.9(10) C(9) C(14) C(13) 120.8(9)
Co(1) C(17) O(1) 176.0(9) Co(1) C(18) O(2) 175.7(10)
14

Table 6. Bond Angles(ffi)
atom atom atom angle atom atom atom angle
C(1) C(2) H(1) 120.9 C(3) C(2) H(1) 120.8

C(2) C(3) H(2) 120.2 C(4) C(3) H(2) 119.7
C(3) C(4) H(3) 119.6 C(5) C(4) H(3) 120.4
C(4) C(5) H(4) 119.2 C(6) C(5) H(4) 119.5
C(1) C(6) H(5) 118.9 C(5) C(6) H(5) 118.8
P(1) C(7) H(6) 109.6 P(1) C(7) H(7) 109.5
P(1) C(7) H(8) 109.5 H(6) C(7) H(7) 109.4
H(6) C(7) H(8) 109.4 H(7) C(7) H(8) 109.3
P(1) C(8) H(9) 109.8 P(1) C(8) H(10) 109.6
P(1) C(8) H(11) 109.5 H(9) C(8) H(10) 109.5
H(9) C(8) H(11) 109.4 H(10) C(8) H(11) 109.1
C(9) C(10) H(12) 118.7 C(11) C(10) H(12) 118.6
C(10) C(11) H(13) 120.7 C(12) C(11) H(13) 120.5
C(11) C(12) H(14) 119.6 C(13) C(12) H(14) 119.1
C(12) C(13) H(15) 120.2 C(14) C(13) H(15) 119.9
C(9) C(14) H(16) 119.6 C(13) C(14) H(16) 119.6
P(2) C(15) H(17) 109.5 P(2) C(15) H(18) 109.5
P(2) C(15) H(19) 109.6 H(17) C(15) H(18) 109.3
H(17) C(15) H(19) 109.4 H(18) C(15) H(19) 109.4
P(2) C(16) H(20) 109.7 P(2) C(16) H(21) 109.9
P(2) C(16) H(22) 109.6 H(20) C(16) H(21) 109.4
H(20) C(16) H(22) 109.0 H(21) C(16) H(22) 109.3
15

Table 7. Torsion Angles(ffi)
atom atom atom atom angle atom atom atom atom angle
I(1) Co(1) P(1) C(1) -63.1(4) I(1) Co(1) P(1) C(7) 59.0(4)
I(1) Co(1) P(1) C(8) 176.3(4) I(1) Co(1) P(2) C(9) -179.1(3)
I(1) Co(1) P(2) C(15) 61.4(4) I(1) Co(1) P(2) C(16) -60.2(4)
I(1) Co(1) C(17) O(1) 164(12) I(1) Co(1) C(18) O(2) 170(11)
Co(1) P(1) C(1) C(2) -93.7(8) Co(1) P(1) C(1) C(6) 84.5(8)
Co(1) P(2) C(9) C(10) 98.6(8) Co(1) P(2) C(9) C(14) -80.2(8)
P(1) Co(1) P(2) C(9) -79(2) P(1) Co(1) P(2) C(15) 160(2)
P(1) Co(1) P(2) C(16) 39(2) P(1) Co(1) C(17) O(1) -103(12)
P(1) Co(1) C(18) O(2) 78(11) P(1) C(1) C(2) C(3) 179.8(7)
P(1) C(1) C(6) C(5) 179.8(9) P(2) Co(1) P(1) C(1) -162(2)
P(2) Co(1) P(1) C(7) -40(2) P(2) Co(1) P(1) C(8) 76(2)
P(2) Co(1) C(17) O(1) 77(12) P(2) Co(1) C(18) O(2) -99(11)
P(2) C(9) C(10) C(11) -178.1(8) P(2) C(9) C(14) C(13) 177.6(7)
O(1) C(17) Co(1) C(18) -13(12) O(2) C(18) Co(1) C(17) -11(11)
C(1) P(1) Co(1) C(17) -179.5(5) C(1) P(1) Co(1) C(18) 51.5(5)
C(1) C(2) C(3) C(4) -1(1) C(1) C(6) C(5) C(4) 1(1)
C(2) C(1) P(1) C(7) 139.2(8) C(2) C(1) P(1) C(8) 31.8(9)
C(2) C(1) C(6) C(5) -1(1) C(2) C(3) C(4) C(5) 1(1)
C(3) C(2) C(1) C(6) 1(1) C(3) C(4) C(5) C(6) -1(2)
C(6) C(1) P(1) C(7) -42.7(9) C(6) C(1) P(1) C(8) -150.0(8)
C(7) P(1) Co(1) C(17) -57.4(5) C(7) P(1) Co(1) C(18) 173.6(5)
C(8) P(1) Co(1) C(17) 59.9(5) C(8) P(1) Co(1) C(18) -69.2(5)
C(9) P(2) Co(1) C(17) -62.6(5) C(9) P(2) Co(1) C(18) 66.4(5)
C(9) C(10) C(11) C(12) 0(1) C(9) C(14) C(13) C(12) 0(1)
16

Table 7. Torsion Angles(ffi) (continued)
atom atom atom atom angle atom atom atom atom angle
C(10) C(9) P(2) C(15) -135.9(9) C(10) C(9) P(2) C(16) -26.1(9)
C(10) C(9) C(14) C(13) -1(1) C(10) C(11) C(12) C(13) -1(1)
C(11) C(10) C(9) C(14) 0(1) C(11) C(12) C(13) C(14) 1(1)
C(14) C(9) P(2) C(15) 45.2(9) C(14) C(9) P(2) C(16) 155.0(8)
C(15) P(2) Co(1) C(17) 177.9(5) C(15) P(2) Co(1) C(18) -53.1(5)
C(16) P(2) Co(1) C(17) 56.3(5) C(16) P(2) Co(1) C(18) -174.7(5)
17

Table 8. non –bonded Contacts out to 3.30 Å

Atom atom distance ADC atom atom distance ADC

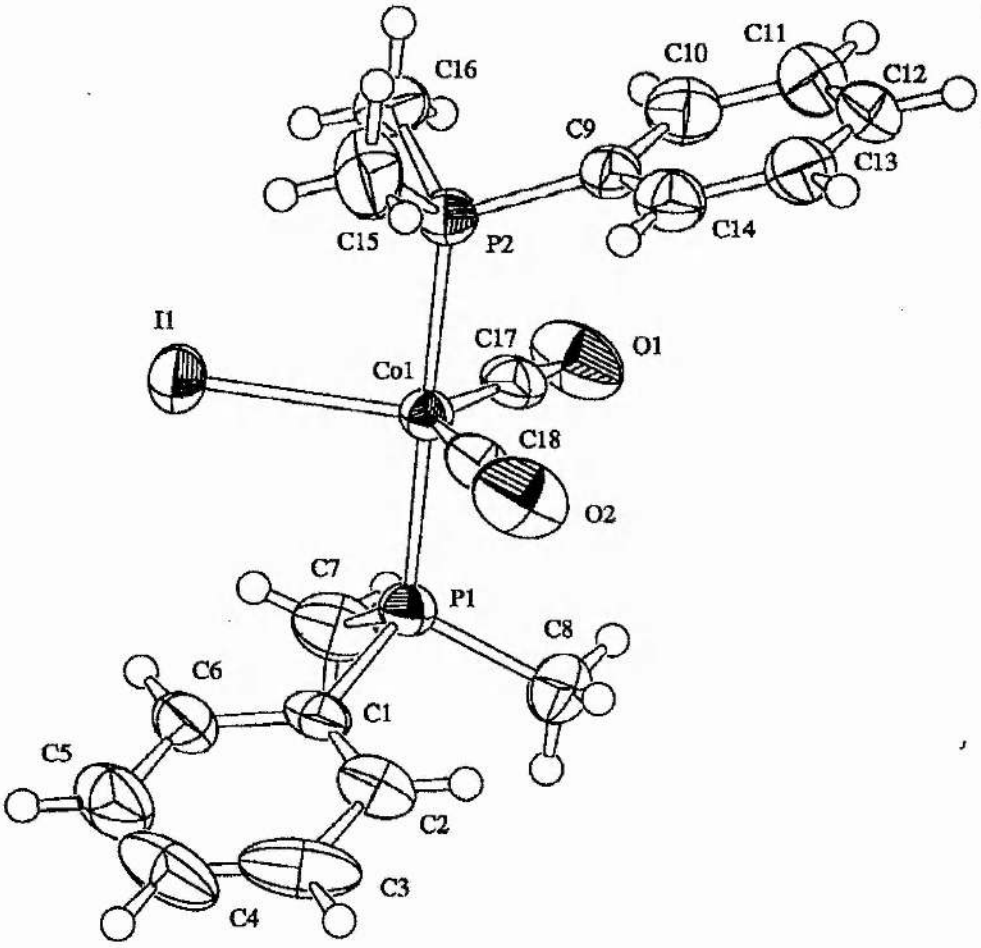
C16
C10
C11
C12
C9
C13
C15
P2
C14
I1
C17
O1
Co1
C18
O2
C7
P1
C8
C6
C1
C5
C2
C3
C4

X-ray Structure Report
Mon Aug 31 1998
acm189c

EXPERIMENTAL DETAILS

Crystal Data
Empirical Formula C 11 H 15 CoOI 2
Formula Weight 475.98
Crystal Color, Habit broun, plate
Crystal Dimensions 0.40 X 0.30 X 0.05 mm
Crystal System monoclinic
Lattice Type Primitive
No. of Reflections Used for Unit
Cell Determination (2` range) 25 (24.4 - 25.0 ffi)
Omega Scan Peak Width
at Half-height 0.40 ffi
Lattice Parameters a = 7.150(4) š A
b = 12.707(3) š A
c = 8.607(4) š A
fi = 112.77(4) ffi
V = 721.0(6) š A 3
Space Group P2 1 /m (#11)
Z value 2
D calc 2.192 g/cm 3
F 000 444.00
¯(MoKff) 54.04 cm
Radiation MoKff (– = 0.71069 A)
graphite monochromated
Attenuator Zr foil (factor = 8.53)
Take-o
Angle 6.0 ffi
Detector Aperture 9.0 mm horizontal
13.0 mm vertical
Crystal to Detector Distance 235 mm
Temperature 220.0 ffi C
Scan Type !-2`
Scan Rate 16.0 ffi /min (in !) (up to 4 scans)
Scan Width (1.68 + 0.35 tan `) ffi
2` max 50.0 ffi
No. of Reections Measured Total: 1455
Unique: 1345 (R int = 0.016)
Corrections Lorentz-polarization
Absorption
(trans. factors: 0.5018 - 1.0000)

Structure Solution and Renement
Structure Solution Direct Methods (SIR92)
Renement Full-matrix least-squares
Function Minimized w (jFoj 2
Least Squares Weights 1
oe 2 (Fo) = 4Fo 2
oe 2 (Fo 2)
p-factor 0.0380
Anomalous Dispersion All non-hydrogen atoms
No. Observations (I?3.00oe(I)) 1082
No. Variables 78
Reection/Parameter Ratio 13.87
Residuals: R; Rw 0.025 ; 0.034
6

Goodness of Fit Indicator 1.23
Max Shift/Error in Final Cycle 0.01
Maximum peak in Final Diff. Map 0.50 e 3
Minimum peak in Final Diff. Map -0.40 e

Table 1. Atomic coordinates and B iso /B eq
atom x y z B eq
I(1) 0.73724(6) 0.2500 0.99760(6) 4.09(1)
I(2) 0.8088(1) 0.12253(8) 1.4109(1) 4.06(2)
Co(1) 0.5582(1) 0.2500 1.20691(9) 2.35(2)
O(1) 0.821(2) 0.080(1) 1.402(2) 9.6(5)
C(1) 0.727(2) 0.1437(8) 1.324(2) 3.9(2)

C(2) 0.3294(9) 0.2500 1.2972(8) 3.2(1)
C(3) 0.3059(6) 0.1599(4) 1.1942(6) 3.24(9)
C(4) 0.2819(6) 0.1937(4) 1.0321(5) 3.25(9)
C(5) 0.354(1) 0.2500 1.4782(10) 6.0(2)
C(6) 0.2928(8) 0.0484(4) 1.2469(9) 6.4(2)
C(7) 0.2387(9) 0.1234(6) 0.8822(8) 6.6(2)
H(1) 0.2393 0.2180 1.4879 7.2120
H(2) 0.4728 0.2116 1.5433 7.2120
H(3) 0.3666 0.3204 1.5181 7.2120
H(4) 0.1804 0.0416 1.2791 7.6506
H(5) 0.2754 0.0025 1.1552 7.6506
H(6) 0.4140 0.0307 1.3393 7.6506
H(7) 0.1141 0.0876 0.8587 7.9132
H(8) 0.2295 0.1646 0.7874 7.9132
H(9) 0.3451 0.0735 0.9057 7.9132
B eq = 8
3 ß 2 (U 11 (aa 3) 2 + U 22 (bb 3) 2 + U 33 (cc 3) 2 + 2U 12 aa 3 bb 3 cos fl + 2U 13 aa 3 cc 3 cos fi + 2U 23 bb 3 cc 3 cos ff)
8

Table 2. Anisotropic Displacement Parameters
atom U 11 U 22 U 33 U 12 U 13 U 23
I(1) 0.0371(3) 0.0762(4) 0.0507(3) 0.0000 0.0264(2) 0.0000
I(2) 0.0356(3) 0.0593(5) 0.0517(5) 0.0082(3) 0.0086(3) 0.0205(4)
Co(1) 0.0226(4) 0.0364(4) 0.0294(4) 0.0000 0.0091(3) 0.0000
C(2) 0.029(3) 0.064(4) 0.032(3) 0.0000 0.013(3) 0.0000
C(3) 0.023(2) 0.044(2) 0.056(3) -0.005(2) 0.016(2) 0.004(2)
C(4) 0.026(2) 0.061(3) 0.036(2) -0.009(2) 0.012(2) -0.013(2)
C(5) 0.059(5) 0.138(8) 0.040(4) 0.0000 0.029(4) 0.0000
C(6) 0.055(3) 0.058(3) 0.129(6) -0.013(3) 0.035(3) 0.023(4)
C(7) 0.062(3) 0.119(6) 0.068(4) -0.036(4) 0.024(3) -0.057(4)
The general temperature factor expression:
exp(2 (a 32 U 11 h 2 + b 32 U 22 k 2 + c 32 U 33 l 2 + 2a 3 b 3 U 12 hk + 2a 3 c 3 U 13 hl + 2b 3 c 3 U 23 kl))
9

Table 3. Bond Lengths(§ A)
atom atom distance atom atom distance
I(1) Co(1) 2.583(1) I(2) Co(1) 2.546(1)
I(2) O(1) 0.56(2) I(2) C(1) 0.80(1)
Co(1) C(1) 1.83(1) Co(1) C(1) 1.83(1)
Co(1) C(2) 2.064(6) Co(1) C(3) 2.103(4)
Co(1) C(3) 2.103(4) Co(1) C(4) 2.092(4)
Co(1) C(4) 2.092(4) O(1) C(1) 1.10(2)
C(2) C(3) 1.417(6) C(2) C(3) 1.417(6)
C(2) C(5) 1.499(9) C(3) C(4) 1.406(6)
C(3) C(6) 1.503(7) C(4) C(4) 1.431(10)
C(4) C(7) 1.500(6)
10

Table 4. Bond Lengths(§ A)
atom atom distance atom atom distance
C(5) H(1) 0.95 C(5) H(1) 0.95
C(5) H(2) 0.95 C(5) H(2) 0.95
C(5) H(3) 0.95 C(5) H(3) 0.95
C(6) H(4) 0.95 C(6) H(5) 0.95
C(6) H(6) 0.95 C(7) H(7) 0.95
C(7) H(8) 0.95 C(7) H(9) 0.95
11

Table 5. Bond Angles(ffi)
atom atom atom angle atom atom atom angle
Co(1) I(2) O(1) 128(1) Co(1) I(2) C(1) 22.2(7)
O(1) I(2) C(1) 107(1) I(1) Co(1) I(2) 94.26(4)
I(1) Co(1) I(2) 94.26(4) I(1) Co(1) C(1) 89.0(3)
I(1) Co(1) C(1) 89.0(3) I(1) Co(1) C(2) 160.3(2)
I(1) Co(1) C(3) 127.6(1) I(1) Co(1) C(3) 127.6(1)
I(1) Co(1) C(4) 94.8(1) I(1) Co(1) C(4) 94.8(1)
I(2) Co(1) I(2) 79.02(5) I(2) Co(1) C(1) 9.5(3)
I(2) Co(1) C(1) 87.2(3) I(2) Co(1) C(2) 100.9(1)
I(2) Co(1) C(3) 92.9(1) I(2) Co(1) C(3) 138.0(1)
I(2) Co(1) C(4) 119.7(1) I(2) Co(1) C(4) 158.5(1)
I(2) Co(1) C(1) 87.2(3) I(2) Co(1) C(1) 9.5(3)

I(2) Co(1) C(2) 100.9(1) I(2) Co(1) C(3) 138.0(1)
I(2) Co(1) C(3) 92.9(1) I(2) Co(1) C(4) 158.5(1)
I(2) Co(1) C(4) 119.7(1) C(1) Co(1) C(1) 95.0(6)
C(1) Co(1) C(2) 104.1(3) C(1) Co(1) C(3) 89.8(3)
C(1) Co(1) C(3) 143.1(3) C(1) Co(1) C(4) 112.4(4)
C(1) Co(1) C(4) 152.3(3) C(1) Co(1) C(2) 104.1(3)
C(1) Co(1) C(3) 143.1(3) C(1) Co(1) C(3) 89.8(3)
C(1) Co(1) C(4) 152.3(3) C(1) Co(1) C(4) 112.4(4)
C(2) Co(1) C(3) 39.8(2) C(2) Co(1) C(3) 39.8(2)
C(2) Co(1) C(4) 66.8(2) C(2) Co(1) C(4) 66.8(2)
C(3) Co(1) C(3) 66.0(2) C(3) Co(1) C(4) 39.1(2)
C(3) Co(1) C(4) 66.2(2) C(3) Co(1) C(4) 66.2(2)
C(3) Co(1) C(4) 39.1(2) C(4) Co(1) C(4) 40.0(3)
12

Table 5. Bond Angles(ffi) (continued)
atom atom atom angle atom atom atom angle
I(2) O(1) C(1) 43(1) I(2) C(1) Co(1) 148.4(10)
I(2) C(1) O(1) 29.2(9) Co(1) C(1) O(1) 174(1)
Co(1) C(2) C(3) 71.6(3) Co(1) C(2) C(3) 71.6(3)
Co(1) C(2) C(5) 126.8(5) C(3) C(2) C(3) 107.7(5)
C(3) C(2) C(5) 126.0(3) C(3) C(2) C(5) 126.0(3)
Co(1) C(3) C(2) 68.6(3) Co(1) C(3) C(4) 70.0(2)
Co(1) C(3) C(6) 130.6(3) C(2) C(3) C(4) 108.3(4)
C(2) C(3) C(6) 125.4(5) C(4) C(3) C(6) 126.2(5)
Co(1) C(4) C(3) 70.8(2) Co(1) C(4) C(4) 70.0(1)
Co(1) C(4) C(7) 130.2(3) C(3) C(4) C(4) 107.8(3)
C(3) C(4) C(7) 125.3(5) C(4) C(4) C(7) 126.6(3)
13

Table 6. Bond Angles(ffi)
atom atom atom angle atom atom atom angle
C(2) C(5) H(1) 109.4 C(2) C(5) H(1) 109.4
C(2) C(5) H(2) 109.4 C(2) C(5) H(2) 109.4
C(2) C(5) H(3) 109.4 C(2) C(5) H(3) 109.4
H(1) C(5) H(1) 50.7 H(1) C(5) H(2) 109.5
H(1) C(5) H(2) 140.7 H(1) C(5) H(3) 109.5
H(1) C(5) H(3) 61.8 H(1) C(5) H(2) 140.7
H(1) C(5) H(2) 109.5 H(1) C(5) H(3) 61.8
H(1) C(5) H(3) 109.5 H(2) C(5) H(2) 61.8
H(2) C(5) H(3) 109.5 H(2) C(5) H(3) 50.7
H(2) C(5) H(3) 50.7 H(2) C(5) H(3) 109.5
H(3) C(5) H(3) 140.7 C(3) C(6) H(4) 109.4
C(3) C(6) H(5) 109.4 C(3) C(6) H(6) 109.4
H(4) C(6) H(5) 109.5 H(4) C(6) H(6) 109.6
H(5) C(6) H(6) 109.5 C(4) C(7) H(7) 109.4
C(4) C(7) H(8) 109.4 C(4) C(7) H(9) 109.4
H(7) C(7) H(8) 109.5 H(7) C(7) H(9) 109.5
H(8) C(7) H(9) 109.5
14

Table 7. Torsion Angles(ffi)
atom atom atom atom angle atom atom atom atom angle
I(1) Co(1) I(2) O(1) -67(2) I(1) Co(1) I(2) C(1) -56(1)
I(1) Co(1) I(2) O(1) 67(2) I(1) Co(1) I(2) C(1) 56(1)
I(1) Co(1) C(1) I(2) 123(1) I(1) Co(1) C(1) O(1) -177(13)
I(1) Co(1) C(1) I(2) -123(1) I(1) Co(1) C(1) O(1) 177(13)
I(1) Co(1) C(2) C(3) 58.3(2) I(1) Co(1) C(2) C(3) -58.3(2)
I(1) Co(1) C(2) C(5) 180.0000(1) I(1) Co(1) C(3) C(2) -158.7(2)
I(1) Co(1) C(3) C(4) -38.7(3) I(1) Co(1) C(3) C(6) 82.3(6)
I(1) Co(1) C(3) C(2) 158.7(2) I(1) Co(1) C(3) C(4) 38.7(3)
I(1) Co(1) C(3) C(6) -82.3(6) I(1) Co(1) C(4) C(3) 150.2(2)
I(1) Co(1) C(4) C(4) -91.74(4) I(1) Co(1) C(4) C(7) 29.8(5)
I(1) Co(1) C(4) C(3) -150.2(2) I(1) Co(1) C(4) C(4) 91.74(4)
I(1) Co(1) C(4) C(7) -29.8(5) I(2) Co(1) I(2) O(1) 161(2)
I(2) Co(1) I(2) C(1) 150(1) I(2) Co(1) C(1) O(1) 58(12)
I(2) Co(1) C(1) O(1) -87(13) I(2) Co(1) C(2) C(3) -81.3(3)
I(2) Co(1) C(2) C(3) 162.0(2) I(2) Co(1) C(2) C(5) 40.39(3)
I(2) Co(1) C(3) C(2) 103.6(3) I(2) Co(1) C(3) C(4) -136.3(2)
I(2) Co(1) C(3) C(6) -15.3(5) I(2) Co(1) C(3) C(2) -26.9(3)
I(2) Co(1) C(3) C(4) -146.9(2) I(2) Co(1) C(3) C(6) 92.1(5)
I(2) Co(1) C(4) C(3) 52.5(3) I(2) Co(1) C(4) C(4) 170.6(1)

I(2) Co(1) C(4) C(7) -67.9(5) I(2) Co(1) C(4) C(3) 95.3(4)
I(2) Co(1) C(4) C(4) -22.7(3) I(2) Co(1) C(4) C(7) -144.3(4)
I(2) O(1) C(1) Co(1) -66(13) I(2) C(1) Co(1) C(1) 34(2)
I(2) C(1) Co(1) C(2) -71(1) I(2) C(1) Co(1) C(3) -108(1)
I(2) C(1) Co(1) C(3) -61(2) I(2) C(1) Co(1) C(4) -141(1)
15

Table 7. Torsion Angles(ffi) (continued)
atom atom atom atom angle atom atom atom atom angle
I(2) C(1) Co(1) C(4) -137(1) Co(1) I(2) O(1) C(1) 4(1)
Co(1) I(2) C(1) O(1) -170(2) Co(1) I(2) O(1) C(1) -4(1)
Co(1) I(2) C(1) O(1) 170(2) Co(1) C(1) I(2) O(1) 170(2)
Co(1) C(1) I(2) O(1) -170(2) Co(1) C(2) C(3) C(4) -59.0(3)
Co(1) C(2) C(3) C(6) 125.4(4) Co(1) C(2) C(3) C(4) 59.0(3)
Co(1) C(2) C(3) C(6) -125.4(4) Co(1) C(3) C(2) C(3) 62.9(4)
Co(1) C(3) C(2) C(5) -122.6(6) Co(1) C(3) C(4) C(4) -60.6(1)
Co(1) C(3) C(4) C(7) 126.2(5) Co(1) C(3) C(2) C(3) -62.9(4)
Co(1) C(3) C(2) C(5) 122.6(6) Co(1) C(3) C(4) C(4) 60.6(1)
Co(1) C(3) C(4) C(7) -126.2(5) Co(1) C(4) C(3) C(2) 58.1(3)
Co(1) C(4) C(3) C(6) -126.3(4) Co(1) C(4) C(4) C(3) -61.1(2)
Co(1) C(4) C(4) C(7) 125.8(4) Co(1) C(4) C(3) C(2) -58.1(3)
Co(1) C(4) C(3) C(6) 126.3(4) Co(1) C(4) C(4) C(3) 61.1(2)
Co(1) C(4) C(4) C(7) -125.8(4) O(1) I(2) Co(1) C(1) -11(3)
O(1) I(2) Co(1) C(1) -156(2) O(1) I(2) Co(1) C(2) 99(2)
O(1) I(2) Co(1) C(3) 60(2) O(1) I(2) Co(1) C(3) 116(2)
O(1) I(2) Co(1) C(4) 30(2) O(1) I(2) Co(1) C(4) 46(2)
O(1) C(1) Co(1) C(1) 93(13) O(1) C(1) Co(1) C(2) -12(13)
O(1) C(1) Co(1) C(3) -50(13) O(1) C(1) Co(1) C(3) -3(13)
O(1) C(1) Co(1) C(4) -83(13) O(1) C(1) Co(1) C(4) -79(13)
C(1) I(2) Co(1) C(2) 110(1) C(1) I(2) Co(1) C(3) 71(1)
C(1) I(2) Co(1) C(3) 127(1) C(1) I(2) Co(1) C(4) 41(1)
C(1) I(2) Co(1) C(4) 57(1) C(1) Co(1) C(2) C(3) -72.2(4)
C(1) Co(1) C(2) C(3) 171.2(4) C(1) Co(1) C(2) C(5) 49.5(3)
16

Table 7. Torsion Angles(ffi) (continued)
atom atom atom atom angle atom atom atom atom angle
C(1) Co(1) C(3) C(2) 112.6(4) C(1) Co(1) C(3) C(4) -127.4(4)
C(1) Co(1) C(3) C(6) -6.4(6) C(1) Co(1) C(3) C(2) -14.4(6)
C(1) Co(1) C(3) C(4) -134.4(6) C(1) Co(1) C(3) C(6) 104.6(7)
C(1) Co(1) C(4) C(3) 59.3(4) C(1) Co(1) C(4) C(4) 177.3(4)
C(1) Co(1) C(4) C(7) -61.2(6) C(1) Co(1) C(4) C(3) 112.7(8)
C(1) Co(1) C(4) C(4) -5.3(7) C(1) Co(1) C(4) C(7) -126.8(9)
C(2) Co(1) C(3) C(4) 120.0(4) C(2) Co(1) C(3) C(6) -119.0(6)
C(2) Co(1) C(3) C(4) -120.0(4) C(2) Co(1) C(3) C(6) 119.0(6)
C(2) Co(1) C(4) C(3) -37.0(2) C(2) Co(1) C(4) C(4) 81.0(1)
C(2) Co(1) C(4) C(7) -157.5(6) C(2) Co(1) C(4) C(3) 37.0(2)
C(2) Co(1) C(4) C(4) -81.0(1) C(2) Co(1) C(4) C(7) 157.5(6)
C(2) C(3) Co(1) C(3) -38.7(3) C(2) C(3) Co(1) C(4) -120.0(4)
C(2) C(3) Co(1) C(4) -81.7(3) C(2) C(3) C(4) C(4) -2.4(4)
C(2) C(3) C(4) C(7) -175.7(5) C(2) C(3) Co(1) C(3) 38.7(3)
C(2) C(3) Co(1) C(4) 81.7(3) C(2) C(3) Co(1) C(4) 120.0(4)
C(2) C(3) C(4) C(4) 2.4(4) C(2) C(3) C(4) C(7) 175.7(5)
C(3) Co(1) C(2) C(5) 121.7(2) C(3) Co(1) C(3) C(4) -81.3(3)
C(3) Co(1) C(3) C(6) 157.7(5) C(3) Co(1) C(4) C(4) 118.1(2)
C(3) Co(1) C(4) C(7) -120.4(6) C(3) Co(1) C(4) C(4) -37.5(2)
C(3) Co(1) C(4) C(7) -159.0(6) C(3) C(2) Co(1) C(4) 36.5(3)
C(3) C(2) Co(1) C(4) 80.2(3) C(3) C(2) C(3) C(4) -3.9(6)
C(3) C(2) C(3) C(6) 171.7(3) C(3) C(4) Co(1) C(4) -118.1(2)
C(3) C(4) C(4) C(3) 0.0 C(3) C(4) C(4) C(7) -173.1(5)
C(4) Co(1) C(2) C(5) 158.2(1) C(4) Co(1) C(3) C(6) 121.0(6)
17

Table 7. Torsion Angles(ffi) (continued)
atom atom atom atom angle atom atom atom atom angle
C(4) Co(1) C(3) C(6) -159.3(6) C(4) Co(1) C(4) C(7) -121.5(5)
C(4) C(3) C(2) C(5) 178.5(6) C(4) C(4) C(3) C(6) -173.2(4)
C(5) C(2) C(3) C(6) 2.8(9) C(5) C(2) C(3) C(6) -2.8(9)
C(6) C(3) C(4) C(7) 0.0(7) C(7) C(4) C(4) C(7) 0.0
18

Table 8. Non-bonded Contacts out to 3.20 § A

atom atom distance ADC atom atom distance ADC
O(1) O(1) 3.19(3) 75803
19

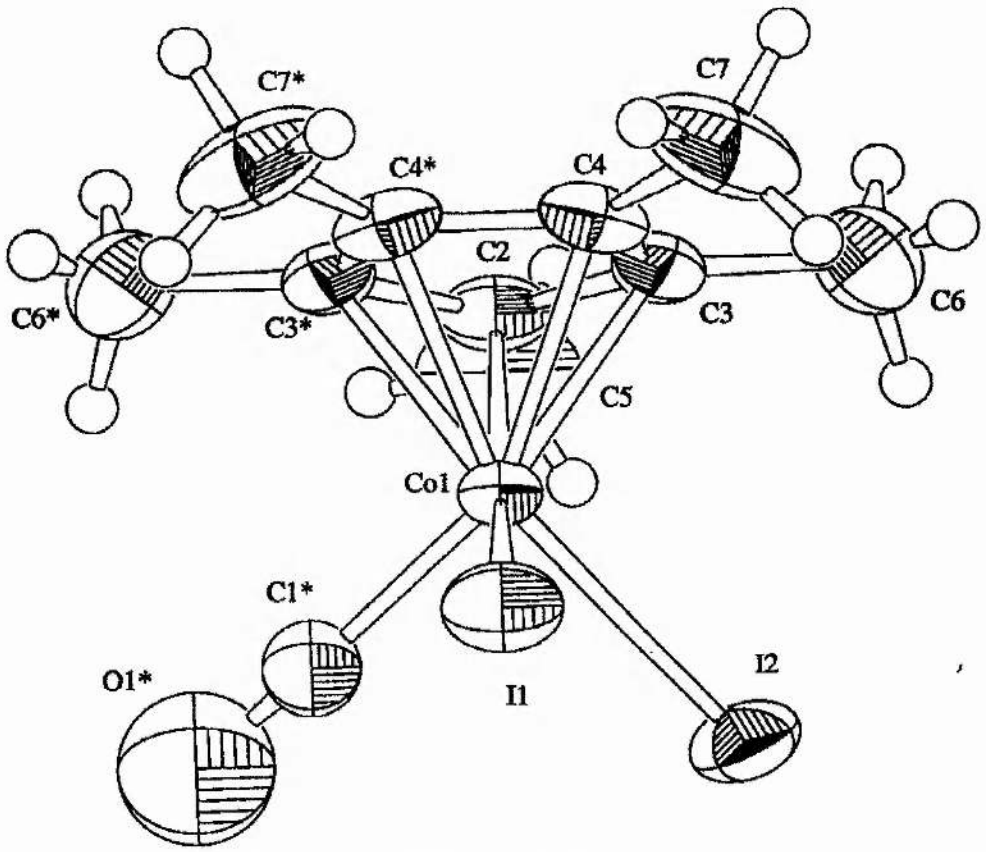

EXPERIMENTAL DETAILS

Crystal Data
Empirical Formula C 14 H 30 O 2 CoIP 2
Formula Weight 478.18
Crystal Color, Habit colorless, block
Crystal Dimensions 0.30 X 0.25 X 0.20 mm
Crystal System orthorhombic
Lattice Type Primitive
No. of Reflections Used for Unit
Cell Determination (2` range) 20 (6.6 - 12.1 ffi)
Omega Scan Peak Width
at Half-height 0.29 ffi
Lattice Parameters a = 15.95(1) š A
b = 19.482(9) š A
c = 13.312(10) š A
V = 4136(4) š A 3
Space Group P2 1 2 1 2 1 (#19)
Z value 8
D calc 1.536 g/cm 3
F 000 1920.00
¯(MoKff) 24.58 cm
graphite monochromated
Attenuator Zr foil (factor = 8.53)
Take-off Angle 6.0 ffi
Detector Aperture 9.0 mm horizontal
13.0 mm vertical
Crystal to Detector Distance 235 mm
Temperature 230.0 ffi C
Scan Type !-2`
Scan Rate 16.0 ffi /min (in !) (up to 4 scans)
Scan Width (1.05 + 0.35 tan `) ffi
2` max 40.0 ffi
No. of Reflections Measured Total: 1917
Corrections Lorentz-polarization

Structure Solution and Refinement
Structure Solution Direct Methods (SIR92)
Refinement Full-matrix least-squares
Function Minimized 6w(jFoj 2
Least Squares Weights 1
oe 2 (Fo) = 4Fo 2
oe 2 (Fo 2)
p-factor 0.0050
Anomalous Dispersion All non-hydrogen atoms
No. Observations (I?3.00oe(I)) 1622
No. Variables 221
Reflection/Parameter Ratio 7.34
Residuals: R; Rw 0.040 ; 0.037
Goodness of Fit Indicator 2.69
Max Shift/Error in Final Cycle 0.03
6

Maximum peak in Final Diff. Map 0.62 e 3
Minimum peak in Final Diff. Map -0.42 e

Table 1. Atomic coordinates and B iso /B eq
atom x y z B eq
I(1) 0.87349(10) 0.03780(7) 0.1154(1) 3.98(4)
I(2) 0.85752(10) 0.27715(7) -0.5085(1) 5.22(4)
Co(1) 0.7541(2) 0.1044(1) 0.0172(2) 2.74(7)
Co(2) 0.7596(2) 0.3755(1) -0.4366(2) 2.77(7)
P(1) 0.8286(4) 0.1996(3) 0.0285(4) 3.6(2)
P(2) 0.6790(3) 0.0081(3) 0.0087(4) 3.1(1)
P(3) 0.8628(4) 0.4517(3) -0.4404(4) 3.4(2)
P(4) 0.6551(4) 0.3007(3) -0.4339(4) 3.2(2)
O(1) 0.6270(9) 0.1685(6) 0.1402(10) 5.3(4)
O(2) 0.756(1) 0.1139(8) -0.1985(9) 5.8(5)
O(3) 0.759(1) 0.3891(7) -0.2189(9) 6.0(5)

O(4) 0.6613(7) 0.4640(6) -0.5565(10) 3.9(4)
C(1) 0.677(1) 0.141(1) 0.094(2) 3.9(6)
C(2) 0.759(1) 0.108(1) -0.111(2) 4.0(5)
C(3) 0.835(1) 0.228(1) 0.156(2) 4.9(5)
C(4) 0.896(2) 0.290(1) 0.180(2) 7.7(7)
C(5) 0.938(1) 0.197(1) -0.009(2) 5.0(6)
C(6) 0.955(2) 0.170(1) -0.111(2) 7.7(7)
C(7) 0.784(1) 0.268(1) -0.042(2) 4.8(6)
C(8) 0.693(1) 0.285(1) -0.032(2) 6.8(7)
C(9) 0.633(1) -0.0139(9) 0.130(1) 4.3(5)
C(10) 0.575(1) -0.074(1) 0.134(2) 5.5(6)
C(11) 0.729(1) -0.0708(9) -0.027(1) 3.7(5)
C(12) 0.782(1) -0.064(1) -0.125(2) 6.1(6)
8

Table 1. Atomic coordinates and B iso /B eq (continued)
atom x y z B eq
C(13) 0.592(1) 0.0144(10) -0.076(1) 3.7(5)
C(14) 0.530(2) 0.070(1) -0.058(2) 7.1(7)
C(15) 0.760(1) 0.380(1) -0.300(2) 3.9(5)
C(16) 0.703(1) 0.4277(10) -0.515(2) 3.9(5)
C(17) 0.965(1) 0.424(1) -0.407(2) 6.2(6)
C(18) 0.972(2) 0.388(1) -0.304(2) 7.3(7)
C(19) 0.846(1) 0.525(1) -0.354(2) 5.8(6)
C(20) 0.767(2) 0.560(1) -0.367(2) 8.1(7)
C(21) 0.878(2) 0.496(1) -0.556(2) 5.4(6)
C(22) 0.899(1) 0.451(1) -0.648(1) 4.9(6)
C(23) 0.668(1) 0.2320(9) -0.343(1) 3.6(5)
C(24) 0.600(1) 0.177(1) -0.340(2) 6.1(6)
C(25) 0.554(1) 0.3390(9) -0.399(1) 3.6(5)
C(26) 0.549(1) 0.372(1) -0.295(2) 6.1(6)
C(27) 0.631(2) 0.251(1) -0.548(1) 5.3(6)
C(28) 0.629(2) 0.298(1) -0.646(2) 8.0(7)
H(1) 0.7801 0.2416 0.1758 5.8597
H(2) 0.8527 0.1904 0.1953 5.8597
H(3) 0.9524 0.2781 0.1658 9.3133
H(4) 0.8812 0.3294 0.1401 9.3133
H(5) 0.8916 0.3028 0.2493 9.3133
H(6) 0.9598 0.2419 -0.0047 6.0463
H(7) 0.9668 0.1680 0.0378 6.0463
H(8) 0.9351 0.1242 -0.1166 9.3196
9

Table 1. Atomic coordinates and B iso /B eq (continued)
atom x y z B eq
H(9) 0.9272 0.1980 -0.1593 9.3196
H(10) 1.0137 0.1709 -0.1238 9.3196
H(11) 0.8147 0.3083 -0.0249 5.7385
H(12) 0.7936 0.2575 -0.1111 5.7385
H(13) 0.6812 0.2968 0.0363 8.2132
H(14) 0.6792 0.3224 -0.0741 8.2132
H(15) 0.6601 0.2461 -0.0499 8.2132
H(16) 0.6775 -0.0223 0.1758 5.2302
H(17) 0.6017 0.0250 0.1527 5.2302
H(18) 0.5549 -0.0805 0.2008 6.6694
H(19) 0.5293 -0.0674 0.0900 6.6694
H(20) 0.6049 -0.1146 0.1142 6.6694
H(21) 0.7659 -0.0845 0.0264 4.4238
H(22) 0.6877 -0.1050 -0.0361 4.4238
H(23) 0.8070 -0.1069 -0.1411 7.4441
H(24) 0.7461 -0.0505 -0.1790 7.4441
H(25) 0.8244 -0.0304 -0.1165 7.4441
H(26) 0.6136 0.0211 -0.1415 4.4881
H(27) 0.5621 -0.0278 -0.0733 4.4881
H(28) 0.5572 0.1134 -0.0606 8.4590
H(29) 0.4871 0.0684 -0.1074 8.4590
H(30) 0.5053 0.0643 0.0069 8.4590
H(31) 0.9838 0.3928 -0.4579 7.5661
H(32) 1.0009 0.4630 -0.4069 7.5661
10

Table 1. Atomic coordinates and B iso /B eq (continued)
atom x y z B eq
H(33) 0.9545 0.4181 -0.2521 8.7538
H(34) 0.9375 0.3479 -0.3031 8.7538
H(35) 1.0287 0.3744 -0.2919 8.7538
H(36) 0.8482 0.5088 -0.2868 6.9758
H(37) 0.8895 0.5577 -0.3643 6.9758
H(38) 0.7641 0.5989 -0.3239 9.8591
H(39) 0.7616 0.5751 -0.4351 9.8591
H(40) 0.7220 0.5297 -0.3519 9.8591
H(41) 0.8276 0.5206 -0.5707 6.4503
H(42) 0.9223 0.5280 -0.5469 6.4503
H(43) 0.8550 0.4185 -0.6583 5.9375
H(44) 0.9057 0.4783 -0.7055 5.9375
H(45) 0.9498 0.4263 -0.6349 5.9375
H(46) 0.7193 0.2096 -0.3567 4.3473
H(47) 0.6703 0.2524 -0.2779 4.3473
H(48) 0.5475 0.1979 -0.3249 7.3236
H(49) 0.5969 0.1548 -0.4028 7.3236
H(50) 0.6130 0.1445 -0.2889 7.3236
H(51) 0.5407 0.3733 -0.4477 4.3148
H(52) 0.5124 0.3038 -0.4019 4.3148
H(53) 0.5615 0.3391 -0.2447 7.3797
H(54) 0.5887 0.4088 -0.2907 7.3797
H(55) 0.4943 0.3901 -0.2838 7.3797
H(56) 0.6728 0.2168 -0.5566 6.3042
11

Table 1. Atomic coordinates and B iso /B eq (continued)
atom x y z B eq
H(57) 0.5778 0.2300 -0.5401 6.3042
H(58) 0.6818 0.3192 -0.6550 9.6087
H(59) 0.6166 0.2700 -0.7029 9.6087
H(60) 0.5867 0.3319 -0.6389 9.6087
B eq = 8
3 ß 2 (U 11 (aa 3) 2 + U 22 (bb 3) 2 + U 33 (cc 3) 2 + 2U 12 aa 3 bb 3 cos fl + 2U 13 aa 3 cc 3 cos fi + 2U 23 bb 3 cc 3 cos ff)
12

Table 2. Anisotropic Displacement Parameters
atom U 11 U 22 U 33 U 12 U 13 U 23
I(1) 0.044(1) 0.0606(10) 0.0459(8) 0.0019(10) -0.0090(9) 0.0041(9)
I(2) 0.046(1) 0.0505(9) 0.102(1) 0.0090(9) 0.021(1) -0.005(1)
Co(1) 0.039(2) 0.038(2) 0.028(2) -0.003(2) 0.001(2) -0.001(1)
Co(2) 0.031(2) 0.035(2) 0.039(2) 0.003(2) -0.001(2) 0.002(1)
P(1) 0.057(5) 0.045(4) 0.035(4) -0.002(3) 0.006(3) -0.002(3)
P(2) 0.043(4) 0.045(3) 0.030(3) -0.009(3) -0.005(3) 0.006(3)
P(3) 0.034(4) 0.048(4) 0.049(3) -0.003(4) 0.001(4) 0.005(3)
P(4) 0.035(5) 0.043(3) 0.046(4) 0.010(3) -0.008(3) -0.005(3)
O(1) 0.06(1) 0.062(10) 0.08(1) 0.00(1) 0.01(1) -0.030(9)
O(2) 0.10(1) 0.10(1) 0.023(9) 0.00(1) -0.007(10) 0.014(9)
O(3) 0.12(2) 0.09(1) 0.018(8) -0.05(1) 0.006(10) -0.008(9)
O(4) 0.022(10) 0.040(8) 0.09(1) 0.008(8) -0.014(8) 0.033(9)
The general temperature factor expression:
exp(2 (a 32 U 11 h 2 + b 32 U 22 k 2 + c 32 U 33 l 2 + 2a 3 b 3 U 12 hk + 2a 3 c 3 U 13 hl + 2b 3 c 3 U 23 kl))
13

Table 3. Bond Lengths(§ A)
atom atom distance atom atom distance
I(1) Co(1) 2.649(3) I(2) Co(2) 2.651(3)
Co(1) P(1) 2.208(6) Co(1) P(2) 2.229(6)
Co(1) C(1) 1.75(2) Co(1) C(2) 1.71(2)
Co(2) P(3) 2.217(6) Co(2) P(4) 2.214(6)
Co(2) C(15) 1.82(2) Co(2) C(16) 1.72(2)
P(1) C(3) 1.78(2) P(1) C(5) 1.81(2)
P(1) C(7) 1.78(2) P(2) C(9) 1.83(2)
P(2) C(11) 1.80(2) P(2) C(13) 1.79(2)
P(3) C(17) 1.78(2) P(3) C(19) 1.85(2)
P(3) C(21) 1.78(2) P(4) C(23) 1.82(2)
P(4) C(25) 1.84(2) P(4) C(27) 1.84(2)
O(1) C(1) 1.14(2) O(2) C(2) 1.17(2)
O(3) C(15) 1.09(2) O(4) C(16) 1.11(2)

C(3) C(4) 1.59(3) C(5) C(6) 1.49(3)
C(7) C(8) 1.50(3) C(9) C(10) 1.49(2)
C(11) C(12) 1.56(3) C(13) C(14) 1.48(3)
C(17) C(18) 1.55(3) C(19) C(20) 1.44(3)
C(21) C(22) 1.55(2) C(23) C(24) 1.51(3)
C(25) C(26) 1.54(3) C(27) C(28) 1.59(3)
14

Table 4. Bond Lengths(§ A)
atom atom distance atom atom distance
C(3) H(1) 0.95 C(3) H(2) 0.95
C(4) H(3) 0.95 C(4) H(4) 0.96
C(4) H(5) 0.95 C(5) H(6) 0.95
C(5) H(7) 0.95 C(6) H(8) 0.95
C(6) H(9) 0.95 C(6) H(10) 0.95
C(7) H(11) 0.95 C(7) H(12) 0.95
C(8) H(13) 0.95 C(8) H(14) 0.95
C(8) H(15) 0.95 C(9) H(16) 0.95
C(9) H(17) 0.95 C(10) H(18) 0.95
C(10) H(19) 0.95 C(10) H(20) 0.95
C(11) H(21) 0.95 C(11) H(22) 0.95
C(12) H(23) 0.95 C(12) H(24) 0.95
C(12) H(25) 0.95 C(13) H(26) 0.95
C(13) H(27) 0.95 C(14) H(28) 0.95
C(14) H(29) 0.95 C(14) H(30) 0.95
C(17) H(31) 0.95 C(17) H(32) 0.95
C(18) H(33) 0.96 C(18) H(34) 0.95
C(18) H(35) 0.95 C(19) H(36) 0.95
C(19) H(37) 0.95 C(20) H(38) 0.95
C(20) H(39) 0.95 C(20) H(40) 0.95
C(21) H(41) 0.95 C(21) H(42) 0.95
C(22) H(43) 0.95 C(22) H(44) 0.95
C(22) H(45) 0.95 C(23) H(46) 0.95
C(23) H(47) 0.95 C(24) H(48) 0.95
15

Table 4. Bond Lengths(§ A) (continued)
atom atom distance atom atom distance
C(24) H(49) 0.95 C(24) H(50) 0.95
C(25) H(51) 0.95 C(25) H(52) 0.95
C(26) H(53) 0.95 C(26) H(54) 0.95
C(26) H(55) 0.95 C(27) H(56) 0.95
C(27) H(57) 0.95 C(28) H(58) 0.95
C(28) H(59) 0.95 C(28) H(60) 0.95
16

Table 5. Bond Angles(ffi)
atom atom atom angle atom atom atom angle
I(1) Co(1) P(1) 89.5(2) I(1) Co(1) P(2) 89.9(2)
I(1) Co(1) C(1) 114.4(7) I(1) Co(1) C(2) 118.6(7)
P(1) Co(1) P(2) 179.0(3) P(1) Co(1) C(1) 89.7(7)
P(1) Co(1) C(2) 90.5(7) P(2) Co(1) C(1) 89.8(7)
P(2) Co(1) C(2) 90.5(7) C(1) Co(1) C(2) 127(1)
I(2) Co(2) P(3) 92.2(2) I(2) Co(2) P(4) 88.5(2)
I(2) Co(2) C(15) 113.1(7) I(2) Co(2) C(16) 121.2(7)
P(3) Co(2) P(4) 179.0(3) P(3) Co(2) C(15) 89.6(7)
P(3) Co(2) C(16) 88.8(7) P(4) Co(2) C(15) 90.8(7)
P(4) Co(2) C(16) 90.2(7) C(15) Co(2) C(16) 125(1)
Co(1) P(1) C(3) 110.9(7) Co(1) P(1) C(5) 118.3(7)
Co(1) P(1) C(7) 112.3(7) C(3) P(1) C(5) 102(1)
C(3) P(1) C(7) 106.9(10) C(5) P(1) C(7) 105(1)
Co(1) P(2) C(9) 111.6(7) Co(1) P(2) C(11) 119.6(7)
Co(1) P(2) C(13) 113.0(7) C(9) P(2) C(11) 102.2(9)
C(9) P(2) C(13) 105.0(9) C(11) P(2) C(13) 104.0(9)
Co(2) P(3) C(17) 118.2(8) Co(2) P(3) C(19) 113.3(8)
Co(2) P(3) C(21) 116.5(8) C(17) P(3) C(19) 102(1)
C(17) P(3) C(21) 103(1) C(19) P(3) C(21) 100.2(9)
Co(2) P(4) C(23) 114.3(7) Co(2) P(4) C(25) 113.5(6)
Co(2) P(4) C(27) 119.3(7) C(23) P(4) C(25) 103.2(9)
C(23) P(4) C(27) 100.9(9) C(25) P(4) C(27) 103.6(10)
Co(1) C(1) O(1) 175(1) Co(1) C(2) O(2) 173(2)
P(1) C(3) C(4) 117(1) P(1) C(5) C(6) 115(1)17

Table 5. Bond Angles(ffi) (continued)

atom atom atom angle atom atom atom angle
P(1) C(7) C(8) 119(1) P(2) C(9) C(10) 117(1)
P(2) C(11) C(12) 112(1) P(2) C(13) C(14) 117(1)
Co(2) C(15) O(3) 172(2) Co(2) C(16) O(4) 171(2)
P(3) C(17) C(18) 115(1) P(3) C(19) C(20) 114(1)
P(3) C(21) C(22) 115(1) P(4) C(23) C(24) 117(1)
P(4) C(25) C(26) 116(1) P(4) C(27) C(28) 112(1)

Table 6. Bond Angles(ffi)

atom atom atom angle atom atom atom angle
P(1) C(3) H(1) 107.7 P(1) C(3) H(2) 107.6
C(4) C(3) H(1) 107.2 C(4) C(3) H(2) 106.9
H(1) C(3) H(2) 109.3 C(3) C(4) H(3) 110.4
C(3) C(4) H(4) 110.0 C(3) C(4) H(5) 110.6
H(3) C(4) H(4) 108.5 H(3) C(4) H(5) 108.9
H(4) C(4) H(5) 108.5 P(1) C(5) H(6) 108.1
P(1) C(5) H(7) 107.8 C(6) C(5) H(6) 107.8
C(6) C(5) H(7) 107.5 H(6) C(5) H(7) 109.5
C(5) C(6) H(8) 109.8 C(5) C(6) H(9) 109.6
C(5) C(6) H(10) 109.8 H(8) C(6) H(9) 109.2
H(8) C(6) H(10) 109.2 H(9) C(6) H(10) 109.3
P(1) C(7) H(11) 106.9 P(1) C(7) H(12) 106.9
C(8) C(7) H(11) 106.7 C(8) C(7) H(12) 106.7
H(11) C(7) H(12) 109.5 C(7) C(8) H(13) 109.8
C(7) C(8) H(14) 109.8 C(7) C(8) H(15) 109.8
H(13) C(8) H(14) 109.2 H(13) C(8) H(15) 109.1
H(14) C(8) H(15) 109.2 P(2) C(9) H(16) 107.5
P(2) C(9) H(17) 107.3 C(10) C(9) H(16) 107.7
C(10) C(9) H(17) 107.4 H(16) C(9) H(17) 109.3
C(9) C(10) H(18) 109.8 C(9) C(10) H(19) 109.8
C(9) C(10) H(20) 109.6 H(18) C(10) H(19) 109.3
H(18) C(10) H(20) 109.1 H(19) C(10) H(20) 109.1
P(2) C(11) H(21) 108.7 P(2) C(11) H(22) 108.9
C(12) C(11) H(21) 108.4 C(12) C(11) H(22) 108.7

Table 6. Bond Angles(ffi) (continued)

atom atom atom angle atom atom atom angle
H(21) C(11) H(22) 109.3 C(11) C(12) H(23) 110.0
C(11) C(12) H(24) 109.7 C(11) C(12) H(25) 110.0
H(23) C(12) H(24) 109.0 H(23) C(12) H(25) 109.1
H(24) C(12) H(25) 109.0 P(2) C(13) H(26) 107.6
P(2) C(13) H(27) 107.7 C(14) C(13) H(26) 107.1
C(14) C(13) H(27) 107.3 H(26) C(13) H(27) 109.4
C(13) C(14) H(28) 110.1 C(13) C(14) H(29) 110.0
C(13) C(14) H(30) 109.9 H(28) C(14) H(29) 109.0
H(28) C(14) H(30) 109.0 H(29) C(14) H(30) 108.8
P(3) C(17) H(31) 107.9 P(3) C(17) H(32) 108.0
C(18) C(17) H(31) 108.1 C(18) C(17) H(32) 108.4
H(31) C(17) H(32) 109.1 C(17) C(18) H(33) 109.4
C(17) C(18) H(34) 109.7 C(17) C(18) H(35) 110.1
H(33) C(18) H(34) 108.8 H(33) C(18) H(35) 109.3
H(34) C(18) H(35) 109.5 P(3) C(19) H(36) 108.5
P(3) C(19) H(37) 108.7 C(20) C(19) H(36) 107.7
C(20) C(19) H(37) 108.0 H(36) C(19) H(37) 109.2
C(19) C(20) H(38) 110.0 C(19) C(20) H(39) 109.7
C(19) C(20) H(40) 109.9 H(38) C(20) H(39) 109.1
H(38) C(20) H(40) 109.0 H(39) C(20) H(40) 109.1
P(3) C(21) H(41) 108.0 P(3) C(21) H(42) 108.2
C(22) C(21) H(41) 107.7 C(22) C(21) H(42) 108.1
H(41) C(21) H(42) 109.4 C(21) C(22) H(43) 109.7
C(21) C(22) H(44) 109.8 C(21) C(22) H(45) 109.3

Table 6. Bond Angles(ffi) (continued)

atom atom atom angle atom atom atom angle
H(43) C(22) H(44) 109.6 H(43) C(22) H(45) 109.2
H(44) C(22) H(45) 109.2 P(4) C(23) H(46) 107.6
P(4) C(23) H(47) 107.6 C(24) C(23) H(46) 107.4
C(24) C(23) H(47) 107.5 H(46) C(23) H(47) 109.5

C(23) C(24) H(48) 109.9 C(23) C(24) H(49) 109.9
C(23) C(24) H(50) 109.9 H(48) C(24) H(49) 109.1
H(48) C(24) H(50) 109.1 H(49) C(24) H(50) 109.0
P(4) C(25) H(51) 107.8 P(4) C(25) H(52) 107.8
C(26) C(25) H(51) 107.8 C(26) C(25) H(52) 107.7
H(51) C(25) H(52) 109.4 C(25) C(26) H(53) 109.5
C(25) C(26) H(54) 109.4 C(25) C(26) H(55) 109.6
H(53) C(26) H(54) 109.3 H(53) C(26) H(55) 109.6
H(54) C(26) H(55) 109.5 P(4) C(27) H(56) 108.6
P(4) C(27) H(57) 108.8 C(28) C(27) H(56) 108.5
C(28) C(27) H(57) 108.8 H(56) C(27) H(57) 109.4
C(27) C(28) H(58) 109.8 C(27) C(28) H(59) 109.8
C(27) C(28) H(60) 109.5 H(58) C(28) H(59) 109.3
H(58) C(28) H(60) 109.1 H(59) C(28) H(60) 109.2
21

Table 7. Torsion Angles(ffi)
atom atom atom atom angle atom atom atom atom angle
I(1) Co(1) P(1) C(3) -68.0(8) I(1) Co(1) P(1) C(5) 49.9(9)
I(1) Co(1) P(1) C(7) 172.5(7) I(1) Co(1) P(2) C(9) 73.7(8)
I(1) Co(1) P(2) C(11) -45.4(8) I(1) Co(1) P(2) C(13) -168.2(7)
I(1) Co(1) C(1) O(1) 143(23) I(1) Co(1) C(2) O(2) -179(18)
I(2) Co(2) P(3) C(17) -38.3(9) I(2) Co(2) P(3) C(19) -158.1(8)
I(2) Co(2) P(3) C(21) 86.4(9) I(2) Co(2) P(4) C(23) 67.8(7)
I(2) Co(2) P(4) C(25) -174.2(7) I(2) Co(2) P(4) C(27) -51.7(8)
I(2) Co(2) C(15) O(3) 145(18) I(2) Co(2) C(16) O(4) 168(12)
Co(1) P(1) C(3) C(4) 172(1) Co(1) P(1) C(5) C(6) 54(1)
Co(1) P(1) C(7) C(8) 49(1) Co(1) P(2) C(9) C(10) 175(1)
Co(1) P(2) C(11) C(12) -50(1) Co(1) P(2) C(13) C(14) -56(1)
Co(2) P(3) C(17) C(18) -53(1) Co(2) P(3) C(19) C(20) -53(1)
Co(2) P(3) C(21) C(22) -60(1) Co(2) P(4) C(23) C(24) -177(1)
Co(2) P(4) C(25) C(26) -60(1) Co(2) P(4) C(27) C(28) -45(2)
P(1) Co(1) P(2) C(9) 20(14) P(1) Co(1) P(2) C(11) -98(13)
P(1) Co(1) P(2) C(13) 138(13) P(1) Co(1) C(1) O(1) 54(23)
P(1) Co(1) C(2) O(2) -89(18) P(2) Co(1) P(1) C(3) -15(14)
P(2) Co(1) P(1) C(5) 102(13) P(2) Co(1) P(1) C(7) -134(13)
P(2) Co(1) C(1) O(1) -126(23) P(2) Co(1) C(2) O(2) 90(18)
P(3) Co(2) P(4) C(23) -158(14) P(3) Co(2) P(4) C(25) -40(14)
P(3) Co(2) P(4) C(27) 82(14) P(3) Co(2) C(15) O(3) 53(18)
P(3) Co(2) C(16) O(4) -100(12) P(4) Co(2) P(3) C(17) -172(14)
P(4) Co(2) P(3) C(19) 68(14) P(4) Co(2) P(3) C(21) -47(14)
P(4) Co(2) C(15) O(3) -126(18) P(4) Co(2) C(16) O(4) 79(12)
22

Table 7. Torsion Angles(ffi) (continued)
atom atom atom atom angle atom atom atom atom angle
O(1) C(1) Co(1) C(2) -35(24) O(2) C(2) Co(1) C(1) 0(19)
O(3) C(15) Co(2) C(16) -35(18) O(4) C(16) Co(2) C(15) -11(13)
C(1) Co(1) P(1) C(3) 46(1) C(1) Co(1) P(1) C(5) 164(1)
C(1) Co(1) P(1) C(7) -73.1(10) C(1) Co(1) P(2) C(9) -40(1)
C(1) Co(1) P(2) C(11) -159(1) C(1) Co(1) P(2) C(13) 77.4(10)
C(2) Co(1) P(1) C(3) 173(1) C(2) Co(1) P(1) C(5) -68(1)
C(2) Co(1) P(1) C(7) 53(1) C(2) Co(1) P(2) C(9) -167(1)
C(2) Co(1) P(2) C(11) 73(1) C(2) Co(1) P(2) C(13) -49(1)
C(3) P(1) C(5) C(6) 176(1) C(3) P(1) C(7) C(8) -72(1)
C(4) C(3) P(1) C(5) 44(1) C(4) C(3) P(1) C(7) -65(1)
C(5) P(1) C(7) C(8) 179(1) C(6) C(5) P(1) C(7) -72(1)
C(9) P(2) C(11) C(12) -174(1) C(9) P(2) C(13) C(14) 65(1)
C(10) C(9) P(2) C(11) -55(1) C(10) C(9) P(2) C(13) 52(1)
C(11) P(2) C(13) C(14) 172(1) C(12) C(11) P(2) C(13) 76(1)
C(15) Co(2) P(3) C(17) 74(1) C(15) Co(2) P(3) C(19) -44(1)
C(15) Co(2) P(3) C(21) -160(1) C(15) Co(2) P(4) C(23) -45.3(10)
C(15) Co(2) P(4) C(25) 72(1) C(15) Co(2) P(4) C(27) -164(1)
C(16) Co(2) P(3) C(17) -159(1) C(16) Co(2) P(3) C(19) 80(1)
C(16) Co(2) P(3) C(21) -34(1) C(16) Co(2) P(4) C(23) -171.1(10)
C(16) Co(2) P(4) C(25) -53.0(10) C(16) Co(2) P(4) C(27) 69(1)
C(17) P(3) C(19) C(20) 177(1) C(17) P(3) C(21) C(22) 71(1)
C(18) C(17) P(3) C(19) 71(1) C(18) C(17) P(3) C(21) 175(1)
C(19) P(3) C(21) C(22) 176(1) C(20) C(19) P(3) C(21) 71(1)
C(23) P(4) C(25) C(26) 63(1) C(23) P(4) C(27) C(28) -171(1)
23

Table 7. Torsion Angles(ffi) (continued)
atom atom atom atom angle atom atom atom atom angle
C(24) C(23) P(4) C(25) 58(1) C(24) C(23) P(4) C(27) -48(1)
C(25) P(4) C(27) C(28) 81(1) C(26) C(25) P(4) C(27) 168(1)
24
Table 8. Non-bonded Contacts out to 3.20 š A
atom atom distance ADC atom atom distance ADC
25

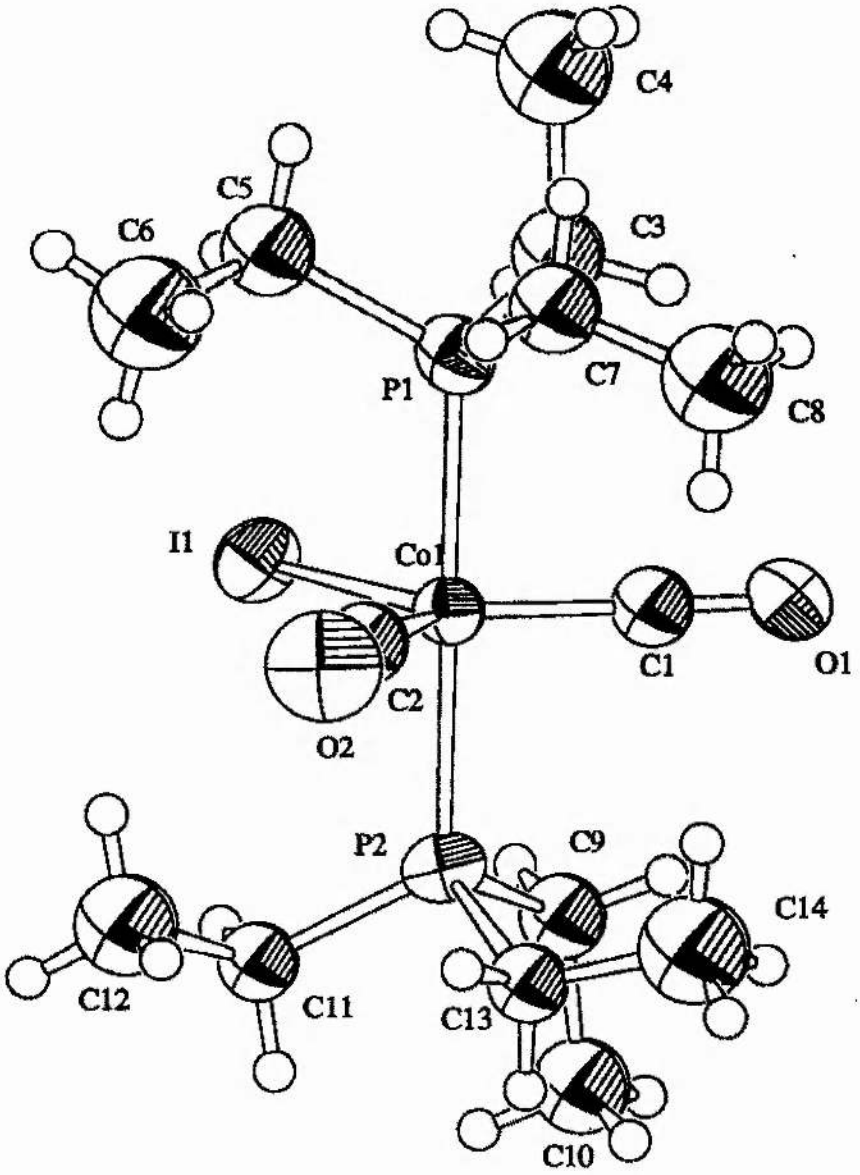

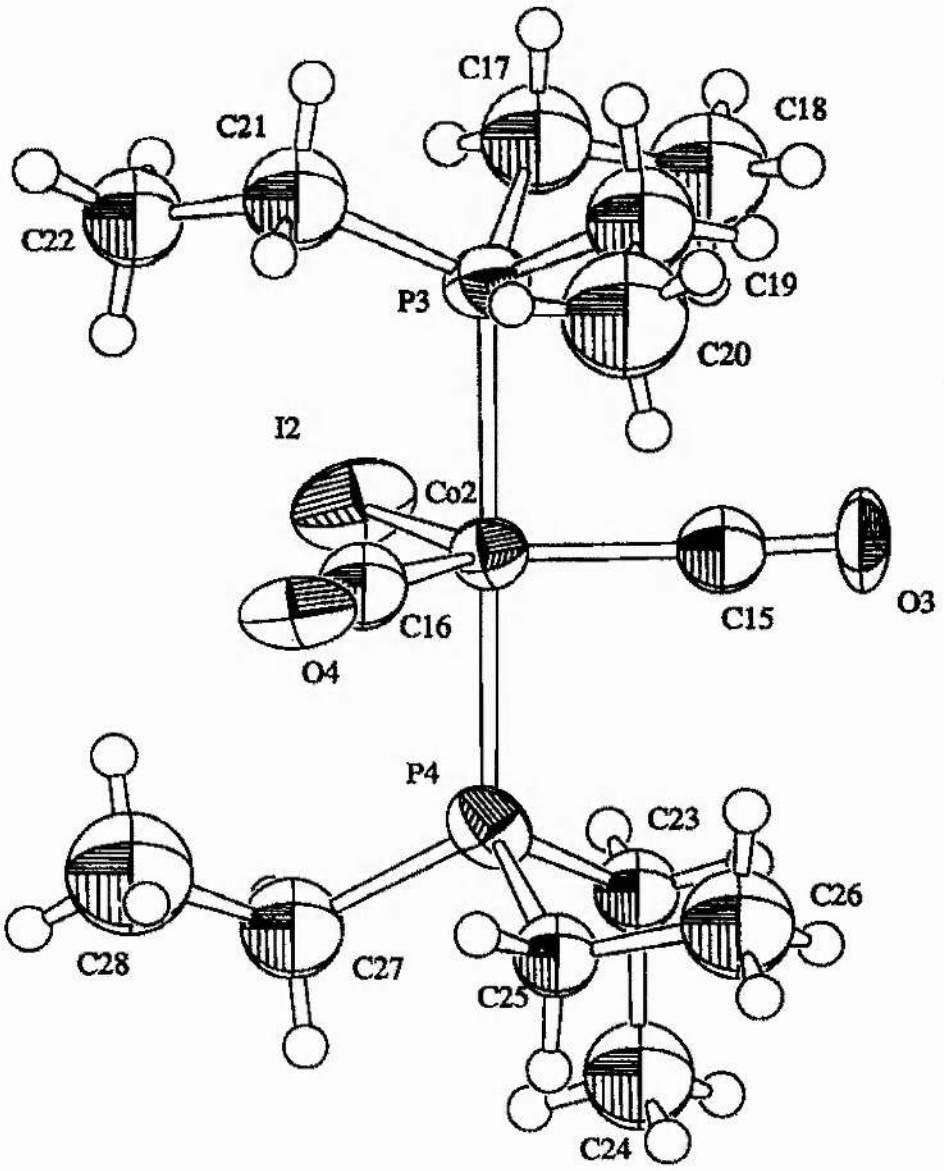
C17
C18
C21
C22
C19
P3
C20
I2
Co2
C16
C15
O3
O4
P4
C23
C26
C28
C27
C25
C24

X-ray Structure Report
Thu Sep 3 1998
acm192a

EXPERIMENTAL DETAILS

Crystal Data
Empirical Formula C 13 H 18 IRhO 2
Formula Weight 436.09
Crystal Color, Habit purple, plate
Crystal Dimensions 0.35 X 0.20 X 0.05 mm
Crystal System monoclinic
Lattice Type Primitive
No. of Reflections Used for Unit
Cell Determination (2` range) 25 (20.4 - 24.7 ffi)
Omega Scan Peak Width
at Half-height 0.28 ffi
Lattice Parameters a = 12.804(7) š A
b = 8.859(7) š A
c = 14.403(7) š A
fi = 113.41(3) ffi
V = 1499(1) š A 3
Space Group P2 1 /c (#14)
Z value 4
D calc 1.932 g/cm 3
F 000 840.00
¯(MoKff) 31.85 cm
Radiation MoKff (– = 0.71069 A)
graphite monochromated
Attenuator Zr foil (factor = 8.53)
Take-o
Angle 6.0 ffi
Detector Aperture 9.0 mm horizontal
13.0 mm vertical
Crystal to Detector Distance 235 mm
Temperature 220.0 ffi C
Scan Type !-2`
Scan Rate 16.0 ffi /min (in !) (up to 4 scans)
Scan Width (1.00 + 0.35 tan `) ffi
2` max 50.0 ffi
No. of Reections Measured Total: 2970
Unique: 2839 (R int = 0.052)
Corrections Lorentz-polarization
Absorption
(trans. factors: 0.6135 - 1.0000)

Structure Solution and Renement
Structure Solution Direct Methods (SIR92)
Renement Full-matrix least-squares
Function Minimized w (jFoj 2
Least Squares Weights 1
oe 2 (Fo) = 4Fo 2
oe 2 (Fo 2)
p-factor 0.0030
Anomalous Dispersion All non-hydrogen atoms
No. Observations (I?3.00oe(I)) 1995
No. Variables 154
Reection/Parameter Ratio 12.95
Residuals: R; Rw 0.037 ; 0.037
6

Goodness of Fit Indicator 1.96
Max Shift/Error in Final Cycle 0.00
Maximum peak in Final Diff. Map 1.09 e 3
Minimum peak in Final Diff. Map -1.29 e

Table 1. Atomic coordinates and B iso /B eq
atom x y z B eq
I(1) 0.16363(5) 0.31609(7) 0.48247(4) 3.63(1)
Rh(1) 0.21700(5) 0.14509(7) 0.64796(5) 2.25(1)
O(1) -0.0231(6) 0.0835(9) 0.6192(6) 6.4(2)
O(2) 0.3106(6) 0.4153(7) 0.7555(5) 4.5(2)
C(1) 0.0645(8) 0.113(1) 0.6302(8) 4.1(2)

C(2) 0.2212(9) 0.3509(10) 0.7176(6) 3.6(2)
C(3) 0.1140(9) 0.417(1) 0.7153(7) 4.6(3)
C(4) 0.3804(7) 0.0647(8) 0.7695(6) 2.9(2)
C(5) 0.4000(6) 0.0920(9) 0.6823(6) 2.7(2)
C(6) 0.3330(7) -0.0166(8) 0.6039(6) 2.5(2)
C(7) 0.2712(7) -0.1053(8) 0.6433(6) 2.8(2)
C(8) 0.2946(7) -0.0485(8) 0.7455(6) 2.9(2)
C(9) 0.4426(8) 0.135(1) 0.8702(6) 4.5(2)
C(10) 0.4825(7) 0.203(1) 0.6697(8) 4.5(2)
C(11) 0.3378(8) -0.033(1) 0.5027(7) 3.7(2)
C(12) 0.1987(9) -0.2398(10) 0.5964(7) 4.4(2)
C(13) 0.2503(9) -0.124(1) 0.8177(8) 4.5(3)
H(1) 0.1207 0.4346 0.7826 5.5436
H(2) 0.0998 0.5105 0.6796 5.5436
H(3) 0.0528 0.3499 0.6823 5.5436
H(4) 0.4135 0.0976 0.9169 5.3594
H(5) 0.5213 0.1118 0.8935 5.3594
H(6) 0.4329 0.2418 0.8647 5.3594
H(7) 0.5576 0.1775 0.7151 5.3742
8

Table 1. Atomic coordinates and B iso /B eq (continued)
atom x y z B eq
H(8) 0.4775 0.1983 0.6021 5.3742
H(9) 0.4645 0.3016 0.6839 5.3742
H(10) 0.3654 -0.1304 0.4970 4.4779
H(11) 0.2637 -0.0197 0.4514 4.4779
H(12) 0.3874 0.0416 0.4952 4.4779
H(13) 0.1668 -0.2778 0.6411 5.3240
H(14) 0.1393 -0.2112 0.5343 5.3240
H(15) 0.2439 -0.3159 0.5841 5.3240
H(16) 0.2747 -0.0678 0.8790 5.4574
H(17) 0.1694 -0.1261 0.7877 5.4574
H(18) 0.2789 -0.2237 0.8315 5.4574
B eq = 8
3 ß 2 (U 11 (aa 3) 2 + U 22 (bb 3) 2 + U 33 (cc 3) 2 + 2U 12 aa 3 bb 3 cos fl + 2U 13 aa 3 cc 3 cos fi + 2U 23 bb 3 cc 3 cos ff)
9

Table 2. Anisotropic Displacement Parameters
atom U 11 U 22 U 33 U 12 U 13 U 23
I(1) 0.0586(4) 0.0395(3) 0.0438(3) 0.0078(3) 0.0247(3) 0.0129(3)
Rh(1) 0.0302(4) 0.0228(3) 0.0347(3) 0.0011(3) 0.0153(3) 0.0034(3)
O(1) 0.039(4) 0.091(6) 0.119(7) -0.005(4) 0.038(5) 0.030(5)
O(2) 0.067(5) 0.029(3) 0.069(5) -0.007(3) 0.022(4) -0.014(3)
C(1) 0.035(6) 0.042(5) 0.082(7) 0.011(4) 0.027(5) 0.015(5)
C(2) 0.078(7) 0.033(5) 0.032(5) 0.016(5) 0.030(5) 0.007(4)
C(3) 0.080(8) 0.046(6) 0.066(7) 0.016(5) 0.047(6) 0.006(5)
C(4) 0.040(5) 0.024(4) 0.039(5) 0.009(4) 0.008(4) 0.001(3)
C(5) 0.023(4) 0.031(4) 0.045(5) 0.003(3) 0.008(4) 0.011(4)
C(6) 0.030(5) 0.028(4) 0.037(4) 0.006(3) 0.014(4) -0.002(4)
C(7) 0.030(5) 0.025(4) 0.048(5) 0.006(3) 0.013(4) 0.003(4)
C(8) 0.043(5) 0.026(4) 0.044(5) 0.012(4) 0.021(4) 0.012(4)
C(9) 0.060(7) 0.063(6) 0.034(5) 0.005(5) 0.006(5) -0.010(5)
C(10) 0.026(5) 0.047(6) 0.099(8) -0.013(4) 0.028(5) 0.000(6)
C(11) 0.055(6) 0.045(5) 0.049(5) 0.010(5) 0.029(5) 0.005(4)
C(12) 0.063(7) 0.028(5) 0.075(7) -0.004(5) 0.026(6) 0.002(5)
C(13) 0.073(7) 0.041(6) 0.076(7) 0.024(5) 0.048(6) 0.024(5)
The general temperature factor expression:
exp(2 (a 32 U 11 h 2 + b 32 U 22 k 2 + c 32 U 33 l 2 + 2a 3 b 3 U 12 hk + 2a 3 c 3 U 13 hl + 2b 3 c 3 U 23 kl))
10

Table 3. Bond Lengths(ß A)
atom atom distance atom atom distance
I(1) Rh(1) 2.6737(8) Rh(1) C(1) 1.887(9)
Rh(1) C(2) 2.071(9) Rh(1) C(4) 2.244(8)
Rh(1) C(5) 2.244(8) Rh(1) C(6) 2.326(7)
Rh(1) C(7) 2.333(7) Rh(1) C(8) 2.189(7)
O(1) C(1) 1.10(1) O(2) C(2) 1.20(1)
C(2) C(3) 1.48(1) C(4) C(5) 1.40(1)
C(4) C(8) 1.43(1) C(4) C(9) 1.49(1)
C(5) C(6) 1.47(1) C(5) C(10) 1.50(1)

C(6) C(7) 1.39(1) C(6) C(11) 1.49(1)
C(7) C(8) 1.47(1) C(7) C(12) 1.50(1)
C(8) C(13) 1.52(1)
11

Table 4. Bond Lengths(§ A)
atom atom distance atom atom distance
C(3) H(1) 0.95 C(3) H(2) 0.95
C(3) H(3) 0.95 C(9) H(4) 0.95
C(9) H(5) 0.95 C(9) H(6) 0.95
C(10) H(7) 0.95 C(10) H(8) 0.95
C(10) H(9) 0.95 C(11) H(10) 0.95
C(11) H(11) 0.95 C(11) H(12) 0.95
C(12) H(13) 0.95 C(12) H(14) 0.95
C(12) H(15) 0.95 C(13) H(16) 0.95
C(13) H(17) 0.95 C(13) H(18) 0.95
12

Table 5. Bond Angles(ffi)
atom atom atom angle atom atom atom angle
I(1) Rh(1) C(1) 94.6(3) I(1) Rh(1) C(2) 83.2(2)
I(1) Rh(1) C(4) 134.7(2) I(1) Rh(1) C(5) 101.0(2)
I(1) Rh(1) C(6) 94.0(2) I(1) Rh(1) C(7) 119.1(2)
I(1) Rh(1) C(8) 155.0(2) C(1) Rh(1) C(2) 91.4(4)
C(1) Rh(1) C(4) 130.7(4) C(1) Rh(1) C(5) 158.8(3)
C(1) Rh(1) C(6) 127.5(4) C(1) Rh(1) C(7) 99.1(3)
C(1) Rh(1) C(8) 98.7(3) C(2) Rh(1) C(4) 93.7(3)
C(2) Rh(1) C(5) 104.7(4) C(2) Rh(1) C(6) 141.0(3)
C(2) Rh(1) C(7) 154.2(3) C(2) Rh(1) C(8) 117.4(3)
C(4) Rh(1) C(5) 36.2(3) C(4) Rh(1) C(6) 61.2(3)
C(4) Rh(1) C(7) 61.6(3) C(4) Rh(1) C(8) 37.5(3)
C(5) Rh(1) C(6) 37.5(3) C(5) Rh(1) C(7) 60.7(3)
C(5) Rh(1) C(8) 61.7(3) C(6) Rh(1) C(7) 34.6(3)
C(6) Rh(1) C(8) 61.1(3) C(7) Rh(1) C(8) 37.8(3)
Rh(1) C(1) O(1) 174.7(9) Rh(1) C(2) O(2) 118.5(7)
Rh(1) C(2) C(3) 119.6(7) O(2) C(2) C(3) 121.9(8)
Rh(1) C(4) C(5) 71.9(4) Rh(1) C(4) C(8) 69.2(4)
Rh(1) C(4) C(9) 126.8(6) C(5) C(4) C(8) 107.5(7)
C(5) C(4) C(9) 125.9(8) C(8) C(4) C(9) 126.5(8)
Rh(1) C(5) C(4) 71.9(5) Rh(1) C(5) C(6) 74.3(4)
Rh(1) C(5) C(10) 124.0(6) C(4) C(5) C(6) 108.6(7)
C(4) C(5) C(10) 127.4(8) C(6) C(5) C(10) 123.8(8)
Rh(1) C(6) C(5) 68.2(4) Rh(1) C(6) C(7) 73.0(5)
Rh(1) C(6) C(11) 127.2(5) C(5) C(6) C(7) 108.0(7)
13

Table 5. Bond Angles(ffi) (continued)
atom atom atom angle atom atom atom angle
C(5) C(6) C(11) 125.1(7) C(7) C(6) C(11) 126.7(8)
Rh(1) C(7) C(6) 72.4(4) Rh(1) C(7) C(8) 65.8(4)
Rh(1) C(7) C(12) 129.1(6) C(6) C(7) C(8) 107.1(7)
C(6) C(7) C(12) 128.3(8) C(8) C(7) C(12) 124.6(8)
Rh(1) C(8) C(4) 73.4(4) Rh(1) C(8) C(7) 76.4(4)
Rh(1) C(8) C(13) 125.7(6) C(4) C(8) C(7) 108.3(7)
C(4) C(8) C(13) 127.1(8) C(7) C(8) C(13) 123.5(8)
14

Table 6. Bond Angles(ffi)
atom atom atom angle atom atom atom angle
C(2) C(3) H(1) 109.5 C(2) C(3) H(2) 109.5
C(2) C(3) H(3) 109.5 H(1) C(3) H(2) 109.5
H(1) C(3) H(3) 109.5 H(2) C(3) H(3) 109.5
C(4) C(9) H(4) 109.5 C(4) C(9) H(5) 109.5
C(4) C(9) H(6) 109.5 H(4) C(9) H(5) 109.5
H(4) C(9) H(6) 109.5 H(5) C(9) H(6) 109.5
C(5) C(10) H(7) 109.5 C(5) C(10) H(8) 109.5
C(5) C(10) H(9) 109.5 H(7) C(10) H(8) 109.4
H(7) C(10) H(9) 109.5 H(8) C(10) H(9) 109.4
C(6) C(11) H(10) 109.5 C(6) C(11) H(11) 109.5
C(6) C(11) H(12) 109.5 H(10) C(11) H(11) 109.5
H(10) C(11) H(12) 109.5 H(11) C(11) H(12) 109.5
C(7) C(12) H(13) 109.5 C(7) C(12) H(14) 109.5

C(7) C(12) H(15) 109.5 H(13) C(12) H(14) 109.5
H(13) C(12) H(15) 109.5 H(14) C(12) H(15) 109.5
C(8) C(13) H(16) 109.5 C(8) C(13) H(17) 109.5
C(8) C(13) H(18) 109.5 H(16) C(13) H(17) 109.5
H(16) C(13) H(18) 109.4 H(17) C(13) H(18) 109.5
15

Table 7. Torsion Angles(ffi)
atom atom atom atom angle atom atom atom atom angle
I(1) Rh(1) C(1) O(1) 118(11) I(1) Rh(1) C(2) O(2) -93.5(7)
I(1) Rh(1) C(2) C(3) 83.8(7) I(1) Rh(1) C(4) C(5) -25.9(6)
I(1) Rh(1) C(4) C(8) -143.5(4) I(1) Rh(1) C(4) C(9) 95.8(8)
I(1) Rh(1) C(5) C(4) 161.6(4) I(1) Rh(1) C(5) C(6) -82.3(4)
I(1) Rh(1) C(5) C(10) 38.1(8) I(1) Rh(1) C(6) C(5) 102.8(4)
I(1) Rh(1) C(6) C(7) -139.1(4) I(1) Rh(1) C(6) C(11) -15.6(7)
I(1) Rh(1) C(7) C(6) 48.3(5) I(1) Rh(1) C(7) C(8) 167.0(4)
I(1) Rh(1) C(7) C(12) -77.1(8) I(1) Rh(1) C(8) C(4) 86.6(7)
I(1) Rh(1) C(8) C(7) -27.6(8) I(1) Rh(1) C(8) C(13) -149.3(6)
Rh(1) C(4) C(5) C(6) -65.7(5) Rh(1) C(4) C(5) C(10) 119.4(8)
Rh(1) C(4) C(8) C(7) 69.1(5) Rh(1) C(4) C(8) C(13) -122.5(8)
Rh(1) C(5) C(4) C(8) 60.3(5) Rh(1) C(5) C(4) C(9) -122.8(8)
Rh(1) C(5) C(6) C(7) -62.5(5) Rh(1) C(5) C(6) C(11) 121.0(8)
Rh(1) C(6) C(5) C(4) 64.2(5) Rh(1) C(6) C(5) C(10) -120.7(8)
Rh(1) C(6) C(7) C(8) -56.8(5) Rh(1) C(6) C(7) C(12) 126.4(8)
Rh(1) C(7) C(6) C(5) 59.5(5) Rh(1) C(7) C(6) C(11) -124.1(8)
Rh(1) C(7) C(8) C(4) -67.0(5) Rh(1) C(7) C(8) C(13) 124.1(8)
Rh(1) C(8) C(4) C(5) -62.0(5) Rh(1) C(8) C(4) C(9) 121.1(8)
Rh(1) C(8) C(7) C(6) 61.0(6) Rh(1) C(8) C(7) C(12) -122.1(8)
O(1) C(1) Rh(1) C(2) -158(11) O(1) C(1) Rh(1) C(4) -62(11)
O(1) C(1) Rh(1) C(5) -18(11) O(1) C(1) Rh(1) C(6) 19(11)
O(1) C(1) Rh(1) C(7) -1(11) O(1) C(1) Rh(1) C(8) -40(11)
O(2) C(2) Rh(1) C(1) 172.1(7) O(2) C(2) Rh(1) C(4) 41.2(7)
O(2) C(2) Rh(1) C(5) 6.1(8) O(2) C(2) Rh(1) C(6) -5.5(10)
16

Table 7. Torsion Angles(ffi) (continued)
atom atom atom atom angle atom atom atom atom angle
O(2) C(2) Rh(1) C(7) 57(1) O(2) C(2) Rh(1) C(8) 71.6(8)
C(1) Rh(1) C(2) C(3) -10.6(7) C(1) Rh(1) C(4) C(5) 155.0(5)
C(1) Rh(1) C(4) C(8) 37.4(7) C(1) Rh(1) C(4) C(9) -83.3(9)
C(1) Rh(1) C(5) C(4) -62(1) C(1) Rh(1) C(5) C(6) 53(1)
C(1) Rh(1) C(5) C(10) 174(1) C(1) Rh(1) C(6) C(5) -158.3(5)
C(1) Rh(1) C(6) C(7) -40.2(7) C(1) Rh(1) C(6) C(11) 83.3(8)
C(1) Rh(1) C(7) C(6) 148.8(5) C(1) Rh(1) C(7) C(8) -92.5(6)
C(1) Rh(1) C(7) C(12) 23.3(9) C(1) Rh(1) C(8) C(4) -152.2(6)
C(1) Rh(1) C(8) C(7) 93.6(5) C(1) Rh(1) C(8) C(13) -28.1(8)
C(2) Rh(1) C(4) C(5) -110.0(5) C(2) Rh(1) C(4) C(8) 132.4(5)
C(2) Rh(1) C(4) C(9) 11.8(8) C(2) Rh(1) C(5) C(4) 75.8(5)
C(2) Rh(1) C(5) C(6) -168.0(4) C(2) Rh(1) C(5) C(10) -47.6(8)
C(2) Rh(1) C(6) C(5) 18.6(7) C(2) Rh(1) C(6) C(7) 136.7(5)
C(2) Rh(1) C(6) C(11) -99.7(8) C(2) Rh(1) C(7) C(6) -98.6(9)
C(2) Rh(1) C(7) C(8) 20(1) C(2) Rh(1) C(7) C(12) 136.0(9)
C(2) Rh(1) C(8) C(4) -56.1(6) C(2) Rh(1) C(8) C(7) -170.3(5)
C(2) Rh(1) C(8) C(13) 68.0(9) C(3) C(2) Rh(1) C(4) -141.5(7)
C(3) C(2) Rh(1) C(5) -176.6(6) C(3) C(2) Rh(1) C(6) 171.8(6)
C(3) C(2) Rh(1) C(7) -124.9(8) C(3) C(2) Rh(1) C(8) -111.1(7)
C(4) Rh(1) C(5) C(6) 116.2(6) C(4) Rh(1) C(5) C(10) -123.4(10)
C(4) Rh(1) C(6) C(5) -37.2(4) C(4) Rh(1) C(6) C(7) 80.9(5)
C(4) Rh(1) C(6) C(11) -155.6(8) C(4) Rh(1) C(7) C(6) -79.6(5)
C(4) Rh(1) C(7) C(8) 39.1(5) C(4) Rh(1) C(7) C(12) 154.9(9)
C(4) Rh(1) C(8) C(7) -114.2(7) C(4) Rh(1) C(8) C(13) 124.1(10)
17

Table 7. Torsion Angles(ffi) (continued)
atom atom atom atom angle atom atom atom atom angle
C(4) C(5) Rh(1) C(6) -116.2(6) C(4) C(5) Rh(1) C(7) -81.1(5)
C(4) C(5) Rh(1) C(8) -37.8(5) C(4) C(5) C(6) C(7) 1.7(9)
C(4) C(5) C(6) C(11) -174.8(7) C(4) C(8) Rh(1) C(5) 36.5(5)
C(4) C(8) Rh(1) C(6) 79.5(5) C(4) C(8) Rh(1) C(7) 114.2(7)
C(4) C(8) C(7) C(6) -6.1(9) C(4) C(8) C(7) C(12) 170.9(7)
C(5) Rh(1) C(4) C(8) -117.6(7) C(5) Rh(1) C(4) C(9) 121(1)
C(5) Rh(1) C(6) C(7) 118.1(6) C(5) Rh(1) C(6) C(11) -118.3(9)

C(5) Rh(1) C(7) C(6) -38.0(4) C(5) Rh(1) C(7) C(8) 80.7(5)
C(5) Rh(1) C(7) C(12) -163.5(9) C(5) Rh(1) C(8) C(7) -77.7(5)
C(5) Rh(1) C(8) C(13) 160.6(9) C(5) C(4) Rh(1) C(6) 38.6(4)
C(5) C(4) Rh(1) C(7) 78.2(5) C(5) C(4) Rh(1) C(8) 117.6(7)
C(5) C(4) C(8) C(7) 7.1(9) C(5) C(4) C(8) C(13) 175.5(7)
C(5) C(6) Rh(1) C(7) -118.1(6) C(5) C(6) Rh(1) C(8) -80.3(5)
C(5) C(6) C(7) C(8) 2.7(9) C(5) C(6) C(7) C(12) -174.1(8)
C(6) Rh(1) C(4) C(8) -79.0(5) C(6) Rh(1) C(4) C(9) 160.3(9)
C(6) Rh(1) C(5) C(10) 120.4(9) C(6) Rh(1) C(7) C(8) 118.7(7)
C(6) Rh(1) C(7) C(12) -125(1) C(6) Rh(1) C(8) C(7) -34.7(4)
C(6) Rh(1) C(8) C(13) -156.4(9) C(6) C(5) Rh(1) C(7) 35.1(4)
C(6) C(5) Rh(1) C(8) 78.4(5) C(6) C(5) C(4) C(8) -5.4(9)
C(6) C(5) C(4) C(9) 171.5(7) C(6) C(7) Rh(1) C(8) -118.7(7)
C(6) C(7) C(8) C(13) -174.9(7) C(7) Rh(1) C(4) C(8) -39.4(5)
C(7) Rh(1) C(4) C(9) -160.1(9) C(7) Rh(1) C(5) C(10) 155.5(9)
C(7) Rh(1) C(6) C(11) 123.6(9) C(7) Rh(1) C(8) C(13) -121.7(10)
C(7) C(6) Rh(1) C(8) 37.8(5) C(7) C(6) C(5) C(10) 176.8(7)
18

Table 7. Torsion Angles(ffi) (continued)
atom atom atom atom angle atom atom atom atom angle
C(7) C(8) C(4) C(9) -169.8(8) C(8) Rh(1) C(4) C(9) -120(1)
C(8) Rh(1) C(5) C(10) -161.2(9) C(8) Rh(1) C(6) C(11) 161.4(8)
C(8) Rh(1) C(7) C(12) 115.8(10) C(8) C(4) C(5) C(10) 179.7(8)
C(8) C(7) C(6) C(11) 179.1(7) C(9) C(4) C(5) C(10) -3(1)
C(9) C(4) C(8) C(13) -1(1) C(10) C(5) C(6) C(11) 0(1)
C(11) C(6) C(7) C(12) 2(1) C(12) C(7) C(8) C(13) 2(1)
19

Table 8. Non-bonded Contacts out to 3.30 § A
atom atom distance ADC atom atom distance ADC
20

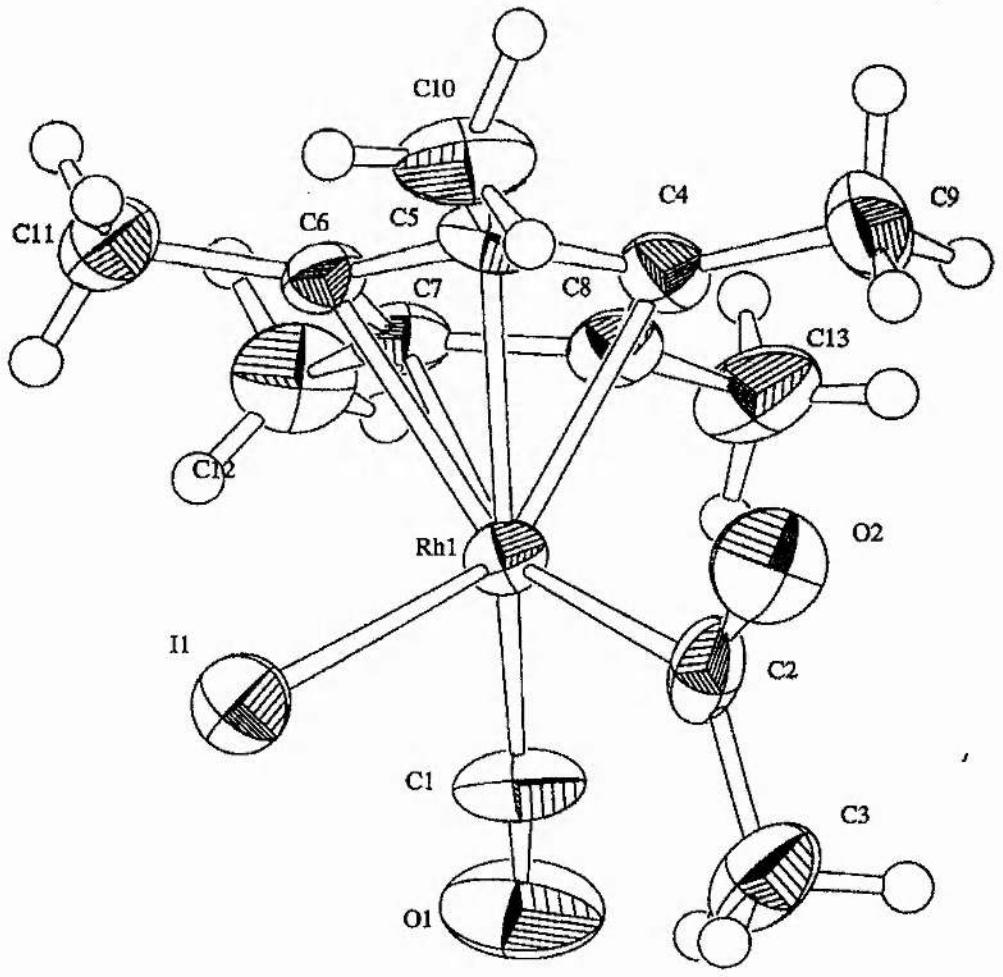

X-ray Structure Report
Wed Dec 17 1997
acm140

EXPERIMENTAL DETAILS

Crystal Data
Empirical Formula C 12 H 32 CoI 3 P 4
Formula Weight 739.93
Crystal Color, Habit brown, plate
Crystal Dimensions 0.50 X 0.40 X 0.05 mm
Crystal System monoclinic
Lattice Type C-centered
No. of Reflections Used for Unit
Cell Determination (2` range) 25 (23.6 - 25.0 ffi)
Omega Scan Peak Width
at Half-height 0.33 ffi
Lattice Parameters a = 13.599(5) š A
b = 26.059(8) š A
c = 9.199(5) š A
fi = 129.86(2) ffi
V = 2502(2) š A 3
Space Group C2/c (#15)
Z value 4
D calc 1.964 g/cm 3
F 000 1400.00
¯(MoKff) 46.37 cm
Radiation MoKff (– = 0.71069 A)
graphite monochromated
Attenuator Zr foil (factor = 8.53)
Take-o
Angle 6.0 ffi
Detector Aperture 9.0 mm horizontal
13.0 mm vertical
Crystal to Detector Distance 235 mm
Temperature 200.0 ffi C
Scan Type !-2`
Scan Rate 16.0 ffi /min (in !) (up to 4 scans)
Scan Width (1.68 + 0.35 tan `) ffi
2` max 50.0 ffi
No. of Reections Measured Total: 2362
Unique: 2263 (R int = 0.030)
Corrections Lorentz-polarization
Absorption
(trans. factors: 0.4724 - 1.0000)

Structure Solution and Renement
Structure Solution Direct Methods (SIR92)
Renement Full-matrix least-squares
Function Minimized w (jFoj 2
Least Squares Weights 1
oe 2 (Fo) = 4Fo 2
oe 2 (Fo 2)
p-factor 0.0010
Anomalous Dispersion All non-hydrogen atoms
No. Observations (I?3.00oe(I)) 1809
No. Variables 93
Reection/Parameter Ratio 19.45
Residuals: R; Rw 0.105 ; 0.124
6

Goodness of Fit Indicator 8.62
Max Shift/Error in Final Cycle 0.00
Maximum peak in Final Diff. Map 3.64 e 3
Minimum peak in Final Diff. Map -5.61 e

Table 1. Atomic coordinates and B iso /B eq
atom x y z B eq
I(1) 0.5000 0.2313(2) 0.7500 5.9(1)
I(2) 0.5000 0.03549(10) 0.7500 2.54(6)
I(3) 0.0000 0.1629(1) 0.7500 3.68(7)
Co(1) 0.5000 0.1357(2) 0.7500 1.27(9)
P(1) 0.3360(6) 0.1356(3) 0.4335(9) 1.8(1)

P(2) 0.3487(6) 0.1381(3) 0.7828(9) 1.8(1)
C(1) 0.328(3) 0.089(1) 0.279(4) 3.7(7)
C(2) 0.302(3) 0.195(1) 0.306(4) 2.8(6)
C(3) 0.189(2) 0.124(1) 0.402(3) 2.5(6)
C(4) 0.197(2) 0.153(1) 0.546(4) 2.6(6)
C(5) 0.303(3) 0.080(1) 0.835(4) 3.5(8)
C(6) 0.366(3) 0.185(1) 0.945(4) 2.5(6)
H(1) 0.2445 0.0896 0.1588 4.4190
H(2) 0.3891 0.0978 0.2648 4.4190
H(3) 0.3457 0.0559 0.3330 4.4190
H(4) 0.3047 0.2224 0.3752 3.3762
H(5) 0.3648 0.1997 0.2919 3.3762
H(6) 0.2197 0.1926 0.1852 3.3762
H(7) 0.1161 0.1342 0.2793 2.9894
H(8) 0.1824 0.0880 0.4174 2.9894
H(9) 0.1270 0.1441 0.5406 3.0700
H(10) 0.1936 0.1887 0.5214 3.0700
H(11) 0.2343 0.0875 0.8342 4.2050
H(12) 0.2769 0.0549 0.7421 4.2050
8

Table 1. Atomic coordinates and B iso /B eq (continued)
atom x y z B eq
H(13) 0.3742 0.0677 0.9565 4.2050
H(14) 0.4291 0.1737 1.0714 3.0132
H(15) 0.3912 0.2171 0.9286 3.0132
H(16) 0.2863 0.1889 0.9182 3.0132
B eq = 8
3 ß 2 (U 11 (aa 3) 2 + U 22 (bb 3) 2 + U 33 (cc 3) 2 + 2U 12 aa 3 bb 3 cos fl + 2U 13 aa 3 cc 3 cos fi + 2U 23 bb 3 cc 3 cos ff)
9

Table 2. Anisotropic Displacement Parameters
atom U 11 U 22 U 33 U 12 U 13 U 23
I(1) 0.067(2) 0.089(3) 0.063(2) 0.0000 0.039(2) 0.0000
I(2) 0.043(2) 0.020(1) 0.037(1) 0.0000 0.027(1) 0.0000
I(3) 0.023(1) 0.080(3) 0.032(2) 0.0000 0.016(1) 0.0000
Co(1) 0.018(2) 0.018(3) 0.013(2) 0.0000 0.010(2) 0.0000
P(1) 0.022(3) 0.029(4) 0.014(3) -0.001(3) 0.010(3) -0.004(3)
P(2) 0.024(3) 0.029(4) 0.018(3) 0.000(3) 0.015(3) 0.000(3)
C(1) 0.05(2) 0.06(2) 0.02(1) 0.01(2) 0.01(1) 0.00(1)
C(2) 0.04(2) 0.04(2) 0.02(1) 0.01(1) 0.01(1) 0.01(1)
C(3) 0.02(1) 0.05(2) 0.01(1) 0.00(1) 0.00(1) 0.00(1)
C(4) 0.02(1) 0.05(2) 0.03(1) 0.01(1) 0.02(1) 0.02(1)
C(5) 0.04(2) 0.05(2) 0.04(2) -0.01(2) 0.03(2) 0.00(2)
C(6) 0.04(2) 0.04(2) 0.02(1) 0.01(1) 0.03(1) 0.00(1)
The general temperature factor expression:
exp(2 (a 32 U 11 h 2 + b 32 U 22 k 2 + c 32 U 33 l 2 + 2a 3 b 3 U 12 hk + 2a 3 c 3 U 13 hl + 2b 3 c 3 U 23 kl))
10

Table 3. Bond Lengths(§ A)
atom atom distance atom atom distance
I(1) Co(1) 2.490(7) I(2) Co(1) 2.611(5)
Co(1) P(1) 2.264(6) Co(1) P(1) 2.264(6)
Co(1) P(2) 2.263(6) Co(1) P(2) 2.263(6)
P(1) C(1) 1.81(3) P(1) C(2) 1.80(3)
P(1) C(3) 1.85(3) P(2) C(4) 1.84(2)
P(2) C(5) 1.81(3) P(2) C(6) 1.82(3)
C(3) C(4) 1.47(4)
11

Table 4. Bond Lengths(§ A)
atom atom distance atom atom distance
C(1) H(1) 0.95 C(1) H(2) 0.95
C(1) H(3) 0.95 C(2) H(4) 0.95
C(2) H(5) 0.95 C(2) H(6) 0.95
C(3) H(7) 0.95 C(3) H(8) 0.95
C(4) H(9) 0.95 C(4) H(10) 0.95
C(5) H(11) 0.95 C(5) H(12) 0.95
C(5) H(13) 0.95 C(6) H(14) 0.95
C(6) H(15) 0.95 C(6) H(16) 0.95
12

Table 5. Bond Angles(ffi)

atom atom atom angle atom atom atom angle
I(1) Co(1) I(2) 180.0000(1) I(1) Co(1) P(1) 90.1(2)
I(1) Co(1) P(1) 90.1(2) I(1) Co(1) P(2) 88.4(2)
I(1) Co(1) P(2) 88.4(2) I(2) Co(1) P(1) 89.9(2)
I(2) Co(1) P(1) 89.9(2) I(2) Co(1) P(2) 91.6(2)
I(2) Co(1) P(2) 91.6(2) P(1) Co(1) P(1) 179.8(4)
P(1) Co(1) P(2) 86.6(2) P(1) Co(1) P(2) 93.4(2)
P(1) Co(1) P(2) 93.4(2) P(1) Co(1) P(2) 86.6(2)
P(2) Co(1) P(2) 176.9(4) Co(1) P(1) C(1) 121.6(10)
Co(1) P(1) C(2) 117.6(9) Co(1) P(1) C(3) 106.0(8)
C(1) P(1) C(2) 101(1) C(1) P(1) C(3) 104(1)
C(2) P(1) C(3) 104(1) Co(1) P(2) C(4) 105.8(8)
Co(1) P(2) C(5) 120(1) Co(1) P(2) C(6) 118.4(9)
C(4) P(2) C(5) 100(1) C(4) P(2) C(6) 106(1)
C(5) P(2) C(6) 103(1) P(1) C(3) C(4) 108(1)
P(2) C(4) C(3) 109(1)
13

Table 6. Bond Angles(ffi)

atom atom atom angle atom atom atom angle
P(1) C(1) H(1) 109.5 P(1) C(1) H(2) 109.5
P(1) C(1) H(3) 109.5 H(1) C(1) H(2) 109.5
H(1) C(1) H(3) 109.5 H(2) C(1) H(3) 109.5
P(1) C(2) H(4) 109.5 P(1) C(2) H(5) 109.5
P(1) C(2) H(6) 109.5 H(4) C(2) H(5) 109.5
H(4) C(2) H(6) 109.5 H(5) C(2) H(6) 109.5
P(1) C(3) H(7) 109.6 P(1) C(3) H(8) 109.6
C(4) C(3) H(7) 109.6 C(4) C(3) H(8) 109.6
H(7) C(3) H(8) 109.5 P(2) C(4) H(9) 109.5
P(2) C(4) H(10) 109.5 C(3) C(4) H(9) 109.5
C(3) C(4) H(10) 109.5 H(9) C(4) H(10) 109.5
P(2) C(5) H(11) 109.5 P(2) C(5) H(12) 109.5
P(2) C(5) H(13) 109.5 H(11) C(5) H(12) 109.5
H(11) C(5) H(13) 109.5 H(12) C(5) H(13) 109.5
P(2) C(6) H(14) 109.5 P(2) C(6) H(15) 109.5
P(2) C(6) H(16) 109.5 H(14) C(6) H(15) 109.5
H(14) C(6) H(16) 109.5 H(15) C(6) H(16) 109.5
14

Table 7. Torsion Angles(ffi)

atom atom atom atom angle atom atom atom atom angle
I(1) Co(1) P(1) C(1) 141(1) I(1) Co(1) P(1) C(2) 15(1)
I(1) Co(1) P(1) C(3) -100.0(10) I(1) Co(1) P(1) C(1) 141(1)
I(1) Co(1) P(1) C(2) 15(1) I(1) Co(1) P(1) C(3) -100.0(10)
I(1) Co(1) P(2) C(4) 77(1) I(1) Co(1) P(2) C(5) -169(1)
I(1) Co(1) P(2) C(6) -41(1) I(1) Co(1) P(2) C(4) 77(1)
I(1) Co(1) P(2) C(5) -169(1) I(1) Co(1) P(2) C(6) -41(1)
I(2) Co(1) P(1) C(1) -38(1) I(2) Co(1) P(1) C(2) -164(1)
I(2) Co(1) P(1) C(3) 80.0(10) I(2) Co(1) P(1) C(1) -38(1)
I(2) Co(1) P(1) C(2) -164(1) I(2) Co(1) P(1) C(3) 80.0(10)
I(2) Co(1) P(2) C(4) -102(1) I(2) Co(1) P(2) C(5) 10(1)
I(2) Co(1) P(2) C(6) 138(1) I(2) Co(1) P(2) C(4) -102(1)
I(2) Co(1) P(2) C(5) 10(1) I(2) Co(1) P(2) C(6) 138(1)
Co(1) P(1) C(3) C(4) 40(2) Co(1) P(2) C(4) C(3) 41(2)
Co(1) P(2) C(4) C(3) 41(2) P(1) Co(1) P(1) C(1) -38(1)
P(1) Co(1) P(1) C(2) -164(1) P(1) Co(1) P(1) C(3) 80.0(10)
P(1) Co(1) P(2) C(4) -12(1) P(1) Co(1) P(2) C(5) 99(1)
P(1) Co(1) P(2) C(6) -131(1) P(1) Co(1) P(2) C(4) 167(1)
P(1) Co(1) P(2) C(5) -79(1) P(1) Co(1) P(2) C(6) 48(1)
P(1) C(3) C(4) P(2) -53(2) P(2) Co(1) P(1) C(1) -130(1)
P(2) Co(1) P(1) C(2) 104(1) P(2) Co(1) P(1) C(3) -11(1)
P(2) Co(1) P(1) C(1) 52(1) P(2) Co(1) P(1) C(2) -72(1)
P(2) Co(1) P(1) C(3) 171(1) P(2) Co(1) P(2) C(4) 77(1)
P(2) Co(1) P(2) C(5) -169(1) P(2) Co(1) P(2) C(6) -41(1)
C(1) P(1) C(3) C(4) 170(1) C(2) P(1) C(3) C(4) -83(2)
15

Table 7. Torsion Angles(ffi) (continued)

atom atom atom atom angle atom atom atom atom angle
C(3) C(4) P(2) C(5) -84(2) C(3) C(4) P(2) C(6) 168(1)

Table 8. Non-bonded Contacts out to 3.30 § A
atom atom distance ADC atom atom distance ADC